

The Study of Late Transition Metal Catalyzed C–H Bond
Activation and Functionalization

Junqi Chen
Wuhan, China

B.S. Chemistry, Peking University, 2013

A Dissertation Presented to the Graduate Faculty
of the University of Virginia in Candidacy for the Degree of
Doctor of Philosophy

Department of Chemistry

University of Virginia
April 30, 2019

ABSTRACT

CHEN, JUNQI The Study of Late Transition Metal Catalyzed C–H Bond Activation and Functionalization. (Under the direction of Professor T. Brent Gunnoe)

The catalytic partial oxidation of hydrocarbons using late transition metals is an important but challenging process. Two key steps are typically involved: C–H bond activation to form a M–C and reductive elimination to form a C–O bond. In this Dissertation, a series of rationally designed “capping arene” supported Rh(III) complexes are synthesized and used to study reductive functionalization of a Rh(III)–Me bond. This type of ligand can block an axial coordination site of the Rh(III) center, which destabilizes the complex and leads to a more facile Rh(I)/Rh(III) redox cycle. The complex (5-FP)Rh(TFA)₂Me [5-FP = 1,2-bis(*N*-7-azaindoly)benzene, TFA = trifluoroacetate] gives 94% yield of MeTFA in acetonitrile with AgOTf (OTf = trifluoromethanesulfonate) as an additive.

The 5-FP ligand has also been used to prevent the Rh(I) complex, (5-FP)Rh(TFA)(η^2 -C₂H₄), from undergoing undesired oxidation in the olefin hydroarylation reaction with benzene and α -olefins. This new Rh catalyst precursor achieves efficient oxidative olefin hydroarylation using either air or Cu(II) salts as oxidants. Under optimized conditions, the conversion of propylene and benzene to linear alkenyl arenes is achieved with over 13,000 turnovers without evidence of catalyst decomposition after 2 weeks at 150 °C. At a lower temperature (80 °C), a linear to branched ratio of ~18:1 has also been observed. The longevity and stability of this catalyst is an improvement on earlier systems and the potential commercialization of the process is being explored.

When investigating the olefin hydroarylation reaction with Rh catalysts, phenyl acetate is produced as a byproduct through a side reaction with benzene and Cu(II) oxidant. As

phenyl acetate is a desirable precursor for phenol production, we sought to generate it selectively. A series of copper salts have been tested for the functionalization of the C–H bond of benzene. Two competing mechanistic pathways are involved in the reaction. Under the anaerobic conditions, the organometallic pathway is favored, while the reaction occurs through the radical pathway under aerobic conditions. Interestingly, the addition of a radical reagent, TEMPO ((2,2,6,6-Tetramethylpiperidin-1-yl)oxyl), can shift the reaction from the radical pathway to the non-radical mechanism under aerobic conditions. In addition, the reaction rate is greatly increased when TEMPO is used as an additive.

Hydroamination of alkenes or alkynes is one of the most straightforward methods to form C–N bonds and N-containing heterocycles. This method involves direct addition of amines to carbon-carbon multiple bonds without the formation of any by-products. Al(OTf)₃ has been used as an effective catalyst for the intramolecular hydroamination of unactivated alkenes. The mechanism for this transformation has been studied. Triflic acid which is generated *in situ* from Al(OTf)₃ is demonstrated to be the active catalyst for the hydroamination reaction. In addition, other metal triflates such as Bi(OTf)₃ and Mg(OTf)₂ have been shown to catalyze the hydroamination reaction through a similar reaction mechanism.

ACKNOWLEDGEMENTS

Chasing a PhD degree is like a long journey in which you will have a lot of ups and downs and finally reach the destination. You will try to expand the knowledge of human a little bit to get the degree. Every discovery you have in your experiments is the first time that human knows about it. It is impossible to accomplish the PhD degree by yourself and here I want to thank all the people who help me survive through my PhD life.

Firstly, thank you to my advisor Brent Gunnoe. You are the nicest advisor in the world and you are always full of passion and enthusiasm about chemistry and catalysis. Thank you for being so supportive and considerate through my PhD journey. It is the greatest thing that have a professor like you to be my advisor. Although all the group members do not like sub-group meeting and monthly report, those reports and presentation slides help me a lot when I am trying to write my dissertation. I enjoy every time when we talk about science and how we can move the project forward. You will be a mentor through my life and I wish you earn the Nobel Prize someday! My thanks extend to Trecia and Leah; your party hosting, delicious foods and smiling faces are gratefully received.

I want thank my committee, Dr. Dean Harman, Dr. Lin Pu, Dr. Ian Harrison and Dr Chris Paolucii for all your feedback over the past six years and for reading this dissertation.

The Gunnoe group is like a big family and I want to say thanks for all the past and present group members. To Sarah and Steve, thank you for being my mentors when I join the group. I learn not only experiment skills but also the rigorous altitude toward scientific researches. To Jiajun Mei, thank you for helping me through both experiments and life in the new country. To Xiaofan and Nichole, it is so nice to have you two in the lab with me

for 5 years and share my happiness and sorrow. To Mike, thank you for teaching me how to handle hydroarylation experiments and how to survive in endless meetings. To Fanji, Shunyan and Weihao, thank you for working closely with me on different research projects and I wish all of you have a bright future. To Abigail, thank you for being the best undergraduate in Gunnoe lab. Many thanks for all the group member for sharing my PhD journey and it is my greatest honor to have you all in my life.

To Diane, Jeff and Earl, thank you for all your help with NMR, XRD and equipment. To Michael, it is great to have someone who can cheer you up whenever you are down.

To my friends near and far, thank you for supporting me during these years. Special thanks to Jiahan, thank you for being my closest friend here and sharing room with me in my first year. Special thanks to Dota 2 squad, Wei Wu and Gengyu, I enjoy every game with you. Special thanks for Jingxin, Huiling and Fengqi, thank you for tolerating massive phone calls when I am down and cheer me up every time. You are the greatest treasures in my life. Special thanks to Tian Qiu, Lihua and Zhuo Chen, I need not to worry about anything when I stay with you. We have known each other for 20 years and we will be life time friends forever. Last special thanks to Karen, thank you for being my special person for three years and I wish you have a better one in the future,

To my family, Mum and Dad, grandpa and grandma, aunts and uncles, Yihui, Xilan and Cheng; and all my nieces and nephews, thank you. You have always supported my, believed in me, trusted me, encouraged me and loved me. Thanks for understanding all my decisions and sharing me the best moments in my life.

TABLE OF CONTENTS

| | |
|--|------------|
| LIST OF SCHEMES | IX |
| LIST OF FIGURES | XI |
| LIST OF TABLES | XIV |
| | |
| 1 Introduction | 1 |
| 1.1 General Concept of Catalysis | 1 |
| 1.2 Examples for Heterogeneous and Homogeneous Catalysts | 4 |
| 1.2.1 Three-way Catalysts..... | 4 |
| 1.2.2 Hydroformylation..... | 5 |
| 1.2.3 Acetic Acid Production (BASF, Monsanto and Cativa Process)..... | 6 |
| 1.2.4 Wacker Process for Acetaldehyde Production..... | 9 |
| 1.3 Alkane C–H Activation | 10 |
| 1.3.1 General Concept for Alkane Activation | 11 |
| 1.3.2 The Conversion of Methane to Methanol..... | 11 |
| 1.3.3 Methane to Methanol via Syngas..... | 14 |
| 1.3.4 Methane Functionalization via Heterogenous Catalysis..... | 14 |
| 1.3.5 Hydrocarbon Functionalization via Organometallic Catalysis..... | 15 |
| 1.3.6 Examples for Methane Functionalization via Organometallic Routes..... | 17 |
| 1.3.7 Reductive Elimination of MeX..... | 21 |
| 1.4 Arene Functionalization | 28 |
| 1.4.1 Overview of Alkyl Arenes..... | 28 |
| 1.4.2 Late Transition Metal Catalyzed Olefin Hydroarylation..... | 31 |
| 1.4.3 Examples for Late Transition Metal Catalyzed Olefin Hydroarylation.... | 34 |
| 1.5 Acetoxylation of Non-directed Arene | 45 |
| 1.6 Summary and Thesis Aims | 49 |
| 1.7 References | 50 |
| | |
| 2 Reductive Functionalization of Rh–Me Bonds with “Capping Arene” Supported Rh(III) complexes | 64 |
| 2.1 Introduction | 64 |
| 2.2 Results and Discussions | 67 |
| 2.2.1 Synthesis of Rh Capping Arene Complexes..... | 67 |
| 2.2.2 Structure Comparison of Two Different Capping Arene Complexes..... | 71 |
| 2.2.3 Solvent Screening for RE of MeX from Complex 1..... | 73 |
| 2.2.4 Temperature Optimization for RE of MeX from Complex 1..... | 77 |
| 2.2.5 Influence of Acid Additive effect on RE of MeX from Complex 1..... | 78 |
| 2.2.6 Influence of Silver Oxidant Additives on RE of MeX from Complex 1..... | 79 |
| 2.3 Conclusion | 81 |
| 2.4 Experimental Section | 81 |

| | | |
|------------|--|------------|
| 2.5 | References..... | 89 |
| 3 | The Development and Study of Rh(I) Complexes with “Capping Arene” ligands for Hydroarylation with Benzene and α-Olefin..... | 91 |
| 3.1 | Basic Concept for Rh Catalyzed Hydroarylation..... | 91 |
| 3.2 | Results and Discussion..... | 97 |
| 3.2.1 | Catalysts Design, Synthesis and Characterization..... | 97 |
| 3.2.2 | Catalytic Oxidative Olefin Hydroarylation..... | 100 |
| 3.2.3 | Attempt to Copper Oxidant Recycle..... | 105 |
| 3.2.4 | Access to Aerobic Reaction Condition and <i>in situ</i> Copper Oxidant Regeneration..... | 108 |
| 3.2.5 | Investigation of Product Inhibition and Cu(II) Oxidant Dependence..... | 113 |
| 3.3 | Computational Studies..... | 116 |
| 3.3.1 | Reaction Pathway Prediction..... | 116 |
| 3.3.2 | Linear Selectivity Modeling..... | 118 |
| 3.2.5 | Resistance Towards Oxidation Explanation..... | 119 |
| 3.4 | Conclusion..... | 121 |
| 3.5 | Experimental Section..... | 122 |
| 3.6 | References..... | 126 |
| | | |
| 4 | Undirected Arene Acetoxylation with Cu Catalysts..... | 131 |
| 4.1 | Introduction..... | 131 |
| 4.2 | Results and Discussions..... | 137 |
| 4.2.1 | Cu(OAc) ₂ Mediated Benzene Acetoxylation and Optimization of Reaction Conditions..... | 137 |
| 4.2.2 | Cu(II) Oxidant Screening for Benzene C–H Functionalization..... | 139 |
| 4.2.3 | Ligand Additives Screening..... | 141 |
| 4.2.4 | Elucidation of Reaction Mechanism..... | 145 |
| 4.2.5 | Attempt Towards Catalytic Turnovers..... | 151 |
| 4.3 | Conclusion..... | 152 |
| 4.4 | Experimental Section..... | 153 |
| 4.5 | References..... | 155 |
| | | |
| 5 | Brønsted acid-catalysed intramolecular hydroamination of unactivated alkenes..... | 158 |
| 5.1 | Introduction..... | 158 |
| 5.2 | Results and Discussion..... | 164 |
| 5.2.1 | Al(OTf) ₃ Catalyzed Hydroamination: Alkenylamine Substrates Scope... | 164 |
| 5.2.2 | Lewis and Brønsted Acid Catalyzed Hydroamination: Catalyst Screening. | 166 |
| 5.2.3 | Base Additives Study..... | 170 |
| 5.2.4 | Kinetic Study of Hydroamination..... | 172 |
| 5.2.5 | Solvent Effect Study..... | 175 |
| 5.3 | Proposed Mechanism and Conclusion..... | 176 |

| | | |
|------------|--|------------|
| 5.4 | Experimental Section..... | 178 |
| 5.5 | References..... | 186 |
| 6 | Future Outlook..... | 191 |
| 6.1 | Future Direction of Reductive Elimination of Rh–Me..... | 191 |
| 6.2 | Future Direction of Hydroarylation with Rh Catalysts..... | 193 |
| 6.3 | Future Direction of Copper Catalyzed Arene C–H Functionalization..... | 194 |
| 6.4 | References..... | 196 |

LIST OF SCHEMES
CHAPTER 1

| | |
|---|----|
| Scheme 1.2.1. Reactions in the three-way catalysis..... | 4 |
| Scheme 1.2.2. Heck-Brewslow mechanism for cobalt-catalyzed hydroformylation..... | 6 |
| Scheme 1.2.3. Catalytic cycle for Monsanto process..... | 8 |
| Scheme 1.2.4. Water-gas shift reaction equation..... | 9 |
| Scheme 1.2.5. Mechanism for Wacker process..... | 10 |
| Scheme 1.3.1. Current industrial production of synthesis gas and methanol..... | 14 |
| Scheme 1.3.2. Proposed catalytic cycle for Shilov system..... | 17 |
| Scheme 1.3.3. Proposed catalytic cycle for Pt(bpy)Cl ₂ /H ₂ SO ₄ system..... | 18 |
| Scheme 1.3.4. Iodate/chloride oxidant of alkanes, which is proposed to be catalytic in chloride..... | 21 |
| Scheme 1.3.5. The effect of geometry on RE reaction..... | 22 |
| Scheme 1.3.6. Mechanism of RE of MeI from (dppe)Pt(Me) ₃ I..... | 23 |
| Scheme 1.3.7. Reductive elimination of MeI from PCP Rh complexes..... | 26 |
| Scheme 1.3.8. Three possible pathways for RE of PNP ligated Rh complexes..... | 27 |
| Scheme 1.4.1. The synthesis and use of alkyl arenes..... | 28 |
| Scheme 1.4.2. Mechanism for acid catalyzed Friedel-Crafts alkylation..... | 29 |
| Scheme 1.4.3. Examples for branched alkyl benzenes (BABs), linear alkyl benzenes (LABs) and super linear alkyl benzenes (SLABs)..... | 31 |
| Scheme 1.4.4. Proposed mechanism for transition metal catalyzed hydroarylation with benzene and α -olefin. | 32 |
| Scheme 1.4.5. Linear to branched selectivity and the in olefin insertion s t e p 3 3 | 33 |
| Scheme 1.4.6. Ir(acac) complexes..... | 35 |
| Scheme 1.4.7. Mechanism of Ir(acac) catalyzed olefin hydroarylation..... | 36 |
| Scheme 1.4.8. Mechanism for TpRu(CO)(NCMe)Ph catalyzed olefin hydroarylation..... | 39 |
| Scheme 1.4.9. Mechanistic comparison between TpRu and MeOTMM based catalyst... | 41 |
| Scheme 1.4.10. Proposed mechanism for (pyridyl)pyrrolide ligand supported Pt(II) complex catalyzed hydroarylation of olefins..... | 42 |
| Scheme 1.4.11. Structures of different (pyridyl)pyrrolide ligand supported Pt(II) complexes and steric effect on olefin insertion..... | 43 |
| Scheme 1.5.1 Summary of Pd(OAc) ₂ catalyzed benzene acetoxylation..... | 46 |
| Scheme 1.5.2. Mechanism for Pd(OAc) ₂ catalyzed benzene acetoxylation with pyridine additive..... | 48 |

CHAPTER 2

| | |
|--|----|
| Scheme 2.1.1. DFT calculation of three pathways for reductive functionalization of a terpyridine Rh ^{III} -Me complex..... | 66 |
|--|----|

CHAPTER 3

| | |
|---|-----|
| Scheme 3.1.1. Current processes for the synthesis of styrene, linear alkyl benzenes (LABs) the synthesis of alkenyl benzenes such as styrene, that can be hydrogenated to form super linear alkyl benzenes (SLABs) | 92 |
| Scheme 3.1.2. Mechanism for Friedel-Crafts alkylation with an α -olefin..... | 94 |
| Scheme 3.2.1. Cu(OAc) ₂ thermo decomposition. | 103 |
| Scheme 3.2.2. Possible steric or electronic effect on oxidative hydrophenylation with styrene and propenyl benzenes..... | 105 |

CHAPTER 4

| | |
|---|-----|
| Scheme 4.1.1. Industrial processes for phenol production..... | 132 |
| Scheme 4.1.2. Proposed mechanism for PIP group directed Cu catalyzed hydroxylation /acetoxylation..... | 133 |
| Scheme 4.1.3. Proposed mechanism for benzoic acid group directed Cu catalyzed hydroxylation..... | 134 |
| Scheme 4.1.4. Cu catalyzed C–H bond functionalization with Daugulis’s directing group..... | 137 |

CHAPTER 5

| | |
|--|-----|
| Scheme 5.1.1. Proposed mechanisms for intramolecular hydroamination of alkene with different types of catalysts | 159 |
| Scheme 5.1.2 Simplified mechanism for organolanthanide catalyzed bicyclization..... | 160 |
| Scheme 5.1.3. Proposed mechanisms for NHC ligand supported Cu complexes catalyzed hydroamination..... | 162 |
| Scheme 5.1.4 Proposed mechanisms for Al(OTf) ₃ catalyzed hydroalkoxylations..... | 164 |
| Scheme 5.2.1 Kinetic isotope effect experiments with Al(OTf) ₃ and Bi(OTf) ₃ | 174 |
| Scheme 5.3.1 Proposed mechanism for metal triflate catalyzed hydroamination..... | 178 |

CHAPTER 6

| | |
|--|-----|
| Scheme 6.1.1. Proposed synthetic routes for di-“capping arene” ligands..... | 192 |
|--|-----|

LIST OF FIGURES
CHAPTER 1

| | |
|--|----|
| Figure 1.1. Simple energy diagram of catalyzed and uncatalyzed reaction pathways..... | 2 |
| Figure 1.2. Simple energy diagram of methane oxidation..... | 13 |
| Figure 1.3. Different mechanisms for metal complex mediated C–H activation..... | 16 |
| Figure 1.4.1. Structure of [Ir(Ph)(py)(trop-O,O) ₂] and <i>trans</i> -(hfac-O,O) ₂ Rh(Ph)(py)..... | 38 |
| Figure 1.4.2. Summarized results from Ru system..... | 39 |
| Figure 1.4.3 Structures of [(^α bpy)Pt(Ph)THF][BAR' ₄] and [(dpm)Pt(Ph)(THF)][BAR' ₄]..... | 45 |

CHAPTER 2

| | |
|--|----|
| Figure 2.2.1. Synthetic routes for (5-FP)Rh(TFA) ₂ Me (1) and (6-FP)Rh(TFA) ₂ Me (2).... | 67 |
| Figure 2.2.2. ¹ H NMR spectrum for (5-FP)Rh(Cl)(η^2 -C ₂ H ₄) in DCM- <i>d</i> ₂ | 69 |
| Figure 2.2.3. ¹ H NMR spectrum for three isomer of (5-FP)Rh(Cl)(I)Me in DCM- <i>d</i> ₂ | 70 |
| Figure 2.2.4. ¹ H NMR spectrum for (5-FP)Rh(TFA) ₂ Me (1) in DCM- <i>d</i> ₂ | 71 |
| Figure 2.2.5. ORTEP of (6-FP)Rh(TFA) ₂ Me (2)..... | 72 |
| Figure 2.2.6. ORTEP of (5-FP)Rh(TFA)(η^2 -C ₂ H ₄) and (6-FP)Rh(TFA)(η^2 -C ₂ H ₄)..... | 72 |
| Figure 2.2.7. Stacked ¹ H NMR spectra for RE of MeX from complex 1 in benzene..... | 75 |
| Figure 2.2.8. Stacked ¹ H NMR spectra for RE of MeX from complex 1 in MeCN at 90°C..... | 76 |
| Figure 2.2.9. Stacked ¹ H NMR spectra for RE of MeX from complex 1 in DMSO..... | 77 |
| Figure 2.4.1. ¹³ C NMR spectrum for (5-FP)Rh(TFA) ₂ Me (1) DCM- <i>d</i> ₂ | 84 |
| Figure 2.4.2. ¹⁹ F NMR spectrum for (5-FP)Rh(TFA) ₂ Me (1) DCM- <i>d</i> ₂ | 85 |
| Figure 2.4.3. ¹ H NMR spectrum for (6-FP)Rh(TFA) ₂ Me (2) DCM- <i>d</i> ₂ | 86 |
| Figure 2.4.4. ¹³ C NMR spectrum for (6-FP)Rh(TFA) ₂ Me (2) DCM- <i>d</i> ₂ | 86 |
| Figure 2.4.5. ¹⁹ F NMR spectrum for (6-FP)Rh(TFA) ₂ Me (2) DCM- <i>d</i> ₂ | 87 |
| Figure 2.4.6. ¹ H NMR spectrum for (6-FP)RhCl(η^2 -C ₂ H ₄) DCM- <i>d</i> ₂ | 88 |
| Figure 2.4.7. ¹ H NMR spectrum for three isomer of (6-FP)Rh(Cl)(I)Me DCM- <i>d</i> ₂ | 88 |

CHAPTER 3

| | |
|--|-----|
| Figure 3.1.1. Proposed cycle for transition metal–catalyzed styrene production from benzene and ethylene using CuX ₂ as an oxidant..... | 94 |
| Figure 3.2.1. ¹ H NMR spectrum of (5-FP)Rh(TFA)(η^2 -C ₂ H ₄) 1 in DCM- <i>d</i> ₂ | 98 |
| Figure 3.2.2. ¹³ C NMR spectrum of (5-FP)Rh(TFA)(η^2 -C ₂ H ₄) 1 in DCM- <i>d</i> ₂ | 98 |
| Figure 3.2.3. ORTEP of (5-FP)Rh(TFA)(η^2 -C ₂ H ₄) 1 | 100 |
| Figure 3.2.4. Structure comparison between (5-FP)Rh(TFA)(η^2 -C ₂ H ₄) (1) and previously reported "capping arene" complex..... | 100 |
| Figure 3.2.5. Photographs of reactors over the course of the reaction..... | 107 |
| Figure 3.2.6. Oxidative hydrophenylation of propylene with <i>in situ</i> Cu oxidant regeneration..... | 107 |

| | |
|---|---------|
| Figure 3.2.7. Plot of turnovers versus time for catalytic oxidative hydrophenylation of propylene with Cu(II) oxidant that is regenerated <i>in situ</i> (using (5-FP)Rh(TFA)(η^2 -C ₂ H ₄) (1) as catalyst)..... | 108 |
| Figure 3.2.8. Hydrophenylation of propylene under aerobic conditions..... | 110-111 |
| Figure 3.2.9. Alkenyl arenes products decomposition study with (5-FP)Rh(TFA)(η^2 -C ₂ H ₄) (1)..... | 111-112 |
| Figure 3.2.10. Catalytic oxidative hydrophenylation of propylene using air as oxidant with (5-FP)Rh(TFA)(η^2 -C ₂ H ₄) (1)..... | 112 |
| Figure 3.2.11. Catalytic oxidative hydrophenylation of propylene using (5-FP)Rh(TFA)(η^2 -C ₂ H ₄) (1) with different Cu(OPiv) ₂ loading..... | 115 |
| Figure 3.3.1. Free energies (kcal/mol) at 423 K from DFT calculations (M06, including PBF solvation) of the proposed catalytic cycle for conversion of ethylene and benzene to styrene..... | 117 |
| Figure 3.3.2. Free energies (kcal/mol) at 423 K from DFT calculations of our proposed catalytic cycle for the oxidative hydroarylation of propene..... | 119 |
| Figure 3.3.3. Free energies (kcal/mol) at 423 K from DFT calculations for reactions of oxidants with the rhodium hydride 8..... | 121 |

CHAPTER 4

| | |
|---|-----|
| Figure 4.1.1. Directing groups for Cu catalyzed hydroxylation..... | 134 |
| Figure 4.2.1. Ligands structures..... | 142 |
| Figure 4.2.2. The results of the acetoxylation reaction with different phosphines and phosphine oxide ligands..... | 145 |
| Figure 4.2.3. Structures of phosphines and phosphine oxide ligands | 145 |
| Figure 4.2.4. Cu(OHex) ₂ mediated benzene C–H functionalization with different radical traps..... | 147 |
| Figure 4.2.5. Cu(OHex) ₂ mediated benzene C–H functionalization with different TEMPO loadings..... | 14 |
| 8 | |
| Figure 4.2.6. Catalytic acetoxylation of benzene with Cu(OAc) ₂ | 152 |

CHAPTER 5

| | |
|---|-----|
| Figure 5.2.1. Kinetic data for determination of reaction order with respect to 1c and catalysts..... | 173 |
| Figure 5.2.2. KIE determination for HOTf and Al(OTf) ₃ catalyzed hydroamination of 1c | 174 |
| Figure 5.2.3. KIE determination for Al(OTf) ₃ and Bi(OTf) ₃ catalyzed hydroamination of 1c or 1c-d₂ | 175 |
| Figure 5.4.1. ¹ H NMR spectrum (600 MHz, CD ₂ Cl ₂) of 4-methoxybenzyl(2,2-diphenyl-4- | |

| | |
|---|-----|
| pentenyl)amine..... | 179 |
| Figure 5.4.2. $^{13}\text{C}\{^1\text{H}\}$ NMR spectrum (150 MHz, CD_2Cl_2) of 4-methoxybenzyl(2,2-diphenyl-4-pentenyl)amine..... | 180 |
| Figure 5.4.3. ^1H NMR spectrum (600 MHz, CDCl_3) of 1c-d₂ | 181 |
| Figure 5.4.4. ^1H NMR spectrum (600 MHz, $\text{C}_6\text{D}_5\text{NO}_2$) of hydroamination product of 1a | 182 |
| Figure 5.4.5. ^1H NMR spectrum (600 MHz, $\text{C}_6\text{D}_5\text{NO}_2$) of hydroamination product of 1b | 182 |
| Figure 5.4.6. ^1H NMR spectrum (600 MHz, $\text{C}_6\text{D}_5\text{NO}_2$) of hydroamination product of 1c | 183 |
| Figure 5.4.7. ^1H NMR spectrum (600 MHz, $\text{C}_6\text{D}_5\text{NO}_2$) of hydroamination product of methyl 4-[(2,2-diphenyl-4-pentenylamino)-methyl]benzoate..... | 183 |
| Figure 5.4.8. ^1H NMR spectrum (600 MHz, $\text{C}_6\text{D}_5\text{NO}_2$) of hydroamination product of 4-nitrobenzyl(2,2-diphenyl-4-pentenyl) amine..... | 184 |
| Figure 5.4.9. ^1H NMR spectrum (600 MHz, $\text{C}_6\text{D}_5\text{NO}_2$) of hydroamination product of 4-methoxybenzyl(2,2-diphenyl-4-pentenyl)amine..... | 184 |
| Figure 5.4.10. ^1H NMR spectrum (600 MHz, $\text{C}_6\text{D}_5\text{NO}_2$) of hydroamination product of 4-bromobenzyl(2,2-diphenyl-4-pentenyl)amine..... | 185 |

CHAPTER 6

| | |
|---|-----|
| Figure 6.1.1. Structure for proposed “capping arene” ligands..... | 192 |
| Figure 6.2.1. Structures of proposed NHC ligands..... | 194 |
| Figure 6.3.1. Structures of TEMPO and additional radicals with N-O linkages..... | 195 |
| Figure 6.3.2. Structures of radical precursors with N-O linkages..... | 195 |
| Figure 6.3.3. Structures of potential ligands to support $\text{Cu}(\text{OAc})_2$ | 195 |

LIST OF TABLES

CHAPTER 1

| | |
|---|----|
| Table 1.1. Selected result from RE from Pd(II) thiolate complexes..... | 24 |
| Table 1.2. Selected result from RE from Pd(II) phosphine dimer..... | 24 |

CHAPTER 2

| | |
|--|----|
| Table 2.2.1. Solvent screening for RE of MeX from complex 1 | 74 |
| Table 2.2.2. Temperature optimization for RE of MeX from complex 1 in MeCN..... | 78 |
| Table 2.2.3. Influence of acid additive on the RE of MeX from complex 1 in MeCN..... | 79 |
| Table 2.2.4. Silver oxidant effect on RE of MeX from complex 1 in MeCN..... | 81 |

CHAPTER 3

| | |
|---|-----|
| Table 3.1.1. Comparison of arene alkylation using AlCl ₃ as the primary catalyst versus [Rh(μ -OAc)(η^2 -C ₂ H ₄) ₂]..... | 96 |
| Table 3.2.1. Results for oxidative hydrophenylation of ethylene using (5-FP)Rh(TFA)(η^2 -C ₂ H ₄) (1) as catalyst precursor..... | 101 |
| Table 3.2.2. Catalytic oxidative hydrophenylation of propylene using 1 | 105 |
| Table 3.2.3. Study of product inhibition of Rh catalyzed oxidative hydrophenylation of ethylene or propylene using styrene and allylbenzene..... | 114 |

CHAPTER 4

| | |
|---|-----|
| Table 4.1.1. Cu(OAc) ₂ -mediated C–H functionalization with pyridine as the directing group..... | 133 |
| Table 4.2.1. Cu(OAc) ₂ mediated benzene acetoxylation..... | 139 |
| Table 4.2.2. Cu(II) oxidant screening for benzene C–H functionalization..... | 140 |
| Table 4.2.3. Ligand additives screening for Cu(OAc) ₂ mediated benzene acetoxylation..... | 142 |
| Table 4.2.4. Optimization of the L6 loading on Cu(OAc) ₂ mediated benzene acetoxylation..... | 142 |
| Table 4.2.5. Comparison of ligand effect of various ligands L6 and L9 | 144 |
| Table 4.2.6. Cu(OAc) ₂ catalyzed acetoxylation of cyclohexane..... | 149 |
| Table 4.2.7. Cu(OAc) ₂ catalyzed acetoxylation of toluene..... | 151 |

CHAPTER 5

| | |
|---|-----|
| Table 5.2.1. Al(OTf) ₃ -catalysed hydroamination of alkenylamines..... | 165 |
| Table 5.2.2. Effect of electron-withdrawing and electron-donating groups in the <i>para</i> position of the phenyl ring for hydroamination of alkenylamines using Al(OTf) ₃ | 166 |

| | |
|---|-----|
| Table 5.2.3. Screening Lewis acids as catalyst precursors for intramolecular olefin hydroamination using 2,2-diphenyl-4-pentenylamine (1c)..... | 167 |
| Table 5.2.4. Screening Brønsted acid as catalyst precursors for intramolecular olefin hydroamination using 2,2-diphenyl-4-pentenylamine (1c)..... | 169 |
| Table 5.2.5. Base additive effects on Al(OTf) ₃ and HOTf catalyzed intramolecular olefin hydroamination using 2,2-diphenyl-4-pentenylamine (1c)..... | 171 |
| Table 5.2.6. Influence of water on Al(OTf) ₃ catalyzed hydroamination..... | 175 |
| Table 5.2.7. Solvent effect on the hydroamination of benzyl(2,2-diphenyl-4-pentenyl)amine (1a)..... | 176 |

1. Introduction

1.1 General Concept of Catalysis:

Catalytic technologies make human society much better in the twentieth century. The world without catalysis will be dirtier, hungrier and weaker against diseases. A lot of benefits have been brought by catalysis to everyday life.^[1] There are a lot of important industrial processes that haven been developed based on catalytic technologies. The Haber-Bosch Process is one of the most well-known technologies that can convert atmospheric nitrogen and hydrogen to valuable ammonia. The production of ammonia today exceeds 100 million tones and is largely used as fertilizers that can help raise the yields of crops. The development of the Haber-Bosch Process is also a history describing how human improve the efficiency of the catalyst based on its mechanism. Scientists put over 80 years of effort to study this complex system. For example, the iron catalyst requires several different phases to be present, each of which has a role in the dissociation of the reactants and in the stepwise recombination of the N and H atoms.^[2] Nowadays, the efficiency of the Haber-Bosch Process is even better than the biological system for nitrogen fixation. Catalytic technologies are highly involved in the production of everyday items. From plastic bags to pharmaceuticals, from automobile gasoline to DNA analytical techniques, catalytic technologies are everywhere.^[1]

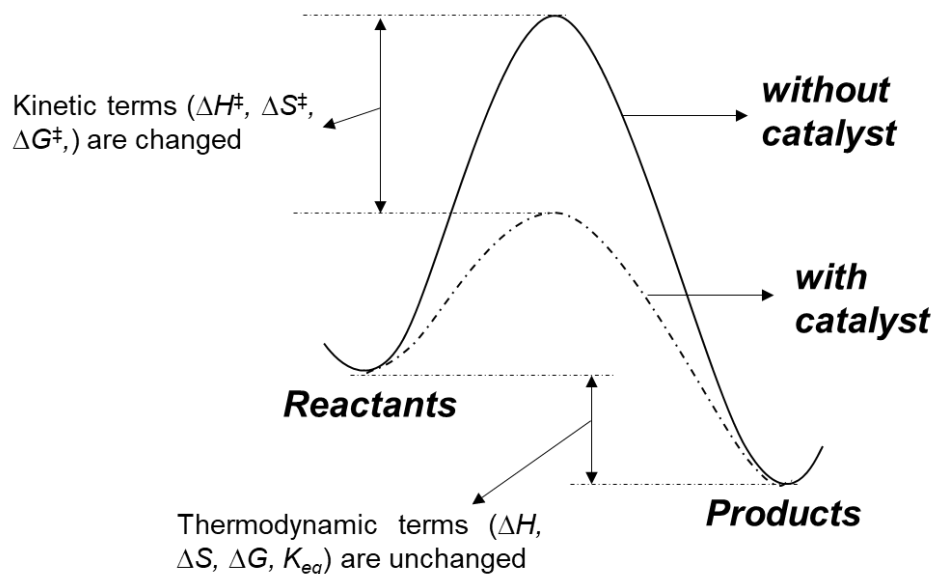


Figure 1.1. Simple energy diagram of catalyzed and uncatalyzed reaction pathways.

Catalysis is the process that can increase the chemical reaction rate by adding a substance which is known as catalyst. The term “catalyst” was first introduced in 1836 by Berzelius and defined by Ostwald in 1894. The catalyst is a substance that can accelerate the reaction by bringing down the activation barrier without itself being consumed.^[3] The simple energy diagram of catalyzed and uncatalyzed reaction is shown in Figure 1.1. A catalyst cannot change the thermodynamic terms such as changes in enthalpy (H), entropy (S), Gibbs free energy (G) and equilibrium constant (K_{eq}), which are only dependent on the difference between products and reactants. However, catalysts can greatly reduce the energy that is needed to overcome the activation barrier, which makes the reaction faster. During a catalytic reaction, the catalyst undergoes a series of transformation to generate the product and regenerate itself. We usually draw the whole series of transformation into a cycle, which is called catalytic cycle.^[3] When the catalyst goes through the catalytic cycle once, we call this process a turnover (TO). The total turnovers that a catalyst can reach before it is deactivated is called turnover number (TON), which is an important term that

represents the longevity of the catalyst. The activity of a catalyst is regularly reported by turnover frequency (TOF), which is defined as the number of turnovers (TOs) per unit time. Different products can be produced with the same reactants through different reaction pathways. If the catalyst can facilitate one of the routes, the reaction will selectively produce the target compounds. The ratio of target products versus side products is called catalyst selectivity. TON, TOF, and selectivity are three significant values to evaluate catalyst performance.

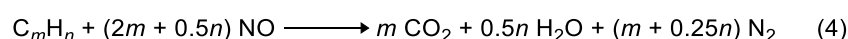
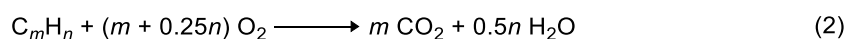
Generally, catalysts can be categorized into two major types: homogeneous and heterogeneous catalysts. Homogeneous catalysts are dissolved in the same phase with reactants. Heterogeneous catalysts, usually solids, operate in a different phase than the reactants, which are often in the gas or liquid phase. Heterogeneous catalysts are responsible for 60% to 75% of the current chemical processes due to their advantages such as high stability and good recyclability. Many important industrial processes, including but not limited to Haber-Bosch Process (ammonia synthesis),^[2] Ostwald process (nitric acid synthesis)^[5] and Ziegler-Natta polymerization (olefin polymerization),^[6] are based on heterogeneous catalysis. However, the mechanism of a heterogeneous catalytic reaction is often difficult to identify. As noted above, scientists spent over 80 years elucidating the mechanism of the Haber-Bosch Process. Compared to heterogeneous catalysis, homogeneous catalysts have some attractive properties, such as the possibility of tuning to achieve higher selectivity, more accessible catalytic metal center and often more detailed mechanistic studies are possible.^[7] With a deeper understanding of mechanisms, the catalytic processes often can be further optimized with improved catalyst designs. As

described below, by utilizing late transition metal homogeneous catalysts, many industrial processes have achieved great success.

1.2 Examples for Heterogeneous and Homogeneous Catalysts

1.2.1 Three-way Catalysts

The wide usage of automobiles offers a lot of convenience for our everyday life. However, the significant amount of exhaust gases from the increased number of cars and trucks have become one of the major sources of air pollution. The major components of vehicle emissions are carbon monoxide (CO), unburned and partially oxidized hydrocarbons (HC) and oxides of nitrogen (NO_x).^[8] In order to reduce air pollution, the three-way catalysis was designed to convert those pollutants to less hazardous compounds (carbon dioxide, nitrogen, and water). The detailed reactions are shown below:



Scheme 1.2.1. Reactions in the three-way catalysis.

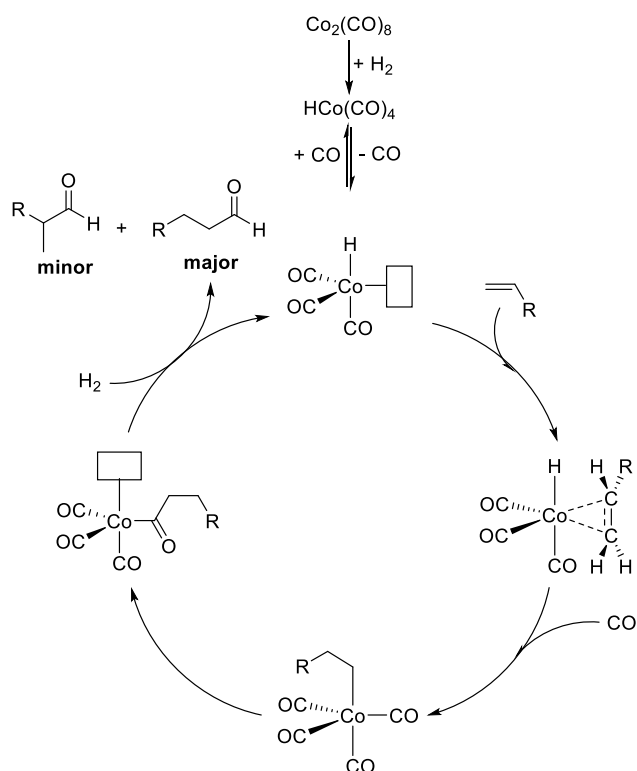
In the three-way catalysis converter, the active species are precious metals (mainly platinum, palladium, and rhodium) located on a metal oxide support. Platinum (Pt) and palladium (Pd) are generally used for catalyzing reaction (1) and (2) in Scheme 1.2.1. The Pt catalyst is less likely to be poisoned by sulfur and lead, while Pd has higher resistance to high-temperature aging and more reactive at a lean cold start.^[9] Rhodium (Rh) is mainly used in reduction steps {Scheme 1.2.1, reaction (3) and (4)}, which shows superior activity

towards NO reduction and highly selective for N₂ as the product, whereas Pt and Pd tend to form NH₃ and N₂O instead. Today, the three-way catalyst can reach very high conversion of the major pollutants CO, HC and NO_x, and can reduce over 80% of the overall emissions after reaching operating temperature. However, there is still no success to replace precious metals with less expensive metals.

1.2.2 Hydroformylation

The hydroformylation of alkenes, also known as oxo synthesis, is an important industrial process for the production of aldehydes. The reaction adds a formyl group (CHO) and a hydrogen atom to a carbon–carbon double bond.^[10] Back in 1938, the first example of hydroformylation was reported by Otto Roelen, using Co₂(CO)₈ as the catalyst at high temperature (120-170 °C) under a high pressure (200-300 bar) mixture of carbon monoxide and hydrogen.^[11] The proposed reaction mechanism for this reaction by Heck and Breslow is shown in Scheme 1.2.2.^[12,13] The active catalyst HCo(CO)₄ is generated from the reaction of Co₂(CO)₈ dimer with H₂, then one molecule of the ligated CO is dissociated to open an empty coordination site to allow olefin coordination. The ligated olefin inserts into the Co–H bond to generate the RCH₂CH₂Co(CO)₄ intermediate. Then the migratory insertion of CO gives the RCH₂CH₂C(O)Co(CO)₃ which leads to an open spot for H₂ coordination. Finally, after oxidative addition of H₂ followed by reductive elimination of the target aldehyde, the Co catalyst can be regenerated.^[10] A mixture of linear (major) and branched (minor) aldehyde is normally observed as products from the hydroformylation reaction, since the selectivity is determined in olefin insertion step. BASF, ExxonMobil and Shell have developed manufacture processes based on this homogeneous Co catalysts,^[14,15] and

great successes have been achieved by using medium to long chain olefins as the reactant. However, only moderate linear selectivities were observed when using propene as the starting material.^[16] Therefore the Ruhrchemie/Rhone-Poulenc process (RCRPP) was designed to improve the selectivity. By using a rhodium catalyst with water-soluble 3,3',3''-phosphanetriyltris(benzenesulfonic acid) trisodium salt as the ligand, the products were found to be up to 98% linear.^[17]

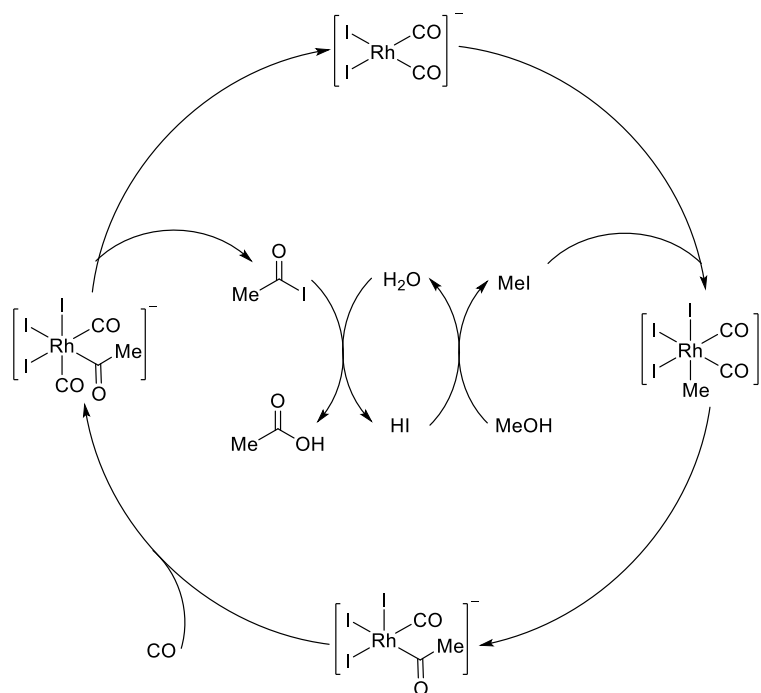


Scheme 1.2.2. Heck-Brewslow mechanism for cobalt-catalyzed hydroformylation.

1.2.3 Acetic Acid Production (BASF, Monsanto and Cativa Process)

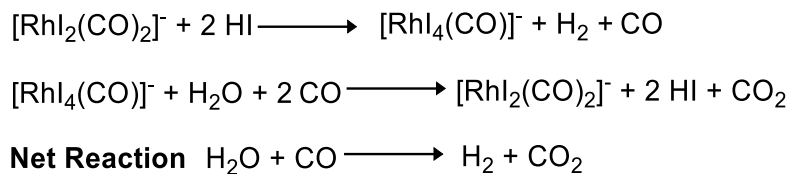
Acetic acid could be found in many plant and animal systems and is well known as an important content in vinegar which was produced by fermentation of wine 5000 years ago.^[18] The first industrial process to produce acetic acid from non-petroleum-based

feedstocks was developed by Reppe at BASF in 1941.^[19,20] Cobalt(II) iodide was used with CO and H₂O/H₂ to *in situ* generate Co₂(CO)₈ and HI, which could catalyze the carbonylation of MeOH to produce acetic acid. By this type of processes, acetic acid could be formed with over 90% yield based on MeOH and 70% yield based on CO. However, the BASF process requires harsh conditions such as extreme pressure (700 bar) and high temperature (250 °C).^[21,22] In the late 1960s, Monsanto developed an iodide-promoted rhodium-based catalyst system, which showed significant improvements over cobalt-based processes. Methanol can be converted to acetic acid even at atmospheric pressure with a yield of 99% based on MeOH and 90% based on CO respectively. In addition, the operating condition of this process (30 bar and 180 °C) is milder compared to the BASF process. Hence, the Monsanto process was commercialized and beat the BASF process the competition.^[23] The mechanism for the Monsanto process is shown in Scheme 1.2.3. The catalyst [Rh(I)₂(CO)₂]⁻ first mediates oxidative addition of methyl iodide (MeI) to form the [Rh(I)₃(CO)₂(Me)]⁻ intermediate. Then CO inserts into the Rh–Me bond followed by coordination of another equivalent of CO to form [Rh(I)₃(CO)₂(C(O)Me)]⁻. After reductively eliminating acetyl iodide, the Rh catalyst is regenerated. Acetyl iodide quickly reacts with water to produce acetic acid and regenerate HI and HI will convert MeOH to MeI to fulfill the reagent used in the initial oxidative addition step.



Scheme 1.2.3. Catalytic cycle for Monsanto process.

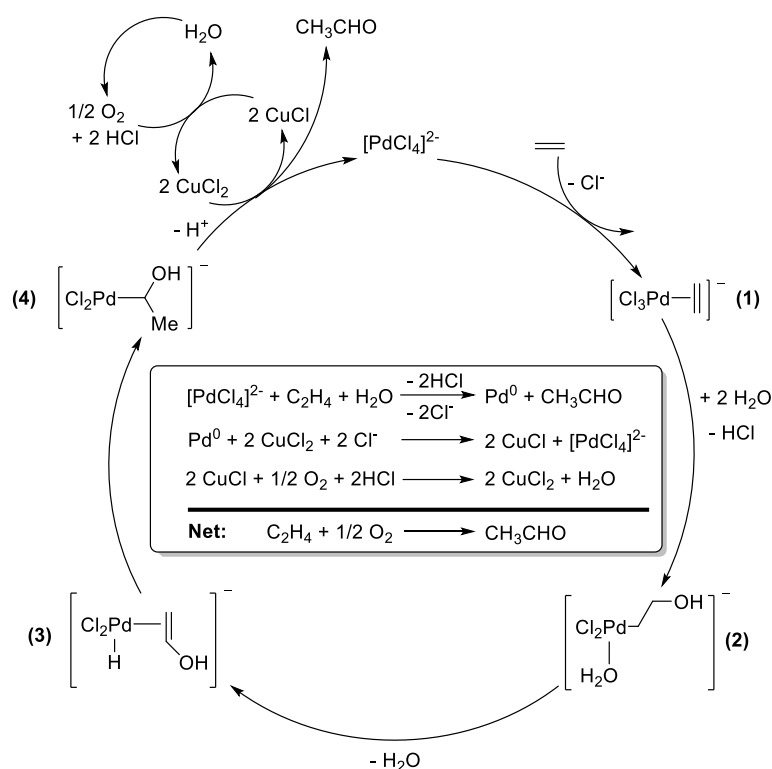
Although the Monsanto process has achieved great success in acetic acid production, a few important drawbacks remained unsolved. The Monsanto process requires high water concentration ($[\text{H}_2\text{O}] > 14\%$) to maintain the maximum rhodium catalyst ($[\text{Rh}(\text{I})_2(\text{CO})_2]$) stability. However, the Rh catalyst itself can also facilitate the water gas shift reaction, which leads to the primary byproducts and major inefficiency of CO in rhodium catalyzed process (Scheme 1.2.4).^[23-26] In order to further improve acetic acid production process, British Petroleum (BP) developed the first commercial low-pressure methanol carbonylation process based on iridium (Ir) catalyst ($\text{H}[\text{IrI}_2(\text{CO})_2]$), which is called the Cativa process.^[27] Initially, the Ir catalysts was found to be less active than Rh catalysts, however, Ir based catalyst can be promoted by ruthenium (Ru) additive, which makes it a superior system to Monsanto process. The switch from Rh to Ir has allowed for less water usage which suppresses the water-gas shift reaction.



Scheme 1.2.4. Water-gas shift reaction equation.

1.2.4 Wacker Process for Acetaldehyde Production

As one of the most important aldehydes, acetaldehyde, occurs naturally in coffee, bread, ripe fruit and can be produced by plants.^[28] The global production of acetaldehyde is about 1 million metric tons per year. Historically, acetaldehyde was made by hydration of acetylene catalyzed by a mercurous/mercuric sulfate system at 95 °C and atmospheric pressure. In the 1960s, the oxidation of ethylene-based ethanol has become the primary route to synthesize acetaldehyde, which requires high temperature (450 °C) and high pressure (3 bar) with air over a silver catalyst. In the 1950s, chemists at Wacker Chemie developed the Wacker process for the production of acetaldehyde, which requires a stoichiometric amount of palladium salt as the oxidant. By adding copper(II) chloride in the reaction mixture, palladium catalyst can be recycled. Importantly, the copper oxidant can be recycled with oxygen, which greatly reduces the cost of the Wacker process.^[29] The detailed mechanism is shown in Scheme 1.2.5.^[30]



Scheme 1.2.5. Mechanism for Wacker process.

The reaction is initiated with ethylene coordination to the Pd center and followed by hydroxide addition to the carbon-carbon double bond to form the intermediate **2**. Then the intermediate undergoes through β -hydride elimination to form **3** and after rearrangement the stable intermediate **4** is found. By the deprotonation of OH group, acetaldehyde is released, and the catalyst is recycled by $CuCl_2$. The recycle of the copper oxidant is the key step in the Wacker process. The regeneration can be accomplished by one step *in situ* or two steps using *ex situ* generation. Both methods have advantages and disadvantages. The *in situ* regeneration requires purified oxygen, which increases the cost. The *ex situ* regeneration can utilize unpurified air, however, it needs the separation of the copper oxidant and additional reactor space.^[31]

1.3 Alkane C–H Activation

1.3.1 General Concept for Alkane Activation

Alkanes are also called “paraffins” which is from the Latin *parum affinis* meaning without affinity. Alkanes may also be called the “the noble gases of organic chemistry” which represents that the activation of alkanes is not an easy job.^[32] Typically alkane C–H bonds exhibit high bond dissociation energies (98-104 kcal/mol) and are non-polar, which makes them highly unreactive. There are generally three different methods for possible alkane activation. The first one does not involve any metals species. By applying high temperature (900-2000 °C) or high energy irradiation to alkanes, it can *in situ* generate highly reactive radicals and carbenes.^[33,34] The second method involves solid metals or their oxides, which play an important role in the chemical industry for oxidation, dehydrogenation, cracking and many other processes.^[35,36] It requires a high temperature (> 200 °C) to sustain efficiency. The last method is metal complexes mediated alkane activations, which is one focus of this thesis. Transition metal complexes have been reported for alkanes oxidation or metal mediated H/D exchange. Examples and mechanisms will be reviewed later in this chapter.

1.3.2 The Conversion of Methane to Methanol

In the 19th century, natural gas was obtained as a by-product of oil production. Unwanted natural gas was a disposal problem in active oil fields. However, natural gas was then found to be a very important energy source. The world has over 180,000 km³ gas reserves in 2013,^[37] and about 900,000 km³ of “unconventional” gas, such as shale gas, has been predicted.^[38] Many studies have predicted natural gas will be the largest energy source

for electricity and heat generation in the future.^[39] As the main component in natural gas, methane, has the highest heat of combustion in hydrocarbons. However, natural gas is only the third energy supply of world energy consumption behind oil and coal during the last 50 years.^[40] The expense of transportation of natural gas (especially methane) plays an important role. Compared to oil and coal, which are in liquid and solid form, respectively, methane's non-polar and light molecular weight properties make it as a gas form with a very low boiling point (-162 °C at 1 atm), hence the transportation efficiency of methane is significantly affected. Compressed natural gas (CNG) can be transported over a short distance, and liquefied natural gas (LNG) is preferred for long distance transportation. However, the capital price of LNG is very high, for example, a conventional LNG tank costs over 200 million dollars.^[40-41] A well-known example is the abandoned Alaska Pipeline Project, which was a planned pipeline (by TransCanada Corp. and ExxonMobil) from the Alaska North Slope to Alberta or Valdez to serve the natural gas from the Prudhoe Bay Oil field for North American markets. The predicted cost is over 45 billion dollars.^[41]

A possible solution is to methane's transportation challenge the partial oxidation of methane to methanol. Since methanol is liquid, transportation is more facile. Methanol is also a raw material for many valuable chemicals as well as a possible gasoline replacement and precursor to diesel fuel. Through the Formox process,^[41] methanol can be converted to formaldehyde which is the raw material for phenolic resin. Through the Monsanto or Cativa process, methanol can be converted to more valuable acetic acid.

The selective oxidation of methane to methanol is challenging due to the fact that the BDE of methanol C-H bond is about ~96 kcal/mol which is significantly lower than that

of methane (~105 kcal/mol). If the oxidation goes through the free radical pathway, the homolytic C–H bond cleavage can be 4 times more rapid in methanol, which often leads to over-oxidation. Another difficulty of methane partial oxidation is the low solubility of methane (1 mM at 1 atm, 25 °C) in suitable reaction solvents such as water. As shown in Figure 1.2, step 1 is the oxidation of methane to methanol (rate constant k_1) and step 2 is the oxidation of methanol to CO₂ and water (rate constant k_2). In order to achieve high conversion of methane to methanol, we need to accelerate step 1 and kinetically suppress step 2. However, the low solubility of methane will greatly limit the reaction rate in methanol production. Assuming a reactor with 1:1 gas to liquid ratio and 500 psig methane pressure, the kinetic model shows that the k_1 to k_2 ratio must be at least 20:1 to selectively produce methanol with over 15% methane conversion.^[43] In this case, catalyst design is essential.

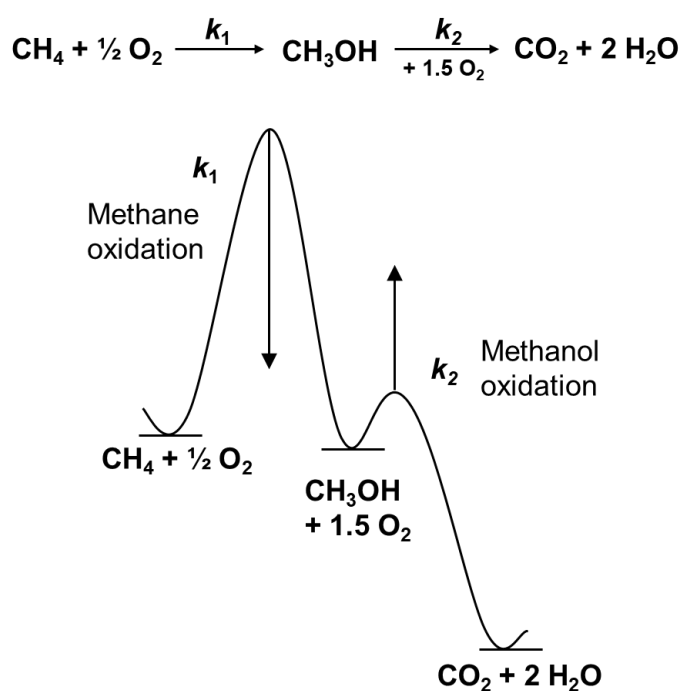
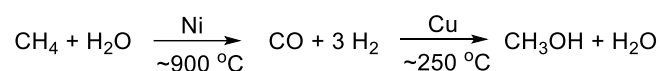


Figure 1.2. Simple energy diagram of methane oxidation.

1.3.3 Methane to Methanol via Syngas

Currently, the most common way to convert methane to methanol is via synthesis gas (syngas, H₂ + CO). Syngas was originally commercial process obtained from the reaction of coal with steam but more recently process to convert natural gas with steam to syngas have been commercialized. However, the process requires a high temperature (ca. 900 °C) and pressure. In addition, the capital expense for syngas is very high which limits its application.^[44]



Scheme 1.3.1. Current industrial production of synthesis gas and methanol.

1.3.4 Methane Functionalization via Heterogeneous Catalysis

Several categories of heterogeneous catalysts have been reported for methane functionalization, which includes coupling oxidation of methane using basic oxide,^[45,46] partial oxidation by transition metal oxides,^[47] and iron complexes supported on zeolites.^[48] In order to break the strong C–H bond in methane, high temperature (> 250 °C) is often necessary for the catalysis to achieve high conversion. However, as mentioned formerly in this chapter, over-oxidation is the major problem for methane partial oxidation. Under high-temperature conditions, the reaction selectivity is usually low. To the best of our knowledge, the catalysis process with high selectivity (> 90%) at high conversion (> 70%) has not been reported yet. For example, Hutchings and co-workers has reported a low temperature methane conversion catalysis using Fe-silicalite-1, which can achieve 96% selectivity to partial oxidation products (CH₃OH, HCOOH, MeOOH with 8% selectivity for MeOH) at 70 °C with 10.5% conversion. With Cu additives, the reaction can selectively produce

MeOH as the only partial oxidation product (with 7% CO₂ as over oxidation product) with 10.1% conversion. However, the reaction requires hydrogen peroxide as the oxidant and the best conversion is about 10%. In addition, the catalyst needs a pre-treatment at 550 °C to maintain its reactivity.^[49] Ronny Neuman and co-workers reported a bipyrimidinylplatinum-polyoxometalate catalyst that can access aerobic oxidation of methane at 50 °C. However, it also suffers from poor selectivity and low conversion. Under the optimal condition, a similar amount of CH₃CHO was produced along with MeOH with ~1% overall conversion.

1.3.5 Hydrocarbon Functionalization via Organometallic Catalysis

Homogeneous catalysts have been suggested as a possible solution for methane partial oxidation. One of the benefits of late transition metal complexes is that the formation of M–C bonds can compensate for breaking the strong C–H bond. In this case, the reaction conditions are usually much milder than heterogeneous catalysis, which often generate free methyl radicals and do not form M–C bond. Another advantage is that normally there is no free radical involved in metal complex catalyzed C–H activation, which leads to a better product selectivity. Several recognized C–H activation mechanisms are summarized in Figure 1.3.

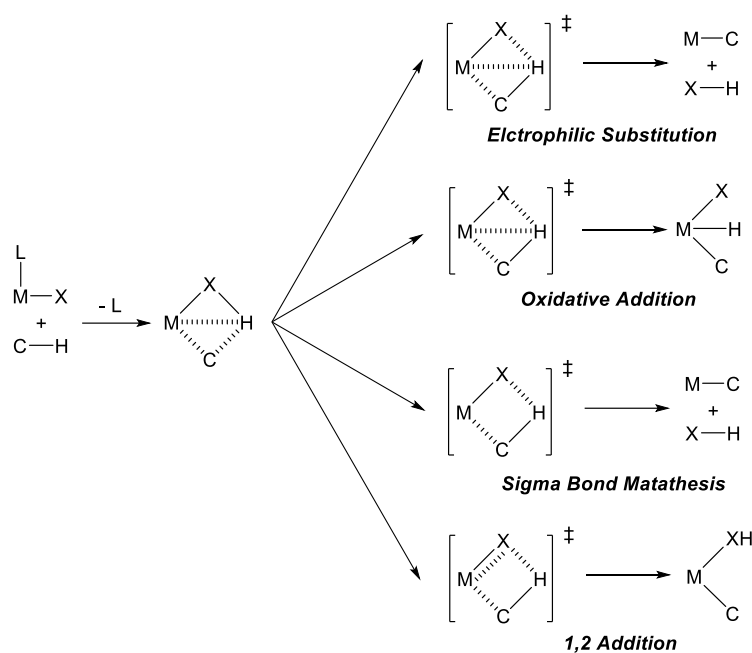
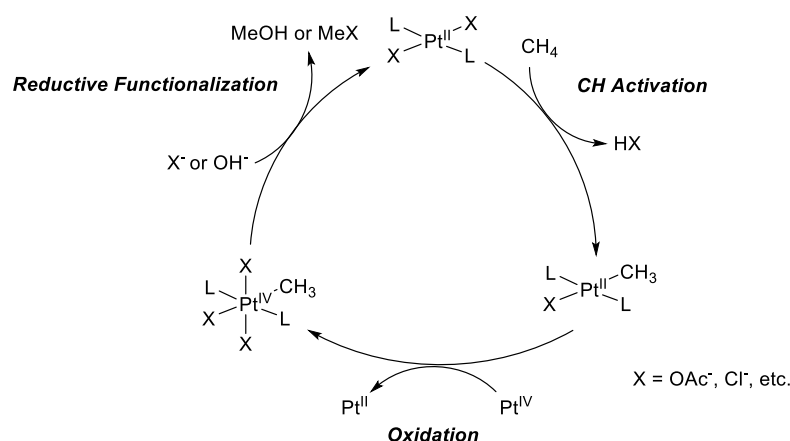


Figure 1.3. Different mechanisms for metal complex mediated C–H activation.^[43]

There are generally two steps required for hydrocarbon functionalization, C–H bond activation and C–X (X = O, N, halide, etc.) bond formation, and both of them are challenging. C–H bond activation generally involves at least two different steps: 1) coordination of alkanes to metal center and 2) C–H bond cleavage. The coordination step can be viewed as an inner sphere ligand displacement or interchange and is often energetically uphill.^[51] Compared to other possible ligands in the reaction mixture, such as OAc^- , halide or solvent molecule, alkanes are not good ligands due to the poor binding characteristics. In some cases, calculation shows that the ΔH^\ddagger for methane coordination is about 4 times higher than the ΔH^\ddagger for C–H bond cleavage. In addition, the ligation of the hydroxy group in partial oxidation products can compete the coordination of alkanes to metal center, which could further hinder the C–H bond activation process. The C–X bond formation step is not easy either. Reductive elimination is the most common strategy to form a C–X bond, and a high oxidation state metal center is often required.

1.3.6 Examples for Methane Functionalization via Organometallic Routes

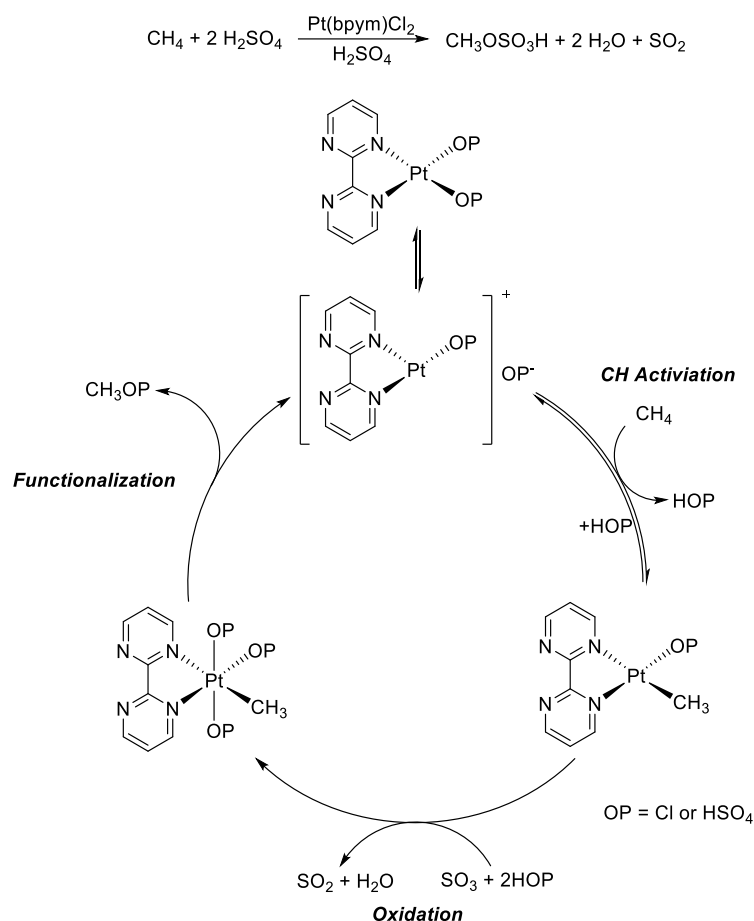
In the 1960s, Shilov and co-workers reported methane partial oxidation to methanol catalyzed by $[\text{PtCl}_4]^{2-}$.^[52] The proposed mechanism for Shilov system is shown in Scheme 1.3.2. The reaction is initiated with C–H activation by a Pt^{II} complex to generate a $\text{Pt}^{\text{II}}\text{–Me}$ species. The $\text{Pt}^{\text{II}}\text{–Me}$ intermediate is oxidized by Pt^{IV} oxidant to generate a $\text{Pt}^{\text{IV}}\text{–Me}$ complex, followed by reductive elimination to produce MeX or MeOH via nucleophilic attack of OH^- or X^- ($\text{X} = \text{Cl}^-$, OAc^- , etc.). However, reported reaction rates and conversions are very low with the Shilov process. In addition, a stoichiometric amount of Pt oxidant is required in the original report. Also, the Pt catalyst is not stable due to irreversible decomposition to $\text{Pt}(0)$ or insoluble, polymeric Pt salts such $(\text{PtCl}_2)_n$.



Scheme 1.3.2. Proposed catalytic cycle for Shilov system.

In order to overcome challenges with the Shilov system, Periana and co-workers developed catalysis using $\text{Pt}(\text{bpym})\text{Cl}_2/\text{H}_2\text{SO}_4$ {bpym = κ^2 -(2,2'-bipyrimidyl)} which is stable and active for converting methane to methyl bisulfate in concentrated sulfuric acid.^[53] The affinity of the bpym ligand for $\text{Pt}(\text{II})$ is sufficient to keep the Pt complex stable in the hot H_2SO_4 solution. In addition, bpym can convert insoluble $(\text{PtCl}_2)_n$ or Pt black to soluble $\text{Pt}(\text{II})$ species, which solves primary problem of the original Shilov system. Under

optimized conditions (3400 kPa CH₄, 80 mL 102% H₂SO₄ at 220 °C), the Pt(bpym)Cl₂/H₂SO₄ system achieves 71% one-pass yield with 81% selectivity for MeOSO₃H based on methane. The TON is over 500 with a TOF of $\sim 10^{-2}$ s⁻¹.



Scheme 1.3.3. Proposed catalytic cycle for Pt(bpym)Cl₂/H₂SO₄ system.

The reaction mechanism is similar to Shilov system except for SO₃ is the oxidant, and conversion of SO₂ to SO₃ can be easily accomplished with air. Another important feature is that the production of the methyl bisulfate has been estimated to be 100 times slower than methane toward C–H activation by the Pt^{II} catalyst.^[54] In this case, the strong electron withdrawing group HSO₄⁻ likely protects the product from over oxidation. An issue is that the concentration of product is limited to 1 M, which is too low for cost-effective product separation. With the reaction proceeds, the concentration of H₂SO₄ drops. The methanol or

H₂O will present in the solution. The energy of Pt–H₂OH or Pt–MeOH is about 5 kcal/mol lower than Pt–HSO₄ which leads to the inhibition of the catalyst. This phenomenon is called ground state inhibition. The catalyst will completely lose activity due to methanol or water coordination.

With the success of Pt/H₂SO₄ system, a series of late transitional metals including Hg,^[55] Au,^[56] and Pd^[57] complexes have been reported to be active for methane partial oxidation. Hg complexes share a similar condition with the Pt system, however, it could use unpurified natural gas as the reactant.^[55] The “soft” metal center Au(I) and Au(III) are proposed to be active for methane oxidation and by using H₂SeO₄ as solvent as well as the oxidant, it can reach over 30 TON with 90% selectivity.^[56] Different from other systems, the Pd complex will selectively produce acetic acid rather than methanol.^[57] Recently, Schüth and co-workers detailed a series of Pt(II) complexes for methane functionalization. By using 20% oleum as oxidant and solvent, simple Pt(II) salts K₂PtCl₄ proved to be very active at low concentration. TOF, over 24,000 h⁻¹ could be reached with the optimized conditions, which indicated possible applications in industrial production.^[58]

The primary issues with Periana Pt system are production inhibition and product separation in super-acidic solvents such as oleum. In order to solve this problem, trifluoroacetic acid (HTFA) has been considered as a possible replacement for oleum. Trifluoroacetate has a very strong electron withdrawing ability, which can provide the similar benefit as sulfate to prevent methyl trifluoroacetate (MeTFA), the product of methane functionalization, from further oxidation. In addition, the boiling point of MeTFA (43 °C) is significantly lower than that of HTFA (b.p. 72 °C), which means that the product

can be likely removed easily from the reaction mixture by distillation.

Sen and co-workers reported Pd(II) salts catalyze methane oxidation to MeTFA using Pd(II) salts with hydrogen peroxide as the oxidant.^[59,60] Strassner and co-workers reported BisNHC (NHC = N-Heterocyclic Carbene) ligand supported Pd(II) complexes, which can catalyze methane functionalization with $K_2S_2O_8$.^[61,62] Co(II) salts such as $Co(OAc)_2$, $CoCl_2$, $Co(NO_3)_2$ have also been shown to be active catalysts for methane oxidation with oxygen to yield MeTFA in HTFA and trifluoroacetic anhydride (TFAA) mixture.^[63] TFAA is essential to protect the Co catalysts from deactivation. Under the optimal condition, $Co(NO_3)_2$ turns out to be the best catalyst, which can achieve 50% MeTFA yield based on methane. However, up to 50% of TFAA was consumed, and the formation of insoluble cobalt fluorides results in the catalyst deactivation. Recently, Periana and co-workers reported main-group compounds, $Tl(TFA)_3$ and $Pb(TFA)_4$, can selectively stoichiometrically oxidize the mixture of methane, ethane and propane to alcohol esters.^[64] Pb^{IV} and Tl^{III} are much better electrophiles especially with ethane in HTFA, which leads to the high reactivity of those main group metal compounds towards alkane oxidation. Although a stoichiometric amount of metal compounds are needed as the oxidant, the oxidative conversion of $Tl(I)$ to $Tl(III)$ is potentially accessible with O_2 .^[65]

Our group reported a hypervalent iodine/chloride alkane oxidation (HIAO) process that uses iodate salts with a sub-stoichiometric chlorine source in HTFA media to selectively functionalize light alkanes.^[66,67] In the initial study, at optimal conditions, a 24% yield of MeTFA based on methane with over 90% mono-functionalization product was achieved (Scheme 1.3.4). The process can use a wide range of alkane pressure (240-6900

kPa) at temperatures < 235 °C. The reaction is inefficient in the absence of chloride. The HIAO process is proposed to occur through H-atom abstraction by free radical species including Cl• and IO₂• to generate alkyl radicals to initiate the reaction. Iodine, which forms by *in situ* reduction of iodate, traps alkyl radicals as alkyl iodides that are subsequently converted to alkyl esters in HTFA solvent.^[68]

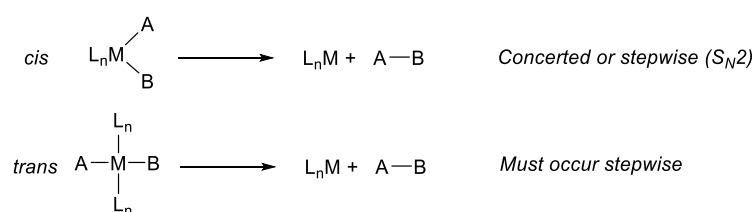


Scheme 1.3.4. Iodate/chloride oxidation of alkanes which is proposed to be catalytic in chloride.

1.3.7 Reductive Elimination of MeX

Reductive elimination (RE) of MeX (X= halide, OAc⁻, TFA⁻, HSO₄⁻, OH⁻, etc.) from metal intermediates is the key step of Shilov-type and other hydrocarbon functionalization reactions. The rate of RE can be influenced by many factors including: 1) steric effect of the metal complex, more sterically hindered complexes can react faster than less sterically hindered complexes; 2) electronic effect of the metal center. Since the RE will formally reduce the metal center, it has often been suggested that metals with less electron density (e.g. high oxidation state) undergo more facile the RE reactions. However, effects that influence reductive elimination and oxidative addition reactions can be more subtle. Generally, the rate of RE is first row > second row > third row, which is likely because of trends in M–C BDE. 3) The effect of coordination number. This effect results from changes in frontier orbitals. Three- or five-coordinate metal complexes tend to undergo RE faster than those of four- and six-coordinate metal complexes. The RE from four- and six-coordinate complexes will occupy an orbital in the intermediate that is strongly metal-ligand antibonding. However, the RE from three- and five-coordinate complexes lead to

the occupation of a nonbonding orbital.^[69] 4) The effect of geometry. Complex with less structural reorganization will have a faster RE rate. For example, the *cis* orientation is required for RE with a concerted mechanism. The complexes with two ligands located *trans* to each other will undergo stepwise mechanism or isomerization to its *cis* isomer prior to RE, which may lead to slower reaction rate (Scheme 1.3.5).



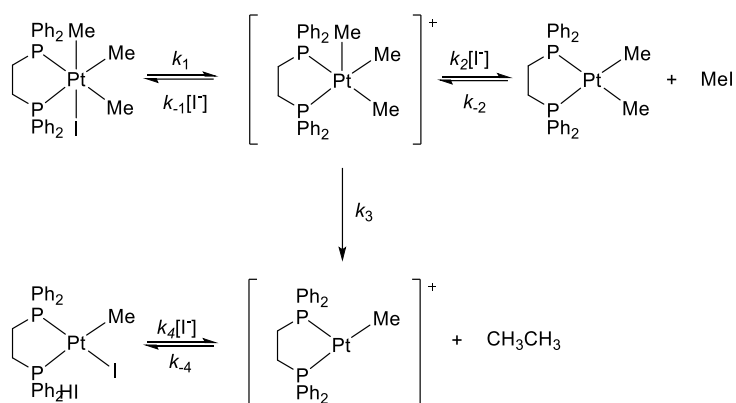
Scheme 1.3.5. The effect of geometry on RE reaction.

The RE of MeX with Pt, Pd, Rh, Au and Ni complexes will be reviewed later in this chapter.

Reductive Elimination of MeX from Pt(IV) complexes

In 1994, Goldberg and co-workers reported that the bidentate phosphine complex (dppe)Pt(Me)₃I (dppe = 1,2-Bis(diphenylphosphino)ethane) undergoes competitive RE of MeI and ethane respectively.^[70,71] The RE of MeI went through a common two-step S_N2 pathway, in which the iodide anion dissociates from Pt complex to form a cationic Pt(IV) intermediate, and subsequent nucleophilic attack of iodide on the methyl ligand yields MeI. The five coordinate Pt intermediate can also undergo RE of ethane, which is kinetic competition reaction against RE of MeI. When tracing the reaction, MeI and (dppe)Pt(Me)₂ will eventually all convert to (dppe)Pt(Me)I and ethane. This result indicated that the RE of MeI is reversible and the production of ethane is thermodynamically favored pathway. The S_N2 mechanism was further confirmed by adding an excess amount of NaI added to

the solution. The initial rate of RE of MeI was not affected, however, the production of ethane was greatly inhibited. The increased amount of iodide will inhibit the dissociation of iodide from the Pt complex to form the five coordinate intermediate, which greatly limit the RE of ethane. Increased iodide concentration can accelerate the nucleophilic attack on the methyl, so the initial reaction rate of MeI production was unaffected. The detailed mechanism is shown in Scheme 1.3.6.



Scheme 1.3.6. Mechanism of RE of MeI from $(dppe)Pt(Me)_3I$.

Reductive Elimination to Form C–X Bond with Pd Complexes

The example for RE of methyl halide from Pd complexes has not been reported, however, there are several examples about C–X bond formation can resemble its insight. The RE from Pd(II) is believed to often undergo through a three-centered concerted mechanism. In this case, the heteroatom ligands with covalently bonding property is more favored.^[72] Base on hard-soft-acid-base (HSAB) theory, Pd(II) complexes with softer and more electron donating heteroatom ligands undergo RE faster than those containing harder and less electron donating ligands.^[70,73] Second, reductive eliminations that form carbon-heteroatom bonds from arylpalladium(II) complexes are faster than those that form carbon-heteroatom bonds from alkylpalladium(II) complexes,^[74] The selected results are shown in

Table 1.1.^[74] The RE reaction rate follow the order: vinyl > aryl > alkenyl > Me. This may be the reason why very limited example of RE of MeX has been reported.

Table 1.1. Selected result from RE from Pd(II) thiolate complexes.

| R | Temp./°C | $t_{1/2}$ /min |
|---|----------|----------------|
| -Me | 95 | 580 |
| -CHC(Me) ₂ | 50 | 17 |
| -Ph | 50 | 48 |
| -C≡C(CH ₂) ₃ CH ₃ | 95 | 87 |

The RE from Pd(II) to form C(*sp*²)-X bond has been widely studied. Hartwig and co-workers have reported RE of aryl halide from a series of tris(*o*-tolyl)phosphine [P(*o*-tol)₃] supported Pd dimer.^[74] The results are summarized in Table 1.2. The chloride anion gives the largest driving force for reductive elimination and iodine gives the smallest due to the thermodynamic properties. However, the reaction rates show an opposite trend. The low yield of chloroarene from the reaction of **1d** is consistent with the slow rates for the reaction of the more hindered chloride **1a** and with generally slow rates for the microscopic reverse, oxidative addition of aryl chloride.

Table 1.2. Selected result from RE from Pd(II) phosphine dimer.

R₁ = *t*-Bu, R₂ = Me, R₃ = H R₁ = R₂ = H, R₃ = *t*-Bu
 X = Cl: **1a**, X = Br: **1b**, X = I: **1c** X = Cl: **1d**, X = Br: **1e**

| complex | Yield of ArX (%) | K_{eq} |
|-----------|------------------|-------------------------|
| 1a | 70 | $9(3) \times 10^{-2}$ |
| 1b | 70 | $2.3(3) \times 10^{-3}$ |
| 1c | 39 | $3.7(2) \times 10^{-5}$ |

| | | |
|-----------|----|-------------------------|
| 1d | 30 | not measured |
| 1e | 75 | $3.3(6) \times 10^{-4}$ |

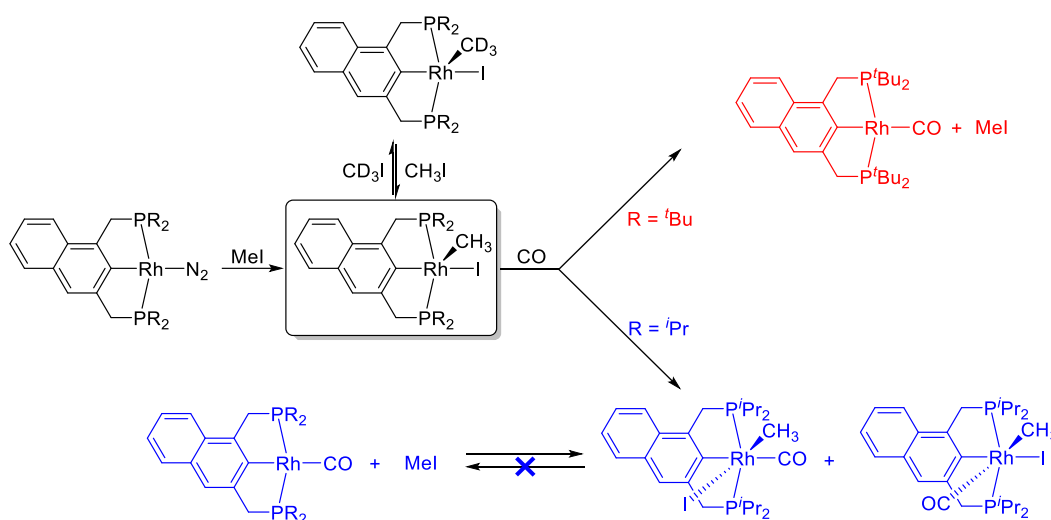
Another interesting example of reductive elimination from dinuclear Pd(III) complexes $\{[\text{Pd}(\text{X})_2(\text{bhq})]_2, \text{bhq} = \text{benzo}[\text{h}]\text{quinoline}, \text{X} = \text{OAc}^- \text{ or } \text{Cl}^-\}$ has been reported by Ritter and co-workers.^[75] The bimetallic Pd(III) complex has a Pd–Pd bond to help stabilizing its structure. Due to the high oxidation state of Pd, the formation of a series of C–O, C–Cl bond via RE can be achieved at a much lower temperature (23 °C for C–Cl bond formation). A bimetallic mechanism has been shown to be likely using experiments and calculations. In addition, C–F bond formation can be achieved through RE from high-valent palladium fluoride complex. Strong fluorination reagent such as XeF₂, Selectfluor and ArIF₂ were essential to accomplish the transformation.^[76-78]

Reductive Elimination of MeX from Rh(III) Complexes

Rh-based catalysis is a possible replacement for Pt-based methane functionalization system. The Rh^I/Rh^{III} redox couple offers a few attractive properties: 1) Rh^I/Rh^{III} redox cycle is easily accessible and allows for potentially air-recyclable oxidants to be used; 2) the Rh metal center is expected to be less electrophilic than late metals might coordinate to water and functionalized product more weakly. 3) The formation of Rh(s) is less thermodynamically favored than Pt(s) and Pd(s).

Milstein and co-workers reported RE of MeI from a series of naphthyl-based PCP-type ligand supported Rh(III) complexes.^[79] Reactions are shown in Scheme 1.3.7. The steric effect is dramatically important in this type of complexes. With the addition of CO, the (tBuPCP)Rh(III) complexes can irreversibly reductively eliminate MeI with high yield. In contrast, less steric hindered (iPrPCP)Rh(III) complexes does not reductively eliminate the

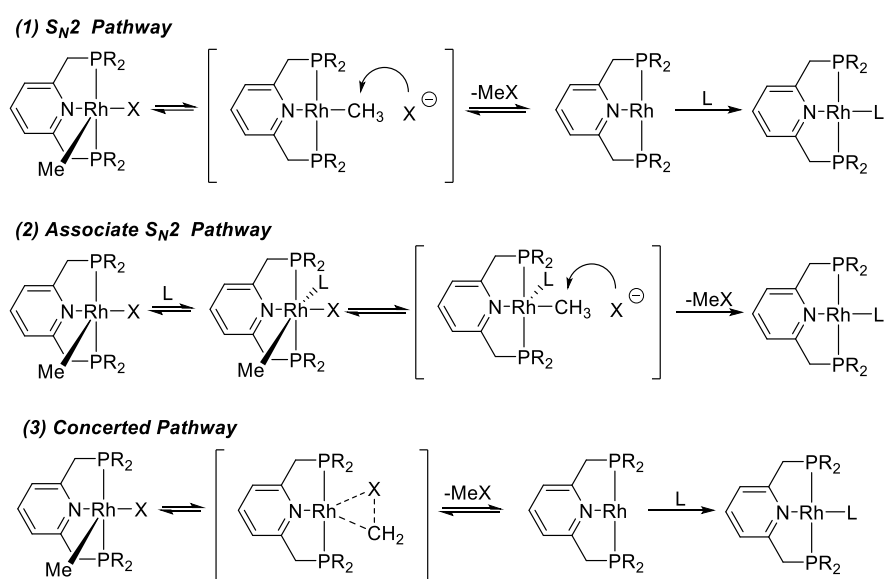
MeI under the same conditions. The reverse reaction, oxidative addition, is favored ($^i\text{PrPCP}$) by Rh(I) complex. In the presence of deuterated methyl iodide (CD_3I), the exchange between CD_3 and CH_3 was observed in ($^t\text{BuPCP}$) the Rh(III) complex, which indicated the RE step is reversible without CO. With the addition of an excess amount of iodide, the CD_3/CH_3 rate is not affected, which indicated the RE of MeI from (PCP)Rh(III) complexes does not have iodide dissociation step.



Scheme 1.3.7. Reductive elimination of MeI from PCP Rh complexes.

Recently, Milstein and co-workers reported a detailed study of a series of ^RPNP-type ligand supported Rh(III) complexes.^[80] Steric effect (^tBu vs ⁱPr), halide ligand effect (Cl⁻, Br⁻, I⁻), ancillary ligand effect (CO, isonitriles, acetonitrile) and solvent (protic polar vs aprotic polar) were investigated. In all different cases, the RE rate is following the trend: I⁻ > Br⁻ > Cl⁻. The ($^t\text{BuPNP}$)Rh(III) complexes gave better RE result than ($^i\text{PrPNP}$)Rh(III), which again indicated the importance of steric effect. When investigating the solvent effect, the author found ($^t\text{BuPNP}$)Rh(III) chloride complex preferred protic polar solvent, which is different from that of iodide and bromide. There are three possible mechanisms proposed in Scheme 1.3.8. While polar protic solvents may increase the halide dissociation step in

pathways (1) and (2) by hydrogen-bonding interaction, such an interaction should also be expected to decrease the nucleophilicity of the dissociated halide. In this case, (PNP)Rh(III) bromide or iodide complexes are more likely to undergo the S_N2 mechanism, while RE of MeCl from (PNP)Rh(III) chloride complex was predicted to go through a concerted mechanism. The ancillary ligand effect is also investigated. The CO ligand promotes the RE of MeX, and the reaction is irreversible. Acetonitrile can also promote the RE of MeX, however, the reaction is reversible. The effect is different from isonitrile, excess amount of ligand will lead to the formation of stable six coordinate Rh(III) complexes, which limits the RE of MeX.



Scheme 1.3.8. Three possible pathways for RE of PNP ligated Rh complexes.

Reductive Elimination to Form C-X Bond with Other Transition Metal Complexes

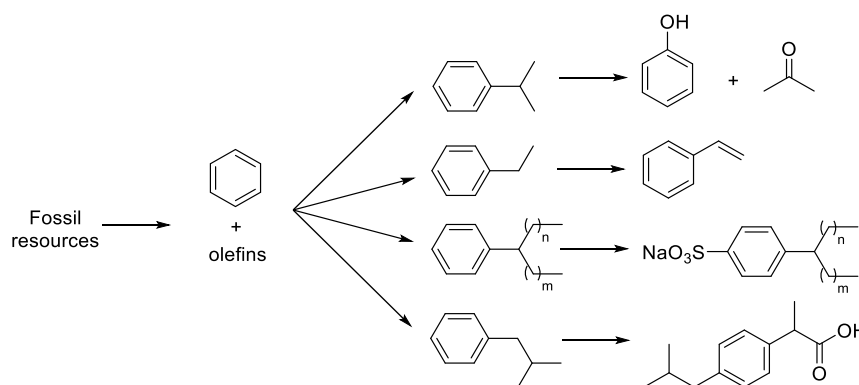
The studies of RE with other metal complex are very limited. Bercaw and co-workers reported RE of MeI from an *N*-heterocyclic carbene (NHC) Au(III) monomethyl complex.^[81] The direct elimination of MeI from three coordinate Au(III) through a concerted pathway was proposed as the most likely mechanism. In addition, Au(III)

complexes with similar NHC ligands were reported for RE of C–F bond with XeF₂ as the fluorination reagent.^[82] Sanford and co-workers reported the first example of Ar–Br bond formation from a nickel aryl halide precursor.^[83] By using CuBr₂ and Br₂ as the oxidant, the nickel complex can be oxidized to high valent Ni^{III} intermediate, which reductively eliminates aryl bromide in high yield.

1.4 Arene Functionalization

1.4.1 Overview of Alkyl Arenes

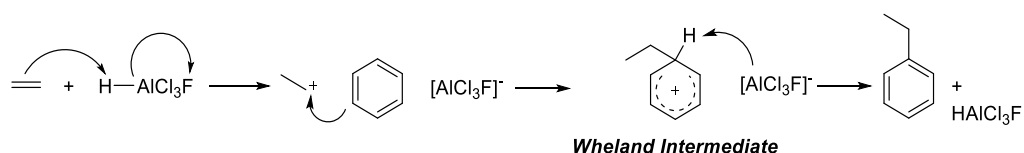
Billions of pounds of alkyl and alkenyl arenes are produced each year, and they serve as precursors for plastics, elastomers, detergents and pharmaceuticals.^[84-88] For example, the global production of ethylbenzene is over 20 million tons annually with approximately 98% of ethylbenzene converted to styrene.^[89-91] Some products from alkyl arenes are summarized in Scheme 1.4.1.



Scheme 1.4.1. The synthesis and usage of alkyl arenes.

Ethylbenzene is one of the simplest and the most important alkyl arenes. After dehydrogenation, ethylbenzene is converted to styrene, which is the starting material for a series of plastics including crystalline polystyrene, rubber-modified impact polystyrene, expandable polystyrene, acrylonitrile–butadiene–styrene copolymer (ABS), styrene–

acrylonitrile resins (SAN), styrene–butadiene latex, styrene–butadiene rubber (qv) (SBR), and unsaturated polyester resins.^[85] Currently, ethylbenzene is produced by Friedel-Crafts or zeolite and catalytic benzene alkylation with ethylene. Use acid based catalysts, such as AlCl_3 and HF or acidic zeolite), high reaction rate can be achieved. The standard mechanism for acid catalysts is shown in Scheme 1.4.2 using HF and AlCl_3 . HF and AlCl_3 will form a superacid intermediate and react with ethylene to form a carbocation. The carbocation then undergoes electrophilic addition to benzene to form a “*Wheland intermediate*”. Deprotonate of the intermediate to give ethylbenzene and regenerate the acid catalyst is the final step.



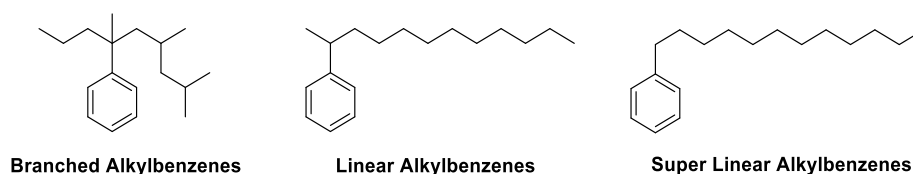
Scheme 1.4.2. Mechanism for acid catalyzed Friedel-Crafts alkylation.

Although the Friedel-Crafts alkylation has been commercialized, there are drawbacks. Ethyl is an electron donating functional group, which makes the benzene ring more electron rich. The increased electron density makes the ethylbenzene more reactive than benzene towards electrophilic attack.^[84] Thus, undesired polyalkylated products cannot be avoided at high conversion. In order to convert polyalkylated products to mono-functionalized product, distillation followed by an energy consuming process called transalkylation are needed.^[92-94] Another disadvantage of Friedel-Crafts alkylation is the limitation of arene substrates. If there is an electron withdrawing functional group on the benzene ring, the reaction rate will be highly reduced. For example, chlorobenzene is about 10 times less reactive compared to benzene. In addition, acid catalysts (AlCl_3 and HF) often cannot be

recycled due to their neutralization during the product extraction process. In order to solve this problem, solid catalysts, zeolites, have been implanted since the 1980s.^[95] However, there are still some processes, such as Monsanto/Lummus Crest, Union Carbide/Badger and Petroflex, that use AlCl_3 based catalysts.^[96]

When using longer chain α -olefin as the substrate, a series important alkyl arenes can be obtained. Cumene, which accounts for about 20% of world benzene consumption,^[97] can be produced through zeolite catalyzed alkylation of benzene with propylene. The majority of cumene is converted to cumene hydroperoxide, which is the important intermediate in the industrial synthesis of phenol and acetone.^[98] Longer chain alkylbenzenes are converted to alkylbenzene sulfonates, which are the active components in detergents, through alkylbenzene sulfonation. Isobutyl benzene is an important starting material for Ibuprofen which is an analgesic, anti-inflammatory drug. However, it cannot be directly synthesized through alkylation of benzene with isobutene. Since Friedel-Crafts alkylation has a carbocation intermediate, the isobutene will generate the tert-butyl carbocation intermediate, which leads to the production of tert-butylbenzene. In order to obtain the isobutene, a sodium/potassium alloy is needed as the catalyst for the reaction of toluene and propylene.^[99] The reaction of benzene with longer chain α -olefins has the same limitation, which makes the production of 1-aryl alkanes impossible with existing catalysts. In the 1960s, branched alkylbenzene sulfonates (BASs), produced by sulfonation of branched alkylbenzenes (Scheme 1.4.3), were used widely as raw materials for domestic detergents. However, their slow biodegradation led to water pollution.^[100] Linear alkylbenzenes (LABs) were introduced in the mid-1960s as a precursor for making linear

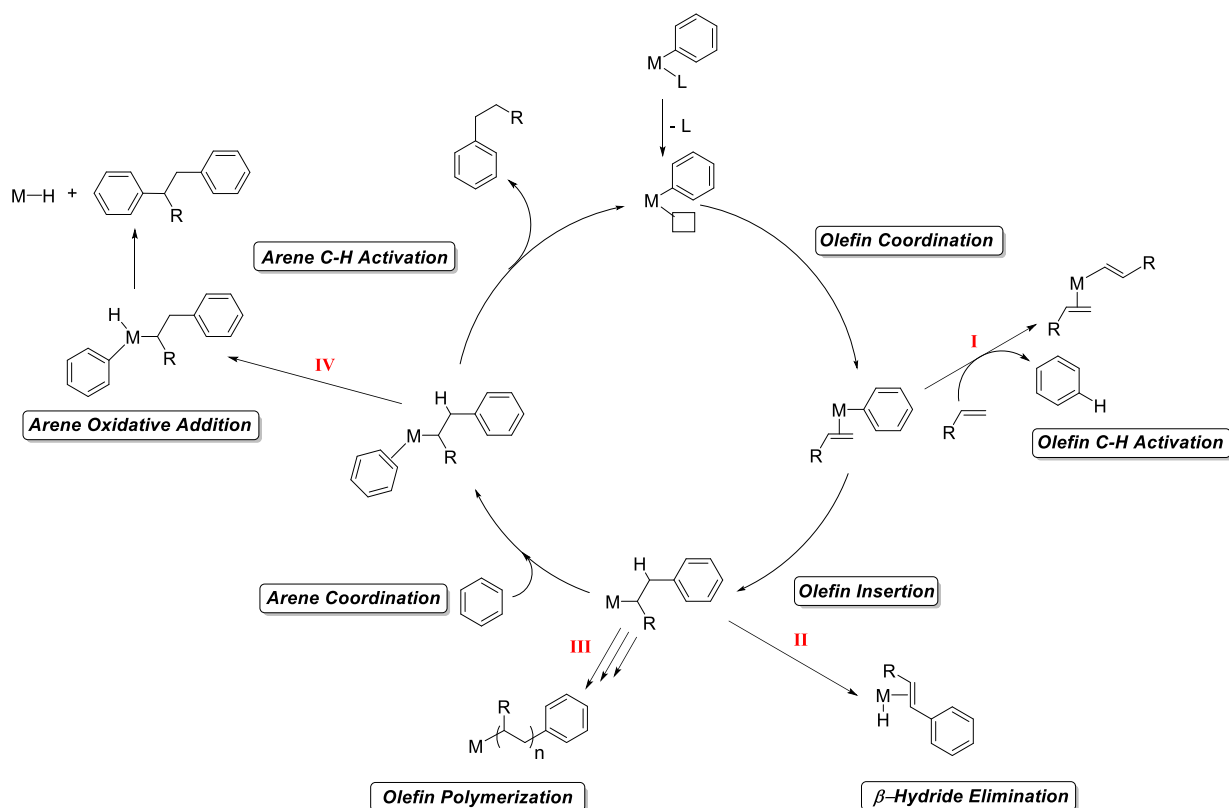
alkylbenzene sulfonates (LASs), which provided more facile biodegradation.^[100,101] The major fractions of LABs are 2- and 3-phenyl alkanes. To differentiate the 1-phenyl alkanes from the predominantly 2-substituted LABs, we have labeled the former super linear alkyl benzenes (SLABs, Scheme 1.4.3), or super linear alkenyl benzenes for their unsaturated variants. Currently, true straight-chain alkyl benzenes can only be produced through Friedel-Crafts acylation followed by a Clemmensen or Wolff-Kishner reduction. The expense of the substrates and the stoichiometric amount of HCl waste limits industrial application.



Scheme 1.4.3. Examples for branched alkyl benzenes (BABs), linear alkyl benzenes (LABs) and super linear alkyl benzenes (SLABs).

1.4.2 Late Transition Metal Catalyzed Hydroarylation of Olefins

Transition metal catalyzed olefin hydroarylation gives an alternative to acid-based catalysis to produce alkyl or alkenyl arenes production. The proposed mechanism for many transition metal catalyzed olefin hydroarylation is shown in Scheme 1.4.4 with benzene and α -olefin. The catalyst dissociates a labile ligand and coordinates an α -olefin to enter the catalytic cycle. The α -olefin then inserts into the M–Ph bond to give a phenalkyl intermediate. Another equivalent of benzene coordinates to the metal center and goes through a C–H activation followed by alkyl benzene dissociation to regenerate the catalyst.^[102-104]

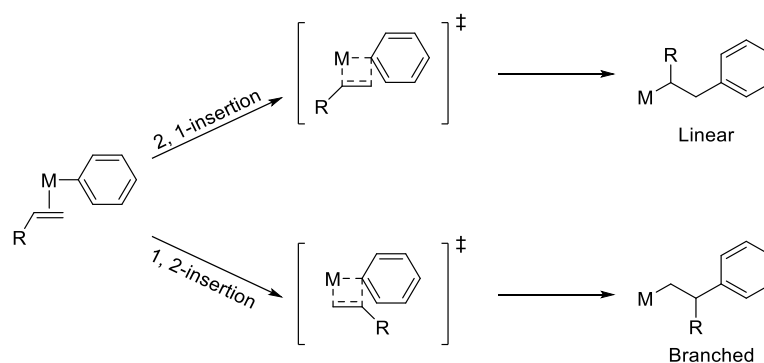


Scheme 1.4.4. Proposed mechanism for transition metal catalyzed hydroarylation with benzene and α -olefin.

Compared to Friedel-Crafts alkylation, several possible advantages of late transition metal catalyzed olefin hydroarylation are listed below (note: assuming the mechanism is or similar to what is shown in Scheme 1.4.4):

- 1) Transition metal catalyzed olefin hydroarylation does not include an electrophilic substitution, which does not require an electron donating group to activate the arene. In this case, a large scope of arenes potentially can be used as substrates, especially those with electron withdrawing groups, such as nitrobenzene, chlorobenzene, etc.
- 2) Since the electron density of the arene might not greatly affect the reaction, the alkylbenzene product will have similar or reduced (due to steric effects) reactivity toward hydroarylation compared to benzene, which can limit polyalkylated arene production.

- 3) When using substituted arene as substrate, the steric effect can dominate product selectivity with *meta*- and *para*- positions more accessible towards alkylation, which is different from *ortho*- and *para*- selectivity of electrophilic substitution reaction.^[105]
- 4) Without the formation of a carbocation intermediate, straight-chain alkyl arenes can be produced directly from alkylation with benzene and α -olefin. The linear to branched selectivity is determined in olefin insertion step (Scheme 1.4.5).
- 5) Transition metal catalyzed pathways also give the possibility to directly product alkenyl arenes.



Scheme 1.4.5. Linear to branched selectivity and the olefin insertion step.

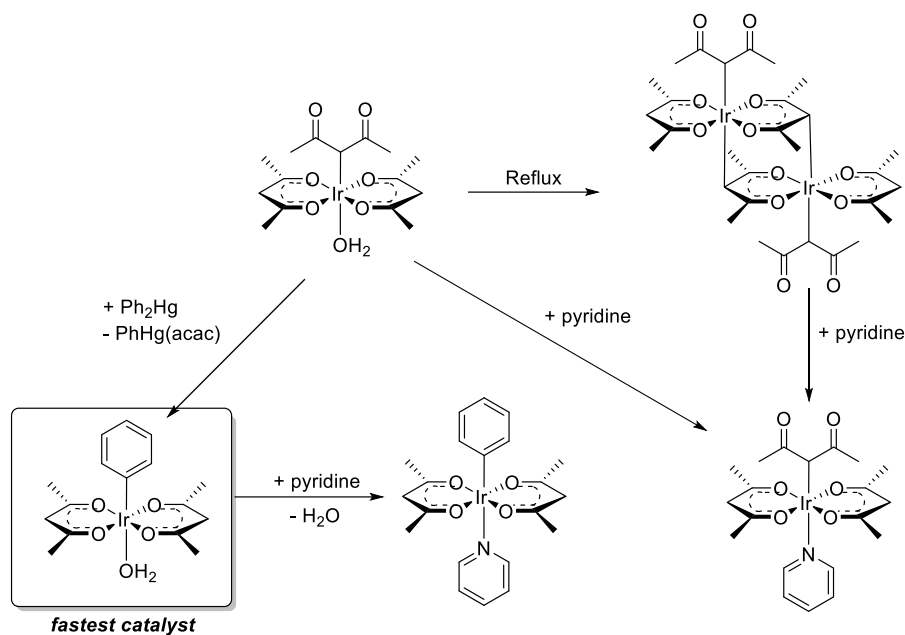
Although transition metal catalyzed hydroarylation has a lot of advantages, it also suffers from some drawbacks. Common off-cycle reactions are shown in Scheme 1.4.4. The BDEs of benzene C–H bond (112 kcal/mol) and olefin C–H bond (112 kcal/mol) are often similar, which leads to the possible olefin C–H activation (pathway I). Irreversible β -hydride elimination of arylalkyl intermediates may also be an issue (pathway II). The β -hydride elimination process will generate metal hydride species, which can lead to decomposition. In order to complete the catalytic cycle, an oxidant is needed to remove metal hydride to keep the catalyst stable. In addition, olefin polymerization can also happen when olefin insertion is too rapid (pathway III). This can generate polymers or oligomers.

Irreversible arene C–H oxidative addition can occur with electron-rich metals. This is proved to be a major pathway for Pd catalyst deactivation.^[106] In order to solve those problems, different ligands are used to tune the steric and electronic property of the metal center.

1.4.3 Examples for Late Transition Metal Catalyzed Olefin Hydroarylation

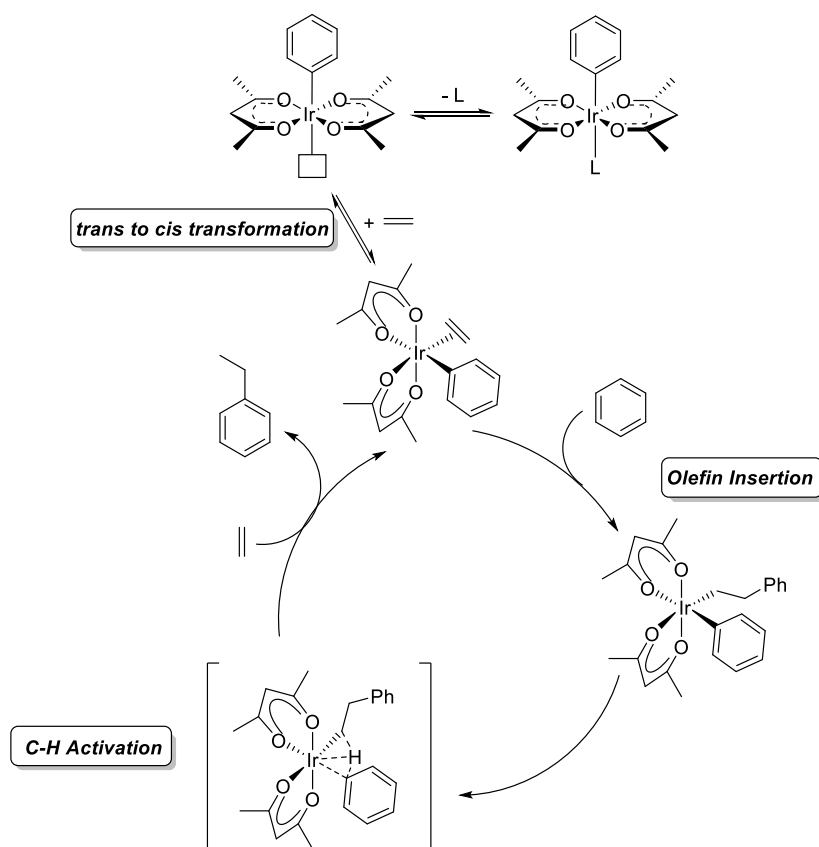
Ir catalysts:

Periana and co-workers published a series of Ir(III) complexes that can catalyze the hydroarylation of olefins.^[107-112] The initial study showed that the bis-acac-O,O-Ir(III) complex $[\text{Ir}(\mu\text{-acac-O,O,C}^3)(\text{acac-O,O})(\text{acac-C}^3)]_2$ (acac = acetylacetonate) can efficiently catalyze olefin hydroarylation. Under 1.9 MPa of ethylene at 180 °C 50 TON after 20 minutes and 455 TON after 3 hours were obtained. The reaction with benzene and longer chain olefins under similar conditions selectively form linear products. The reaction with propylene gives 13 TON with linear to branched (L:B) ratio of 1.6:1 and with iso-butene gives 2 TON with L:B ratio of 4:1. The reaction with 1-hexene gives 1-phenylhexane and 2-phenylhexane with 2.2:1 ratio and 3-phenylhexane was not observed. Further, the hydroarylation of ethylene with toluene produced *m*-ethyltoluene and *p*-ethyltoluene in a 63:37 ratio with no *o*-ethyl toluene observed.^[107] In the follow-up paper, a series of Ir(acac) complexes are synthesized from original Ir dimer and the mono Ir(acac) complex with water and phenyl as ligands proves to be the fastest catalyst (Scheme 1.4.6). The reaction rate is reduced with addition of extra pyridine, which indicates the dissociation of the ligand is needed for catalysis.^[108]



Scheme 1.4.6. Ir(acac) complexes.

The proposed mechanism is similar to general late transition metal catalyzed olefin hydroarylation in Scheme 1.4.7.^[109,110] However, there are several interesting points that need to be noted. A *trans* to *cis* transformation is needed for entering the catalytic cycle. The barrier for this transformation is calculated to be even higher than the C–H activation step. The reaction shows no kinetic isotope effect (KIE) for C₆H₆/C₆D₆ mixture and positive KIE for 1,3,5-C₆D₃H₃, which indicates that the rate determining step in this transformation is not likely C–H activation. In addition, the Ir-phenethyl species was shown to undergo reversible β-hydride elimination based on deuterium labeling studies and the rate for the C–H activation is about twice that of β-hydride elimination reactions.



Scheme 1.4.7. Mechanism of Ir(acac) series complexes catalyzed olefin hydroarylation.

In order to improve their Ir(acac) system, two new complexes have been developed as potential catalysts (Figure 1.4.1). $[\text{Ir}(\text{Ph})(\text{py})(\text{trop-O,O})_2]$ (trop-O,O = κ^2 -O,O-tropolonato) catalyzed H/D of toluene is at least 50 times faster than acac-O,O analogue; however, it shows very similar reaction rate of olefin hydroarylation to acac-O,O analogue.^[111,112] The Rh analogue *trans*-(hfac-O,O)₂Rh(Ph)(py) (hfac-O,O = κ^2 -O,O-1,1,1,5,5,5-hexafluoroacetylacetonato) shows positive results in arene C–H activation, however, it does not catalyze olefin hydroarylation. When monitoring the reaction with benzene and styrene with *trans*-(hfac-O,O)₂Rh(Ph)(py), dihydrostilbene is the major product in short reaction (< 1 hour), however significant amount of polystyrene observed in long reaction (> 1 hour).^[113]

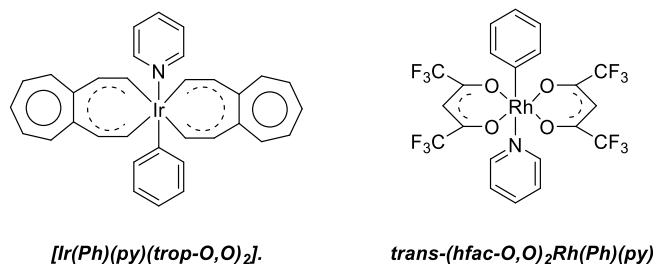


Figure 1.4.1. Structure of $[\text{Ir}(\text{Ph})(\text{py})(\text{trop-O,O})_2]$ and $\text{trans}-(\text{hfac-O,O})_2\text{Rh}(\text{Ph})(\text{py})$.

Ru catalysts:

Our group has reported a series of Ru(II) complexes that catalyze the hydroarylation of olefins.^[114-124] Some important results are summarized in Figure 1.4.2. The initial report showed that $\text{TpRu}(\text{CO})(\text{NCMe})\text{Ph}$ (Tp = hydridotris(pyrazolyl)borate) could catalyze olefin hydroarylation using benzene with ethylene and propylene.^[114] At 90 °C in neat benzene under 25 psig ethylene and with 0.1 mol% Ru catalyst loading, the reaction gave 74 TON after 24 hours. The TOF in the first 4 h is $3.5 \times 10^{-3} \text{ mol}^{-1} \text{ s}^{-1}$ and only a small amount of 1,3- and 1,4- diethylbenzene were produced. In the reaction with propylene, 14 catalytic TOs of *n*-propylbenzene and cumene products were obtained in a 1.6:1 ratio.

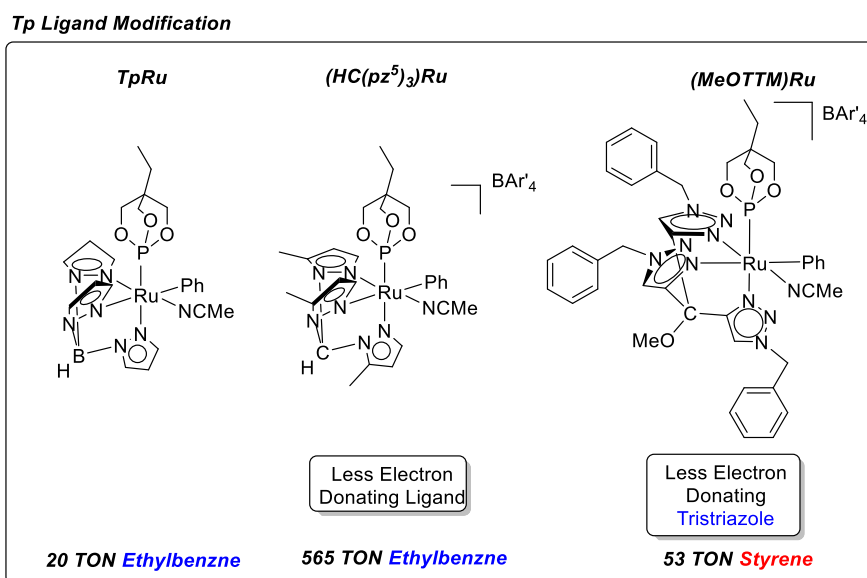
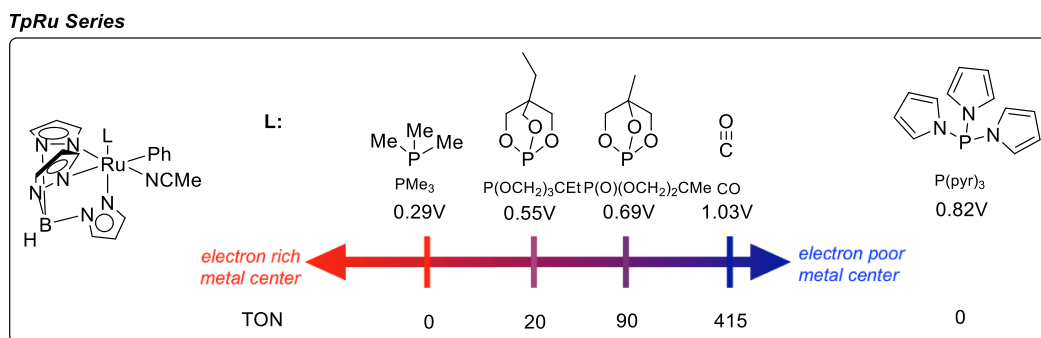
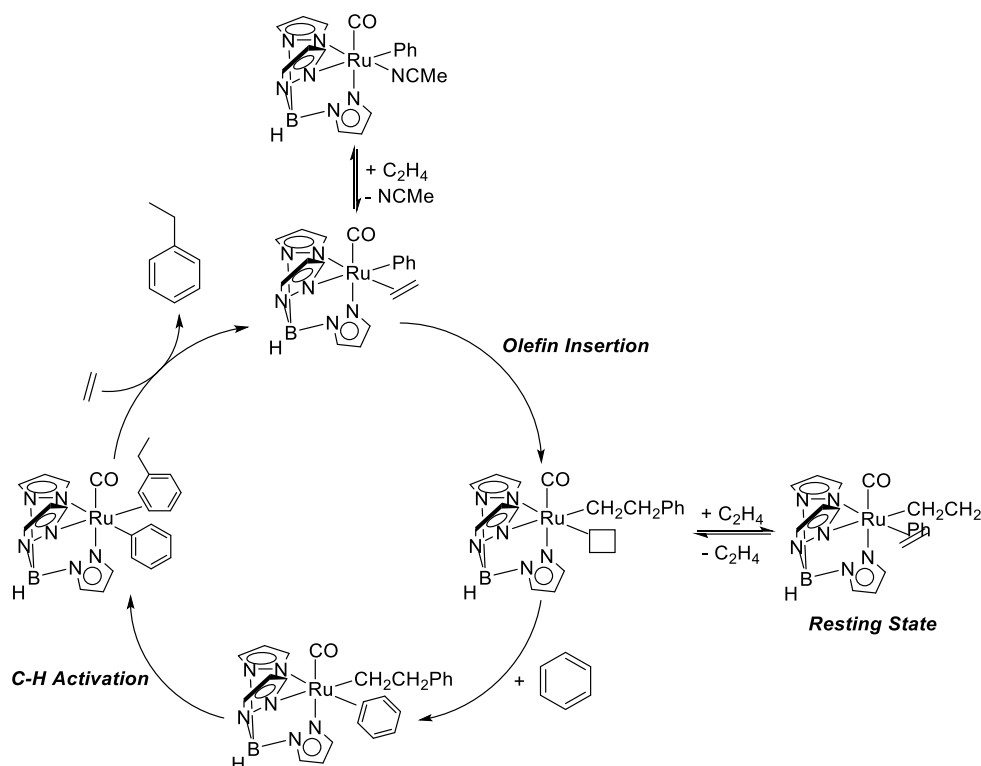


Figure 1.4.2. Summarized results of Ru(II) catalysts for olefin hydroarylation.

In the follow-up paper, computational studies in conjunction with experimental results support the mechanism depicted in Scheme 1.4.8.^[115] The catalyst dissociates acetonitrile and coordinates to one equivalent of ethylene to enter the catalytic cycle. The ethylene then inserts into the Ru–Ph bond to give a phenethyl intermediate. Another equivalent of benzene coordinates to the Ru and goes through a C–H activation followed by ethylene coordination and ethylbenzene dissociation to regenerate the catalyst. The reaction rate shows an inverse dependence on ethylene pressure, indicating that ethylene can coordinate to the phenethyl intermediate to form the resting state, which slows down the reaction. A KIE of 2.1(1) was found through competition experiments, indicating that C–H activation

is or precedes the rate determining step in the catalytic cycle.

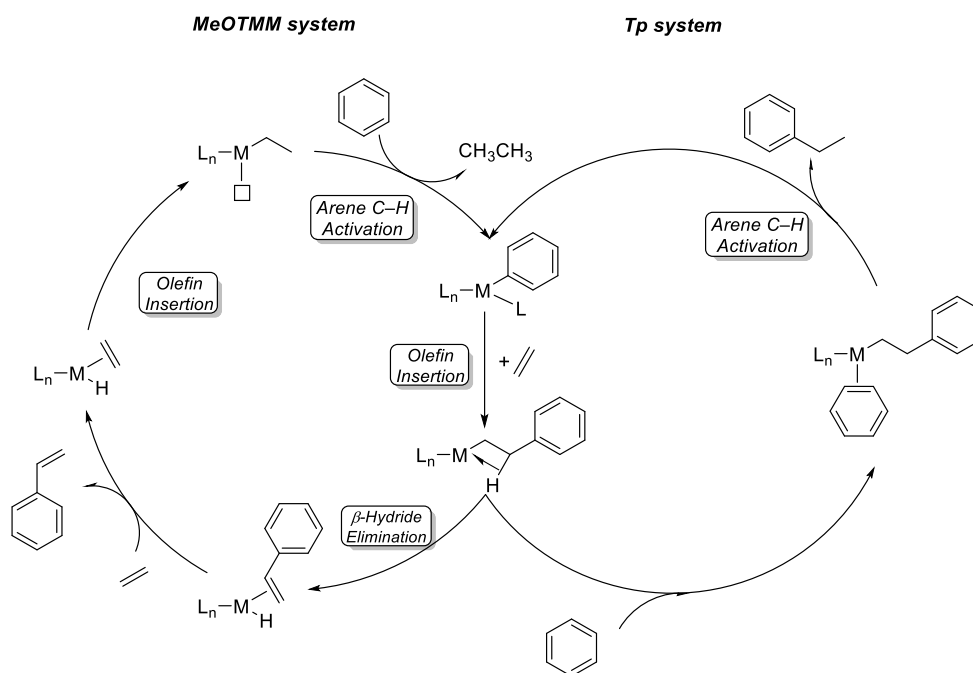


Scheme 1.4.8. Mechanism for $\text{TpRu}(\text{CO})(\text{NCMe})\text{Ph}$ catalyzed olefin hydroarylation.

A series of modifications on ancillary ligand have provided more insight of the TpRu system.^[116-120] PMe_3 , $\text{P}(\text{O})(\text{OCH}_2)_2\text{CMe}$, $\text{P}(\text{N-pyrrolyl})_3$ ($\text{P}(\text{pyr})_3$), $\text{P}(\text{OCH}_3)_2\text{Et}$ and CO were used as ancillary ligands (Figure 1.4.2). The electronics properties of the complex was analyzed by cyclic voltammetry using reversible $\text{Ru}(\text{III}/\text{II})$ potentials. The TON increases with an increase in $\text{Ru}(\text{III}/\text{II})$ potential. The complex with PMe_3 ligand shows no activity towards ethylene hydrophenylation. This result was investigated by DFT calculations, and it was found that the energy difference between ethylene insertion and ethylene activation is the smallest with PMe_3 . $\text{TpRu}(\text{PMe}_3)(\eta^2\text{-C}_2\text{H}_4)(\eta^1\text{-C}_2\text{H}_3)$ is the kinetic product of catalyst deactivation, and this leads to the formation of $\text{TpRu}(\text{PMe}_3)(\eta^3\text{-C}_3\text{H}_4\text{Me})$.^[116] $\text{P}(\text{pyr})_3$ has moderated $\text{Ru}(\text{III}/\text{II})$ potentials, however, it also shows no catalytic ability. The inactivity is due to the steric bulk of the ligand. The cone angle of $\text{P}(\text{pyr})_3$ (145°) is much larger than

other ligands (CO 95°, P(OCH₃)₂Et 101°), which leads to a difficulty of ethylene coordination and insertion. The combined steric and electronic impact on the ethylene coordination/insertion step for olefin hydroarylation, the ΔG of P(pyr)₃ complex (25.0 kcal/mol) is higher than CO complex (9.9 kcal/mol), which leads to its failure to catalyze hydroarylation of ethylene.^[117] Additional study with functionalized arene initiated that the C–H activation step likely occurs through σ -bond metathesis.^[118]

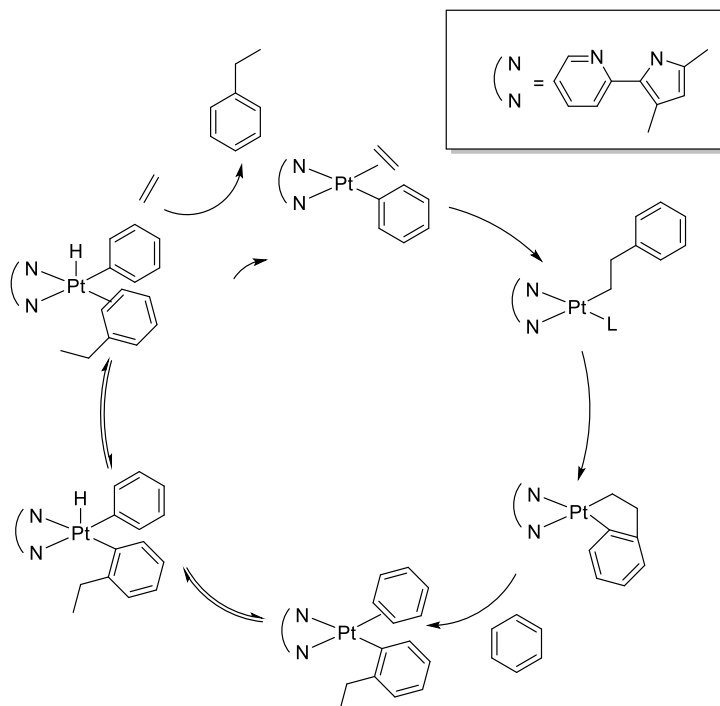
In addition, our group has modified the Tp ligand to look for possible improvement. The more electron deficient ligand HC(pz⁵)₃ (HC(pz⁵)₃ = tris(5-methyl-pyrazolyl)-methane) was used to replace Tp. This causes the catalyst to be cationic rather than neutral. The Ru(III/II) potential is 1.06 for the catalyst [HC(pz⁵)₃Ru(P(OCH₂)₃CEt)(NCMe)Ph][BAR'₄] { BAR'₄ = tetrakis[3,5-bis(trifluoromethyl)phenyl]borate }, which is found to be the most active catalysts. Under the best conditions, it gives 565 TON of ethylbenzene with a 95% yield based on ethylene.^[121] In order to pursue better catalysis result, an even less electron donating tristriazole ligand, MeOTMM [MeOTMM=4,4',4''-(methoxymethanetriyl)-tris(1-benzyl-1H-1,2,3-triazole)], was used to replace Tp. Surprisingly, the main product is styrene instead of ethylbenzene. In addition, the reaction shows a positive dependence on ethylene pressure. The proposed mechanism comparison is shown in Scheme 1.4.9.^[124]



Scheme 1.4.9. Mechanistic comparison between TpRu and MeOTMM based catalyst.

Pt catalysts

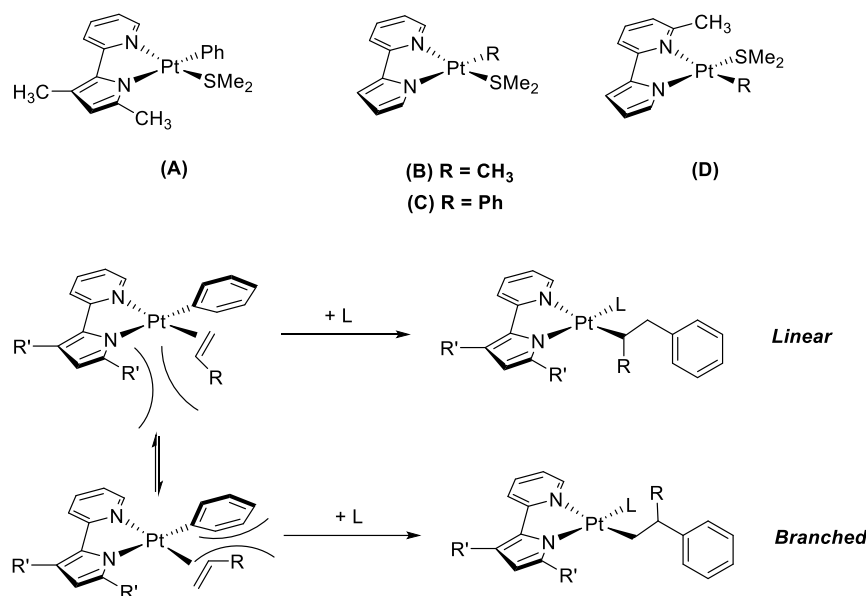
Goldberg and co-workers reported that a (pyridyl)pyrrolide supported Pt(II) complex catalyzes the hydroarylation of unactivated olefins.^[125] The proposed mechanism is shown in Scheme 1.4.10. The catalyst can achieve 26 TON ethylbenzene at 100 °C. When treated with propylene, it gives 8 TON with L:B ratio of 14:86. The L:B ratio of alkyl chain stays the same when switching benzene to substituted benzene. Substitution of the benzene ring with results in *meta/para* selectivity over *ortho* position.



Scheme 1.4.10. Proposed mechanism for (pyridyl)pyrrolide ligand supported Pt(II) complex catalyzed hydroarylation of olefins.

In order to better understand insight of linear to branched product selectivity, a series of Pt(II) complexes with different pyridyl pyrrolide ligands were synthesized and tested for olefin hydroarylation reactions.^[126] As shown in the Scheme 1.4.11, the complex A has a methyl group on the 3,5 position on pyrrolide ring and the complex D has a methyl group on the 6-position on pyridine ring. SMe_2 is a labile ligand, which will dissociate to leave the empty site for olefin coordination. As shown in Scheme 1.4.11, the methyl group brings extra steric barrier against the R group on olefin which leads to the production of branched product. When using propylene as olefin source, complex A gives a L:B ratio of 13:84 and complex B gives L:B ratio of 48:52. The R group on the olefin also has a steric barrier against phenyl group at cis position, which leads to the linear selectivity of product with complex C. The reactions with propylene, 1-hexene and neohexene as olefin source give L:B ratio of 48:52, 57:43 and 90:9 respectively. When using complex D as the catalyst, the

even bigger steric bulk leads to the production of vinyl benzene.



Scheme 1.4.11. Structures of different (pyridyl)pyrrolide ligand supported Pt(II) complexes and steric effect on olefin insertion.

Our group has recently published a series of papers detailing ligand effects, substrate scope, and mechanistic details of Pt(II) catalysts for olefin hydroarylation.^[127-132] The initial Pt catalyst reported was $[(^t\text{bpy})\text{Pt}(\text{Ph})\text{THF}][\text{BAR}'_4]$ (^tbpy = 4,4'-di-*tert*-butyl-2,2'-bipyridine, $\text{Ar}' = 3,5$ -bis(trifluoromethyl)phenyl). At 100 °C with 15 psig ethylene, using 0.1 mol% Pt catalyst, the catalysis gives ~66 TOs of ethylbenzene and ~35 TOs of diethylbenzene after 16 h reaction. The diethylbenzene is highly selective for *meta* and *para* position. When using propylene as olefin source, it gives ~34 TOs of *n*-propylbenzene and cumene with a L:B ratio of ~1:3.^[127] By increasing the chelate size from 5- to 6-member rings with a modified bipyridine ligand dipyrityl methane (dpm), the complex $[(\text{dpm})\text{Pt}(\text{Ph})(\text{THF})][\text{BAR}'_4]$ shows substantial increase in both reactivity and longevity. The catalysis gives 469 TON of ethylbenzene after 110 h of reaction.^[128] A series of dpm ligand with 6,6'-substitution was used to determine their effect on catalysis.^[129] With increased the steric bulk on dpm ring, diethylbenzene formation is reduced. However, when investigating

the reaction with propylene, the L:B ratio was decreased. Changing the chelate size to 7-member ring shuts down the reaction. In order to pursue better catalysis, a series of functional groups were used to substitute the *t*-butyl on the bipyridine ring.^[130,131] The interesting observation is that with the decrease of electron donating ability, the main product changes from ethylbenzene to styrene. In addition, the electron withdrawing functional group facilitates branched product formation when using propylene as reactant (2.9:1 for OMe, 4.6:1 for NO₂). In the computational study, the methyl group on the propylene is either proximal (TS-a) or distal (TS-b) to the phenyl ring to yield branched or linear product respectively. The energy difference is about 4 kcal/mol favored TS-a, which is caused by steric hindrance between the methyl group on propylene and a 6-H on the bipyridyl ligand. A mechanistic study shows that the (bpy)Pt catalyst has a small KIE (~1.4) of ethylene hydrophenylation with C₆H₆ and C₆D₆, which indicates the rate determining step does not involve direct breaking C–H bond. The coordination of C–H bond to Pt center is most likely the rate determining step. An inverse dependence on ethylene pressure was observed on the reaction rate. In this case, the ethylene coordinated phenethyl intermediate is proposed to be the off-cycle resting state for the catalyst.^[132] Other later transition metal catalysts, especially Rh based complexes, will be reviewed in the introduction of Chapter 3.

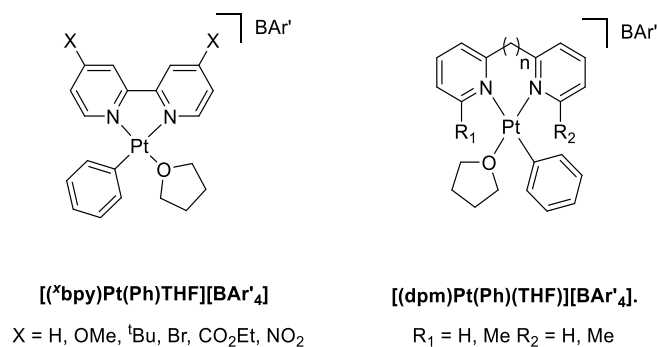
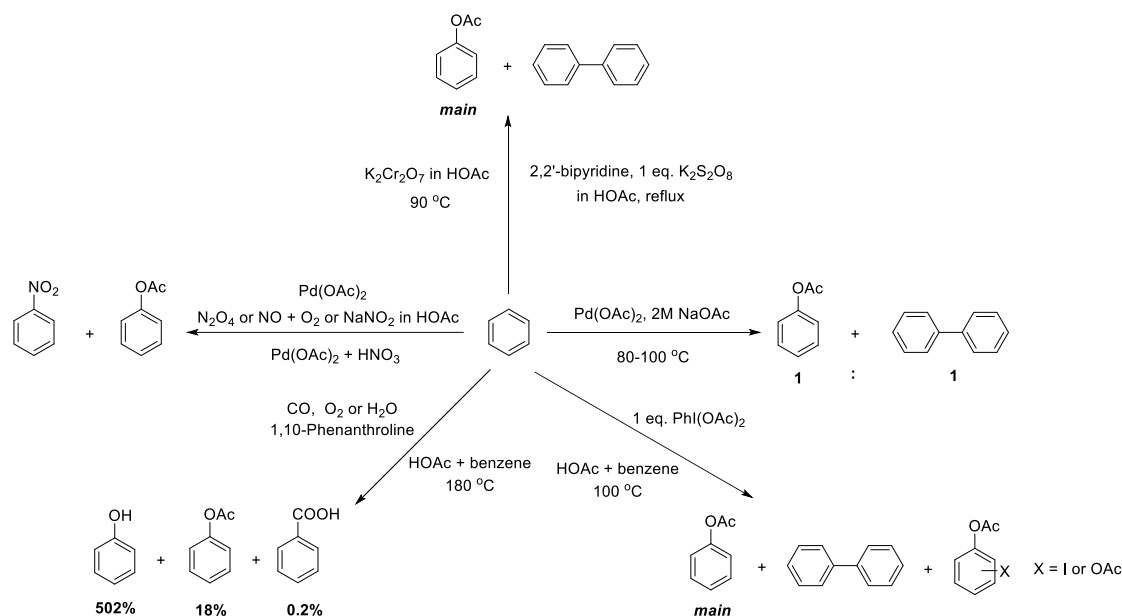


Figure 1.4.3 Structures of $[(^x\text{bpy})\text{Pt}(\text{Ph})\text{THF}][\text{BAR}'_4]$ and $[(\text{dpm})\text{Pt}(\text{Ph})(\text{THF})][\text{BAR}'_4]$.

1.5 Acetoxylation of Non-directed Arenes

Above challenges with C–H bond activation and C–O bond formation with methane were presented. One of the biggest problems is the barrier for C–H bond coordination to the metal center is often quite high. Although arene C–H bond coordination is slightly favored compared to methane, functionalization of C–H bonds in arenes that are lack of functionalization is still challenging. In order to circumvent the C–H coordination problem, functional directing groups on the arene are used to increase the reactivity and selectivity of the C–H functionalization process. Nevertheless, the use of directing groups generally implies the addition of extra steps in the synthetic sequence, the introduction and removal of the directing group, which frustrates the goal of this strategy. The direct oxidation of simple arenes is an attractive process to obtain phenols. Palladium catalyzed C-H acetoxylation of benzene is a potential route. The different methods to accomplish this transformation is summarized in Scheme 1.5.1.



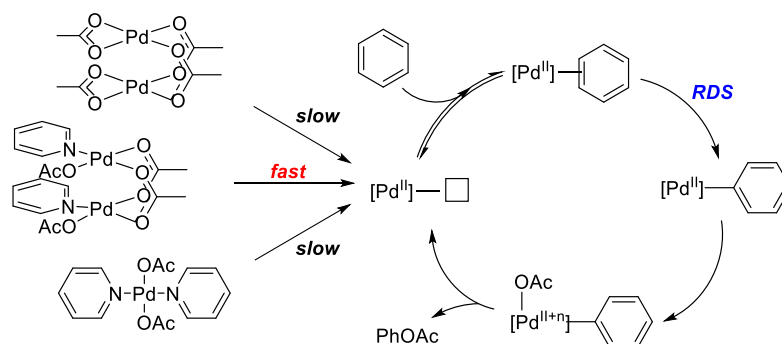
Scheme 1.5.1. Summary of Pd(OAc)₂ catalyzed benzene acetoxylation.

In 1968, Triggs and co-workers studied a series of metal acetate mediated benzene acetoxylation.^[133] Hg(OAc)₂, Pb(OAc)₄ and Pd(OAc)₂ were shown to be effective. A 1:1 ratio of phenyl acetate and biphenyl was observed for the reaction using Pd(OAc)₂ as the oxidant. When reacting with toluene, Hg(OAc)₂, Pb(OAc)₄ selectively produced benzyl acetate, however, tolyl acetate is the main product for Pd(OAc)₂. Thus, it is likely that the acetoxylation with Pd(OAc)₂ occurs through a non-radical pathway. A year later, Downs and co-workers showed that the Pd(OAc)₂ could be used as a catalyst for acetoxylation of benzene. When using NaNO₂ as the oxidant and acetic acid as solvent, Pd(OAc)₂ can give 6 TON of phenyl acetate and 8 TON of nitrobenzene at 100 °C after 18 hours.^[134] Strong oxidants K₂Cr₂O₇ and K₂S₂O₈ can sufficiently oxidize Pd(0) to Pd(II) to regenerate the catalyst.^[135,136] With the help of CO and water, oxygen can be used as sufficient oxidant.^[137,138] At 180 °C with 15 bar oxygen and 15 bar CO, using 1,10-phenanthroline as support ligand, Pd(OAc)₂ can produce 5 TON of phenol and 0.2 TON of phenyl acetate after 12h. No biphenyl is observed in the reaction. In addition, high valent iodine oxidant,

$\text{PhI}(\text{OAc})_2$ is the best oxidant. At 100 °C, $\text{Pd}(\text{OAc})_2$ gives 37 TON phenyl acetate after 20h with 75% yield based on oxidant.^[139]

In the past decade, Sanford and co-workers developed a series of catalysts based on $\text{Pd}(\text{OAc})_2$ that are for acetoxylation of non-directed arenes.^[140-145] In the initial report, $\text{PhI}(\text{OAc})_2$ was used as an oxidant and acetic acid/acetic anhydride ($\text{AcOH}/\text{Ac}_2\text{O}$ 9:1) was used as the solvent.^[140] By adding a cationic bipyridine-based ligand, the reaction rate almost doubled. In a following paper, by changing additive ligand to simple pyridine, the reaction rate was shown to be about 20 times faster than the non-additive condition.^[141] The amount of pyridine is essential to the catalysis, a pyridine: $\text{Pd}(\text{OAc})_2$ ratio of 0.9:1 is optimal. Over 2 equivalents of pyridine will shut down the reaction due to blocking of Pd coordination sites. When reducing the Pd loading to 0.01 mol%, the catalyst can achieve 4,756 TOs of phenyl acetate after 306 hours at 100 °C. In addition, substituted arenes such as chlorobenzene, bromobenzene, dichlorobenzene and benzo-trifluoride are suitable substrates for the reaction. Through detailed kinetic studies, the mechanism in Scheme 1.5.2 was proposed.^[142] A KIE of 3.1 was observed, indicating that C-H bond activation is likely the rate determining step. Since $\text{Pd}(\text{OAc})_2$ is a dimer in the solution without ligand additive. The speed for transferring $\text{Pd}(\text{OAc})_2$ dimer to monomer process is slow, which impacts the reaction rate. Using $\text{Pd}(\text{TFA})_2$ which is a monomer Pd source greatly increases the reaction, which is consistent with this hypothesis. When using 2 equiv. of pyridine as the additive, the $\text{Pd}(\text{OAc})_2$ dimer will quickly change to monomer with two pyridine ligands. However, the dissociation of pyridine is slow. With electron withdrawing group substituted pyridine ligands, a rate enhancement was observed. When using 1 eq. pyridine

as additive, the $\text{Pd}(\text{OAc})_2$ dimer is still a dimer in the solution, but the rate of monomer formation enhanced, which leads to more rapid acetoxylation. The reaction rate is not affected by change pyridine ligand, which proves the pyridine ligand dissociation is not involved in the catalytic cycle. By modifying pyridine ligand and change oxidant from $\text{PhI}(\text{OAc})_2$ to $\text{MesI}(\text{OAc})_2$, control of site selectivity in the Pd-catalyzed C-H acetoxylation of simple arenes was enhanced.^[143] Although $\text{PhI}(\text{OAc})_2$ is an effective oxidant for acetoxylation, the price for this compound is very high. Sanford and co-workers designed a pyridinium-substituted pyridine ligand which can serve as ligand as well as phase transfer reagent to utilize $\text{K}_2\text{S}_2\text{O}_8$ as the oxidant.^[144] Similar yields and selectivities were achieved compared to use of $\text{PhI}(\text{OAc})_2$. In addition, palladium-catalyzed C-H bond acetoxylation via electrochemical oxidation has been developed,^[145] which is selective for the benzyl position of arenes.



Scheme 1.5.2. Mechanism for $\text{Pd}(\text{OAc})_2$ catalyzed benzene acetoxylation with pyridine additive.

Fernández-Ibáñez and co-workers utilize pyridinecarboxylic acid derivatives and S,O-ligands as additive to improve the $\text{PhI}(\text{OAc})_2$ system.^[146,147] Different types of ligands including bis-*N*-heterocyclic carbene and *trans*-chelating bis(pyridyl) supported Pd(II) complexes proved to be effective catalysts for benzene acetoxylation.^[148,149] Recently, a series of polymer-supported Pd(II) carbene complexes turn out to be effective catalysts for

biphenyl and naphthalene. With the heterogeneous support, those catalysts can be recycled four times without loss of activity. In addition, by controlling the size and structure of heterogeneous support, the catalysts show tunable selectivity towards acetoxylation of the α or β position of naphthalene.^[150] Modification of oxidants were also attempted, for example, Stahl and co-workers evaluated a series of NO_x based oxidants and found that 30% fuming HNO₃ with oxygen is an effective oxidant. With this oxidant, Pd(OAc)₂ can achieve 136 TON with 26:1 selectivity toward phenyl acetate over nitrobenzene.^[151] Other PhI(OR)₂ type oxidants such as iodobenzene dibenzoates are used for oxidative functionalization of benzene.^[152] By modifying the R group in the oxidant, different type of functionalization can be achieved in the catalysis, which opens the route for possible synthetic applications.

1.6 Summary and Thesis Aims

The research presented in this dissertation aims to develop transition metal catalysts for C–H activation and functionalization. A series of Rh(III) complexes with different “capping arene” ligands have been synthesized and used to study the reductive functionalization of Rh–Me bonds. By using these specially designed ligands, one of the coordination site of the Rh(III) center has been blocked, which could destabilize Rh intermediates with high oxidation states (*e.g.* Rh(III)). With the success of this design concept, a series of Rh(I) complexes with the same support ligands were used to probe the oxidative alkenylation of benzene. With the help of the ligands, the catalyst is tolerated to *in situ* dioxygen, which leads access to the aerobic conditions. With the help of air and acid, Cu(II) oxidant can be regenerated *in situ*. In addition, using the catalyst with longer chain

α -olefins revealed that the catalysts achieved unprecedented linear to branched ratios of 18:1. For the

Rh catalyzed arene alkenylation reaction, phenylacetate was found to be a side product produced from Cu(II) oxidant. Different simple copper salts were then tested for the acetoxylation of benzene. Reactions with toluene and cyclohexane showed that the copper catalyzed acetoxylation does not likely involve radical intermediates. The addition of TEMPO or compounds with P-O linkage increase the rate of acetoxylation reactions.

Hydroamination of alkenes or alkynes is one of the most straightforward methods to form C–N bonds and N-containing heterocycles. This method involves direct addition of amines to carbon-carbon multiple bonds without the formation of any by-products. Al(OTf)₃ was tested and proved to be an effective catalyst for intramolecular hydroamination of unactivated alkenes. The mechanism for this transformation was then further investigated. The Al(OTf)₃ can *in situ* generate HOTf, which is the actual catalyst for hydroamination reaction. In addition, other metal triflates were proved to go through the similar reaction mechanism.

1.7 References:

- [1] Adams, C., *Chem. Ind. (London)* **1999**, 740.
- [2] Baiker A, Blaser H-U; Ertl G et al. (ed) *Handbook of heterogeneous catalysis*. Wiley VCH, New York, 1997.
- [3] Hartwig, J. F.; Collman, J. P., *Organotransition metal chemistry: from bonding to catalysis*. University Science Books Sausalito, CA: 2010; Vol. 1.

-
- [4] Cornils, B.; Herrmann, W. A., *J. Catal.* **2003**, *216*, 23-31.
- [5] GB 190208300, Ostwald, Wilhelm, "Improvements in and relating to the Manufacture of Nitric Acid and Oxides of Nitrogen"
- [6] Giuliano Cecchin, Giampiero Morini, Fabrizio Piemontesi. "Ziegler–Natta Catalysts" in *Kirk-Othmer Encyclopedia of Chemical Technology*. Wiley-VCH.2003
- [7] Cole-Hamilton, D. J., *Science* **2003**, *299*, 1702-1706.
- [8] Crucq, A.; Frennet, A., *Catalysis and automotive pollution control*. Elsevier: 1987; Vol. 30.
- [9] E. S. Lox, B. Engler: "Environmental Catalysis", G. Ertl, H. Knözinger, J. Weitkamp (eds.): *Handbook of Heterogeneous Catalysis*, VCH, Weinheim, 1997
- [10] I. Ojima, C.-Y. Tsai, M. Tzamarioudaki, D. Bonafoux in *Organic Reactions*, Vol. 50 (Ed.: L. E. Overman), Wiley, New York, 2000.
- [11] Roelen, O. *Ger. Offen.* **1938**, *949*, 548.
- [12] Pino, P.; Piacenti, F.; Bianchi, M.; In *Organic Synthesis via Metal Carbonyls*; John Wiley & Sons: New York, 1977; pp. 43-231.
- [13] Parshall, G. W., *J. Mol. Catal.* **1978**, *4*, 243-270.
- [14] Dümbgen, G.; Neubauer, D., *Chem. Ing. Tech.* **1969**, *41*, 974-980.

-
- [15] Boy Cornils, Wolfgang A. Herrmann, Chi-Huey Wong, Horst -Werner Zanthoff: *Catalysis from A to Z: A Concise Encyclopedia*, Wiley-VCH Verlag GmbH & Co. KGaA: 2012.
- [16] Bianchi, M.; Piacenti, F.; Frediani, P.; Matteoli, U., *J. Organomet. Chem.* **1977**, *137*, 361-365.
- [17] Kohlpaintner, C. W.; Fischer, R. W.; Cornils, B., *Appl. Catal. A.* **2001**, *221*, 219-225.
- [18] Cheung, H.; Tanke, R. S.; Torrence, G. P. Acetic Acid In *Ullmann's Encyclopedia of Industrial Chemistry*; Wiley-VCH Verlag GmbH & Co. KGaA: 2000.
- [19] H. Hohenschutz, N. v. Kutepov and W. Himmele., *Hydrocarbon Process*, **1965**, *45*, 141.
- [20] J.W. Reppe: *Acetylene Chemistry*, Charles A. Meyer & Co., Boston 1949.
- [21] Forster, D.; Singleton, T. C., *J. Mol. Catal.* **1982**, *17*, 299-314.
- [22] Dekleva, T. W.; Forster, D., Mechanistic Aspects of Transition-Metal-Catalyzed Alcohol Carbonylations. In *Advances in Catalysis*, Eley, D. D.; Pines, H.; Weisz, P. B., Eds. Academic Press: 1986; Vol. 34, pp 81-130.
- [23] Forster, D., Mechanistic Pathways in the Catalytic Carbonylation of Methanol by Rhodium and Iridium Complexes. In *Adv. Organomet. Chem.*, Stone, F. G. A.; West, R., Eds. Academic Press: 1979; Vol. 17, pp 255-267.

-
- [24] Baker, E. C.; Hendriksen, D. E.; Eisenberg, R., *J. Am. Chem. Soc.* **1980**, *102*, 1020-1027.
- [25] James, B. R.; Rempel, G. L., *J. Chem. Soc. A.* **1969**, 78-84.
- [26] T.C. Singleton, L.J. Park, D. Forster, *Prepr. Am. Chem. Soc. Div. Pet. Chem.* **1979**, *24*, 329–335.
- [27] Sunley, G. J.; Watson, D. J., *Catal. Today* **2000**, *58*, 293-307.
- [28] Uebelacker, M.; Lachenmeier, D. W., *J. Autom. Methods Manage. Chem.* **2011**, *2011*, 907317-907317.
- [29] Wittcoff, H. A.; Reuben, B. G.; Plotkin, J. S. Chemicals and Polymers from Ethylene In *Industrial Organic Chemicals*; John Wiley & Sons, Inc.: 2012, p 139.
- [30] Keith, J. A.; Henry, P. M., *Angew. Chem. Int. Ed.* **2009**, *48*, 9038-9049.
- [31] Eckert, M.; Fleischmann, G.; Jira, R.; Bolt, H. M.; Golka, K. Acetaldehyde In *Ullmann's Encyclopedia of Industrial Chemistry*; Wiley-VCH Verlag GmbH & Co. KGaA: 2000.
- [32] Shilov, A. E.; Shul'pin, G. B., *Chem. Rev.* **1997**, *97*, 2879-2932.
- [33] *Pyrolysis: Theory and Industrial Practice*; Albright, L. F., Crynes, B. L., Corcoran, W. H., Eds.; Academic Press: New York, 1983.
- [34] Dorofeev, Yu. I.; Skurat, V. E. *Usp. Khim.* **1982**, *51*, 925
- [35] Kung, H. H. *Transition Metal Oxides*; Elsevier: Amsterdam, 1989.
- [36] Minachev, Kh.M., Dergachev, A. A.; Usachev, N. A., *Usp. Khim.* **1991**, *31*, 148.

-
- [37] *The World Factbook*. Central Intelligence Agency. 1 December 2013.
- [38] “Wonderfuel: Welcome to the age of unconventional gas”. *New Scientist*. p44-47.
- [39] “In Natural Gas, U.S. Will Move From Abundance to Imports”. *Greentech Media*.
- [40] BP: “Statistical Review of World Energy”, Workbook (xlsx), London, 2016.
- [41] “Alaska natural gas pipeline project history”. www.arcticgas.gov
- [42] “Formaldehyde – Johnson Matthey”. www.formox.com
- [43] Conley, B. L.; Tenn, W. J.; Young, K. J. H.; Ganesh, S.; Meier, S.; Ziatdinov, V.; Mironov, O.; Oxgaard, J.; Gonzales, J.; Goddard, W. A.; Periana, R. A. In *Activation of Small Molecules*; Wiley-VCH Verlag GmbH & Co. KGaA: 2006, p 235.
- [44] George A. Olah, A. M. *Hydrocarbon Chemistry*; 2nd ed.; John Wiley & Sons, 2003.
- [45] Forlani, O.; Rossini, S., *Mater. Chem. Phys.* **1992**, *31*, 155-158.
- [46] Maitra, A. M., *Appl. Catal. A.* **1993**, *104*, 11-59.
- [47] Krylov, O. V., *Catal. Today* **1993**, *18*, 209-302.
- [48] Raja, R.; Ratnasamy, P., *Appl. Catal. A.* **1997**, *158*, L7-L15.
- [49] Hammond, C.; Forde, M. M.; Ab Rahim, M. H.; Thetford, A.; He, Q.; Jenkins, R. L.; Dimitratos, N.; Lopez-Sanchez, J. A.; Dummer, N. F.; Murphy, D. M.; Carley, A. F.; Taylor, S. H.; Willock, D. J.; Stangland, E. E.; Kang, J.; Hagen, H.; Kiely, C. J.; Hutchings, G. J., *Angew. Chem. Int. Ed.* **2012**, *51*, 5129-5133.
- [50] Bar-Nahum, I.; Khenkin, A. M.; Neumann, R., *J. Am. Chem. Soc.* **2004**, *126*, 10236-10237.

-
- [51] Johansson, L.; Tilset, M., *J. Am. Chem. Soc.* **2001**, *123*, 739-740.
- [52] N. F. Goldshleger; M. B. Tyabin; A. E. Shilov; A. A. Shteinman; *Zhurnal Fizicheskoi Khimii* **1969**, *43*, 2174-2175
- [53] Periana, R. A.; Taube, D. J.; Gamble, S.; Taube, H.; Satoh, T.; Fujii, H., *Science* **1998**, *280*, 560-564.
- [54] Ahlquist, M.; Nielsen, R. J.; Periana, R. A.; Goddard Iii, W. A., *J. Am. Chem. Soc.* **2009**, *131*, 17110-17115.
- [55] Periana, R. A.; Taube, D. J.; Evitt, E. R.; Löffler, D. G.; Wentrcek, P. R.; Voss, G.; Masuda, T., *Science* **1993**, *259*, 340-343.
- [56] Jones, C.; Taube, D.; Ziatdinov, V. R.; Periana, R. A.; Nielsen, R. J.; Oxgaard, J.; Goddard III, W. A., *Angew. Chem. Int. Ed.* **2004**, *43*, 4626-4629.
- [57] Periana, R. A.; Mironov, O.; Taube, D.; Bhalla, G.; Jones, C., *Science* **2003**, *301*, 814-818.
- [58] Zimmermann, T.; Soorholtz, M.; Bilke, M.; Schüth, F., *J. Am. Chem. Soc.* **2016**, *138*, 12395-12400.
- [59] Gretz, E.; Oliver, T. F.; Sen, A., *J. Am. Chem. Soc.* **1987**, *109*, 8109-8111.
- [60] Kao, L. C.; Hutson, A. C.; Sen, A., *J. Am. Chem. Soc.* **1991**, *113*, 700-701.
- [61] Ahrens, S.; Strassner, T., *Inorg. Chim. Acta* **2006**, *359*, 4789-4796.
- [62] Ahrens, S.; Zeller, A.; Taige, M.; Strassner, T., *Organometallics* **2006**, *25*, 5409-5415.

-
- [63] Strassner, T.; Ahrens, S.; Muehlhofer, M.; Munz, D.; Zeller, A., *Eur. J. Inorg. Chem.* **2013**, *2013*, 3659-3663.
- [64] Hashiguchi, B. G.; Konnick, M. M.; Bischof, S. M.; Gustafson, S. J.; Devarajan, D.; Gunsalus, N.; Ess, D. H.; Periana, R. A., *Science* **2014**, *343*, 1232-1237.
- [65] Johnson, R. A. (Halcon Research & Development Corporation).US Patent 4192814.Mar 11, 1980
- [66] Fortman, G. C.; Boaz, N. C.; Munz, D.; Konnick, M. M.; Periana, R. A.; Groves, J. T.; Gunnoe, T. B., *J. Am. Chem. Soc.* **2014**, *136*, 8393-8401.
- [67] Kalman, S. E.; Munz, D.; Fortman, G. C.; Boaz, N. C.; Groves, J. T.; Gunnoe, T. B., *Dalton Trans.* **2015**, *44*, 5294-5298.
- [68] Schwartz, N. A.; Boaz, N. C.; Kalman, S. E.; Zhuang, T.; Goldberg, J. M.; Fu, R.; Nielsen, R. J.; Goddard, W. A.; Groves, J. T.; Gunnoe, T. B., *ACS Catal.* **2018**, *8*, 3138-3149.
- [69] Hartwig, J. F. *Organotransition Metal Chemistry: From Bonding to Catalysis*; University Science Books: Sausalito, 2009.
- [70] Goldberg, K. I.; Yan, J. Y.; Winter, E. L., *J. Am. Chem. Soc.* **1994**, *116*, 1573-1574.
- [71] Goldberg, K. I.; Yan, J.; Breitung, E. M., *J. Am. Chem. Soc.* **1995**, *117*, 6889-6896.
- [72] Macgregor, S. A.; Neave, G. W.; Smith, C., *Faraday Disc.* **2003**, *124*, 111-127.

-
- [73] Williams, B. S.; Holland, A. W.; Goldberg, K. I., *J. Am. Chem. Soc.* **1999**, *121*, 252-253.
- [74] Roy, A. H.; Hartwig, J. F., *J. Am. Chem. Soc.* **2001**, *123*, 1232-1233.
- [75] Powers, D. C.; Benitez, D.; Tkatchouk, E.; Goddard, W. A.; Ritter, T., *J. Am. Chem. Soc.* **2010**, *132*, 14092-14103.
- [76] Furuya, T.; Ritter, T., *J. Am. Chem. Soc.* **2008**, *130*, 10060-10061.
- [77] Kaspi, A. W.; Yahav-Levi, A.; Goldberg, I.; Vigalok, A., *Inorg. Chem.* **2008**, *47*, 5-7.
- [78] McMurtrey, K. B.; Racowski, J. M.; Sanford, M. S., *Org. Lett.* **2012**, *14*, 4094-4097.
- [79] Frech, C. M.; Milstein, D., *J. Am. Chem. Soc.* **2006**, *128*, 12434-12435.
- [80] Feller, M.; Diskin-Posner, Y.; Leitun, G.; Shimon, L. J. W.; Milstein, D., *J. Am. Chem. Soc.* **2013**, *135*, 11040-11047.
- [81] Scott, V. J.; Labinger, J. A.; Bercaw, J. E., *Organometallics* **2010**, *29*, 4090-4096.
- [82] Mankad, N. P.; Toste, F. D., *Chem. Sci.* **2012**, *3*, 72-76.
- [83] Higgs, A. T.; Zinn, P. J.; Simmons, S. J.; Sanford, M. S., *Organometallics* **2009**, *28*, 6142-6144.
- [84] Caro, J.; Noack, M., Chapter 1 - Zeolite Membranes – Status and Prospective. In *Advances in Nanoporous Materials*, Ernst, S., Ed. Elsevier: 2010; Vol. 1, 1-96.
- [85] Chen, S.-S. Styrene in *Kirk-Othmer Encyclopedia of Chemical Technology*; John Wiley & Sons, Inc: Hoboken, NJ, 2006.

-
- [86] Wittcoff, H. A., Reuben, B. G. and Plotkin, J. S. Chemicals and Polymers from Ethylene in *Industrial Organic Chemicals*; John Wiley & Sons, Inc: Hoboken, NJ, 2013.
- [87] Kocal, J. A.; Vora, B. V.; Imai, T., *Appl. Catal. A.*, **2001**, *221*, 295-301.
- [88] Olah, G. A.; Prakash, G. S., *Hydrocarbon Chemistry, 2 Volume Set*. John Wiley & Sons, Inc: Hoboken, NJ, 2017.
- [89] Gerzeliev, I.; Khadzhiev, S.; Sakharova, I., *Petrol. Chem.* **2011**, *51*, 39-48.
- [90] Čejka, J.; Wichterlová, B., *Catal. Rev.* **2002**, *44*, 375-421.
- [91] Perego, C.; Ingallina, P., *Green Chem.* **2004**, *6*, 274-279.
- [92] Corma, A.; García, H., *Chem. Rev.* **2003**, *103*, 4307-4366.
- [93] Macquarrie, D. J. Industrial Friedel–Crafts Chemistry In *Catalytic Asymmetric Friedel–Crafts Alkylations*; Wiley-VCH Verlag GmbH & Co. KGaA: 2009, p 271. 51
- [94] Jan, D.-Y. Y.; Barger, P. T. Processes on Industrial C-C Bond Formation In *Zeolites in Industrial Separation and Catalysis*; Wiley-VCH Verlag GmbH & Co. KGaA: 2010, p 505.
- [95] Perego, C.; Ingallina, P., *Catal. Today* **2002**, *73*, 3-22
- [96] *Production of Ethylbenzene from Benzene and Ethylene by Liquid-phase Alkylation Using Zeolite Catalysts*. Aspen Model Documentation
- [97] Market Study Benzene, published by Ceresana, July 2011
- [98] Weber, M.; Weber, M.; Kleine-Boymann, M. Phenol In *Ullmann's Encyclopedia of Industrial Chemistry*; Wiley-VCH Verlag GmbH & Co. KGaA: 2000.

-
- [99] Production of Isobutylbenzene via The Alkylation of Toluene with Propylene. IHS Markit.
- [100] De Almeida, J.; Dufaux, M.; Taarit, Y. B.; Naccache, C., *J. Am. Oil Chem. Soc.* **1994**, *71*, 675-694.
- [101] Kocal, J. A.; Vora, B. V.; Imai, T., Production of linear alkylbenzenes. *Appl. Catal., A.* **2001**, *221*, 295-301.
- [102] Oxgaard, J.; Periana, R. A.; Goddard, W. A., *J. Am. Chem. Soc.* **2004**, *126*, 11658-11665.
- [103] Oxgaard, J.; Muller, R. P.; Goddard, W. A.; Periana, R. A., *J. Am. Chem. Soc.* **2004**, *126*, 352-363.
- [104] Oxgaard, J.; Goddard, W. A., *J. Am. Chem. Soc.* **2004**, *126*, 442-443.
- [105] Kosswig, K. Surfactants In *Ullmann's Encyclopedia of Industrial Chemistry*; Wiley-VCH Verlag GmbH & Co. KGaA: 2000.
- [106] Crabtree, R. H., *Chem. Rev.* **2015**, *115*, 127-150.
- [107] Matsumoto, T.; Taube, D. J.; Periana, R. A.; Taube, H.; Yoshida, H., *J. Am. Chem. Soc.* **2000**, *122*, 7414-7415.
- [108] Periana, R. A.; Liu, X. Y.; Bhalla, G., *Chem. Commun.* **2002**, 3000-3001.
- [109] Bhalla, G.; Liu, X. Y.; Oxgaard, J.; Goddard, W. A.; Periana, R. A., *J. Am. Chem. Soc.* **2005**, *127*, 11372-11389.
- [110] Bhalla, G.; Bischof, S. M.; Ganesh, S. K.; Liu, X. Y.; Jones, C. J.; Borzenko, A.; Tenn, III W. J.; Ess, D. H.; Hashiguchi, B. G.; Lokare, K. S.; Leung, C. H.; Oxgaard, J.; Goddard, III W. A.; Periana, R. A., *Green Chem.* **2011**, *13*, 69-81.

-
- [111] Bhalla, G.; Periana, R. A., *Angew. Chem. Int. Ed.* **2005**, *44*, 1540-1543.
- [112] Bhalla, G.; Oxgaard, J.; Goddard, W. A.; Periana, R. A., *Organometallics* **2005**, *24*, 3229-3232.
- [113] Tenn, W. J.; Conley, B. L.; Bischof, S. M.; Periana, R. A., *J. Organomet. Chem.* **2011**, *696*, 551-558.
- [114] Lail, M.; Arrowood, B. N.; Gunnoe, T. B., *J. Am. Chem. Soc.* **2003**, *125*, 7506-7507.
- [115] Lail, M.; Bell, C. M.; Conner, D.; Cundari, T. R.; Gunnoe, T. B.; Petersen, J. L., *Organometallics* **2004**, *23*, 5007-5020.
- [116] Foley, N. A.; Lail, M.; Lee, J. P.; Gunnoe, T. B.; Cundari, T. R.; Petersen, J. L., *J. Am. Chem. Soc.* **2007**, *129*, 6765-6781.
- [117] Foley, N. A.; Lail, M.; Gunnoe, T. B.; Cundari, T. R.; Boyle, P. D.; Petersen, J. L., *Organometallics* **2007**, *26*, 5507-5516.
- [118] DeYonker, N. J.; Foley, N. A.; Cundari, T. R.; Gunnoe, T. B.; Petersen, J. L., *Organometallics* **2007**, *26*, 6604-6611.
- [119] Foley, N. A.; Ke, Z.; Gunnoe, T. B.; Cundari, T. R.; Petersen, J. L., *Organometallics* **2008**, *27*, 3007-3017.
- [120] Foley, N. A.; Lee, J. P.; Ke, Z.; Gunnoe, T. B.; Cundari, T. R., *Acc. Chem. Res.* **2009**, *42*, 585-597.
- [121] Burgess, S. A.; Joslin, E. E.; Gunnoe, T. B.; Cundari, T. R.; Sabat, M.; Myers, W. H., *Chem. Sci.* **2014**, *5*, 4355-4366.
- [122] Joslin, E. E.; Quillian, B.; Gunnoe, T. B.; Cundari, T. R.; Sabat, M.; Myers, W. H., *Inorg. Chem.* **2014**, *53*, 6270-6279.

-
- [123] Morello, G. R.; Cundari, T. R.; Gunnoe, T. B., *J. Organomet. Chem.* **2012**, *697*, 15-22.
- [124] Jia, X.; Gary, J. B.; Gu, S.; Cundari, T. R.; Gunnoe, T. B., *Isr. J. Chem.* **2017**, *57*, 1037-1046.
- [125] Luedtke, A. T.; Goldberg, K. I., *Angew. Chem. Int. Ed.* **2008**, *47*, 7694-7696.
- [126] Clement, M. L.; Grice, K. A.; Luedtke, A. T.; Kaminsky, W.; Goldberg, K. I., *Chem. Eur. J.* **2014**, *20*, 17287-17291.
- [127] McKeown, B. A.; Foley, N. A.; Lee, J. P.; Gunnoe, T. B., *Organometallics* **2008**, *27*, 4031-4033.
- [128] McKeown, B. A.; Gonzalez, H. E.; Gunnoe, T. B.; Cundari, T. R.; Sabat, M., *ACS Catal.* **2013**, *3*, 1165-1171.
- [129] McKeown, B. A.; Gonzalez, H. E.; Michaelos, T.; Gunnoe, T. B.; Cundari, T. R.; Crabtree, R. H.; Sabat, M., *Organometallics* **2013**, *32*, 3903-3913.
- [130] McKeown, B. A.; Gonzalez, H. E.; Friedfeld, M. R.; Brosnahan, A. M.; Gunnoe, T. B.; Cundari, T. R.; Sabat, M., *Organometallics* **2013**, *32*, 2857-2865.
- [131] McKeown, B. A.; Prince, B. M.; Ramiro, Z.; Gunnoe, T. B.; Cundari, T. R., *ACS Catal.* **2014**, *4*, 1607-1615.
- [132] McKeown, B. A.; Gonzalez, H. E.; Friedfeld, M. R.; Gunnoe, T. B.; Cundari, T. R.; Sabat, M., *J. Am. Chem. Soc.* **2011**, *133*, 19131-19152.
- [133] Davidson, J. M.; Triggs, C., *J. Chem. Soc. A.* **1968**, 1331-1334.
- [134] Tissue, T.; Downs, W. J., *J. Chem. Soc. D.*, **1969**, 410a-410a.
- [135] Henry, P. M., *J. Org. Chem.* **1971**, *36*, 1886-1890

-
- [136] L. Ebersson, L. Jonsson, *Acta Chem. Scand. B.* **1976**, 361.
- [137] Tetsuro, J.; Hiroshi, T.; Yuzo, F., *Chem. Lett.* **1987**, 16, 1865-1868.
- [138] Jintoku, T.; Takaki, K.; Fujiwara, Y.; Fuchita, Y.; Hiraki, K., *Bull. Chem. Soc. Jpn.* **1990**, 63, 438-441.
- [139] Yoneyama, T.; Crabtree, R. H., *J. Mol. Catal. A: Chem.* **1996**, 108, 35-40.
- [140] Emmert, M. H.; Gary, J. B.; Villalobos, J. M.; Sanford, M. S., *Angew. Chem. Int. Ed.* **2010**, 49, 5884-5886.
- [141] Emmert, M. H.; Cook, A. K.; Xie, Y. J.; Sanford, M. S., *Angew. Chem. Int. Ed.* **2011**, 50, 9409-9412.
- [142] Cook, A. K.; Sanford, M. S., *J. Am. Chem. Soc.* **2015**, 137, 3109-3118.
- [143] Cook, A. K.; Emmert, M. H.; Sanford, M. S., *Org. Lett.* **2013**, 15, 5428-5431.
- [144] Gary, J. B.; Cook, A. K.; Sanford, M. S., *ACS Catal.* **2013**, 3, 700-703.
- [145] Shrestha, A.; Lee, M.; Dunn, A. L.; Sanford, M. S., *Org. Lett.* **2018**, 20, 204-207.
- [146] Valderas, C.; Naksomboon, K.; Fernández-Ibáñez, M. Á., *ChemCatChem* **2016**, 8, 3213-3217.
- [147] Naksomboon, K.; Valderas, C.; Gómez-Martínez, M.; Álvarez-Casao, Y.; Fernández-Ibáñez, M. Á., *ACS Catal.* **2017**, 7, 6342-6346.
- [148] Wang, N.; McCormick, T. M.; Ko, S.-B.; Wang, S., *Eur. J. Inorg. Chem.* **2012**, 2012, 4463-4469.

[149] Desai, S. P.; Mondal, M.; Choudhury, J., *Organometallics* **2015**, *34*, 2731-2736.

[150] Majeed, M. H.; Shayesteh, P.; Wallenberg, L. R.; Persson, A. R.; Johansson, N.;
Ye, L.; Schnadt, J.; Wendt, O. F., *Chem. Eur. J.* **2017**, *23*, 8457-8465.

[151] Zultanski, S. L.; Stahl, S. S., *J. Organomet. Chem.* **2015**, *793*, 263-268.

[152] Li, L.; Wang, Y.; Yang, T.; Zhang, Q.; Li, D., *Tetrahedron Lett.* **2016**, *57*, 5859-5863.

2 Reductive Functionalization of Rh–Me Bonds with “Capping Arene” Supported Rh(III) Complexes

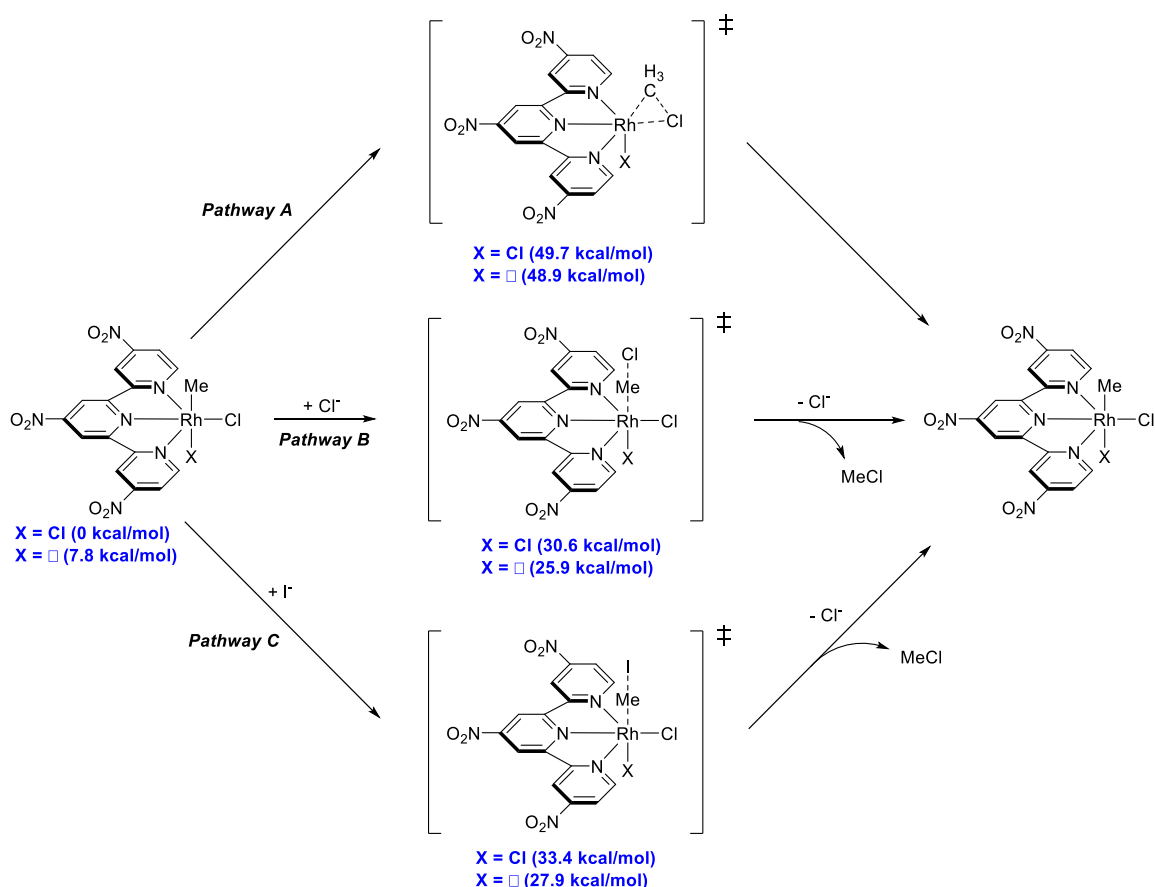
2.1 Introduction

Studies of reductive elimination (RE) of MeX from high-valent metal centers have been reviewed in Chapter 1. Many examples with Pt(IV) and Pd(II)/(III) have been reported. Compared with Pd and Pt, Rh shares several attractive features: 1. The less electrophilic metal should form weaker coordination bonds to water or functionalized product. 2. The Rh(I)/Rh(III) redox cycle are more accessible. 3. The formation of Rh(s) is less favored comparing to Pt(s) or Pd(s).

Milstein and coworkers recently reported that by introducing sterically bulky PCP or PNP pincer ligands destabilize Rh^{III} and lead to more facile RE of alkyl halide.^[1,2] In these reactions, π -acidic ligands (CO, CNR, MeCN) were used to trap and stabilize Rh(I) complexes. Two critical steps in transition metal mediated hydrocarbon functionalization, hydrocarbon C-H activation and reductive elimination of functionalized product, require opposite steric property from the metal complex, where steric crowded ligand will facilitate the RE by destabilizing Rh(III) but blocking the hydrocarbon from coordination to the Rh(I) complex. In order to avoid the complication created from the sterics, tuning electronic properties may provide an alternative approach towards an effective catalyst.

Recently, our group reported a series of terpyridine ligand supported Rh(III) complexes which can reductively eliminate methyl halide without π -acidic ligands.^[3] The electronic properties of terpyridine motif can be easily modulated without changing steric factors by simply appending the functional groups on the 4, 4' and 4'' positions of the ligand, which offers an opportunity to study electronic effect on RE of Rh^{III}–Me bonds. By

anchoring strong electron-withdrawing nitro groups on the terpyridine ligand, the stability of Rh^{III}-Me complexes are reduced, which permits reductive elimination of MeX [X = Cl, TFA (TFA = trifluoroacetic acetate)]. With excess amount (3 equiv.) of Cl⁻ or TFA⁻ additives, the reaction can reach 25% and 28% MeX yield respectively. In contrast, the 4,4',4''-tri-*tert*-butylterpyridine ligand supported Rh^{III}-Me complex did not produce any MeX under the same reaction conditions. Due to the poor solubility of the nitro-substituted terpyridine Rh complexes, the mechanism was only investigated by DFT calculation. Concerted mechanism (pathway A) and Cl⁻ (pathway B) or I⁻ (pathway C) assisted S_N2 mechanisms were calculated (Scheme 2.1.1). Calculated energy barriers of the S_N2 pathways are significantly lower than the concerted pathway. In addition, dissociating the *trans*-halide to form a cationic complex prior to reductive functionalization lowers the transition energy barrier to nucleophilic attack by ~5 kcal/mol. The energy difference of nucleophilic attack with Cl⁻ and I⁻ is very small, which indicated that pathway C is a possible mechanism.



Scheme 2.1.1. DFT calculation of three pathways for reductive functionalization of a terpyridine $\text{Rh}^{\text{III}}\text{-Me}$ complex.

The RE of terpyridine $\text{Rh}^{\text{III}}\text{-Me}$ complex in acidic media has been systematically studied in a follow up paper.^[4] Three different protic solvents (D_2O , DOAc and $\text{HTFA}/\text{C}_6\text{D}_6$ [5:1 v:v]) were used, 41%, 57% and 52% MeX yield were obtained, respectively, with free I^- addition. DFT calculations were used to proposed a $\text{S}_{\text{N}}2$ attack either by I^- or conjugated base (e.g., OAc^- or TFA^-) of acid solvent. The dissociation of the *trans*-halide slightly inhibits the RE reaction, which contrasts to the result of RE in non-acidic media. Proton is predicted to bind to the axial chloride through a hydrogen bond, which makes it a better leaving group. This weaker interaction reduces the energy barrier by 5 kcal/mol in acidic media. The RE in D_2O is unusual in comparison to acetic acid or HTFA . No MeI or MeCl was observed in the reaction. In addition, the addition of Cl^- or I^- additive has a negligible

effect on the yield. This unusual observation indicates that the RE in D₂O may undergo a different pathway and water coordination is an important factor to this conversion. Methane formation from Rh^{III}-Me complex is observed from the reaction, which is undesired side reaction. DFT calculations suggested CH₄ formation via Rh^{III}-Me bond homolysis is more favorable than simple protonation, and high temperature (150 °C) could facilitate the generation of methyl radicals. However, experimental verification of methyl radical was not achieved.

2.2 Results and Discussions

2.2.1 Synthesis of Rh Capping Arene Complexes

Previously, our group developed a series of “capping arene” ligands supported Rh complexes which potentially can be a good candidate for homogenous methane partial oxidation since a coordination site on Rh(III) will be blocked by an arene ring.^[5] Generally, the Rh(III) oxidation state generally favors the formation of octahedral complexes that provide electronically saturated 18-electron structures. However, by blocking one coordination site with a weakly coordinating arene group, the Rh(III) state might be destabilized, which can make Rh(I)/Rh(III) redox cycles more feasible.

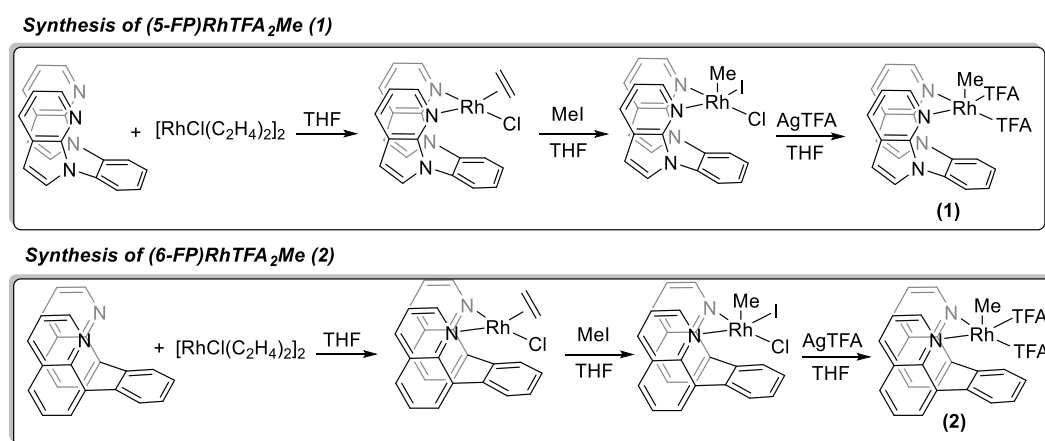


Figure 2.2.1. Synthetic routes for (5-FP)Rh(TFA)₂Me (1) and (6-FP)Rh(TFA)₂Me (2).

Two “capping arene” ligand supported Rh complexes (5-FP)Rh(TFA)₂Me (**1**) [5-FP = 1,2-bis(*N*-7-azaindolyl)benzene] and (6-FP)Rh(TFA)₂Me (**2**) [6-FP = 8,8'-(1,2-phenylene)diquinoline]) were synthesized. Two different fragments in 5-FP and 6-FP, *N*-7-azaindolyl and 8-quinoline respectively, create two different bond angles via the phenyl linkage and result in different distances between Rh metal center and the capping benzene ring under Rh. Both complexes were synthesized through similar synthetic routes (Figure 2.2.1). Using the synthesis of (5-FP)Rh(TFA)₂Me as an example, the first step is mixing the 5-FP ligand and [Rh(μ -Cl)(η^2 -C₂H₄)]₂ in THF solution to form (5-FP)Rh(Cl)(η^2 -C₂H₄). The ¹H NMR spectrum of this Rh(I) complex (Figure 2.2.2), reveals two broad peaks for the coordinated ethylene, which is consistent with rapid rotation of ethylene on the timescale of the NMR experiment. A small coupling constant (~1.5 Hz) is observed between Rh and all the hydrogen atoms on C6 arene ring of the ligand, which indicates weak coordination of arene moiety to the Rh center.

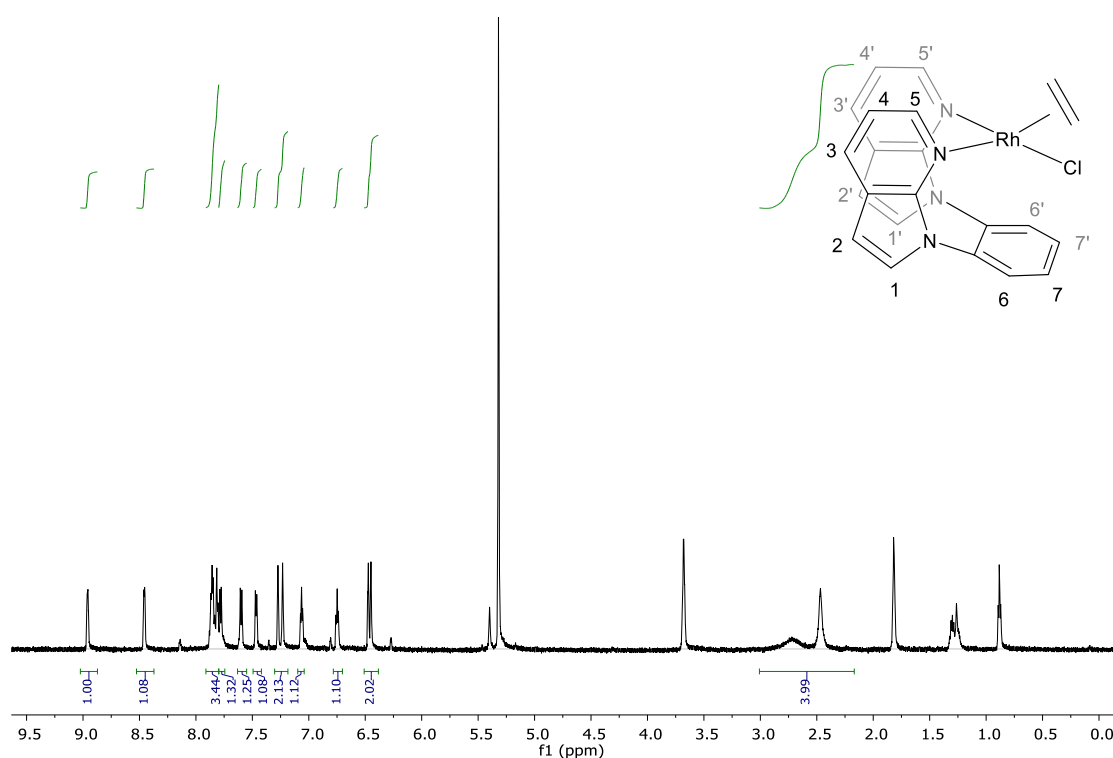


Figure 2.2.2 ^1H NMR spectrum for $(5\text{-FP})\text{Rh}(\text{Cl})(\eta^2\text{-C}_2\text{H}_4)$ in $\text{DCM-}d_2$.

An easy synthetic method to access $\text{Rh}(\text{III})\text{-CH}_3$ complexes is through the oxidative addition of MeX ($\text{X} = \text{OAc}$, TFA or halide) starting from a $\text{Rh}(\text{I})$ complex. However, the $(5\text{-FP})\text{Rh}(\text{Cl})(\eta^2\text{-C}_2\text{H}_4)$ is inert to oxidation of MeOAc or MeTFA even at high temperature ($100\text{ }^\circ\text{C}$) and only undergoes slow oxidation with MeI . The addition of 5 equiv. of MeI is added to the THF solution of $(5\text{-FP})\text{Rh}(\text{Cl})(\eta^2\text{-C}_2\text{H}_4)$, a color change from brown to yellow, which indicates the formation of $\text{Rh}(\text{III})$ complexes. $(5\text{-FP})\text{Rh}(\text{Cl})(\text{I})\text{Me}$ is synthesized after 48 hours at room temperature. Three peaks at 3.36, 3.40 and 3.43 ppm in ^1H NMR spectrum (Figure 2.2.3) reveals the formation of three Rh-CH_3 units, each appearing as a doublet ($^2J_{\text{Rh-H}} = 2\text{ Hz}$). Thus we prospected the $(5\text{-FP})\text{Rh}(\text{Cl})(\text{I})\text{Me}$ is a combination of three isomers, which leads to a complicated aromatic region.

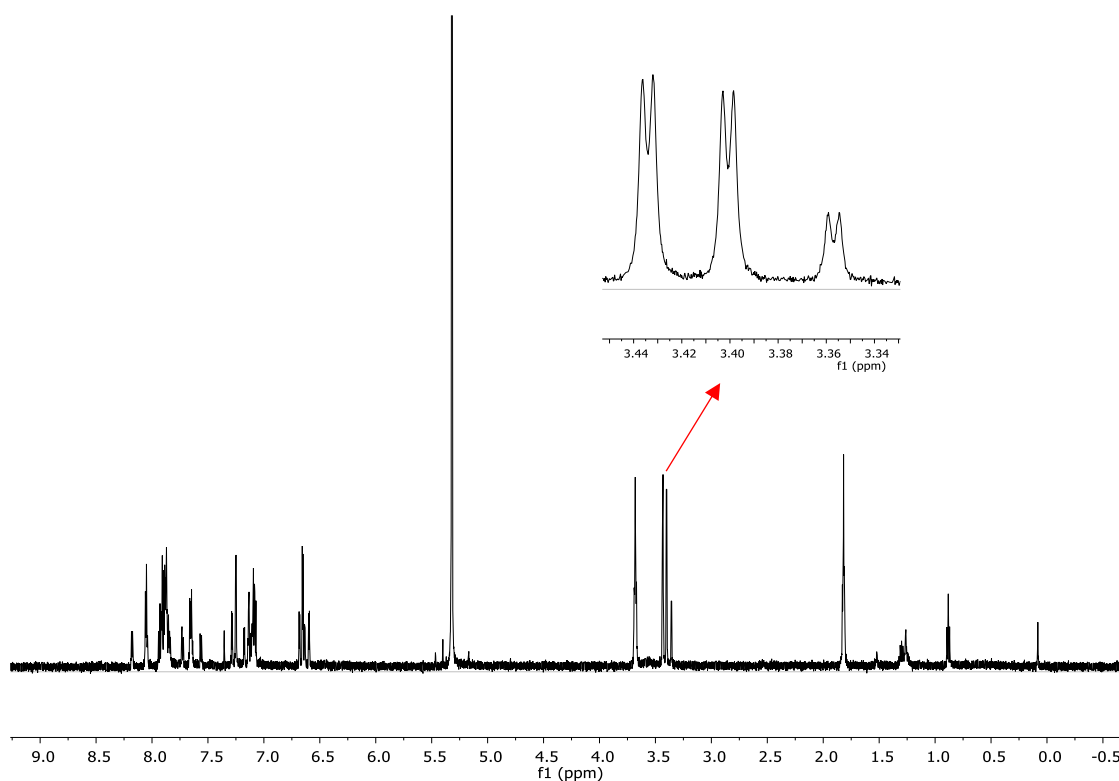


Figure 2.2.3 ^1H NMR spectrum for three isomers of $(5\text{-FP})\text{Rh}(\text{Cl})(\text{I})\text{Me}$ in $\text{DCM-}d_2$.

The substitution of halides by TFA is accomplished by adding two equivalents AgTFA

to a THF solution of (5-FP)Rh(Cl)(I)Me. The immediate formation of a white precipitate indicates successful ligand exchange. After stirring overnight at room temperature, the color of solution changed to light yellow and a white solid is obtained after work-up. The formation of complex **1** was confirmed by ^1H NMR spectroscopy (Figure 2.2.4), a doublet at 3.06 ppm ($^2J_{\text{Rh-H}} = 2$ Hz) reveals the formation of a Rh–CH₃ moiety and the corresponding ^{13}C nucleus resonates at 21.8 ppm ($^1J_{\text{Rh-C}} = 28$ Hz). The synthesis of complex **2** is nearly identical to that of complex **1** except that MeI oxidation step is completed in only 24 hours. This observation may indicate a lower barrier for the oxidative addition of MeI with complex **2** compared to that of complex **1**.

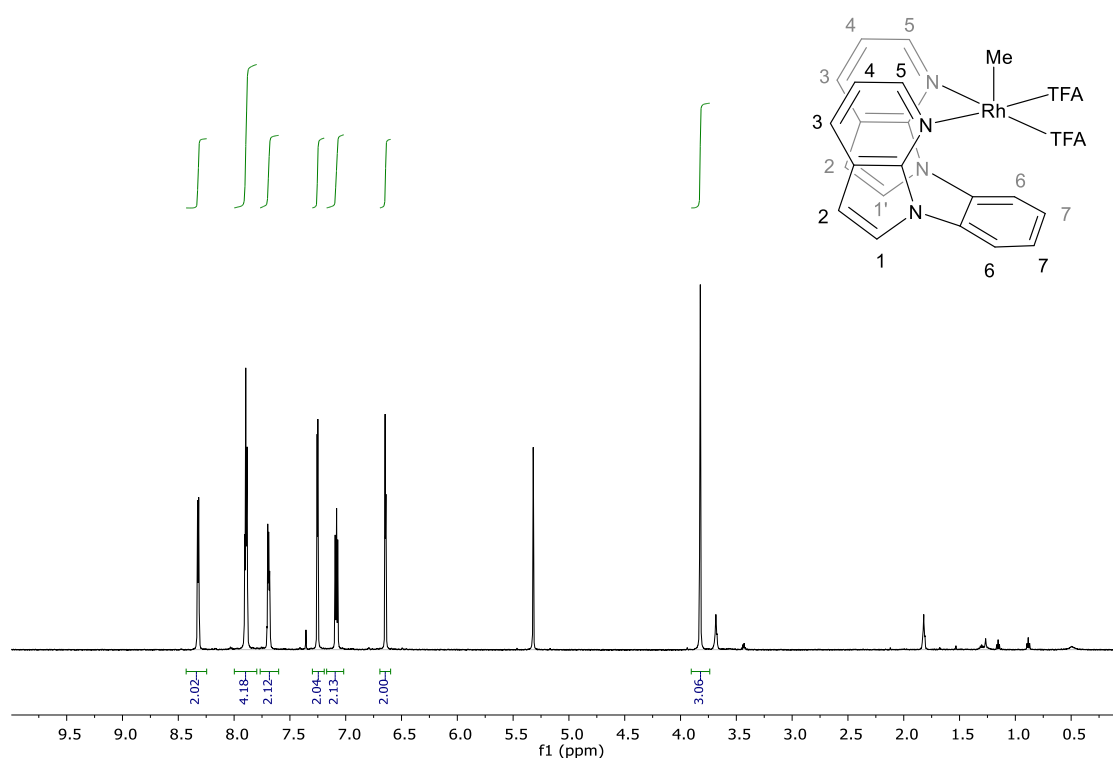


Figure 2.2.4 ^1H NMR spectrum for (5-FP)Rh(TFA)₂Me (**1**) in $\text{DCM-}d_2$.

2.2.2 Structure Comparison of Two Different Capping Arene Complexes

In order to further understand the complex structure and the orientation of the capping

arene ligand, a single crystal of (6-FP)Rh(TFA)₂Me is prepared and used for X-ray diffraction (XRD) characterization (Figure 2.2.5). When investigating the structure of complex **2**, the arene ring of the ligand is positioned with Rh–C10 and Rh–C15 distances of 2.631(2) Å and 2.572(3) Å, respectively. As expected, these distances are longer than a typical Rh–C single bond,^[6-9] which indicates a weak coordination between Rh and the arene moiety. However, the quinoline is distorted in order to bring the C10–C15 underneath the Rh center to make it a suitable η^2 coordination. In addition, the bond length of C10–C15 is 1.415(3) Å, which is the longest bond among the benzene ring.

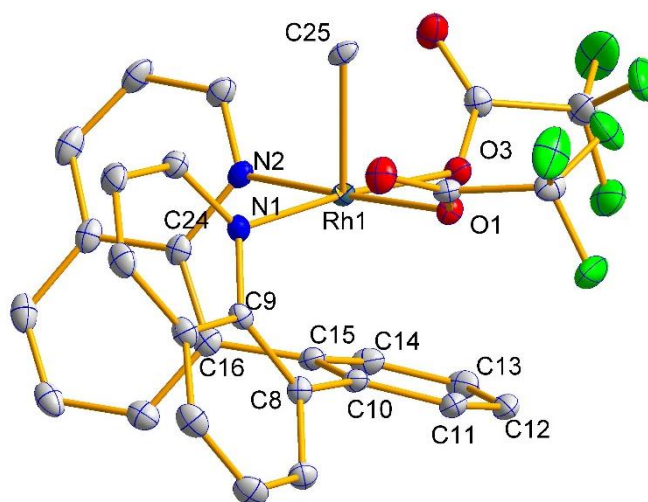


Figure 2.2.5. ORTEP of (6-FP)Rh(TFA)₂Me (**2**). Displacement ellipsoids are drawn at the 50% probability level, and hydrogen atoms are omitted for clarity. Selected bond lengths (Å): Rh1–N1 2.038(2), Rh1–N2 2.056(2), Rh1–O1 2.046(1), Rh1–O3 2.032(1), Rh–C25 2.074(2), Rh–C10 2.631(2), Rh1–C15 2.572(2), Selected bond angles (deg): C9–C8–C10 122.6(2), C24–C16–C15 117.8(2), N1–Rh1–N2 88.99(6), O1–Rh1–O3 80.63(5), N1–Rh1–C25 92.09(7).

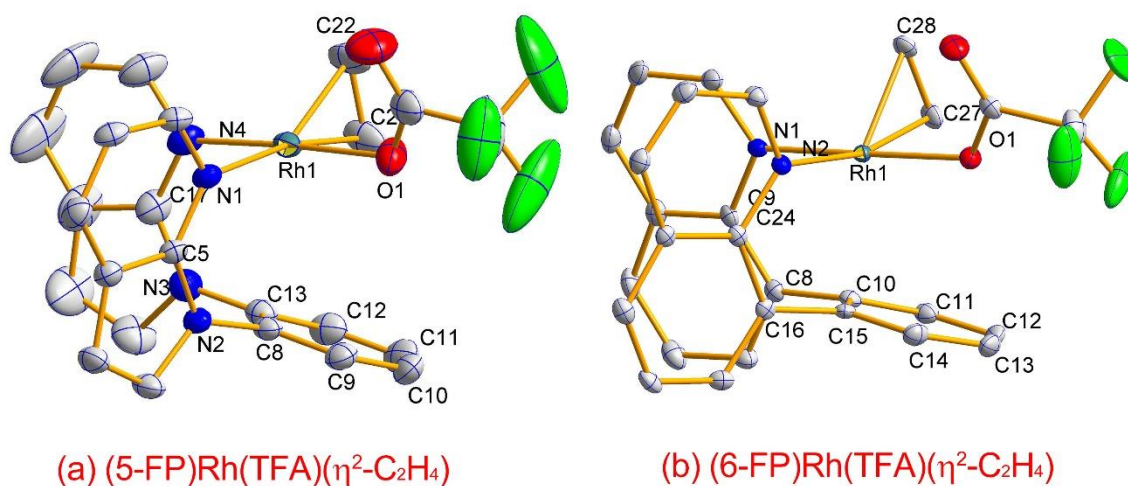


Figure 2.2.6. ORTEP of (5-FP)Rh(TFA)(η^2 -C₂H₄) and (6-FP)Rh(TFA)(η^2 -C₂H₄). Displacement ellipsoids are drawn at the 50% probability level, and hydrogen atoms are omitted for clarity. (a) (5-FP)Rh(TFA)(η^2 -C₂H₄): Selected bond lengths (Å): Rh1–C21 2.101(3), Rh1–C22 2.096(3), C8–Rh1 3.002(3), C13–Rh1 3.008(3), N1–Rh1 2.134(2), N4–Rh1 2.022(2). Selected bond angles (deg): C5–N2–C8 127.0(2), C17–N3–C13 128.4(2), N1–Rh1–N4 86.94(9), C22–Rh1–C21 38.8(1). (b) (6-FP)Rh(TFA)(η^2 -C₂H₄): Selected bond lengths (Å): Rh1–C27 2.087(2), Rh1–C28 2.078(2), C10–Rh1 2.509(2), C15–Rh1 2.649(2), N1–Rh1 2.005(2), N2–Rh1 2.180 (2). Selected bond angles (deg): C24–C16–C15 120.6(2), C9–C8–C10 122.6(2), N1–Rh1–N2 84.32(7), C27–Rh1–C28 39.86(9).

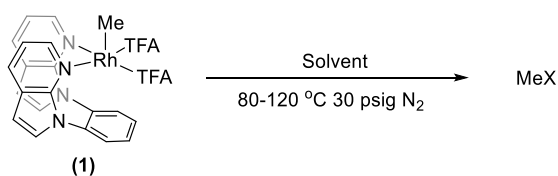
The growth of single crystal of (5-FP)Rh(TFA)₂Me has not been successful so far. Two Rh(I) complexes with a 5-FP and 6-FP ligand respectively [(5-FP)Rh(TFA)(η^2 -C₂H₄) and (5-FP)Rh(TFA)(η^2 -C₂H₄)] are used to compare the difference between two ligands (Figure 2.2.6). When comparing the structure of complex **2** and (6-FP)Rh(TFA)(η^2 -C₂H₄), their bond distances and bond angles are similar, which makes (5-FP)Rh(TFA)(η^2 -C₂H₄) a suitable replacement of complex **1** for structure comparison. The distance of the Rh center to the benzene ring is represented by C8–Rh1 and C13–Rh which are 3.002(3), 3.008(3) respectively in (5-FP)Rh(TFA)(η^2 -C₂H₄). These distances are significant longer than similar distances (Rh–C10 and Rh–C15) in (6-FP)Rh(TFA)(η^2 -C₂H₄) and complex **2**. The bond angle C5–N2–C8 and C17–N3–C13 in (5-FP)Rh(TFA)(η^2 -C₂H₄) that can represent

the linkage of *N*-7-azaindole to the benzene motif are larger than the corresponding angles in 6-FP supported Rh complexes (127.0° vs 120.6°). The larger angle indicates that the 5-FP ligand positions the arene ring further from the Rh center. In addition, the bond length of C8–C13 is 1.398(4) Å, which is nearly identical to C–C bond length in free benzene (1.400 Å). This observation indicates that the η^2 coordination of benzene ring in 5-FP is not accessible or negligible. Based on what we have learned from the crystal structures, we predicted that 5-FP is a better ligand in terms of blocking coordination to a sixth site in Rh^{III} complexes.

2.2.3 Solvent Screening for RE of MeX from Complex 1

(5-FP)Rh(TFA)₂Me was tested for possible RE of MeX in a series of solvents. The results are summarized in Table 2.2.1. All reactions were performed in J-young NMR tubes containing the solvent indicated in the Table 2.2.1 with 0.01M complex **1** and 30 psig N₂. The reaction time was recorded when the MeX yield stop increasing or begin decreasing due to product decomposition. The MeX yield was determined by ¹H NMR spectroscopy using hexamethyldisiloxane in sealed capillary as an internal standard.

Table 2.2.1. Solvent screening for RE of MeX from complex **1**.



| Entry | Solvent | Temperature (°C) | Time (h) | MeX & Yield |
|-------|---------|------------------|----------|-------------|
| 1 | Benzene | 120 | 36 | N.D. |
| 2 | THF | 110 | 36 | N.D. |
| 3 | Acetone | 120 | 36 | 3% MeOH |
| 4 | DCM | 120 | 48 | 8(1)% MeTFA |

| | | | | |
|---|-------------------|-----|----|----------------|
| 5 | MeNO ₂ | 110 | 24 | 5(1) % unknown |
| 6 | DMSO | 120 | 36 | N.D. |
| 7 | MeCN | 80 | 84 | 48 (2)% MeTFA |
| 8 | HOAc | 80 | 75 | 19(2)% MeOAc |
| 9 | HOAc | 100 | 10 | 18(2)% MeOAc |

When heating the complex **1** in benzene, no MeX production was observed. As shown in Figure 2.2.7, the Rh-CH₃ appears at 3.90 ppm in the ¹H NMR spectrum. Complex **1** is relatively stable in benzene at 90 °C and no changes were observed in the spectra after 12 hours. When raising the temperature to 100 °C, complex **1** began to slowly decompose. All peaks decreased simultaneously but a peak for MeX product was not detected. Elevating the temperature to 110 or 120 °C accelerates complex decomposition, which is similar to what we observed in THF.

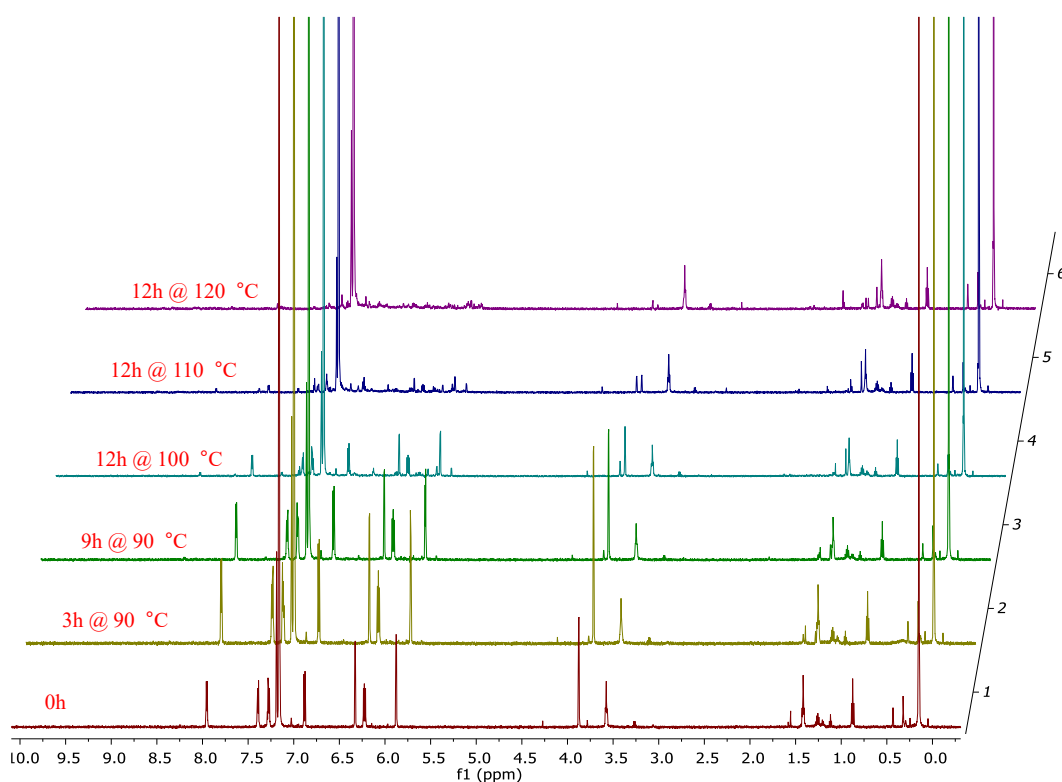


Figure 2.2.7. Stacked ¹H NMR spectra for RE of MeX from complex **1** in benzene-*d*₆.

Heating complex **1** in acetone and DCM gave 3% yield of MeOH and 8% yield of MeTFA. The reaction in MeNO₂ gives an unknown peak at 3.58 ppm, which is possibly a

MeX product, however, we cannot confirm the identity. Among all the solvents, acetonitrile gave the best results leading to 48% yield of MeTFA after 84 hours reaction at 80 °C. In addition, the changes in the ^1H NMR spectra are quite intriguing (Figure 2.2.8). The Rh-CH₃ peak first appears at 3.78 ppm, and it shifts to 3.68 ppm upon heating. The overlapping of peaks in the aromatic region indicated the symmetry of the complex was reduced during the reaction. This observation indicates that MeCN likely coordinates to Rh by displacement of a TFA ligand. The cationic [(5-FP)Rh(TFA)(MeCN)Me][TFA] intermediate can then undergo RE of MeTFA from a 5-coordinate metal center leading to [(5-FP)Rh(MeCN)₂][TFA], which is in agreement with the symmetric product obtained at the end of reaction.

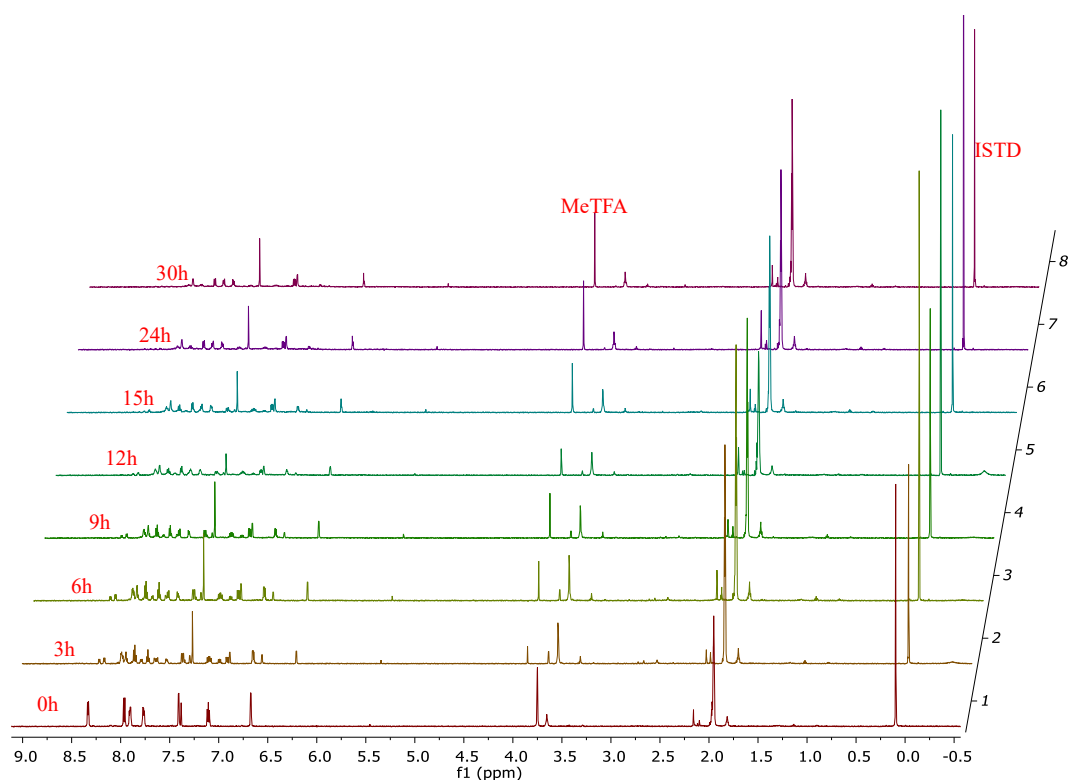


Figure 2.2.8. Stacked ^1H NMR spectra for RE of MeX from complex **1** in MeCN-*d*₄ at 90 °C.

Similar changes in the ^1H NMR spectra during the reaction are also be observed in

DMSO- d_6 (Figure 2.2.9). Instead of displacing one TFA, DMSO appears to replace both TFA ligands in the first coordination sphere, which keeps the complex symmetrical. The Rh-CH₃ peak is shifted up field to 2.02 ppm. However, no MeX product was observed upon heating at 100 °C for 12h. When raising temperature to 120 °C, the methyl peak disappeared and still no MeX product was observed after 24 hours. This result may indicate that the RE of MeX is inhibited by DMSO coordination. Furthermore, the complex **1** was tested in acetic acid, obtaining 19% yield of MeOAc at 80 °C. Raising the temperature to 100 °C accelerated the reaction; however there was no increase in yield of MeOAc (Table 2.2.1, entries 8-9).

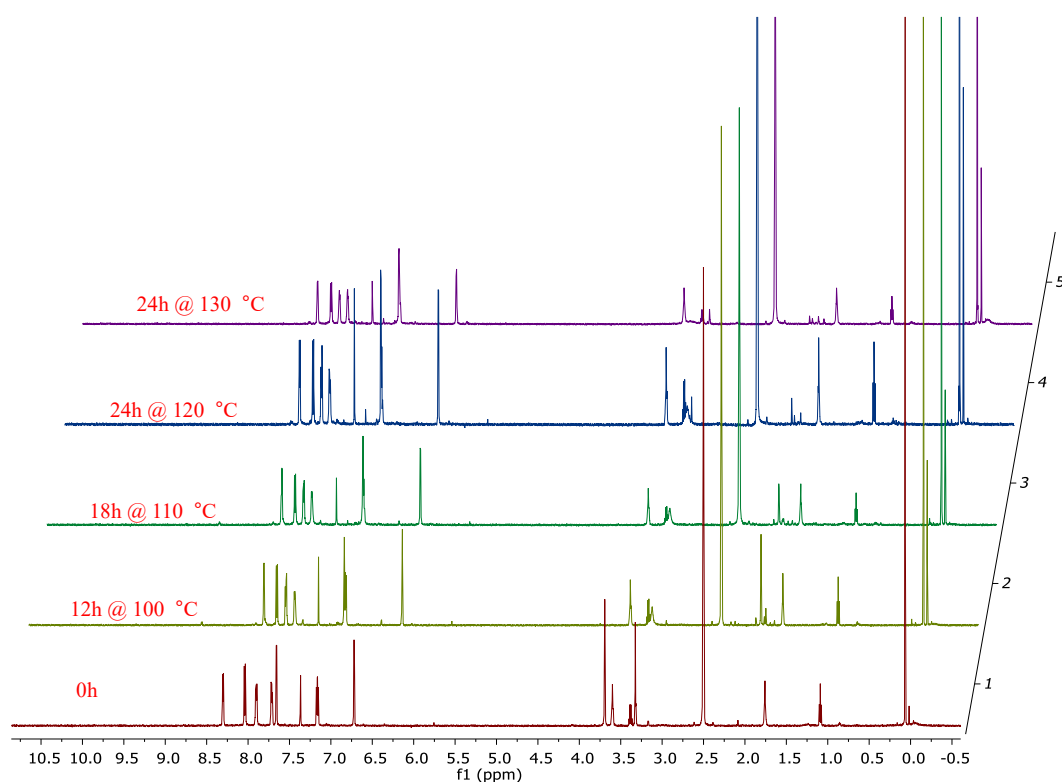


Figure 2.2.9. Stacked ¹H NMR spectra for RE of MeX from complex **1** in DMSO- d_6 .

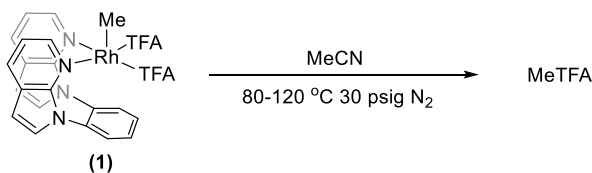
Since complex **1** gave optimal MeX yield in MeCN, (6-FP)Rh(TFA)₂Me (**2**) was tested for possible RE of MeX. In MeCN, complex **2** is stable at 80 °C and slow reductive elimination of MeTFA from complex **2** at 90 °C. After heating in MeCN for 72h, only 4%

yield of MeTFA was observed with ~50% starting material remaining. This observation indicates that complex **1** is likely undergoes RE of MeX more rapidly than complex **2** and the result supports our hypothesis that 5-FP could effectively destabilized the Rh(III) and significantly promotes the RE of MeX. By utilizing the steric effect around the metal center, we can control the electronic property of the Rh. No example of this type of ligand design was reported before.

2.2.4 Temperature Optimization for RE of MeX from Complex 1

Since MeCN proved to be the best solvent for the reductive functionalization of Rh–Me bond in complex **1**, a systematic temperature optimization was carried out. Complex **1** was heated in MeCN from 80 to 120 °C. The yield after 24 hours and at the end of the reaction were recorded for comparison of 80 °C, 85 °C and 90 °C. Less than 12 hours was needed for complete conversion at 100 °C or higher temperatures. At 110 °C and 120 °C, we observed significant complex decomposition and evidence of Rh mirror on the NMR tubes, leading to low yields of MeX. For the reaction below 100 °C, comparable yield was observed in all the reactions, while the reaction rate increased with higher temperatures. Throughout the reactions, 90 °C proved to be the optimal temperature.

Table 2.2.2. Temperature optimization for RE of MeX from complex **1** in MeCN.



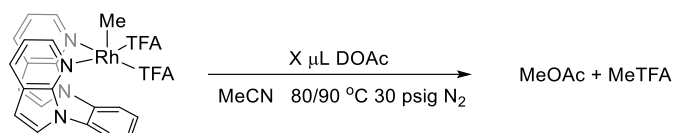
| Entry | Temperature (°C) | Time (h) | MeTFA Yield (%) |
|-------|------------------|----------|-----------------|
| 1 | 80 | 24 | 33(2) |
| 2 | 80 | 84 | 48(2) |
| 3 | 85 | 24 | 46(1) |
| 4 | 85 | 42 | 52(1) |

| | | | |
|---|-----|----|-------|
| 5 | 90 | 24 | 51(1) |
| 6 | 90 | 30 | 55(2) |
| 7 | 100 | 12 | 42(3) |
| 8 | 110 | 12 | 29(3) |
| 9 | 120 | 12 | 11(2) |

2.2.5 Influence of Acid Additive effect on RE of MeX from Complex 1

Acidic solvents are often used for catalytic methane functionalization, as acid media is often poorly coordinating which reduces competition with methane for metal coordination. Also for electrophilic C–H bond activation, the electron withdrawing conjugate base (X^-) can prevent the functionalized MeX product from further oxidation.^[10] In order to investigate the effect of acid on RE of MeX from complex **1**, acetic acid and water were added to the reaction. Different amount of did not give dramatically different results (Table 2.2.3, entries 1-5 and 7). In all cases, the acid additive can increase the MeX yield by approximately 10%. The major effect of acetic acid is that it shifts the MeX formation from MeTFA to MeOAc. The MeOAc : MeTFA ratio increased from 1:5 to 1:1 when increasing the acid addition from 10 μ L to 100 μ L. Addition of a large amount of acid can slightly accelerate the reaction (Table 2.2.3, entry 7). In addition, the water addition can increase the yield of MeX to a similar extent as acetic acid. If the RE and oxidative addition of MeX is in equilibrium, the removal of MeTFA can lead to higher MeX production. Since MeTFA can be converted to MeOH in presence of water, this may be the reason for the increased MeX production.

Table 2.2.3. Influence of acid additive on the RE of MeX from complex **1** in MeCN.



| Entry | Temperature (°C) | Time (h) | Acid Loading (μL) | MeX Yield (%) | | |
|-------|---------------------|-------------|-----------------------|---------------|-------|-------|
| | | | | MeOAc | MeTFA | Total |
| 1 | 80 | 84 | 0 | 0 | 48(2) | 48(2) |
| 2 | 80 | 84 | 10 | 11(1) | 51(1) | 62(2) |
| 3 | 80 | 84 | 20 | 23(1) | 36(3) | 59(3) |
| 4 | 80 | 84 | 50 | 23(1) | 53(1) | 58(2) |
| 5 | 80 | 84 | 10 (D ₂ O) | 7 (MeOH) | 54 | 61 |
| 6 | 90 | 30 | 0 | 0 | 55(2) | 55(2) |
| 7 | 90 | 24 | 100 | 29(1) | 29(5) | 58(6) |

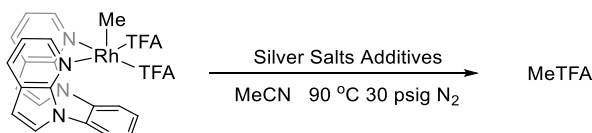
2.2.6 Influence of Silver Oxidant Additives on RE of MeX from Complex 1

Another way to promote MeX production is using oxidizing additives. By adding a strong oxidant to the reaction, Rh(III) is potentially oxidized to a higher oxidation state, which can result in more rapid reductive elimination of MeX. Silver(II) salts are strong oxidants. Three Ag(II) additives AgF₂, AgO and silver picolinate were used in the reaction of RE of MeX from complex 1. Surprisingly, the strong oxidant silver picolinate reduced the MeTFA yield to 23% (compared to 55% yield without the Ag oxidant) and the reaction stopped at 24 hours. Both AgF and AgF₂ can push the yield to ~73%, while the reaction with AgF₂ requires less reaction time than AgF (48h vs 72h). In addition, several Ag(I) oxidants were tested for this transformation. Silver nitrite had no effect on the reaction and AgOAc decreased the yield. Interestingly, no MeOAc was produced with AgOAc, and the MeTFA yield was decreased after 48 hours. AgTFA has similar effect as AgF₂, however, product decomposition was also observed. Among all the oxidant additives, the AgOTf is the most effective oxidant additive for RE of MeX from **1**. With 2 equivalents of AgOTf, the reaction can reach 94% MeTFA yield after 114 hours. This results in the highest MeX

yield among the Rh mediated RE process. By increasing the AgOTf loading to 4 equivalents, the MeTFA yield drops to 85%. However, the reaction rate is slightly enhanced. Through this oxidant additive screening study, the oxidation potential of the silver salts may not be the only factor that influence the MeX production. The counter ion may also play an important role here.

Copper salts are considered to be a prospective replacement for silver oxidant in many cases. However, when adding Cu(OAc)₂, Cu(TFA)₂ or Cu(OTf)₂ to the acetonitrile solution of complex **1**, none of them gives over 20% MeX yield. This result may be explained by the big oxidation potential difference between Cu(I)/Cu(II) and Ag(I)/Ag(0) (+0.34V vs +0.80V).

Table 2.2.4. Silver oxidants effect on RE of MeX from complex **1** in MeCN.



| Entry | Additives | Loading (eq.) | Time (h) | MeTFA Yield (%) |
|-------|---------------------------|---------------|----------|-----------------|
| 1 | AgO | 2 | 60 | 49(5) |
| 2 | AgOTf | 2 | 114 | 94(2) |
| 3 | AgOTf | 4 | 90 | 85(1) |
| 4 | AgF | 2 | 72 | 73 |
| 5 | AgF ₂ | 2 | 48 | 72 |
| 6 | Ag(picolate) ₂ | 2 | 24 | 23(4) |
| 7 | AgNO ₂ | 2 | 24 | 43(4) |
| 8 | AgTFA | 2 | 48 | 72(1) |
| 9 | AgOAc | 2 | 48 | 27(3) |

2.3 Conclusions

In later transition metal catalyzed methane functionalization, C–H activation and

reductive elimination of functionalized product, require opposite steric property from the metal complex, where steric crowded ligand will facilitate the RE by destabilizing Rh(III) but blocking the hydrocarbon from coordination to the Rh(I) complex. In this chapter, we want to use steric effect to control the electron property of the metal center to facilitate the RE step without inhibition of C–H activation step. We developed two different “capping arene” ligands, 5-FP and 6-FP, were coordinated to Rh with the goal of preventing the coordination of a sixth strongly donating ligand to the metal center. In the “capping arene” ligands supported Rh(III) complexes if the Rh-arene interaction is considered negligible, the metal center can only have 5-coordinate 16-electron structures. Through this designed structure, we expect that the Rh(III) oxidation state is destabilized, which could facilitate the reductive elimination of MeX from Rh(III) methyl complexes. Two Rh(III) complexes, (5-FP)Rh(TFA)₂Me and (6-FP)Rh(TFA)₂Me, were synthesized and tested for the reductive elimination reaction. For the 5-FP ligated complex, the benzene motif in the ligand is pushed further away from Rh center to prevent the possible η^2 coordination that discovered in 6-FP ligated complex. In this case, (5-FP)Rh(TFA)₂Me outperformed (6-FP)Rh(TFA)₂Me in MeX elimination. With the help of AgOTf additive, (5-FP)Rh(TFA)₂Me can achieve 94% of MeTFA yield in MeCN at 90 °C, which is the best MeX yield from Rh(III) methyl complexes up to date.

2.4 Experimental Section

[Rh(η^2 -C₂H₄)₂(μ -Cl)]₂, 1,2-bis(*N*-7-azaindoly)benzene (5-FP) and 8,8'-(1,2-phenylene)diquinoline (6-FP) were prepared according to literature procedures.^[11-13] All other reagents were purchased from commercial sources and used as received.

Synthesis of (5-FP)RhCl(η^2 -C₂H₄). A THF solution (10 mL) of 1,2-bis(*N*-7-azaindoly)benzene (0.0810 g, 2.61×10^{-4} mol) was added to a THF solution (10 mL) of [Rh(η^2 -C₂H₄)₂(μ -Cl)]₂ (0.0572 g, 1.47×10^{-4} mol) dropwise and stirred for 24 h. The reaction mixture was dried under vacuum. The resulting solid was dissolved in minimal THF (4 mL), and pentane (30 mL) was added to the solution to give a brown precipitate. The solid was collected by filtration, washed with pentane (3×10 mL), and dried under vacuum to afford the analytically pure (5-FP)RhCl(η^2 -C₂H₄) (0.0890 g, yield = 70%). ¹H NMR (600 MHz, methylene chloride-*d*₂) δ 8.96 (dd, ³*J*_{HH} = 5.3, 1.3 Hz, 1H, 5 or 5'), 8.46 (d, ³*J*_{HH} = 5.6 Hz, 1H, 5 or 5'), 7.89 – 7.80 (m, 3H, three of 6, 6', 7, 7'), 7.78 (dd, ³*J*_{HH} = 7.8, 1.4 Hz, 1H, 3 or 3'), 7.60 (dd, ³*J*_{HH} = 7.9, 1.4 Hz, 1H, 3 or 3'), 7.50 – 7.42 (m, 1H, one of 6, 6', 7 and 7'), 7.27 (d, ³*J*_{HH} = 3.6 Hz, 1H, 1 or 1'), 7.23 (d, ³*J*_{HH} = 3.6 Hz, 1H, 1 or 1'), 7.06 (dd, ³*J*_{HH} = 7.9, 5.3 Hz, 1H, 4 or 4'), 6.75 (dd, ³*J*_{HH} = 7.8, 5.5 Hz, 1H, 4 or 4'), 6.47 (d, ³*J*_{HH} = 3.6 Hz, 1H, 2 or 2'), 6.45 (d, ³*J*_{HH} = 3.6 Hz, 1H, 2 or 2'), 2.59 (br, 4H, ethylene).

Synthesis of (5-FP)RhCl(I)Me. Iodomethane (0.072 mL, 1.16×10^{-3} mol) was added to a THF solution (30 mL) of (5-FP)RhCl(η^2 -C₂H₄) (0.1110 g, 2.32×10^{-4} mol) dropwise and stirred for 48 h. The reaction mixture was dried under vacuum. The resulting solid was dissolved in minimal THF (4 mL), and pentane (30 mL) was added to the solution to give a yellow precipitate. The solid was collected by filtration, washed with pentane (3×10 mL), and dried under vacuum to afford the a combination three isomers of (5-FP)Rh(Cl)(I)Me (0.101 g, yield = 74%).

Synthesis of (5-FP)Rh(TFA)₂Me (1). A THF solution (30 mL) of (5-FP)Rh(Cl)(I)Me

(0.1210 g, 2.05×10^{-4} mol) was prepared and AgTFA (0.0906g, 4.10×10^{-4} mol) was added to the solution and shielded from the light. After stirring for 24h, the reaction mixture was filtered through Celite. The filtrate was dried under vacuum. The resulting solid was dissolved in minimal THF (4 mL), and pentane (30 mL) was added to the solution to give a white precipitate. The solid was collected by filtration, washed with pentane (3 x 10 mL), and dried under vacuum to afford the analytically pure (5-FP)Rh(TFA)₂Me (0.127g, yield = 95%). X-ray quality crystals of **1** were grown by the vapor diffusion method using THF and *n*-pentane. ¹H NMR (600 MHz, methylene chloride-*d*₂): δ = 8.82 (d, ³*J*_{HH} = 5.3 Hz, 2H, 1), 8.14 (dd, ³*J*_{HH} = 8.2, ⁵*J*_{RH} 1.4 Hz, 2H, 3), 7.78 (dd, *J* = 5.9, 3.4 Hz, 2H, 7 or 8), 7.65 (m, 4H, and 7 or 8), 7.51 – 7.43 (m, 4H, 5 and 4 or 6), 7.31 (dd, ³*J*_{HH} = 8.2, 5.4 Hz, 2H, 2), 3.28 (d, ¹*J*_{RhH} = 2.3 Hz, 3H, Me). ¹⁹F NMR (methylene chloride-*d*₂, 600 MHz): δ = -73.9 (s, TFA) ppm. ¹³C {¹H} NMR (150 MHz, methylene chloride-*d*₂): δ = 162.6 (q, ¹*J*_{FC} = 35.5 Hz, CF₃), 156.4 (s, Ar-C), 151.4 (s, Ar-C), 139.6 (s, Ar-C), 137.7 (s, Ar-C), 135.3 (s, Ar-C), 134.0 (s, Ar-C), 133.7 (s, Ar-C), 131.3 (s, Ar-C), 129.2 (s, Ar-C), 128.7 (s, Ar-C), 127.6 (s, Ar-C), 122.0 (s, Ar-C), 23.6 (d, ¹*J*_{RhC} = 27.1 Hz, CH₃).

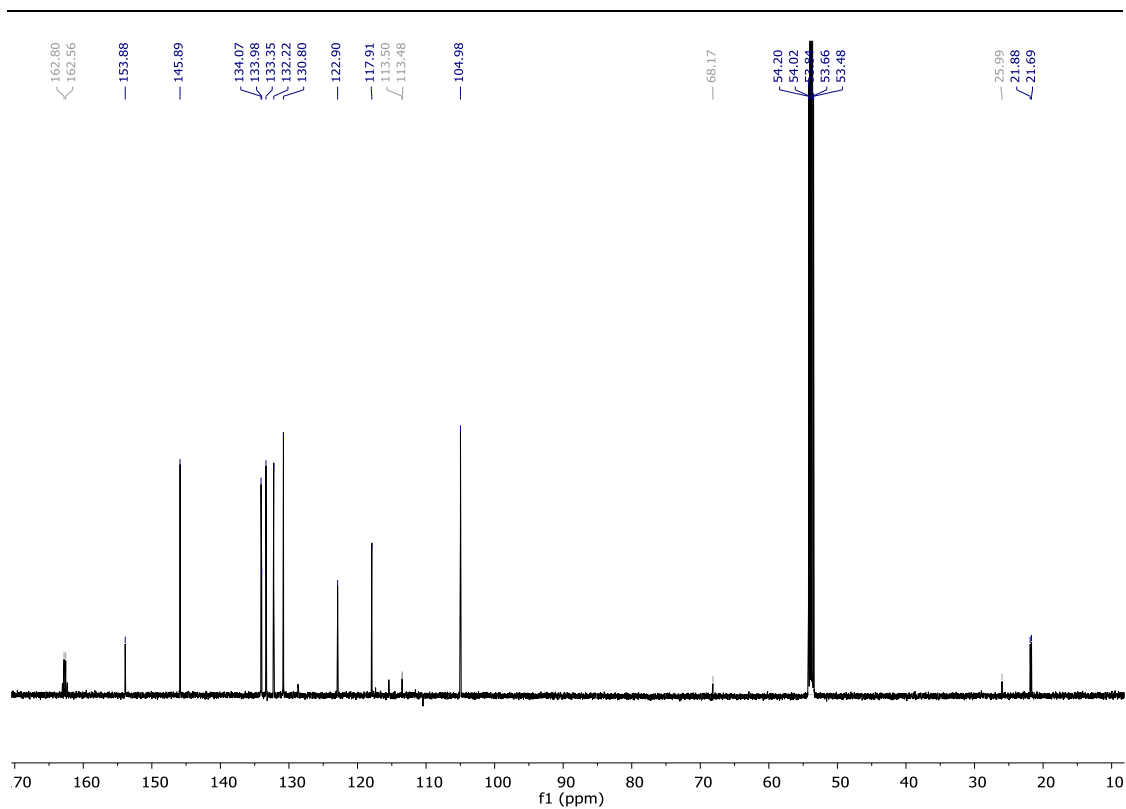


Figure 2.4.1. ^{13}C NMR spectrum of (5-FP)Rh(TFA) $_2$ Me (**1**) in DCM- d_2 .

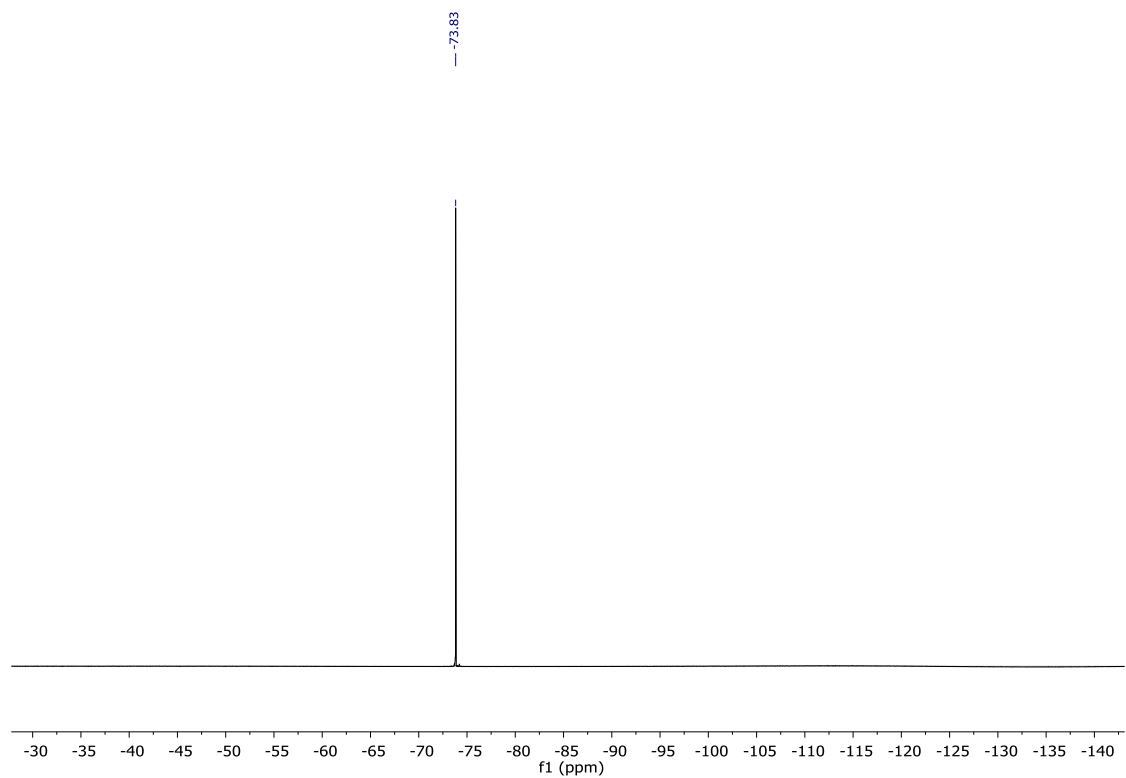


Figure 2.4.2. ^{19}F NMR spectrum of (5-FP)Rh(TFA) $_2$ Me (**2**) in DCM- d_2 .

Synthesis of (6-FP)RhCl(η^2 -C $_2$ H $_4$), (6-FP)Rh(Cl)(I)Me and (6-FP)Rh(TFA) $_2$ Me

are followed similar procedure with (5-FP)RhCl(η^2 -C₂H₄), (5-FP)Rh(Cl)(I)Me and (5-FP)Rh(TFA)₂Me, the 8,8'-(1,2-phenylene)diquinoline (6-FP) was used to replace 1,2-bis(*N*-7-azaindoly)benzene (5-FP) in the procedure. The NMR spectra are shown below:

NMR spectra data for (6-FP)Rh(TFA)₂Me:

¹H NMR (600 MHz, methylene chloride-*d*₂): δ = 8.82 (d, ³*J*_{HH} = 5.3 Hz, 2H, 1), 8.14 (dd, ³*J*_{HH} = 8.2, ⁵*J*_{RH} 1.4 Hz, 2H, 3), 7.78 (dd, *J* = 5.9, 3.4 Hz, 2H, 7 or 8), 7.65 (m, 4H, and 7 or 8), 7.51 – 7.43 (m, 4H, 5 and 4 or 6), 7.31 (dd, ³*J*_{HH} = 8.2, 5.4 Hz, 2H, 2), 3.28 (d, ²*J*_{RH} = 2.3 Hz, 3H, Me). ¹⁹F NMR (methylene chloride-*d*₂, 600 MHz): δ = -73.9 (s, TFA) ppm. ¹³C-{¹H} NMR (150 MHz, methylene chloride-*d*₂): δ = 162.6 (q, ¹*J*_{FC} = 35.5 Hz, CF₃), 156.4 (s, Ar-C), 151.4 (s, Ar-C), 139.6 (s, Ar-C), 137.7 (s, Ar-C), 135.3 (s, Ar-C), 134.0 (s, Ar-C), 133.7 (s, Ar-C), 131.3 (s, Ar-C), 129.2 (s, Ar-C), 128.7 (s, Ar-C), 127.6 (s, Ar-C), 122.0 (s, Ar-C), 23.6 (d, ¹*J*_{RhC} = 27.1 Hz, CH₃).

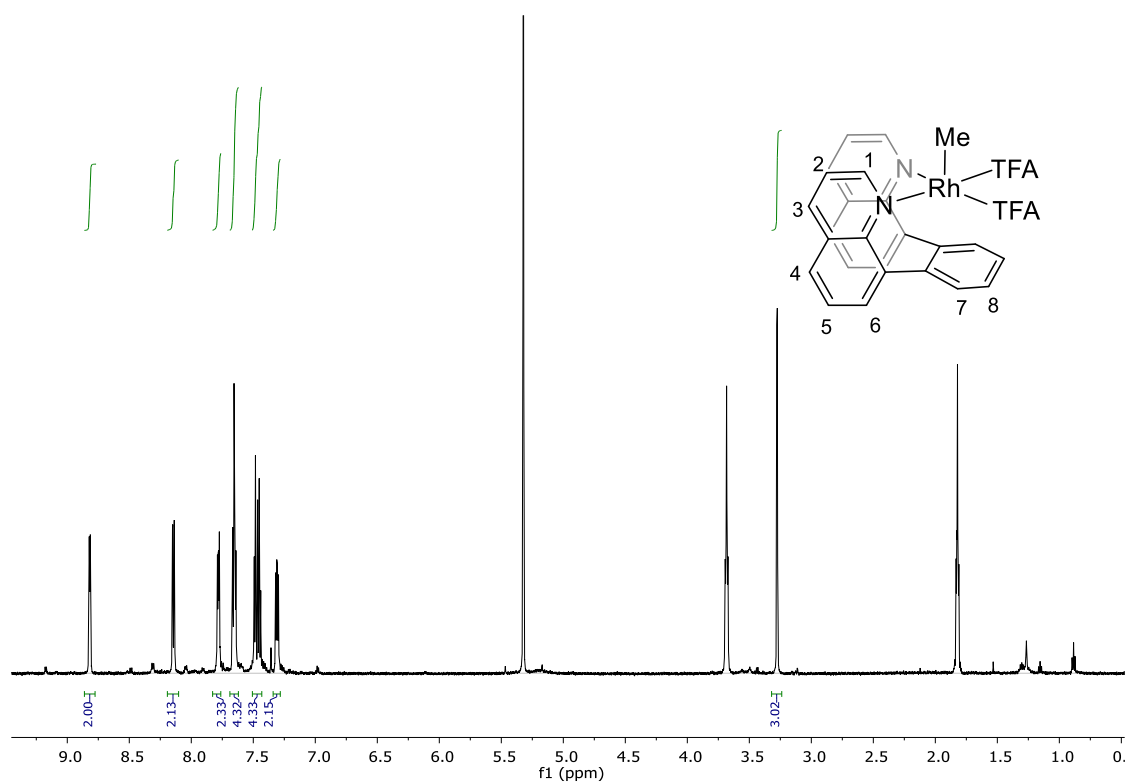


Figure 2.4.3. ¹H NMR spectrum for (6-FP)Rh(TFA)₂Me (2) in DCM-*d*₂.

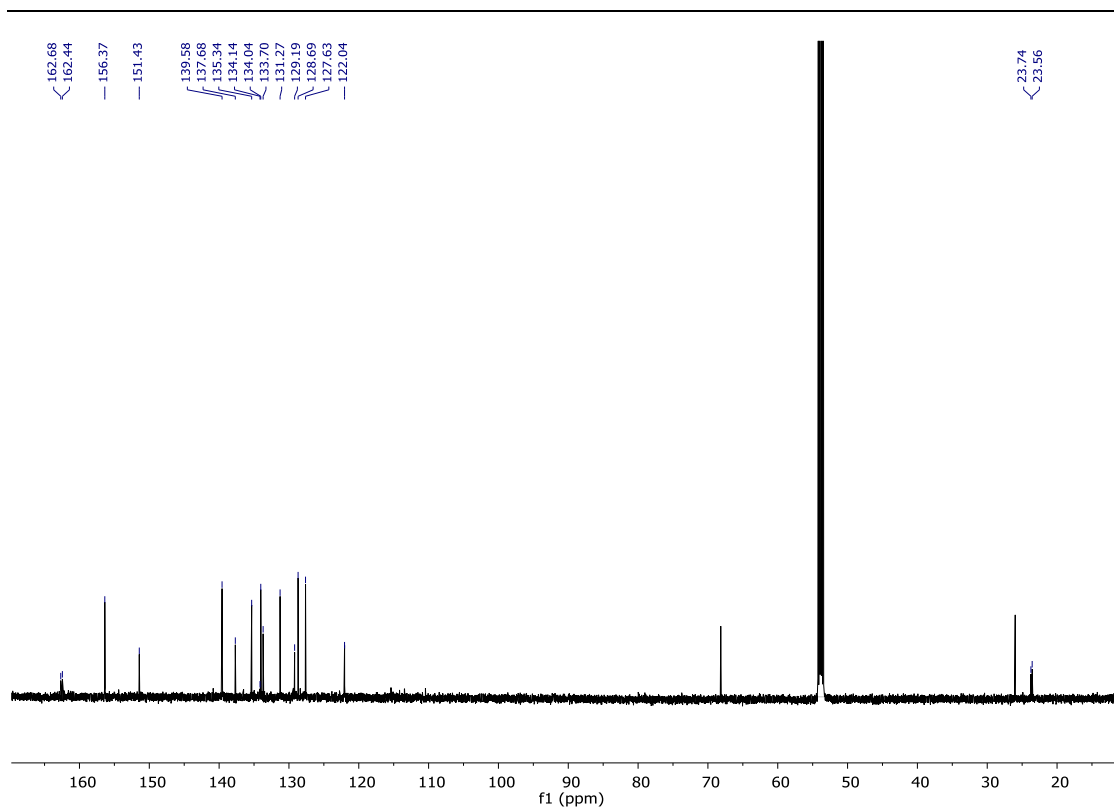


Figure 2.4.4. ^{13}C NMR spectrum of (6-FP)Rh(TFA) $_2$ Me (**2**) in DCM- d_2 .

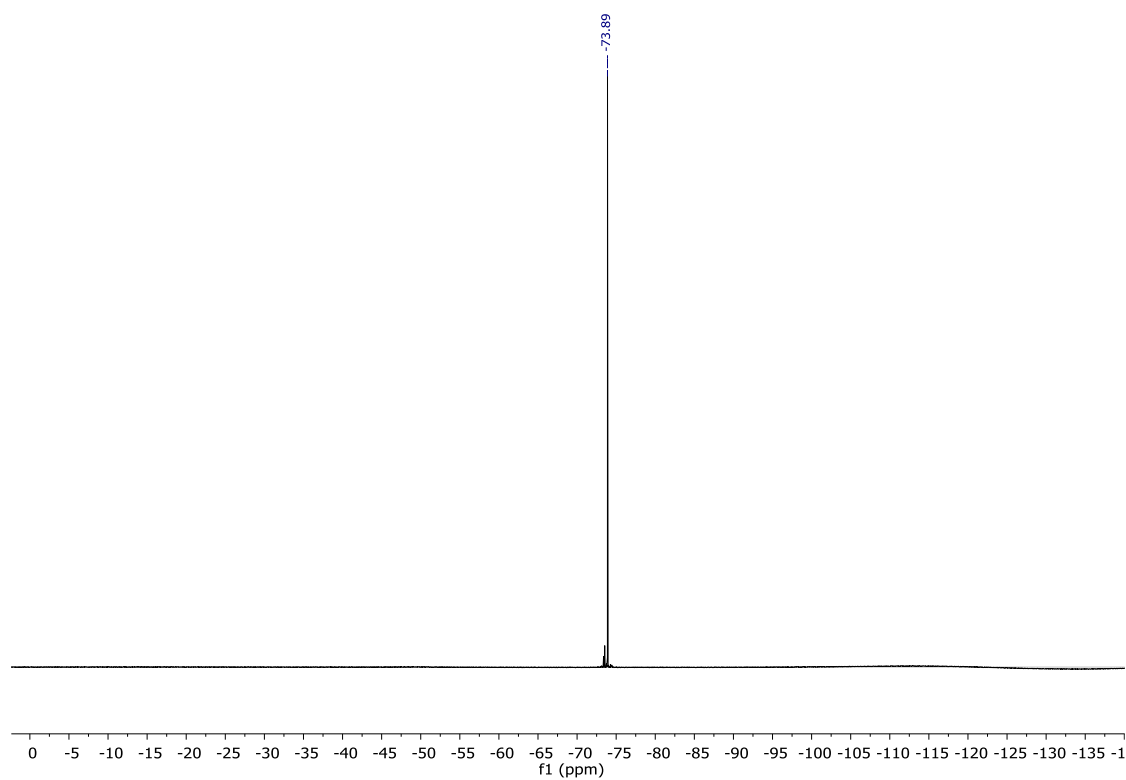


Figure 2.4.5. ^{19}F NMR spectrum for (6-FP)Rh(TFA) $_2$ Me (**2**) in DCM- d_2 .

NMR spectra data for (6-FP)RhCl(η^2 -C $_2$ H $_4$):

^1H NMR (600 MHz, methylene chloride- d_2) δ 9.91 (dd, $J = 4.7, 1.6$ Hz, 1H, 1 or 1'), 8.58 (d, $J = 5.2$ Hz, 1H, 1 or 1'), 8.09 (dd, $J = 8.3, 1.6$ Hz, 1H, 3 or 3'), 8.01 (d, $J = 7.8$ Hz, 1H, 3 or 3'), 7.78 (dd, $J = 7.1, 1.5$ Hz, 1H, 4 or 4'), 7.75 (dd, $J = 8.2, 1.5$ Hz, 1H, 4 or 4'), 7.64 – 7.58 (m, 1H, one of 7, 7', 8 and 8'), 7.57 – 7.46 (m, 5H, three of 7, 7', 8 and 8'; 5 and 5'), 7.21 – 7.14 (m, 2H, 2 or 2' and 6 or 6'), 7.11 (d, $J = 7.6$, 1H, 6 or 6'), 6.78 (dd, $J = 8.2, 5.2$ Hz, 1H, 2 or 2'), 3.55 (br, 1H, ethylene, ethylene), 2.32 (br, 1H, ethylene), 1.80 (br, 1H, ethylene), 1.53 (br, 1H, ethylene).

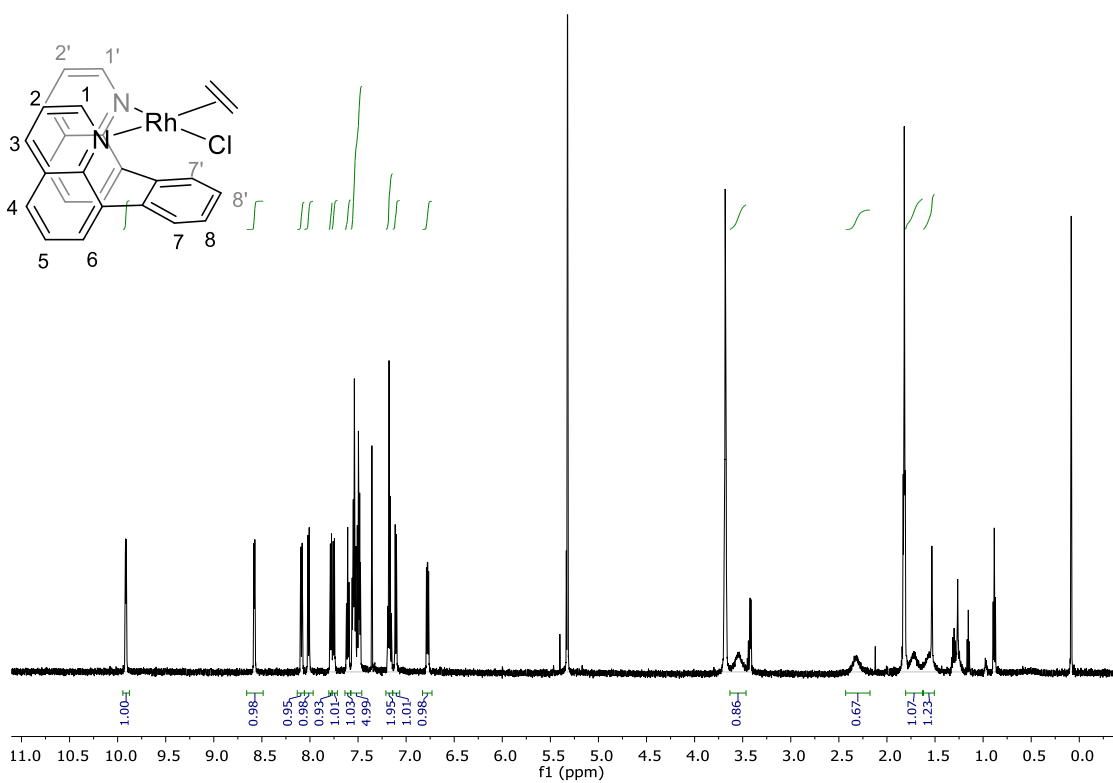


Figure 2.4.6 ^1H -NMR spectra for $(6\text{-FP})\text{RhCl}(\eta^2\text{-C}_2\text{H}_4)$

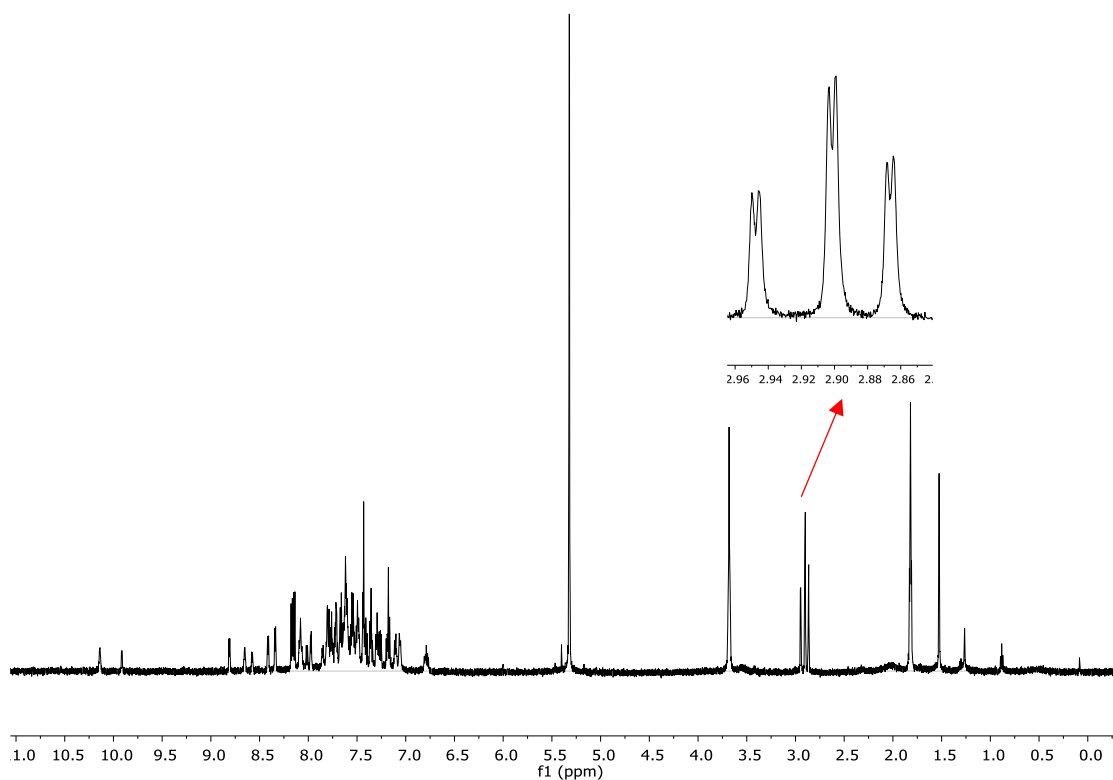


Figure 2.4.7. ^1H -NMR spectrum for three isomer of $(6\text{-FP})\text{Rh}(\text{Cl})(\text{I})\text{Me}$ in $\text{DCM-}d_2$.

2.5 References:

- [1] Feller, M.; Diskin-Posner, Y.; Leitun, G.; Shimon, L. J. W.; Milstein, D., *J. Am. Chem. Soc.* **2013**, *135*, 11040-11047.
- [2] Frech, C. M.; Milstein, D., *J. Am. Chem. Soc.* **2006**, *128*, 12434-12435.
- [3] O'Reilly, M. E.; Pahls, D. R.; Webb, J. R.; Boaz, N. C.; Majumdar, S.; Hoff, C. D.; Groves, J. T.; Cundari, T. R.; Gunnoe, T. B., *Dalton Transactions* **2014**, *43*, 8273-8281.
- [4] O'Reilly, M. E.; Pahls, D. R.; Cundari, T. R.; Gunnoe, T. B., *Organometallics* **2014**, *33*, 6504-6510.

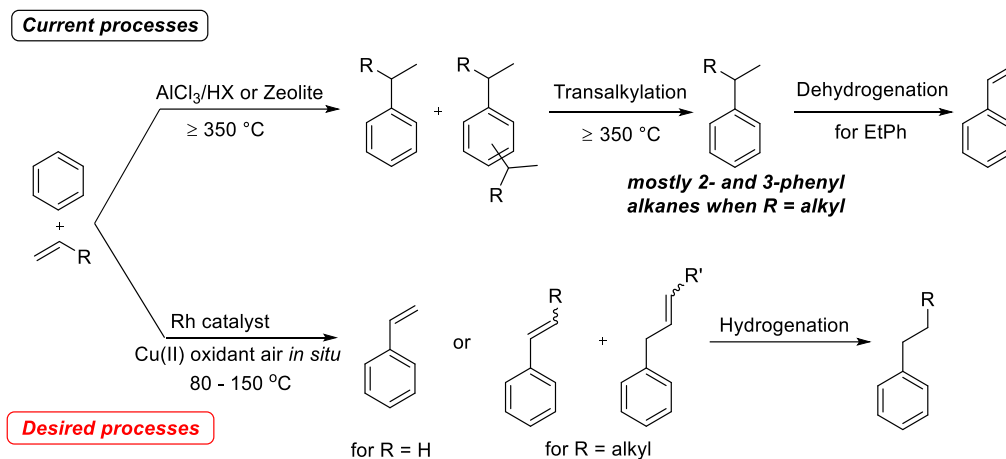
-
- [5] Fu, R.; O'Reilly, M. E.; Nielsen, R. J.; Goddard III, W. A.; Gunnoe, T. B., *Chem. Eur. J.* **2015**, *21*, 1286-1293.
- [6] Liu, Z.; Yamamichi, H.; Madrahimov, S. T.; Hartwig, J. F., *J. Am. Chem. Soc.* **2011**, *133*, 2772-2782.
- [7] Kanas, D. A.; Geier, S. J.; Vogels, C. M.; Decken, A.; Westcott, S. A., *Inorg. Chem.* **2008**, *47*, 8727-8735.
- [8] Geier, S. J.; Chapman, E. E.; McIsaac, D. I.; Vogels, C. M.; Decken, A.; Westcott, S. A., *Inorg. Chem. Commun.* **2006**, *9*, 788-791.
- [9] Budzelaar, P. H. M.; Moonen, N. N. P.; de Gelder, R.; Smits, J. M. M.; Gal, A. W., *Chem. Eur. J.* **2000**, *6*, 2740-2747.
- [10] Webb, J. R.; Bolaño, T.; Gunnoe, T. B., *ChemSusChem* **2011**, *4*, 37-49.
- [11] Cramer, R., *J. Am. Chem. Soc.* **1964**, *86*, 217-222.
- [12] Tan, R.; Jia, P.; Rao, Y.; Jia, W.; Hadzovic, A.; Yu, Q.; Li, X.; Song, D., *Organometallics* **2008**, *27*, 6614-6622.
- [13] Werner, H.; Poelsma, S.; Schneider, M. E.; Windmüller, B.; Barth, D., *Chem. Ber.* **1996**, *129*, 647-652.

3 The Development and Study of Rh(I) Complexes with “Capping Arene” ligands for Hydroarylation with Benzene and α -Olefins

This chapter is adapted from “Chen, J.; Nielsen, R. J.; Goddard, W. A.; McKeown, B. A.; Dickie, D. A.; Gunnoe, T. B. Catalytic Synthesis of Superlinear Alkenyl Arenes Using a Rh (I) Catalyst Supported by a “Capping Arene” Ligand: Access to Aerobic Catalysis. J. Am. Chem. Soc., 2018, 140, 17007-17018.” Copyright 2018 American Chemical Society

3.1 Basic Concept for Rh Catalyzed Hydroarylation

Late transition metal complex catalyzed hydroarylation is considered to be a potential alternative to Friedel Crafts arene alkylation. Using styrene as an example, current industrial processes include several steps: 1. Friedel Crafts alkylation of benzene with ethylene to produce ethylbenzenes or polyethylbenzenes. 2. Distillation to separate ethylbenzene from polyethylbenzenes. 3. Transalkylation of benzene with polyethylbenzenes to optimize the yield of ethylbenzene. 4. Dehydrogenation of ethylbenzene to produce styrene.^[1-6] The overall process is energy consuming. A potential advantageous route is a single-step oxidative benzene alkenylation that uses benzene and ethylene to directly produce styrene. The process comparison is summarized in Scheme 3.1.1.



Scheme 3.1.1. Current processes for the synthesis of styrene, linear alkyl benzenes (LABs) the synthesis of alkenyl benzenes such as styrene, that can be hydrogenated to form super linear alkyl benzenes (SLABs).

Yoshida and co-workers reported that $\text{Rh}(\text{acac})(\text{CO})_2$ ($\text{acac} = \text{acetylacetonate}$) can catalyze oxidative hydrophenylation of ethylene to produce styrene using purified oxygen and $\text{Cu}(\text{OAc})_2$ as the oxidant. At 180°C in 10.6 M acetic acid solution of benzene with 1.55 MPa ethylene and 2.10 MPa oxygen, the catalyst can achieve 29 turnover number (TON) of styrene after 20 minutes reaction. Approximately 10 TON of vinylacetate was produced as a side product. With the addition of excess acacH , vinylacetate production is suppressed; however, the TON of styrene was reduced to 22. Rh(III) complexes ($[(\text{Cp}^*)\text{RhCl}_2]_2$ ($\text{Cp}^* = \text{pentamethylcyclopentadiene}$) and $[\text{Rh}(\text{ppy})_2\text{Cl}]_2$ ($\text{ppy} = 2\text{-phenylpyridine}$)) are also capable of catalyzing olefin hydroarylation reactions, however, the reaction rate is one tenth to that of Rh(I) complexes, such as $\text{Rh}(\text{acac})(\text{ethylene})_2$.^[7] Several different Rh(I), Rh(III), Ir(III) and Pd(II) complexes were tested for the hydrophenylation of ethylene with or without acacH ligand.^[8] The addition of acacH can help reduce the production of vinylacetate. $\text{Pd}(\text{OAc})_2$ was elucidated to be the most active catalyst; however a significant amount of vinylacetate was produced even with acacH additive. The reactivity with Ir

complexes such as $[\text{Ir}(\text{acac})_3]_2$ and $\text{IrCp}^*(\text{acac})_2$ is very limited and Rh complexes give much promising catalysis result. With the addition of acacH, all of the Rh complexes such as $\text{Rh}(\text{acac})(\text{CO})_2$, $\text{Rh}(\text{ppy})_2(\text{OAc})$, $[\text{RhCp}^*\text{Cl}_2]_2$ and $\text{RhCp}^*(\text{acac})\text{Cl}$ give no vinyl acetate production. Among all the Rh complexes, $\text{Rh}(\text{acac})(\text{CO})_2$ stood out as the best catalyst for ethylene hydrophenylation. At the best condition, the maximum TON of styrene is 22.5 without ant vinylacetate production. The longevity of the catalyst is not good.

Recently, our group reported that $(^{\text{Fl}}\text{DAB})\text{Rh}(\text{TFA})(\eta^2\text{-C}_2\text{H}_4)$ ($^{\text{Fl}}\text{DAB} = N,N'$ -bis(pentafluorophenyl)-2,3-dimethyl-1,4-diaza-1,3-butadiene; TFA = trifluoroacetate) serves as a catalyst precursor for the oxidative hydrophenylation of ethylene to produce styrene using Cu(II) salts as the *in situ* oxidant.^[9] The detailed proposed mechanism using a generic metal “M” is shown in Figure 3.1.1. Benzene coordinates to the Rh center and undergoes a C–H activation step to release HX (X = OAc or TFA) and form a Rh–Ph intermediate. Ethylene coordination followed by ethylene insertion into the Rh–Ph bond forms a Rh–CH₂CH₂Ph intermediate, and β -hydride elimination generates coordinated styrene and a Rh-hydride complex. Cu(II) salts are used as *in situ* oxidants to regenerate the catalyst and complete the cycle. Cu(II) salts are attractive as *in situ* oxidants because the reduced Cu(I) complexes with acid can be re-oxidized to Cu(II) with dioxygen, which is demonstrated by the Wacker-Hoechst process for ethylene oxidation.^[6] Under optimal condition, over 800 TOs can be reached after 96 h reaction time and no ethylbenzene or vinyl acetate production was detected.

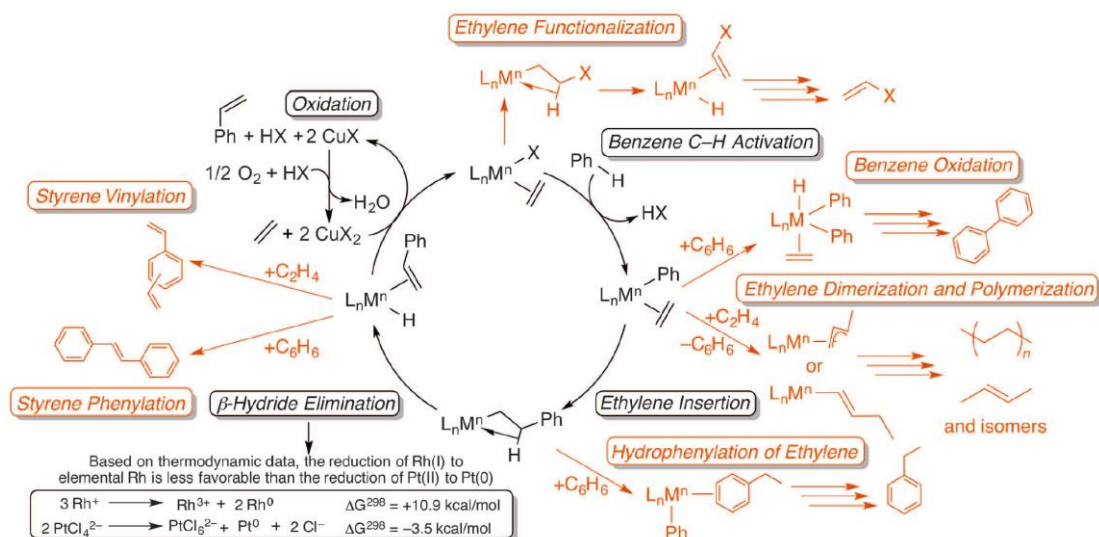
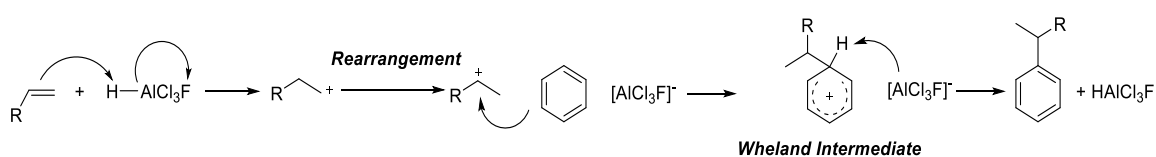


Figure 3.1.1. Proposed cycle for transition metal-catalyzed styrene production from benzene and ethylene using CuX_2 as an oxidant.^[9]

Another advantage of transition metal catalyzed olefin hydroarylation is the opportunity for selective production of linear alkylbenzene. Using traditional Friedel Craft alkylation, carboncationic intermediates are generated, which will go through the rearrangement to form the most stable carboncation. The stability follows the order of primary < secondary < tertiary.^[10,11] Thus the production of 1-aryl alkanes from α -olefin is not impossible (Scheme 3.1.2).



Scheme 3.1.2. Mechanism for Friedel-Crafts alkylation with an α -olefin.

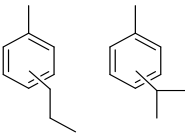
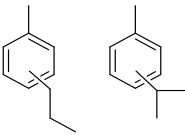
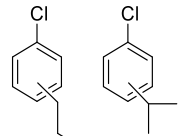
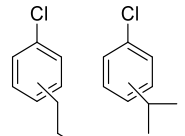
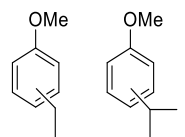
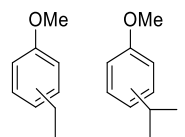
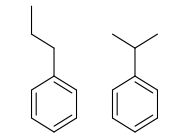
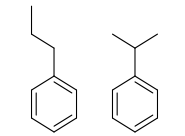
Transition metal catalyzed olefin hydroarylation often involves an olefin insertion into metal-aryl bond, which offers the opportunity for selectivity of linear products. By controlling the regioselectivity of the olefin insertion step (*i.e.*, 1,2- vs 2,1-insertion), it is possible to selectively produce 1-phenyl alkanes or their unsaturated alkenyl variants. During the past decades, a lot of effort has been put into this field. Ru(II) and Ir(III) catalysts have been reported to convert benzene and α -olefins such as propylene or 1-hexene to alkyl

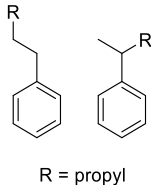
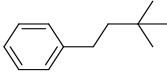
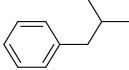
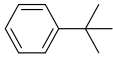
arenes with ~1.6:1 L:B ratios.^[12-16] In contrast, Pt complexes have been shown to catalyze olefin hydroarylation, slightly favoring the generation of branched products in most cases.^[17-20] However, similar to the Ru(II) and Ir(III) catalysts, Goldberg and co-worker reports one example of a Pt catalyst that achieves a L:B ratio of 1.6:1 with 1-hexene as olefin source.^[21] An *in situ* formed Ni(II) *N*-heterocyclic carbene (NHC) complex can mediate olefin hydroarylation with trifluoromethyl-substituted arenes with a L:B ratio up to 19:1; however, a stoichiometric amount of Ni is required to complete the conversion.^[22] In an alternative route, 1-aryl *n*-alkanes can be prepared through dehydrogenation of alkyl arenes followed by olefin cross-metathesis.^[23,24] In addition, Kim and co-workers showed that a Rh complex could generate linear products using hetero-functionalized 2-phenylpyridine and terminal alkenes.^[25] Thus, to the best of our knowledge, the L:B selectivity for catalytic benzene alkylation when using simple α -olefins (*e.g.*, propylene, 1-hexene) either favors branched products or is only modestly selective for linear products with best 1.6:1 L:B ratios.

Recently our group reported that the simple Rh complex $[\text{Rh}(\mu\text{-OAc})(\eta^2\text{-C}_2\text{H}_4)]_2$ is a catalyst precursor to convert α -olefins and arenes to alkenyl arenes with high anti-Markovnikov selectivity (up to a 10:1 L:B ratio) using Cu(II) as oxidant.^[26] The catalytic results with different olefins and arenes are summarized in Table 3.1.1. Catalysis results are dramatically different between AlCl_3 and the Rh catalyst. All the catalysis results with AlCl_3 shows 100% selectivity towards branched product.^[27-31] The catalytic results with the Rh complex are highly selective of linear product and the reaction with isobutylene and neohexene only produce linear alkyl arenes. The two catalysts exhibit different product

distribution of *ortho:meta:para* (*o:m:p*) in catalysis with toluene. AlCl₃ catalyzed alkylation is highly selective for *ortho* and *para*, but Rh complex shows *meta* and *para* selectivity. The *o:m:p* selectivity is likely due to the electronic and steric effects for AlCl₃ and Rh complex, respectively. In addition, Rh complex catalyzed oxidative olefin hydroarylation is not sensitive to the functional group on the arene. The reaction with chlorobenzene and benzene have similar reaction rate. In contrast, the rate of AlCl₃ catalyzed chlorobenzene alkylation (with propylene in nitromethane at 25 °C) is approximately 10 times slower relative to benzene. Under the best conditions, [Rh(μ -OAc)(η^2 -C₂H₄)₂]₂ catalyzed oxidative hydroarylation with benzene and propylene can reach over 1400 TON with an 8:1 L:B ratio.

Table 3.1.1. Comparison of arene alkylation using AlCl₃ as the primary catalyst versus [Rh(μ -OAc)(η^2 -C₂H₄)₂]₂^[26]

| | Arene | Coupling Partner | <i>o:m:p</i> | L:B | TON | Product |
|-------------------|---------------|------------------|--------------|--------|--------|---|
| AlCl ₃ | toluene | propylene | 3:1:2.6 | >98% B | n.r. |  |
| Rh | toluene | propylene | 1:8.9:9.3 | 9.4:1 | 86(17) |  |
| AlCl ₃ | chlorobenzene | 2-chloropropane | 6.4:1:5.1 | 100% B | n.r. |  |
| Rh | chlorobenzene | propylene | 1:11:7 | 10:1 | 116(3) |  |
| AlCl ₃ | anisole | 2-chloropropane | 62:4:34 | 100% B | n.r. |  |
| Rh | anisole | propylene | 1:2.4:6.4 | 7.8:1 | 92(7) |  |
| AlCl ₃ | benzene | propylene | n/a | 100% B | 95 |  |
| Rh | benzene | propylene | n/a | 8:1 | 80(4) |  |
| AlCl ₃ | benzene | 1-hexene | n/a | 100% B | 67 | |

| | | | | | | |
|-------------------|---------|----------------------------|-----|--------|---------|---|
| Rh | benzene | 1-pentene ^[§] | n/a | 8:1 | 122(10) |  R = propyl |
| Rh | benzene | neohexene ^[§] | n/a | 100% L | 30(8) |  |
| Rh | benzene | isobutylene ^[§] | n/a | 100% L | 100(2) |  |
| AlCl ₃ | benzene | isobutylene | n/a | 100% B | n.r. |  |

* The AlCl₃ results are from references. **Rh** = [Rh(μ -OAc)(η^2 -C₂H₄)₂]. Unsaturated products are produced from Rh catalyzed reaction and all the products results shown in the table are after hydrogenation.

3.2 Result and Discussion

3.2.1 Catalysts Design, Synthesis and Characterization

The ligand 1,2-bis(*N*-7-azaindolyl)benzene (5-FP) was synthesized according to a published procedure.^[32] The (5-FP)Rh(TFA)(η^2 -C₂H₄) (**1**) was synthesized by mixing 5-FP and [Rh(μ -TFA)(η^2 -C₂H₄)₂] in THF. Complex **1** has been characterized by ¹³C and ¹H NMR spectroscopy, elemental analysis and a single crystal X-ray diffraction study. The ¹³C and ¹H NMR spectra are shown in Figure 3.2.1 and 3.2.2. The spectra show that complex **1** is an asymmetric complex. For coordinated ethylene, the ¹H NMR spectrum reveals two broad peaks, which is consistent with rapid rotation of ethylene on the timescale of the NMR experiment. A small coupling constant (~1.5 Hz) is observed between Rh and all hydrogens on the C₆ arene ring of the 5-FP ligand in ¹H NMR spectrum, which indicates weak interaction between arene moiety and Rh center.

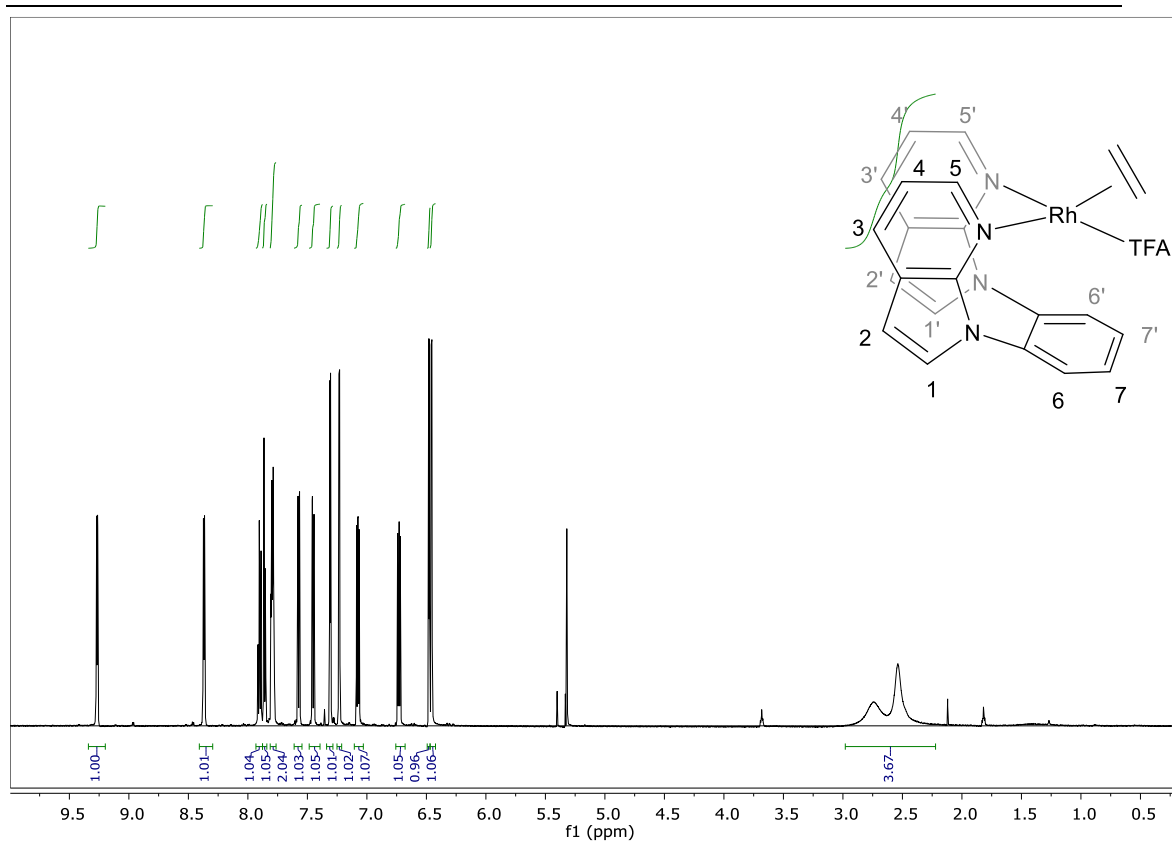


Figure 3.2.1. ^1H NMR spectrum of $(5\text{-FP})\text{Rh}(\text{TFA})(\eta^2\text{-C}_2\text{H}_4)$ **1** in $\text{DCM-}d_2$.

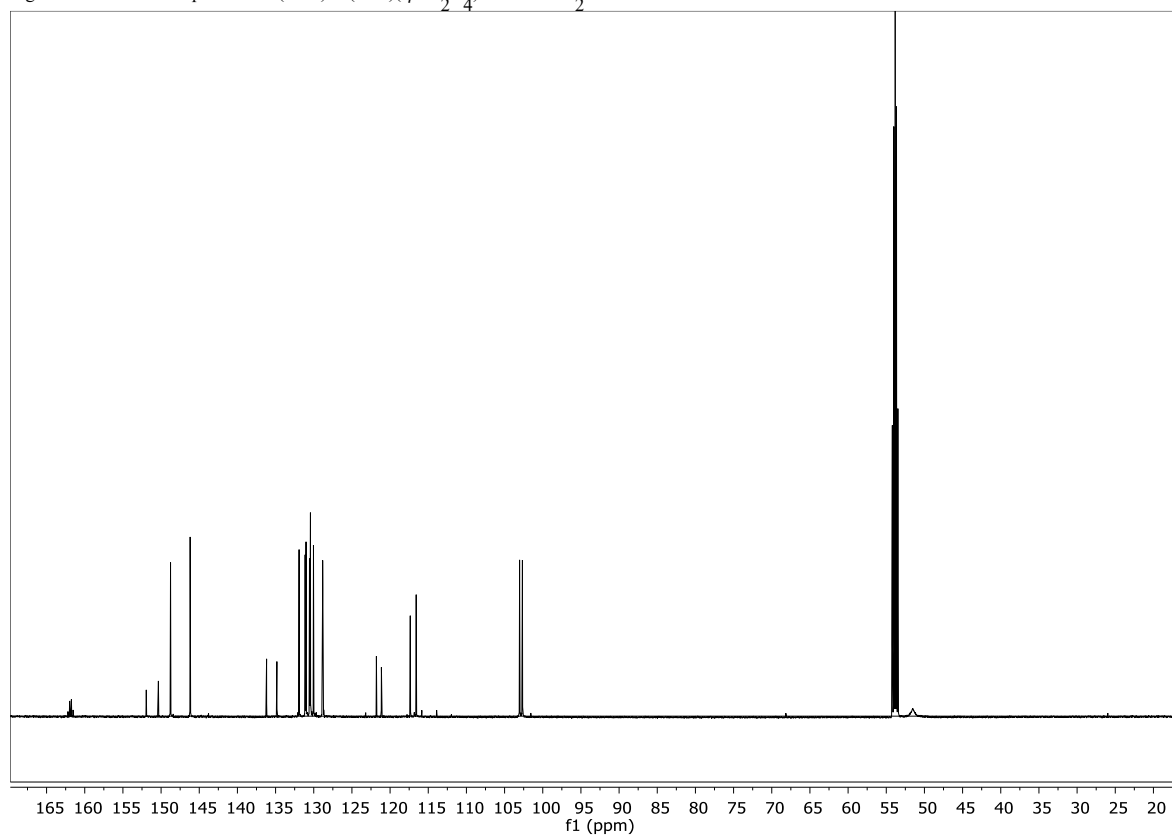


Figure 3.2.2. ^{13}C NMR spectrum of $(5\text{-FP})\text{Rh}(\text{TFA})(\eta^2\text{-C}_2\text{H}_4)$ **1** in $\text{DCM-}d_2$.

The structure of complex **1** was confirmed by single crystal X-ray diffraction. Figure 3.2.3 shows an ORTEP of complex **1**. The arene of the 5-FP ligand is located near the Rh center, and the arene ring of the ligand is positioned with Rh-C8 and Rh-C13 distances of 3.002(3) Å and 3.008(3) Å, respectively. These distances are much longer than a typical Rh–C single bond,^[33-36] which is consistent with weak coordination between Rh and the arene moiety or intermediates by the ¹H NMR spectrum (see above). The coordinated ethylene is oriented approximately perpendicular to the Rh square plane. This is a typical orientation for four-coordinate and d⁸ η^2 -olefin transition metal complexes.^[37-42] Previously, our group reported a similar crystal structure in which the ligand has a quinoline other than 7-azaindole group.^[43] The structure comparison of these two complexes is shown in Figure 3.2.4. The distances between Rh and arene rings were modeled by constructing a centroid with the 6 carbon atoms of the arene ring and then measuring the distance between the Rh atom and the centroid. The measured distance is significant longer for complex **1** (3.354 Å vs. 3.019 Å, Figure 3.2.4) than for the other complex. For **1**, the coordination of the arene ring is likely best described as an η^2 interaction with Rh. Thus, the five-member nitrogen heterocycle of the 7-azaindole group appears to weak the Rh-arene bonding interaction by positioning the arene group farther from the Rh center than the six-member ring of the quinoline-based ligand. This feature seemingly provides an ability to fine-tune the Rh-arene interaction, which could be important to future efforts to control Rh-based redox chemistry.

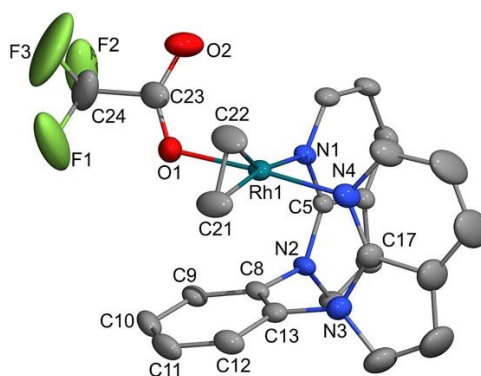


Figure 3.2.3. ORTEP of (5-FP)Rh(TFA)(η^2 -C₂H₄) (**1**). Ellipsoids are drawn at the 50% probability level, and hydrogen atoms are omitted for clarity. Selected bond lengths (Å): Rh1–C21 2.101(3), Rh1–C22 2.096(3), C8–Rh1 3.002(3), C13–Rh1 3.008(3), N1–Rh1 2.134(2), N2–Rh1 2.022(2). Selected bond angles (deg): C5–N2–C8 127.0(2), C17–N3–C13 128.4(2), N1–Rh1–N4 86.94(9), C22–Rh1–C21 38.8(1).

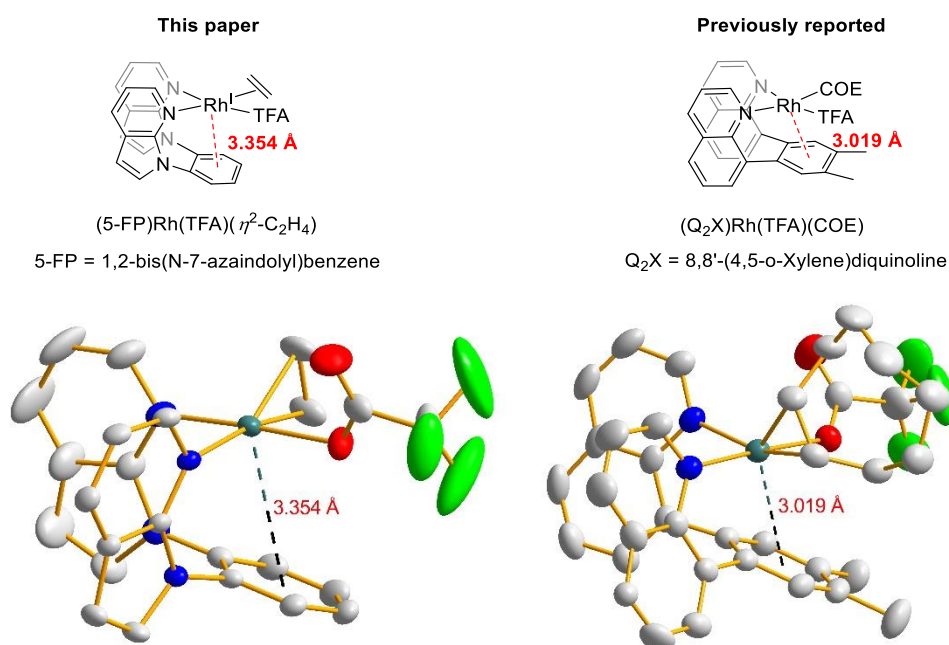


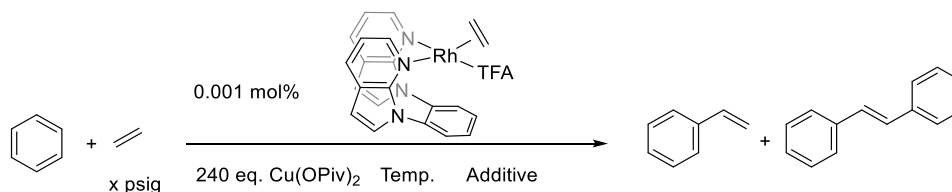
Figure 3.2.4. Structure comparison between (5-FP)Rh(TFA)(η^2 -C₂H₄) (**1**) and previously reported "capping arene" complex (6-FP)Rh(COE)(TFA) [6-FP = 8,8'-(1,2-phenylene)diquinoline, COE = cyclooctene].^[43]

3.2.2 Catalytic Oxidative Olefin Hydroarylation

In order to investigate the reactivity of complex **1** as a catalyst precursor for olefin hydroarylation, the oxidative hydrophenylation of ethylene is used as a model reaction. Some reaction results are summarized in Table 3.2.1. Heating a 10 mL benzene solution of complex **1** (0.001 mol% relative to benzene) with 50 psig ethylene and Cu(OPiv)₂ (240

equivalents relative to **1**, OPiv = trimethylacetic acetate) at 150 °C affords 114(1) TOs of styrene after 1 hour (for all catalytic reactions the average TOs and standard deviations based on at least three independent experiments are given). The percent yields in Table 3.2.1 are based on Cu(II) oxidants as the limiting reagent. Two equivalents of Cu(II) oxidant are required for 1 equivalent styrene production. Trace amounts of phenyl pivalate (PhOPiv) and biphenyl were observed as side products. Biphenyl likely forms from a Rh mediated oxidative benzene coupling reaction, and 1.6 TOs (relative to Rh) of PhOPiv results from a slow background reaction that occurs upon heating Cu(OPiv)₂ to 150 °C in benzene, which has been confirmed by heating (150 °C) same amount of Cu(OPiv)₂ in benzene without Rh complex. A similar amount of PhOPiv was produced. The conversion of benzene, ethylene and Cu(OPiv)₂ to styrene using complex **1** can achieve > 90% yield with high selectivity for styrene (no ethylbenzene was observed in the reactions). Under most conditions, small amounts of *trans*-stilbene from the hydrophenylation of styrene were also detected as shown in Table 3.2.1.

Table 3.2.1 Results for oxidative hydrophenylation of ethylene using (5-FP)Rh(TFA)(η^2 -C₂H₄) (**1**) as catalyst precursor.



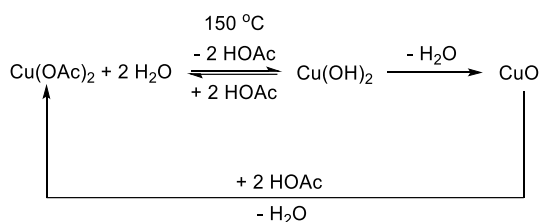
| | Temp./°C | Acid ^[a] /eq. | C ₂ H ₄ /psig | Time/h | Products/TOs | | % Yield styrene ^[b] |
|---|----------|--------------------------|-------------------------------------|--------|--------------|------------------------|--------------------------------|
| | | | | | Styrene | <i>trans</i> -Stilbene | |
| 1 | 120 | / | 50 | 16 | 109(9) | 0.6 | 91 |
| 2 | 130 | / | 50 | 10 | 107(3) | 0.2 | 89 |
| 3 | 150 | / | 50 | 1 | 114(1) | 1.3 | 95 |
| 4 | 180 | / | 50 | 0.5 | 83(8) | 5.2 | 69 |
| 5 | 150 | / | 15 | 4 | 113(7) | 0.4 | 94 |
| 6 | 150 | / | 25 | 2 | 108(3) | 1.0 | 90 |
| 7 | 150 | / | 70 | 1 | 109(4) | 0.2 | 91 |

| | | | | | | | |
|---------------------|-----|------|-----|-----|---------|---------|----|
| 8 | 150 | 240 | 50 | 0.5 | 109(2) | 1.6 | 91 |
| 9 | 150 | 480 | 50 | 0.5 | 108(1) | 2.0 | 90 |
| 10 | 150 | 2400 | 50 | 0.5 | 108(6) | 2.2 | 90 |
| 11 ^[c] | 150 | 2400 | 50 | 7 | 671(42) | 124(12) | 56 |
| 12 ^[c,d] | 150 | / | 500 | 6 | 632(5) | 4 | 53 |
| 13 ^[e] | 150 | 480 | 50 | 40 | 96(5) | 1.4 | 80 |

[a] Acid additive is HOPiv for entries 8-11, HOAc for entry 13. [b] Yields are relative to the limiting reagent Cu(II) oxidant. [c] 2400 eq. Cu(OPiv)₂ were used in the reaction. [d] The reaction is carried out in a stainless steel Parr reactor [e] 240 eq. Cu(OAc)₂ were used in the reaction.

The influence of temperature on the reaction (Table 3.2.1, entries 1-4) was investigated. The reaction time is greatly reduced by raising the temperature from 120 °C to 180 °C; however, the yield decreases at 180 °C with an increase in production of *trans*-stilbene (0.6 TOs vs. 5.2 TOs) and PhOPiv (1.6 TOs and 6.8 TOs). Among the condition studies, optimal temperature is 150 °C, which provides 95% yield of styrene as well as high TOF. Higher ethylene pressure can facilitate the reaction (Table 3.2.1, entries 3, 5-7). The reaction time to achieve > 90% yield was reduced from 4 hours at 15 psig of ethylene (entry 5) to 1 hour at 70 psig of ethylene (entry 7). Now the main focus of chemistry in this Chapter is to access possible *in situ* Cu(II) oxidant regeneration, and acid additive is essential to recycle the Cu. Entries 8-10 in Table 3.2.1 demonstrate the influence of pivalic acid additive. The reaction rate is enhanced and the > 90% yield can be achieved. For example, at 50 psig of ethylene at 150 °C without added pivalic acid, the reaction requires about 1 hour to reach > 90% yield (entry 3), but with added pivalic acid the time to achieve > 90% yield is reduced to 0.5 hour (entries 8-10). Two possible benefits are suggested the pivalic acid addition. First, the solubility of the Cu(OPiv)₂ in benzene is increased with the addition of HOPiv. Secondly, it is known that Cu(OAc) and water will undergo hydrolysis reaction to generate acetic acid and Cu oxide (Scheme 3.2.1).^[44] Oxidation of Cu(I) salts and acid

(pivalic or acetic acid) to Cu(II) produces water. Thus, the inhibition of Cu(I) hydrolysis by the addition of acid could enhance the longevity of the catalysis. (see below for studies of catalyst longevity).



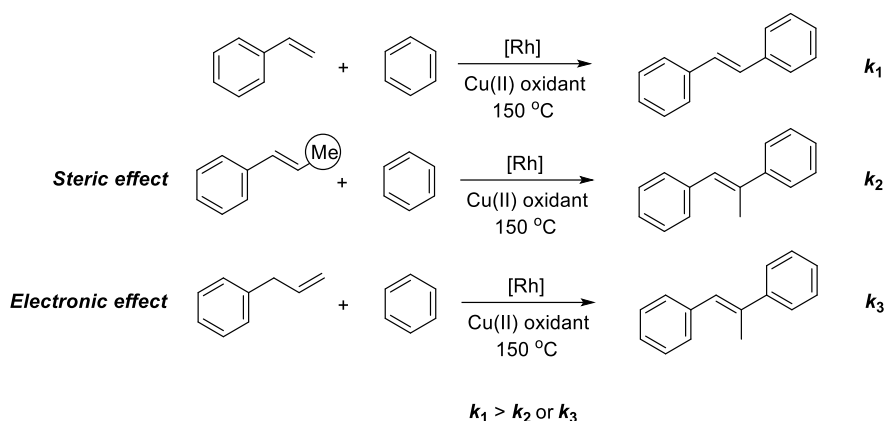
Scheme 3.2.1. Cu(OAc)₂ thermo decomposition.

Using a large amount of Cu(II) (2400 eq. relative to **1**, entry 11) results in decreased yield of styrene (~56%) due to the formation of *trans*-stilbene, which is likely produced by styrene hydrophenylation. To suppress the stilbene production, high ethylene pressure (500 psig) was used to inhibit styrene coordination. These conditions result in > 99:1 selectivity for styrene over *trans*-stilbene (entry 12). Interestingly, an increase in % yield is not observed with high ethylene pressure. This could be due to the undesired olefin activation reaction which produces vinyl pivalate under higher ethylene concentrations. In addition, the reaction in entry 12 used stainless steel reactors, which gives rise to a difference in heating compared to the glass Fischer-Porter vessels. The use of Cu(II) acetate reduces the yield from ~90% with Cu(OPiv)₂ to ~80%, and the reaction requires much longer time to reach the completion (entries 9 and 13, Table 3.2.1). Compared with Cu(OAc)₂, Cu(OPiv)₂ is a better Cu(II) oxidant.

Next, we probed the use of **1** for the oxidative hydrophenylation of propylene to investigate the anti-Markovnikov selectivity. (Table 3.2.2) Heating a 10 mL of benzene solution of complex **1** (0.001 mol% relative to benzene) to 150 °C with 30 psig of propylene with Cu(OPiv)₂ (240 eq. relative to **1**) and HOPiv (480 eq. relative to **1**) over 0.5 h affords

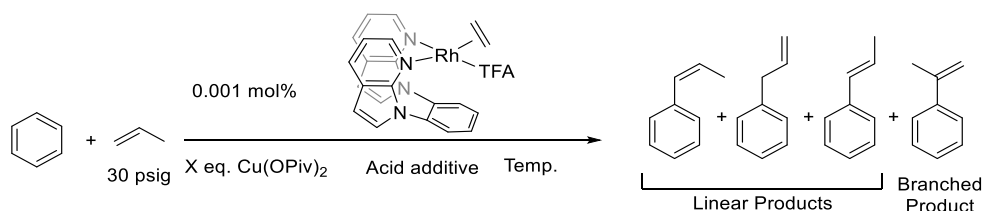
86 TOs with a L:B ratio of ~11:1. Four different alkenyl benzenes are produced from reaction. After hydrogenation of allylbenzene, β -*cis*-methylstyrene and β -*trans*-methylstyrene would produce *n*-propylbenzene, and hydrogenation of α -methylstyrene would yield cumene. Thus, the L:B ratio is determined based on the ratio of *n*-propylbenzene precursors to cumene precursor (**sss**, the ratio of allylbenzene and β -methylstyrenes to amount of α -methylstyrene). When the temperature is decreased from 150 °C to 80 °C, the L:B ratio increases from 11:1 to 18:1. However, catalyst activity and yield are also decreased with lower temperature (Table 3.2.2, entries 1-5). No alkenylbenzene products were produced from reaction when the temperature is under 60 °C.

In order to test catalyst longevity, a large amount of Cu(OPiv)₂ (2400 eq. relative to **1**) was used in the reaction with benzene and propylene. This resulted in 900 TOs (79% yield based on copper) after 10 h. The yield is even greater than reaction with lower Cu(II) oxidant loading (Table 3.2.2, entry 1 and 6). Compared to the oxidative hydrophenylation of ethylene to produce styrene under similar condition (Table 3.2.1, entry 11), which only gives 671 TOs with > 120 TOs stilbene production, the oxidative hydrophenylation of propylene only yields ~20 TOs of 1,1'-(*E*)-1-propene-1,3-diylbis[benzene]. Since the amount of ethylene and propylene is likely similar, the rate of hydrophenylation of propenyl benzenes is likely slower than the hydroarylation of styrene. This rate difference may be due to the steric bulk of methyl group on propenyl arenes and electronic difference between styrene and propenyl benzenes (Scheme 3.2.2).



Scheme 3.2.2. Possible steric or electronic effect on oxidative hydrophenylation with styrene and propenyl benzenes.

Table 3.2.2. Catalytic oxidative hydrophenylation of propylene using **1**.



| | Temp./°C | Acid ^[a] /eq. | Time/h | Products/TOs | L:B Ratio | Yield/% ^[b] |
|------------------|----------|--------------------------|--------|--------------|-----------|------------------------|
| 1 | 150 | 480 | 0.5 | 86(7) | 11 | 72 |
| 2 | 120 | 480 | 4 | 77(1) | 13 | 64 |
| 3 | 100 | 480 | 16 | 66(3) | 15 | 55 |
| 4 | 80 | 480 | 144 | 38(10) | 18 | 32 |
| 5 | 60 | 480 | 110 | 0 | N/A | 0 |
| 6 ^[c] | 150 | 2400 | 10 | 953(48) | 11 | 79 |
| 7 ^[d] | 150 | 480 | 24 | 49(2) | 9 | 41 |

[a] Acid additive is HOPiv for entries 1-6, HOAc for entry 7. [b] Yield is relative to Cu(II). [c] 2400 eq. Cu(OPiv)₂ were added to the reaction. [d] 240 eq. Cu(OAc)₂ were added to the reaction.

3.2.3 Attempt to Copper Oxidant Recycle

One of the drawbacks of our previously reported Rh catalysts is that the catalytic activity is maintained only under inert (dinitrogen) atmosphere. In addition, when heating the non-ligated Rh complex $[\text{Rh}(\mu\text{-OAc})(\eta^2\text{-C}_2\text{H}_4)]_2$ in benzene without Cu(II) oxidant, it rapid decomposition to Rh(0), acetic acid and free ethylene occurs. Since the "capping arene" ligand was selected to protect Rh against oxidative degradation or suppression of

catalysis in the presence of air, reaction with *in situ* aerobic Cu(II) regeneration was probed with 0.001 mol% complex **1**, 30 psig propylene, 240 eq. Cu(OPiv)₂ and 480 eq. HOPiv at 150 °C. Two equivalents copper required to produce one equivalent alkenylbenzene. Thus, without regeneration of Cu(II), using 240 eq. of Cu(OPiv)₂ the maximum TON of alkenylarene is 120. In order to recycle the Cu(II) oxidant, air was added to the reactor after consumption of Cu(II) oxidant, and the reaction mixture was heated at 120 °C for *in situ* Cu(OPiv)₂ regeneration. The color changes are shown in Figure 3.2.5. The original color of the reaction mixture was deep blue, which is the color of soluble copper(II) oxidant. After the reaction reached the completion, all the Cu(II) oxidant were transferred to Cu(I) species and the solution color is little brown. After the addition of air into the reactor, the Cu(II) oxidant was regenerated by oxygen and acid and the solution color came back. After regeneration of Cu(II), air was removed with a propylene purge, and the mixture was again heated at 150 °C after repressurising with propylene to continue oxidative propylene hydrophenylation. Both complex **1** and [Rh(μ -OAc)(η^2 -C₂H₄)₂] were tested to provide a direct comparison of the impact of the “capping arene” ligand to the [Rh(μ -OAc)(η^2 -C₂H₄)₂] catalyst precursor (Figure 3.2.6). Complex **1** maintains activity through 10 air-recycle procedures and 800 TOs of alkenylarene are produced, however, the reaction with [Rh(μ -OAc)(η^2 -C₂H₄)₂] stopped after 5 air-recycle procedures with about 300 TOs. Complex **1** clearly outperforms [Rh(μ -OAc)(η^2 -C₂H₄)₂] in both activity and longevity. As can be seen in Figure 2, after ~800 TOs have been reached, catalytic activity decreases; however, upon addition of pivalic acid and more benzene, catalyst activity resumes (Figure 3.2.7). Thus, the decrease in activity of **1** in Figure 3.2.6 is *not* due to catalyst deactivation.

Since the addition of pivalic acid can remove the decrease in catalyst reactivity, the equilibrium between $\text{Cu}(\text{OPiv})$ and water with pivalic acid and Cu oxide may be the reason for this observation, which inhibit the recycling of the oxidant not the catalyst.

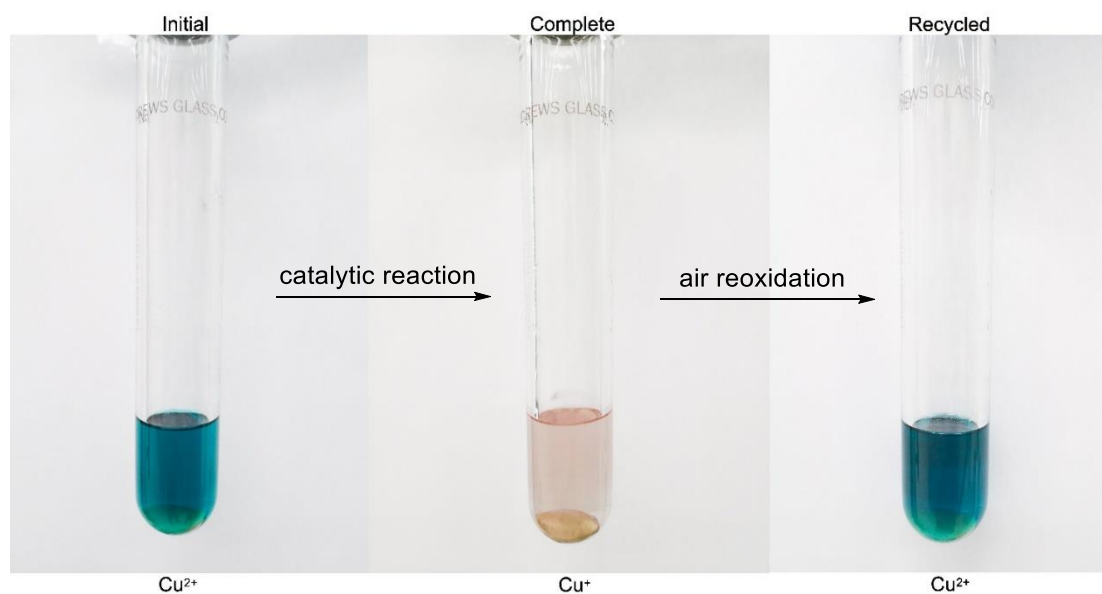


Figure 3.2.5. Photographs of reactors over the course of the reaction.

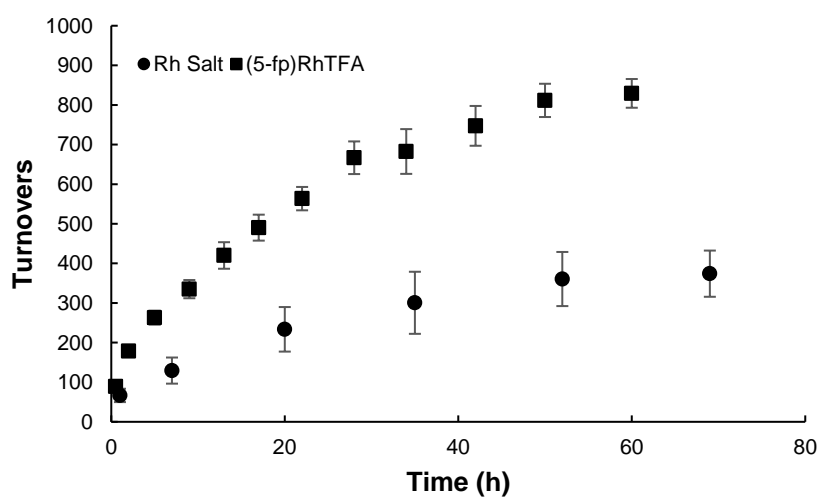


Figure 3.2.6. Oxidative hydrophenylation of propylene with *in situ* Cu oxidant regeneration. A Plot of turnovers of all akenylarene products versus time, reaction conditions: $[\text{Rh}] = 0.001$ mol% of complex 1 or $[\text{Rh}(\mu\text{-OAc})(\eta^2\text{-C}_2\text{H}_4)_2]$ in 10 mL benzene, 240 eq. $\text{Cu}(\text{OPiv})_2$, 480 eq. HOPIv , 30 psig propylene. The reactor is refilled with air and 50 psig N_2 at every sampling point for regenerating Cu oxidant at 120 °C and then removed all air and pressurized with 30 psig propylene.

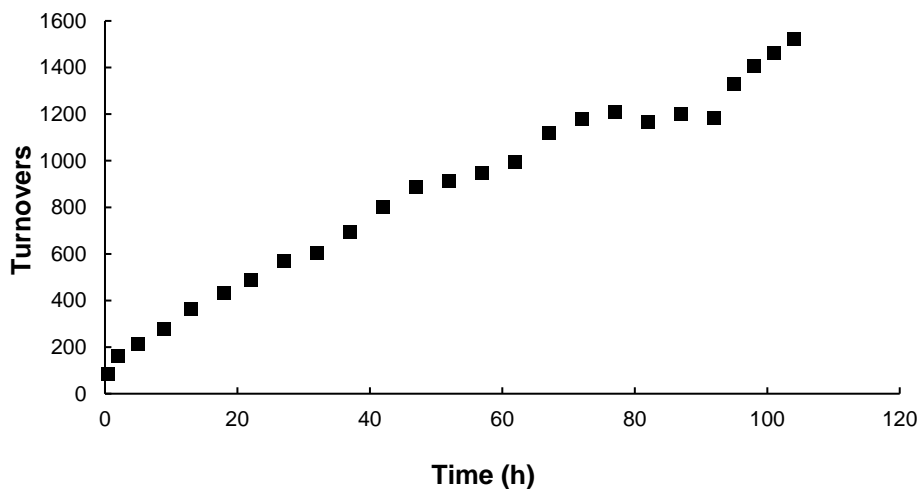


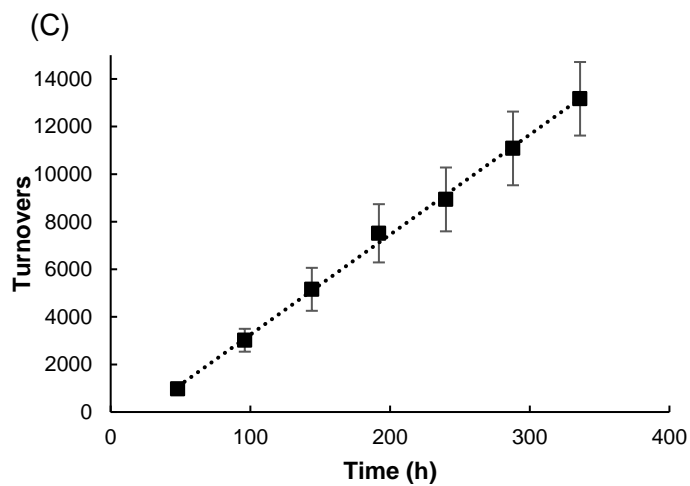
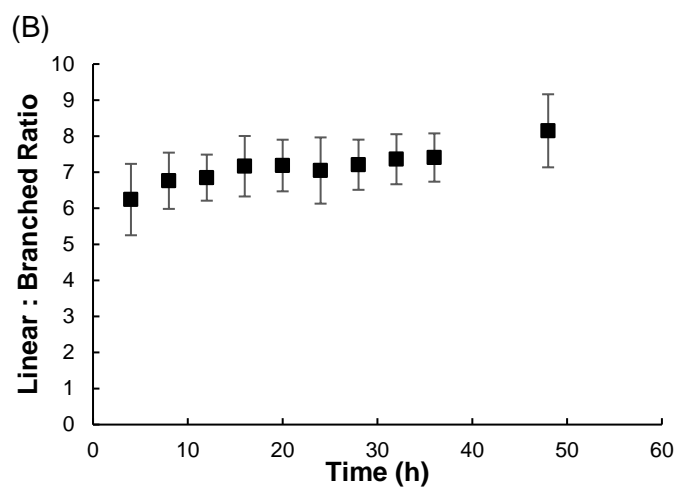
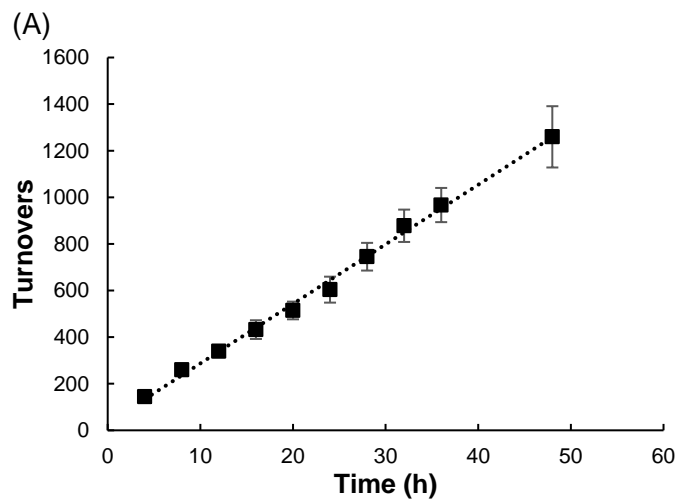
Figure 3.2.7. Plot of turnovers versus time for catalytic oxidative hydrophenylation of propylene with Cu(II) oxidant that is regenerated *in situ* (using (5-FP)Rh(TFA)(η^2 -C₂H₄) (**1**) as catalyst). Reaction conditions: 0.001 mol % Rh, 240 equiv. Cu(OPiv)₂, 480 equiv. HOPiv, 30 psig propylene, at 150 °C. After sampling at the 92h time point, an additional 480 equiv. HOPiv were added.

3.2.4 Access to Aerobic Reaction Condition and *in situ* Copper Oxidant Regeneration

Next, we tested the reactivity of complex **1** for benzene alkenylation under aerobic conditions through the combination of benzene, propylene, Cu(OPiv)₂ and HOPiv in the presence of air. In this case, Cu(II) oxidant was regenerated with air and acid *in situ* during the catalysis. When performing the reaction, the reactor was firstly purged with 1 atm unpurified air and then pressured with propylene. Figure 3.2.8A shows TOs and L:B ratios versus time for 0.001 mol% complex **1**, 30 psig propylene with 1 atm air, 240 eq. Cu(OPiv)₂ and 2400 eq. HOPiv at 150 °C. In the absence of air, the maximum TOs are 120. Catalysis continues over a period of at least two days and linear TOs versus time plot was observed to give > 1200 TOs after 48 hours, which indicated no apparent catalyst deactivation. The L:B ratio is ~7 (Figure 3.2.8B), which is reduced comparing to catalysis under anaerobic conditions (L:B = ~11). As catalysis progresses, the L:B ratio increased from 6:1 (4 h plot)

to 8:1 (48 h plot). One of the possibilities is that the branched product α -methylstyrene is slowly decomposing in the presence of air. In order to test this hypothesis, .1000 eq. allyl benzene and 200 eq. α -methylstyrene were added to the reactor with 0.001 mol% complex **1** and 240 eq. $\text{Cu}(\text{OPiv})_2$. The 1 atm air with 85 psig N_2 were used to replace the propylene. The amount of allyl benzene and α -methylstyrene was monitored during the reaction. (Figure 3.2.9) The α -methylstyrene was consumed over time and the concentration of allyl benzene stayed the same. This result indicates that the increase in L:B ratio is due to the decomposition of branched product. The observed TOF (TOF = turnover frequency, calculated from Table 3.2.1, entry 8 and the first data point in Figure 3.2.8A) is decreased from 0.06 s^{-1} for catalysis under anaerobic conditions to 0.01 s^{-1} when for catalysis under aerobic conditions.

The longevity of the catalyst was further attempted with lower catalyst loading (0.0001 mol% of **1** relative to benzene) and $> 13,000$ TOs can be reached after 336 hours catalysis with no evidence of catalyst deactivation (Figure 3.2.8C). The results suggest that the complex **1** is quite stable under aerobic conditions using unpurified air at $150 \text{ }^\circ\text{C}$. Rh and Ru catalysts are reported to produce alkenyl arenes using purified oxygen as the oxidant,^[7-8,45] complex **1** was investigated using 1 atm **unpurified air** as the sole oxidant in the absence of $\text{Cu}(\text{II})$ oxidant. A large amount of acid is essential for the catalysis and the L:B ratio was reduced. Under the best condition we found > 500 TOs after 240 h with L:B ratio of ~ 5 (see Figure 3.2.10). Thus, complex **1** can catalyze oxidative alkenylarene formation by direct use of the oxygen from air. The observed TOF, however, decreased to $6 \times 10^{-4} \text{ s}^{-1}$ (calculated with the 240h time plot).



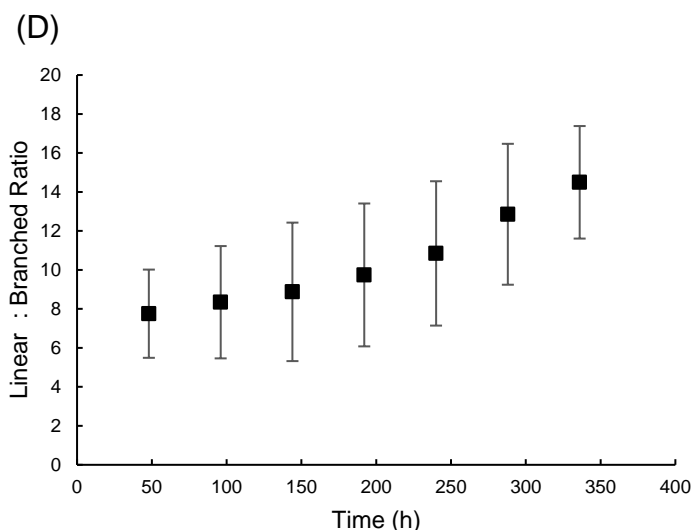
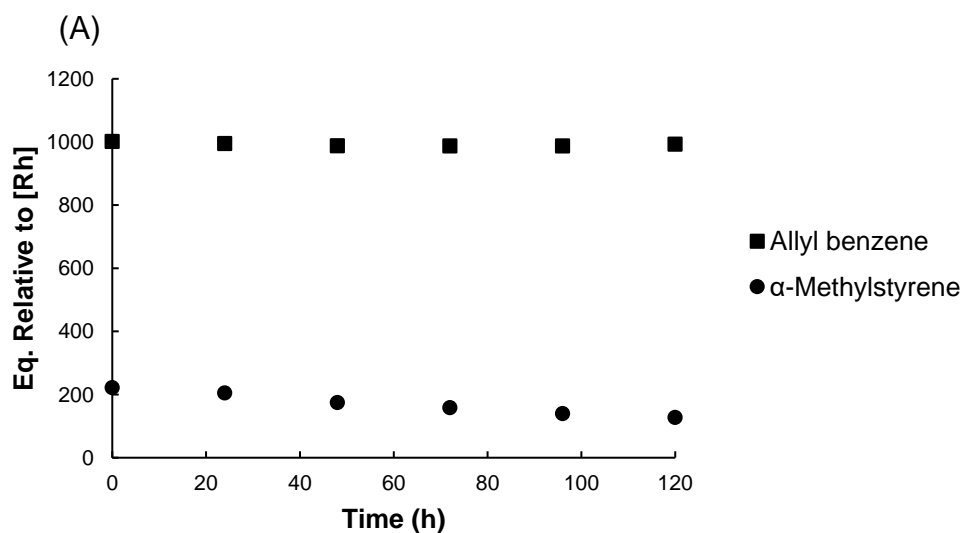


Figure 3.2.8. Hydrophenylation of propylene under aerobic conditions. (A) Plot of turnovers versus time, reaction conditions: $[Rh] = 0.001$ mol% **1** in 10 mL benzene, 240 eq. $Cu(OPiv)_2$, 2400 eq. HOPiv, 30 psig propylene with 1 atm air at 150 °C. The reactor is refilled with air at every sampling point. (B) L:B ratio versus time plot, reaction condition is the same as A. (C) Plot of turnovers versus time, reaction conditions: 0.0001 mol % Rh, 2400 equiv. $Cu(OPiv)_2$, 48000 equiv. HOPiv, 1 atm air, 30 psig propylene, at 150 °C. Fresh air was purged to the reactor every 24 hours and the reaction mixture was sampled every 48 hours at every sample point. The data are from four separate experiments with standard deviations given. (D) L:B ratio versus time plot, reaction condition is the same as C.



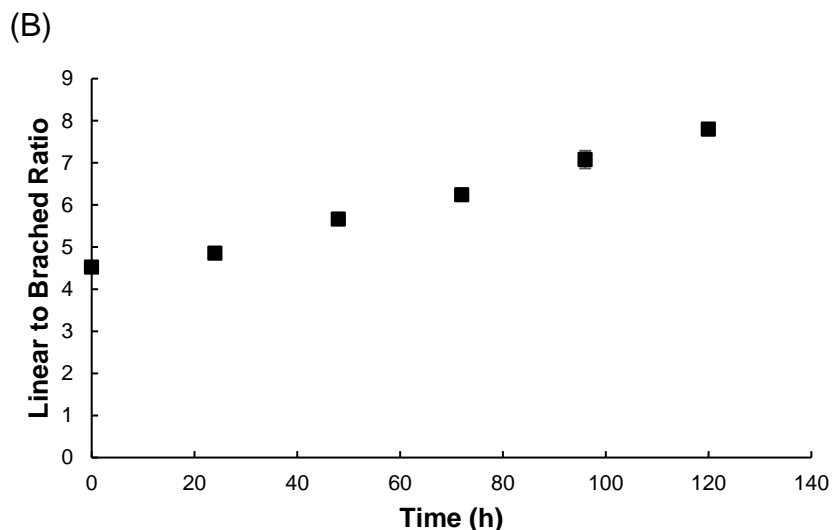


Figure 3.2.9. Alkenyl arenes products decomposition study with (5-FP)Rh(TFA)(η^2 -C₂H₄) (**1**). (A) Plot of remained alkenyl arenes products versus time, reaction conditions: Reaction conditions: 0.001 mol % Rh, 1 atm air, 85 psig N₂, 240 eq. Cu(OPiv)₂ at 150 °C with initial ally benzene (~1000 equivalents to [Rh]) and α -methylstyrene (~200 equivalents to [Rh]) addition. Reactions were sampled every 24 hours and fresh air was purged into reactor with at every sample point. The data are from three separate experiments with standard deviations given. (B) L:B ratio versus time plot, reaction condition is the same as A.

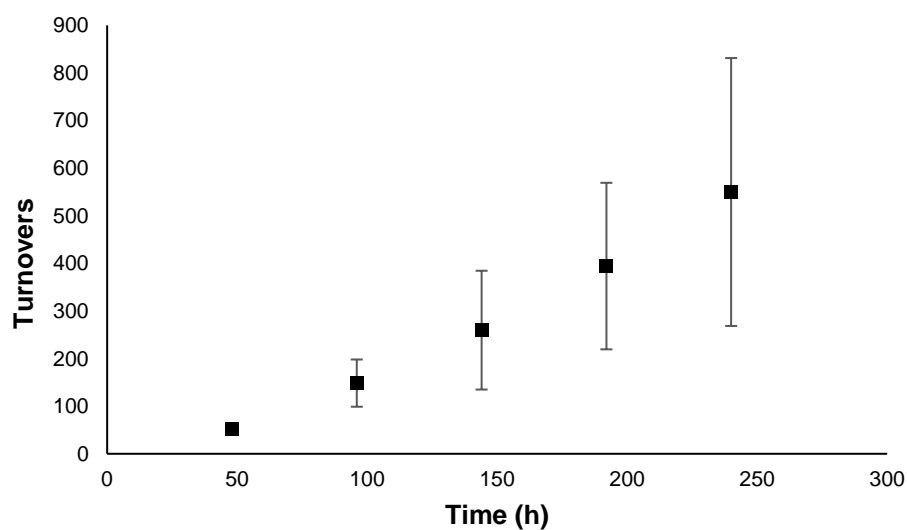


Figure 3.2.10. Catalytic oxidative hydrophenylation of propylene using air as oxidant with (5-FP)Rh(TFA)(η^2 -C₂H₄) (**1**). Reaction conditions: 0.001 mol % Rh 4800 equiv. HOPiv, 1 atm air, 30 psig propylene, at 150 °C. Reactions were sampled every 48 hours and fresh air was purged into reactor with at every sample point. The data are from three separate experiments with standard deviations given.

3.2.5 Investigation of Product Inhibition and Cu(II) Oxidant Dependence

The oxidative hydrophenylation with propylene and ethylene shows different results when using 2400 eq. Cu(OPiv)₂ as oxidant. Increasing the Cu(II) amount (relative to complex **1**) for the ethylene oxidative hydrophenylation resulted in a decrease in the yield compared to lower Cu(II) amounts. For example, the yield drops from 90% to 56% when 2400 eq. Cu(OPiv)₂ was applied comparing with 240 eq. Cu(OPiv)₂ (Table 3.2.1, entries 10 and 11). However, the yield for oxidative hydrophenylation of propylene is not affected by increasing the amount of Cu(II). The yield increased from 72% to 79% when using 2400 eq. Cu(OPiv)₂ compared to 240 eq. Cu(OPiv)₂ (Table 3.2.2, entries 1 and 6). Based on these observations, possible product inhibition was investigated with initial styrene and allylbenzene addition for the hydrophenylation of ethylene and propylene, respectively. Different amounts of styrene and allylbenzene were added at the beginning of the reaction, and the results are summarized in Table 3.2.3. The reaction was greatly inhibited with styrene addition. When 480 eq. of styrene (relative to **1**) were added at the start of the reaction, the percent yield decreased from 95% to 44% after 1 hour (Table 3.2.3, entries 1 and 3). The addition of 960 eq. of styrene nearly terminated the production of styrene, and *trans*-stilbene is the major product. Interestingly, we found that addition of pivalic acid can help moderate the product inhibition, with an increase the percent yield of styrene from 44% to 58% after 1 hour when 480 eq. of pivalic acid (relative to **1**) are added to the reaction (Table 3.2.3, entries 3 and 5). However, the yield still decreases ~40% compared with non-styrene addition trial (Table 3.2.3, entries 1 and 5). Comparing with styrene, allylbenzene exhibits less inhibition, the percent yield decreased from 72% to 57% when 480 eq. of

allylbenzene are added at the beginning of the reaction with propylene and benzene (Table 3.2.3, entries 5 and 7). At this point we cannot assign the increased inhibition of styrene relative to allylbenzene to steric or electronic effects. But it might be expected that other products from hydrophenylation of propylene (α -methylstyrene, *cis*- β -methylstyrene and *trans*- β -methylstyrene), which have less sterically accessible double bonds, will exhibit less product inhibition on the rate of catalysis. (Scheme 3.2.2)

Table 3.2.3. Study of product inhibition of Rh catalyzed oxidative hydrophenylation of ethylene or propylene using styrene and allylbenzene.^[a]

| | Amount of added vinyl arene/eq. ^[b] | HOPIV/eq. ^[c] | Time/h | Products/TOs | | L:B Ratio |
|---|--|--------------------------|--------|-----------------|------------------------|-----------|
| | | | | alkenyl benzene | <i>trans</i> -Stilbene | |
| 1 | / | / | 1 | 114(1) | 1.3 | / |
| 2 | 240 | / | 1 | 78(3) | 5(1) | / |
| 3 | 480 | / | 1 | 53(3) | 9(1) | / |
| 4 | 960 | / | 1 | 3(13) | 22(4) | / |
| 5 | 480 | 480 | 1 | 69(7) | 7(1) | / |
| 6 | / | 480 | 0.5 | 86(4) | / | 11 |
| 7 | 480 | 480 | 0.5 | 68(2) | / | 10 |

[a] Reaction conditions: 0.001 mol% complex **1** relative to benzene, 240 eq. Cu(OPiv)₂, 50 psig ethylene or 30 psig propylene reacted at 150 °C. [b] Styrene is added for entries 1-5 and allylbenzene is added for entry 7. Loading is relative to complex **1**.

In order to investigate the influence of Cu(II) oxidant loading, the oxidative hydrophenylation of propylene using (5-FP)Rh(TFA)(η^2 -C₂H₄) (**1**) with different amount of Cu(OPiv)₂ has performed. The reactor was charged with 10 mL benzene solution of complex **1** (0.001 mol% relative to benzene) with 30 psig propylene, 1 atm air, different amount of Cu(OPiv)₂ (60, 120, 240 and 360 equivalents relative to **1**) and HOPIV (4800 equivalents relative to **1**). Catalysis was monitored at 150 °C and the solution was sampled every 6h. With the addition of excess HOPIV, Cu(OPiv)₂ is completely dissolved in the benzene solution and the concentration of the Cu(II) oxidant is constant along with the reaction. The results are shown in Figure 3.2.11. All the reactions show a linear relation

between products turnovers and reaction time, which indicate no catalyst deactivation (Figure 3.2.11A). When plotting the TOF with Cu(II) oxidant loading, a linear relation was observed. Thus, the reaction rate is likely the first order in Cu(II) oxidant. This result is different from Rh catalyzed olefin hydroarylation under different conditions,^[9] which indicates the catalysis by complex **1** may undergoes a different reaction pathway or, at least, the energetics are altered. This change in dependence of Cu(II) concentration is consistent with our hypothesis to the capping arene ligand inhibits Rh oxidation.

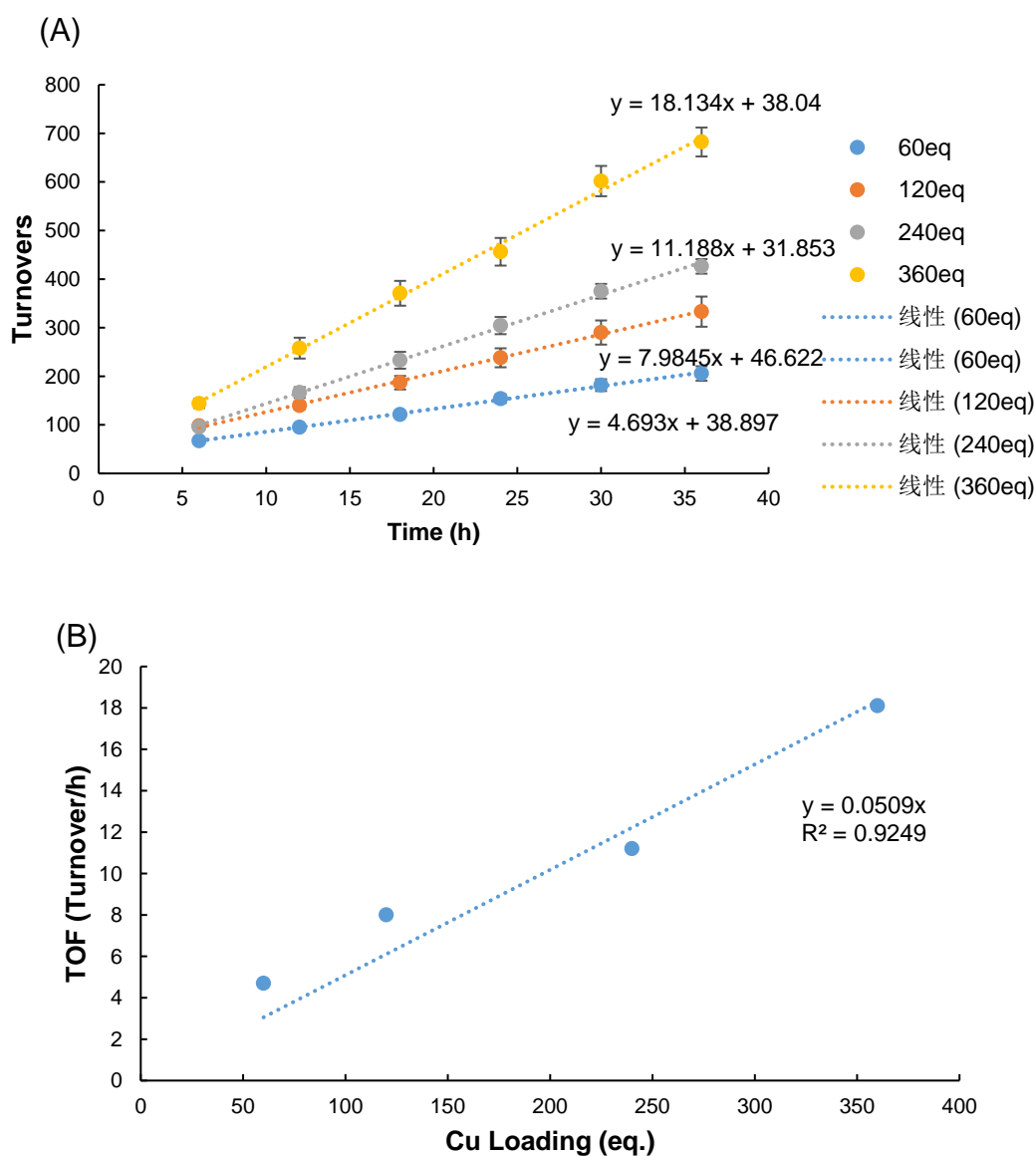


Figure 3.2.11. Catalytic oxidative hydrophenylation of propylene using (5-FP)Rh(TFA)(η^2 -

C₂H₄) (**1**) with different Cu(OPiv)₂ loading. Reaction conditions: 0.001 mol % Rh 4800 equiv. HOPiv, 1 atm air, 30 psig propylene, Cu(OPiv)₂ (60 eq., 120 eq., 240 eq., 360 eq.) at 150 °C. Reactions were sampled every 6 hours and fresh air was purged into reactor with at every sample point. The data are from three separate experiments with standard deviations given. (A) Turnover versus time plot of four different Cu(OPiv)₂ loading. (B) TOF versus Cu(OPiv)₂ loading plot.

3.3 Computational Studies

In this part, all the computational results are from our collaborate Nielsen, R. J. and Goddard, W. A. in Caltech.

3.3.1 Reaction Pathway Prediction

DFT calculations (M06/6-311G**++ including implicit solvation) were used to predict the elementary steps that could be responsible for the reactions of oxidative ethylene and propylene hydrophenylation catalyzed by complex **1**. The predicted free energy surfaces at experimental conditions suggest an oxidative arylation mechanism comprised of benzene C–H activation, olefin insertion, β-hydride elimination and regeneration by O₂ or Cu(II) oxidant. Our predicted L:B ratio of 11:1 from the relative free energies of propene insertion transition states, is consistent with the experimentally observed ratio of 11:1 (Table 3.2.2), which supports the mechanism from the DFT calculations.

At concentrations mimicking reaction conditions, displacement of ethylene from **2** by benzene is predicted from the DFT to be endergonic by 9.2 kcal/mol (Figure 3.3.1). Benzene C–H activation by a concerted metalation-deprotonation (CMD) mechanism has a DFT predicted barrier of 30.6 kcal/mol. Alternatively, oxidative insertion of Rh(I) into a C–H bond followed by reductive elimination of pivalic acid leads to barriers that are lower for both the C–H oxidative addition step (24.4 kcal/mol) and the O–H reductive elimination (26.6 kcal/mol). Thus, despite the observation for many other reactions that the concerted

metalation-deprotonation (CMD) pathway is favored for C–H activation,^[46] the DFT calculations predict that for this system the oxidative addition/reductive elimination process is favored by 4 kcal/mol.

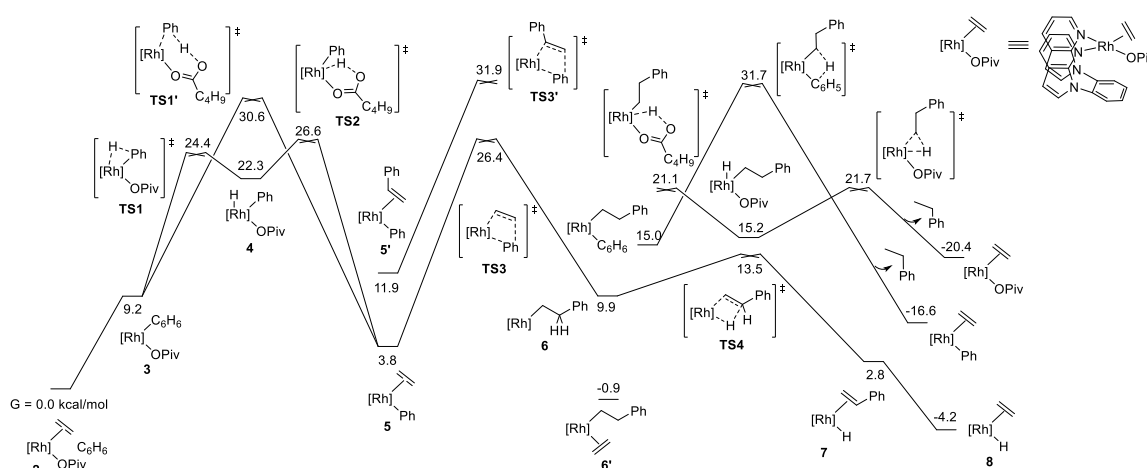


Figure 3.3.1. Free energies (kcal/mol) at 423 K from DFT calculations (M06, including PBF solvation) of the proposed catalytic cycle for conversion of ethylene and benzene to styrene. Conditions: $[\text{Rh}] = 0.11 \text{ mM}$, $[\text{HOPIv}] = 0.053 \text{ M}$, 4.4 atm C_2H_4 , 1 atm O_2 , $[\text{styrene}] = [\text{ethylbenzene}] = 0.1 \text{ M}$, in benzene.

Liberation of HOPIv and coordination of ethylene generates a Rh(I) phenyl species (**5**) that can form a C–C bond via olefin insertion. The DFT predicted transition state for ethylene insertion (**TS3**) lies 26.4 kcal/mol above starting complex **2** and 22.6 kcal/mol above the precursor **5**. The three-coordinate Rh(I) alkyl complex **6** leads to styrene formation via a facile β -hydride elimination through **TS4**, although this can be inhibited by the favorable coordination of an additional ethylene to form **6'**. The resulting Rh(I) hydride with styrene coordinated **7** can undergo ligand exchange with ethylene to form free styrene and complex **8**. Either complex **7** or **8** can potentially react with Cu(II) to regenerate complex **2**.

Minor products can result from branches off this pathway. Protonolysis of the Rh–C

bond in **6** would divert the reaction to produce ethylbenzene. However, using pivalic acid or benzene as a proton source, the barriers for this reaction are predicted to be 8 or 18 kcal/mol higher, respectively, than the β -hydride elimination reaction that leads to the observed product styrene. A more competitive detour is the generation of stilbene by the insertion of styrene in **5'** via **TS3'**. The barrier for the insertion of styrene is only 5 kcal/mol higher than the insertion of ethylene, which is consistent with the experimental observation of stilbene formation once styrene is formed by catalysis. Within the accuracy of DFT calculations we can distinguish whether C–H activation (specifically the reductive elimination transition state **TS2** at 26.6 kcal/mol) or subsequent olefin insertion limits the rate of the overall reaction. Furthermore, the relative rates of these branches are sensitive to the evolving concentrations of ethylene and styrene over the course of reaction.

3.3.2 Linear Selectivity Modeling

Figure 3.3.2 shows the DFT results for the conversion of propylene to linear and branched products. Since propylene is easier to displace by benzene than ethylene, the computed C–H activation barriers are effectively reduced. The resulting phenyl complex lies about 4 kcal/mol uphill and precedes olefin insertion transition states that lead to linear or branched products. The four distinct arrangements of the C_s -symmetric ligand, propylene and phenyl group were predicted by DFT to have free energies of activation within 3 kcal/mol. Both transition states with linear regiochemistry lead to lower activation barriers (24.0 and 25.2 kcal/mol) than those leading to the branched product (26.2 and 26.8 kcal/mol). The ratio of the summed rates through the linear and branched paths predicted using transition state theory at 150 °C predicts a linear:branched ratio of 11.2:1. The lowest-

energy transition state also has a higher vibrational entropy, suggesting the fragments in this arrangement are less tightly packed. The calculated L:B ratio of 11, which is consistent with the value (11:1) observed from experimental observations (see Table 3.2.2), derives from a factor of ~ 2 from the entropic difference and a factor of ~ 5 from the enthalpy differences. The activation energies for β -hydride elimination transition states producing branched or linear olefin are more than 10 kcal/mol lower than the olefin insertion barriers. Therefore, the selectivity determined in the insertion step is not expected to be obscured by β -hydride elimination or product dissociation.

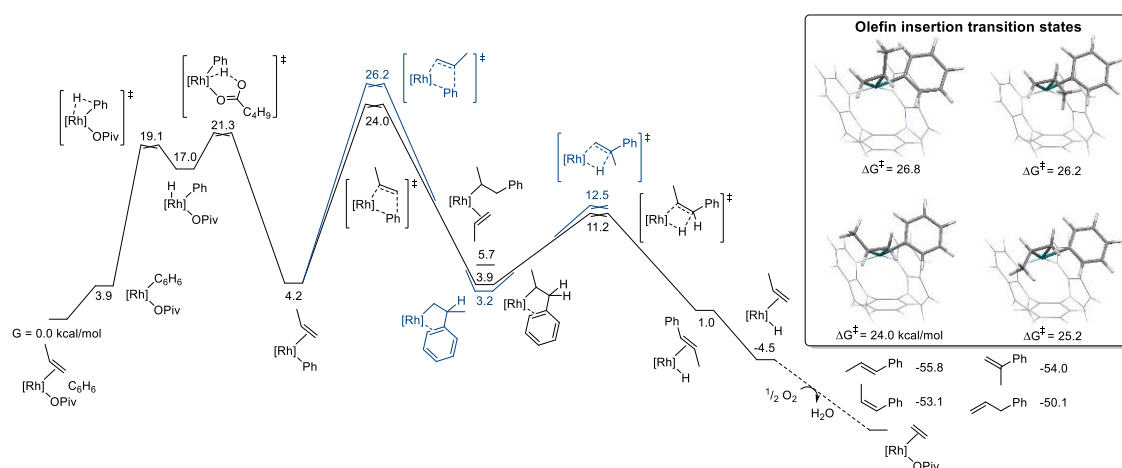


Figure 3.3.2. Free energies (kcal/mol) at 423 K from DFT calculations of our proposed catalytic cycle for the oxidative hydroarylation of propene (conditions as in Figure 3.3.1). The inset displays isomers of the olefin insertion transition state, with the propene and phenyl units drawn as cylinders.

3.3.3 Resistance Towards Oxidation Explanation

As a first step towards understanding the regeneration of **1** by O_2 and $Cu(II)$, intermediates that might result from the reaction of these with the most exergonic, and likely reducing, state in Figure 3.3.1 were considered (Figure 3.3.3). One feasible route involves the $Cu(II)/Cu(I)$ couple, represented computationally by

Cu(OPiv)₂/Cu(OPiv)(C₆H₆). The hydride complex **8** undergoes an exergonic single electron oxidation by Cu(OPiv)₂ via a net carboxyl group transfer. Reductive elimination of pivalic acid to form the the Rh(0) complex **10** is also exergonic. A second oxidation to regenerate **2** is highly exergonic. Direct complexation of O₂ to **8** is unlikely: no complex forms on the triplet surface and the singlet **11** is highly exergonic. A role for the capping arene in activating O₂ was considered, but a singlet Rh(III) complex **12** with O₂ bridging the Rh(III) and an arene carbon lies 26 kcal/mol uphill. Dissociation of ethylene from **8** to create a vacancy is also unlikely ($\Delta G = 27.7$ kcal/mol, **13**). The transition state for an associative substitution of ³O₂ for ethylene was found (**TS5**), which could be the entry to rearrangements that exergonically produce a rhodium peroxide **18**. The activation barrier ($\Delta G^\ddagger = 25.5$ kcal/mol) is high but comparable to those earlier in the mechanism. Slightly more favorable is a direct hydrogen-atom abstraction by ³O₂ (**TS6**, $\Delta G^\ddagger = 22.2$ kcal/mol).^{[47-}

^{51]} However, a radical chain mechanism for converting the hydride is perhaps more likely than the direct involvement of O₂. For example, reaction of **8** with a hydroperoxyl radical (generated photochemically or via decomposition of a peroxide intermediate) yields the Rh(II) complex **14**. The weakened Rh–H bond can easily be broken by ³O₂ to yield **18**, effecting a net insertion of O₂ into the Rh^I–H bond. Alternatively, the Rh(I) superoxide complex **19** is able to abstract a hydrogen atom from **8** exergonically to yield the Rh(0) **10**, which regenerates **19** spontaneously via reaction with O₂.⁷⁶ A full mechanistic study including ligands that do not facilitate aerobic oxidation is beyond the scope of this paper, but these DFT calculations indicate that both anaerobic and aerobic pathways are viable.

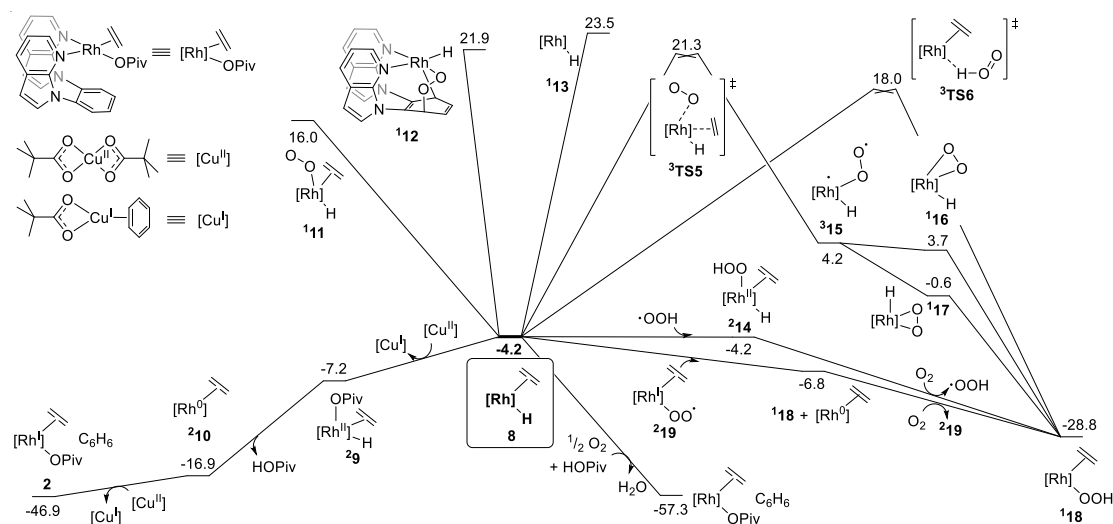


Figure 3.3.3. Free energies (kcal/mol) at 423 K from DFT calculations for reactions of oxidants with the rhodium hydride **8**. Conditions: $[\text{Cu}^{\text{II}}] = [\text{Cu}^{\text{I}}] = [\text{Rh}] = [\cdot\text{OOH}] = 0.11\text{mM}$, $[\text{HOPIv}] = 0.053\text{M}$, 4.4 atm C_2H_4 , 1 atm O_2 , in benzene. Superscripts denote spin multiplicities.

3.4 Conclusion

To our knowledge, there are no previous example of catalytic conversion of benzene and propylene to linear alkylbenzene with high selectivity for anti-Markovnikov products under aerobic conditions. We have reported that a "capping arene" ligand supported Rh(I) complex $(5\text{-FP})\text{Rh}(\text{TFA})(\eta^2\text{-C}_2\text{H}_4)$ serves as catalyst precursor under anaerobic or aerobic conditions. The special designed ligand can prevent Rh(I) center from oxidation. The Rh catalyst is quite stable in air at 150 °C and the catalysis can use air as the direct oxidant without any Cu(II) salts. The Rh catalyst shows a remarkable longevity and stability. Under optimized condition, a significant turnover number ($> 13,000$) can be reached without obvious catalyst deactivation at 150 °C for at least 2 weeks of reaction, and the catalyst can achieve a linear to branched ratio up to 18:1, which is to our knowledge the highest ratio for conversion of hydrocarbon substrates.

3.5 Experimental Section

$[\text{Rh}(\eta^2\text{-C}_2\text{H}_4)_2(\mu\text{-TFA})]_2$ and 1,2-bis(*N*-7-azaindoly)benzene (5-FP) were prepared according to literature procedures.^[32,53] All other reagents were purchased from commercial sources and used as received.

Synthesis of (5-FP)Rh(TFA)($\eta^2\text{-C}_2\text{H}_4$) (1). A THF solution (10 mL) of 1,2-bis(*N*-7-azaindoly)benzene (0.0810 g, 2.61×10^{-4} mol) was added to a THF solution (10 mL) of $[\text{Rh}(\eta^2\text{-C}_2\text{H}_4)_2(\mu\text{-TFA})]_2$ (0.0800 g, 1.47×10^{-4} mol) dropwise and stirred for 48 h. The reaction mixture was dried under vacuum. The resulting solid was dissolved in minimal THF (2 mL), and pentane (30 mL) was added to the solution to give a yellow precipitate. The solid was collected by filtration, washed with pentane (3 x 10 mL), and dried under vacuum to afford the analytically pure **1** (0.110 g, yield = 76%). X-ray quality crystals of **1** were grown by the vapor diffusion method using THF and *n*-pentane. ^1H NMR (CD_2Cl_2 , 600 MHz): δ = 9.27 (dd, $^3J_{\text{HH}} = 5.3$ Hz, 1.4 Hz, 1H, 5 or 5'), 8.37 (d, $^3J_{\text{HH}} = 5.5$ Hz, 1H, 5 or 5'), 7.91 (td, $^3J_{\text{HH}} = 7.7$ Hz, 1.5 Hz, 1H, 7 or 7'), 7.86 (dd, $^3J_{\text{HH}} = 7.9$ Hz, 1.6 Hz, 1H, 6 or 6'), 7.77-7.81 (m, 2H, 1H of 6 or 6' and 1H of 7 or 7'), 7.58 (dd, $^3J_{\text{HH}} = 7.8$ Hz, 1.3 Hz, 1H, 3 or 3'), 7.45 (dd, $^3J_{\text{HH}} = 7.9$, 1.4 Hz, 1H, 3 or 3'), 7.31 (d, $^3J_{\text{HH}} = 3.6$ Hz, 1H, 1 or 1'), 7.23 (d, $^3J_{\text{HH}} = 3.5$ Hz, 1H, 1 or 1'), 7.08 (dd, $^3J_{\text{HH}} = 7.9$ Hz, 5.3 Hz, 1H, 4 or 4'), 6.73 (dd, $^3J_{\text{HH}} = 7.8$ Hz, 5.5 Hz, 1H, 4 or 4'), 6.48 (d, $^3J_{\text{HH}} = 3.6$ Hz, 1H, 2 or 2'), 6.46 (d, $^3J_{\text{HH}} = 3.6$ Hz, 1H, 2 or 2'), 2.75 (br, 2H, ethylene-*H*), and 2.54 (br, 2H, ethylene-*H*) ppm. ^{19}F NMR (CD_2Cl_2 , 600 MHz): δ = -74.0 (s, TFA) ppm. ^{13}C - $\{^1\text{H}\}$ NMR (CD_2Cl_2 , 150 MHz): δ = 161.9 (q, OC(O)CF_3 , $^2J_{\text{CF}} = 34$ Hz), 151.9 (s, Ar-C), 150.4 (s, Ar-C), 148.8 (s, Ar-C), 146.2 (s, Ar-C), 131.2 (s, Ar-C), 134.8 (s, Ar-C), 131.9 (s, Ar-C), 131.1 (s, Ar-C), 131.0 (s, Ar-

C), 130.6 (s, Ar-C), 130.5 (s, Ar-C), 130.4 (s, Ar-C), 130.0 (s, Ar-C), 128.8 (s, Ar-C), 121.8 (s, Ar-C), 121.1 (s, Ar-C), 117.4 (s, Ar-C), 116.6 (s, Ar-C), 103.0 (s, ethylene-C), 102.7 (s, ethylene-C) ppm. Peak of OC(O)CF₃ is overlapped with some Ar-C peaks. Elemental analysis for C₂₄H₁₈F₃N₄O₂Rh: Calculated; C: 52.00%; H: 3.27%; N: 10.11%, Found; C: 51.21%; H: 3.26%; N: 10.00%.

Catalytic Oxidative Hydrophenylation of Ethylene. A representative catalytic reaction is described (Table 3.2.1, entry 9). A stock solution containing **1** (0.0156 g, 0.0280 mmol, 0.001 mol % of rhodium catalyst), hexamethylbenzene (0.0911 g, 0.561 mmol), and benzene (250 mL) was prepared in a volumetric flask. Thick-walled glass Fisher-Porter reactors were charged with stock solution (10 mL), pivalic acid (0.0550 g, 0.539 mmol) and Cu(OPiv)₂ (0.0716 g, 0.269 mmol). The vessels were sealed, pressurized with ethylene (50 psig), and subsequently stirred and heated to 150 °C. The color of the reaction mixture is deep blue at the beginning of the reaction and turns to colorless when all Cu oxidant is consumed. The reaction was sampled when the solution turned colorless. The reactors were cooled to room temperature and aliquots of the reaction mixture (< 200 μL) were analyzed by GC/FID using relative peak areas versus the internal standard (hexamethylbenzene).

Catalytic Oxidative Hydrophenylation of Propylene. A representative catalytic reaction is described (Table 3.2.2, entry 1). A stock solution containing **1** (0.0156 g, 0.0280 mmol, 0.001 mol % of rhodium catalyst), hexamethylbenzene (0.0911 g, 0.561 mmol), and benzene (250 mL) was prepared in a volumetric flask. Thick-walled glass Fisher-Porter reactors were charged with stock solution (10 mL), pivalic acid (0.0550 g, 0.539 mmol) and Cu(OPiv)₂ (0.0716 g, 0.269 mmol). The vessels were sealed, pressurized with propylene

(30 psig), and subsequently stirred and heated to 150 °C. The color of the reaction mixture is deep blue at the beginning of the reaction and turns to colorless when all Cu oxidant is consumed. The reaction was sampled when the solution turned colorless. The reactors were cooled to room temperature and aliquots of the reaction (< 200 µL) mixture were analyzed by GC/FID using relative peak areas versus the internal standard (hexamethylbenzene).

Catalytic Oxidative Hydrophenylation of Propylene with Cu(II) Oxidant Using *in situ* Regeneration. A representative catalytic reaction is described (using **1** as the catalyst). A stock solution containing **1** (0.0156 g, 0.0280 mmol, 0.001 mol % of rhodium catalyst), hexamethylbenzene (0.0911 g, 0.561 mmol), and benzene (250 mL) was prepared in a volumetric flask. Thick-walled glass Fisher-Porter reactors were charged with stock solution (10 mL), pivalic acid (0.0550 g, 0.539 mmol) and Cu(OPiv)₂ (0.0716 g, 0.269 mmol). The vessels were sealed, pressurized with propylene (30 psig), and subsequently stirred and heated to 150 °C. The color of the reaction mixture is deep blue at the beginning of the reaction and turns to colorless when all Cu oxidant is consumed. The reaction was sampled when the solution turned colorless. The reactors were cooled to room temperature and aliquots of the reaction mixture (< 200 µL) were analyzed by GC/FID using relative peak areas versus the internal standard (hexamethylbenzene). After the sampling, 1 atm fresh air was purged into the reactor. Then the reactor was pressurized with 50 psig N₂. The reactor was heated to 120 °C for 15 min for *in situ* Cu(II) oxidant regeneration. After the regeneration, the reactors were cooled to room temperature and purged and pressurized with propylene (30 psig). The vessels were subsequently stirred and heated to 150 °C for the reaction.

Air *in situ* Catalytic Oxidative Hydrophenylation of Propylene. A representative catalytic reaction is described (Figure 3.2.8A). A stock solution containing **1** (0.0156 g, 0.0280 mmol, 0.001 mol % of rhodium catalyst), hexamethylbenzene (0.455 g, 2.24 mmol), and benzene (250 mL) was prepared in a volumetric flask. Thick-walled glass Fisher-Porter reactors were charged with stock solution (1 mL) and benzene (9 mL), pivalic acid (0.550 g, 5.38 mmol) and Cu(OPiv)₂ (0.0716 g, 0.269 mmol). The vessels were sealed and purged with 1 atm air, pressurized with propylene (30 psig), and subsequently stirred and heated to 150 °C. After every 24h, the reactors were cooled down to room temperature first and to 0°C with ice bath. Then the reactor was purged with air (1 atm) and pressurized with propylene (30 psig), and reheated. The reaction mixture was sampled every 48h. Aliquots of the reaction (< 200 µL) mixture were analyzed by GC/FID using relative peak areas versus the internal standard (hexamethylbenzene).

Catalytic Oxidative Hydrophenylation of Propylene Using Air as Oxidant. A stock solution containing **1** (0.0156 g, 0.0280 mmol, 0.001 mol % of rhodium catalyst), hexamethylbenzene (0.0911 g, 0.561 mmol), and benzene (250 mL) was prepared in a volumetric flask. Thick-walled glass Fisher-Porter reactors were charged with stock solution (10 mL) and pivalic acid (0.5500 g, 5.39 mmol). The vessels were sealed and purged with 1 atm air, pressurized with propylene (30 psig), and subsequently stirred and heated to 150 °C. The reaction was sampled every 48 h. At each time point, the reactors were cooled to room temperature, sampled, purged with air (1 atm) and pressurized with propylene (30 psig), and reheated. Aliquots of the reaction mixture (< 200 µL) were analyzed by GC/FID using relative peak areas versus the internal standard

(hexamethylbenzene).

3.6 References

- [1] Caro, J.; Noack, M., Chapter 1 - Zeolite Membranes – Status and Prospective. In *Advances in Nanoporous Materials*, Ernst, S., Ed. Elsevier: 2010; Vol. 1, pp 1-96.
- [2] Perego, C.; Ingallina, P., *Catal. Today* **2002**, *73*, 3-22.
- [3] Gerzeliev, I. M.; Khadzhiev, S. N.; Sakharova, I. E., *Petroleum Chemistry* **2011**, *51*, 39-48.
- [4] Čejka, J.; Wichterlová, B., *Catalysis Reviews* **2002**, *44*, 375-421.
- [5] Perego, C.; Ingallina, P., *Green Chemistry* **2004**, *6*, 274-279.
- [6] Wittcoff, H. A.; Reuben, B. G.; Plotkin, J. S., *Industrial organic chemicals*. John Wiley & Sons, Inc: Hoboken, NJ, 2012.
- [7] Takaya, M.; Hajime, Y., *Chem. Lett.* **2000**, *29*, 1064-1065.
- [8] Matsumoto, T.; Periana, R. A.; Taube, D. J.; Yoshida, H., *J. Catal.* **2002**, *206*, 272-280.
- [9] Vaughan, B. A.; Webster-Gardiner, M. S.; Cundari, T. R.; Gunnoe, T. B., *Science* **2015**, *348*, 421-424.
- [10] Cornils, B.; Herrmann, W. A., *J. Catal.* **2003**, *216*, 23-31.
- [11] Cole-Hamilton, D. J., *Science* **2003**, *299*, 1702-1706.
- [12] Oxgaard, J.; Muller, R. P.; Goddard, W. A.; Periana, R. A., *J. Am. Chem. Soc.* **2004**, *126*, 352-363.
- [13] Periana, R. A.; Liu, X. Y.; Bhalla, G., *Chem. Commun.* **2002**, 3000-3001.

-
- [14] Bhalla, G.; Oxgaard, J.; Goddard, W. A.; Periana, R. A., *Organometallics* **2005**, *24*, 3229-3232.
- [15] Lail, M.; Arrowood, B. N.; Gunnoe, T. B., *J. Am. Chem. Soc.* **2003**, *125*, 7506-7507.
- [16] Lail, M.; Bell, C. M.; Conner, D.; Cundari, T. R.; Gunnoe, T. B.; Petersen, J. L., *Organometallics* **2004**, *23*, 5007-5020.
- [17] Luedtke, A. T.; Goldberg, K. I., *Angew. Chem. Int. Ed.* **2008**, *47*, 7694-7696.
- [18] Clement, M. L.; Grice, K. A.; Luedtke, A. T.; Kaminsky, W.; Goldberg, K. I., *Chem. Eur. J.* **2014**, *20*, 17287-17291.
- [19] McKeown, B. A.; Foley, N. A.; Lee, J. P.; Gunnoe, T. B., *Organometallics* **2008**, *27*, 4031-4033.
- [20] McKeown, B. A.; Prince, B. M.; Ramiro, Z.; Gunnoe, T. B.; Cundari, T. R., *ACS Catal.* **2014**, *4*, 1607-1615.
- [21] Grice, K. A.; Kaminsky, W.; Goldberg, K. I., *Inorg. Chim. Acta* **2011**, *369*, 76-81.
- [22] Bair, J. S.; Schramm, Y.; Sergeev, A. G.; Clot, E.; Eisenstein, O.; Hartwig, J. F., *J. Am. Chem. Soc.* **2014**, *136*, 13098-13101.
- [23] Ahuja, R.; Punji, B.; Findlater, M.; Supplee, C.; Schinski, W.; Brookhart, M.; Goldman, A. S., *Nature Chemistry* **2010**, *3*, 167.
- [24] Dobereiner, G. E.; Yuan, J.; Schrock, R. R.; Goldman, A. S.; Hackenberg, J. D., *J. Am. Chem. Soc.* **2013**, *135*, 12572-12575.
- [25] Lim, Y.-G.; Kang, J.-B.; Kim, Y. H., *J. Chem. Soc., Perkin Trans. 1* **1996**, 2201-2206.

-
- [26] Webster-Gardiner, M. S.; Chen, J.; Vaughan, B. A.; McKeown, B. A.; Schinski, W.; Gunnoe, T. B., *J. Am. Chem. Soc.* **2017**, *139*, 5474-5480.
- [27] Matsumoto, T.; Taube, D. J.; Periana, R. A.; Taube, H.; Yoshida, H., *J. Am. Chem. Soc.* **2000**, *122*, 7414-7415.
- [28] Olah, G. A.; Flood, S. H.; Kuhn, S. J.; Moffatt, M. E.; Overchuck, N. A., *J. Am. Chem. Soc.* **1964**, *86*, 1046-1054.
- [29] Olah, G. A.; Flood, S. H.; Moffatt, M. E., *J. Am. Chem. Soc.* **1964**, *86*, 1060-1064.
- [30] Kovacic, P.; Hiller, J. J., *J. Org. Chem.* **1965**, *30*, 1581-1588.
- [31] Olah, G. A.; Olah, J. A.; Ohyama, T., *J. Am. Chem. Soc.* **1984**, *106*, 5284-5290.
- [32] Zhao, S.-B.; Song, D.; Jia, W.-L.; Wang, S., *Organometallics* **2005**, *24*, 3290-3296.
- [33] Liu, Z.; Yamamichi, H.; Madrahimov, S. T.; Hartwig, J. F., *J. Am. Chem. Soc.* **2011**, *133*, 2772-2782.
- [34] Kanas, D. A.; Geier, S. J.; Vogels, C. M.; Decken, A.; Westcott, S. A., *Inorg. Chem.* **2008**, *47*, 8727-8735.
- [35] Geier, S. J.; Chapman, E. E.; McIsaac, D. I.; Vogels, C. M.; Decken, A.; Westcott, S. A., *Inorg. Chem. Commun.* **2006**, *9*, 788-791.
- [36] Budzelaar, P. H. M.; Moonen, N. N. P.; de Gelder, R.; Smits, J. M. M.; Gal, A. W., *Chem. Eur. J.* **2000**, *6*, 2740-2747.
- [37] Vierkoetter, S. A.; Barnes, C. E.; Garner, G. L.; Butler, L. G., *J. Am. Chem. Soc.* **1994**, *116*, 7445-7446.

-
- [38] Noam, S.; Akito, O.; David, S.; Kazuhiko, S.; Yoshiaki, N.; John, H., *Nickel-Catalyzed Anti-Markovnikov Hydroarylation of Unactivated Alkenes with Unactivated Arenes Facilitated by non-Covalent Interactions*. 2019.
- [39] Caddy, P.; Green, M.; Smart, L. E.; White, N., *J. Chem. Soc., Chem. Commun.* **1978**, 839-841.
- [40] Guggenberger, L. J.; Cramer, R., *J. Am. Chem. Soc.* **1972**, *94*, 3779-3786.
- [41] Mlekuz, M.; Bougeard, P.; Sayer, B. G.; McGlinchey, M. J.; Rodger, C. A.; Churchill, M. R.; Ziller, J. W.; Kang, S. K.; Albright, T. A., *Organometallics* **1986**, *5*, 1656-1663.
- [42] Cramer, R., *J. Am. Chem. Soc.* **1964**, *86*, 217-222.
- [43] O'Reilly, M. E.; Fu, R.; Nielsen, R. J.; Sabat, M.; Goddard, W. A.; Gunnoe, T. B., *J. Am. Chem. Soc.* **2014**, *136*, 14690-14693.
- [44] E. J. Parish, S. A. Kizito. Copper(I) Acetate *e-EROS Encyclopedia of Reagents for Organic Synthesis*; John Wiley & Sons, Inc: Hoboken, NJ, 2001.
- [45] Weissman, H.; Song, X.; Milstein, D., *J. Am. Chem. Soc.* **2001**, *123*, 337-338.
- [46] David, L.; Keith, F., *Chem. Lett.* **2010**, *39*, 1118-1126.
- [47] Keith, J. M.; Nielsen, R. J.; Oxgaard, J.; Goddard, W. A., *J. Am. Chem. Soc.* **2005**, *127*, 13172-13179.
- [48] Keith, J. M.; Muller, R. P.; Kemp, R. A.; Goldberg, K. I.; Goddard, W. A.; Oxgaard, J., *Inorg. Chem.* **2006**, *45*, 9631-9633.
- [49] Decharin, N.; Popp, B. V.; Stahl, S. S., *J. Am. Chem. Soc.* **2011**, *133*, 13268-13271.

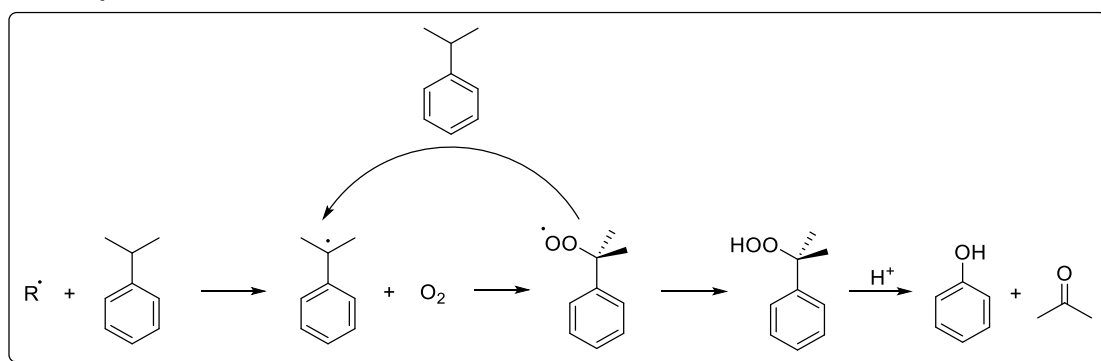
-
- [50] Gaggioli, C. A.; Belpassi, L.; Tarantelli, F.; Zuccaccia, D.; Harvey, J. N.; Belanzoni, P., *Chemical Science* **2016**, 7, 7034-7039.
- [51] Keith, J. M.; Goddard, W. A.; Oxgaard, J., *J. Am. Chem. Soc.* **2007**, 129, 10361-10369.
- [52] Look, J. L.; Wick, D. D.; Mayer, J. M.; Goldberg, K. I., *Inorg. Chem.* **2009**, 48, 1356-1369.
- [53] Werner, H.; Poelsma, S.; Schneider, M. E.; Windmüller, B.; Barth, D., *Chem. Ber.* **1996**, 129, 647-652.

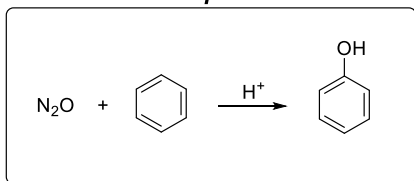
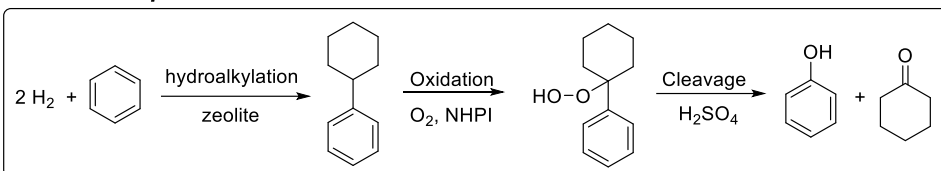
4 Undirected Arene Acetoxylation with Cu Catalysts

4.1 Introduction

Acetoxylation of benzene is considered to be a possible alternative to phenol production. Currently 95% of phenol was produced through Hock process, which uses benzene and propylene as feedstock and involved the partial oxidation of cumene via Hock rearrangement.^[1] The problem with this process is same amount of phenol and acetone were produced, however, the demand for phenol is higher than acetone which cause the price of acetone to fall and penalizes the economics of the entire process. The process developed by Dutch State Mines (DSM) and Solutia utilize N_2O to direct oxidize benzene to phenol. However, the difficulty in finding a low-cost route to N_2O limit its application.^[2] ExxonMobil developed a process in which benzene and hydrogen were used as feedstock. Benzene is firstly hydrogenated to cyclohexene and hydrophenylated to produce cyclohexylbenzene. The latter product is oxidized to hydroperoxide and then cleaved to phenol and cyclohexanone.^[2] (Scheme 4.1.1)

Hock process



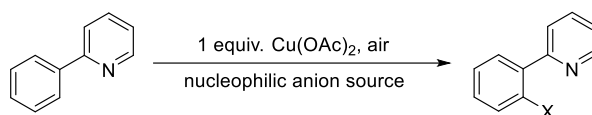
DSM and Solutia process**ExxonMobil process****Scheme 4.1.1.** Industrial processes for phenol production.

$Pd(OAc)_2$ -based acetoxylation of benzene has been reviewed in great detail. Although $Pd(OAc)_2$ catalyzed arene acetoxylation has achieved great success during the past several years, the high price of Pd and easily accessible decomposition to Pd(0) limit its practical use. Copper is considered to be a potential substitute for noble metals; however, its use for catalytic C–H bond functionalization has traditionally been limited as C–H bond functionalization by Cu complexes generally requires the presence of a directing group.^[3,4]

In 2006, Jinquan Yu and co-workers reported functionalization of an inert C–H bond using pyridine as the directing group with $Cu(OAc)_2$ as the promoter.^[3] The use of a stoichiometric amount of $Cu(OAc)_2$ with different anion sources produced a variety of substituted arene products (Table 4.1.1). Although the acetoxylation product was not observed in the reaction, the hydroxylation product could be obtained with moderate yield (Table 4.1.1, entry 9). In addition, by lowering the $Cu(OAc)_2$ loading to 10 mol% in the presence of O_2 , acetoxylation and diacetoxylation products were obtained with 37% and 56% yields, respectively. No kinetic isotope effect (KIE) was observed in an intramolecular competition reaction, which indicates that the reaction likely undergoes a different mechanism than Pd-catalyzed acetoxylation or at least has different energetic parameters.

A single electron transfer (SET) from the aryl ring to the coordinated Cu(II) to produce a radical cation intermediate was suggested as the rate-determining step for the reaction. Cheng and co-workers have utilized anhydride additives to help the acetoxylation with same substrate motif.^[4] In contrast to the report by Yu and co-workers, functionalization was proposed to occur through the disproportionation of Cu(II) to form Cu(III) intermediate rather than through the formation of a radical cation intermediate via SET.^[4]

Table 4.1.1. Cu(OAc)₂-mediated C–H functionalization with pyridine as the directing group.^[3]



| Entry | Anion Source | Solvent | Product (X) | Yield (%) |
|-------|-------------------|--------------------------------------|------------------|-----------|
| 1 | / | Br ₂ CHCHBr ₂ | Br | 65 |
| 2 | I ₂ | ClCH ₂ CH ₂ Cl | I | 61 |
| 3 | TMSCN | MeCN | CN | 42 |
| 4 | / | MeNO ₂ | CN | 67 |
| 5 | TsNH ₂ | MeCN | TsNH | 74 |
| 6 | <i>p</i> -CN-PhOH | MeCN | <i>p</i> -CN-PhO | 35 |
| 7 | PhSH | DMSO | PhS | 40 |
| 8 | MeSSMe | DMSO | MeS | 51 |
| 9 | H ₂ O | DMSO | OH | 22 |

During the past decade, additional directing groups have been developed to facilitate Cu catalyzed hydroxylation (Figure 4.1.1).^[5-8] Yu's group also reported hydroxylation using a series of substituted amide groups as directing groups.^[5] Unfortunately, none of the substrates with *N*-OMe, *N*-isopropyl, *N*-phenyl or *N*-(4-NO₂)-phenyl groups were hydroxylated. However, by using the substrate with a more electron deficient *N*-aryl group (Figure 4.1.1, ArF), 23% yield of the hydroxylation product was obtained when using CuBr as an additive. In addition, a the quinoline-based supporting ligand and added base (Cs₂CO₃

with 1-adamantanecarboxylic acid), the reaction achieves up to 80% yield based on the substrate and demonstrates good functional group tolerance for substituents on the benzene ring. In 2015, Yu and co-workers reported oxazolyamide as a directing group for Cu catalyzed hydroxylation.^[6] In this study, no supporting ligand was required, and water was shown to be essential for this transformation. As opposed to their initial study, the kinetic isotope effect (KIE) study of this reaction showed a k_H/k_D value of 3.2. The addition of the common radical trap TEMPO (2,2,6,6-Tetramethylpiperidin-1-yl)oxyl) had a negligible effect on the reaction, which indicates that the hydroxylation mechanism most likely involves a Cu mediated C–H bond cleavage rather than a pathway involving free radical formation.

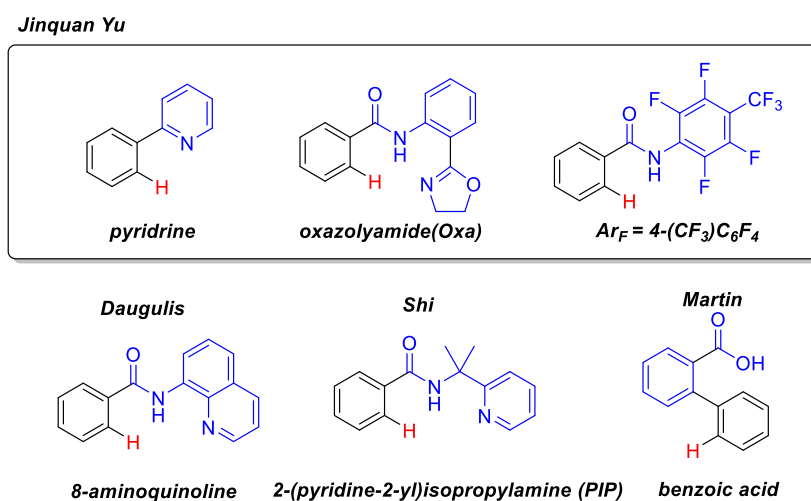
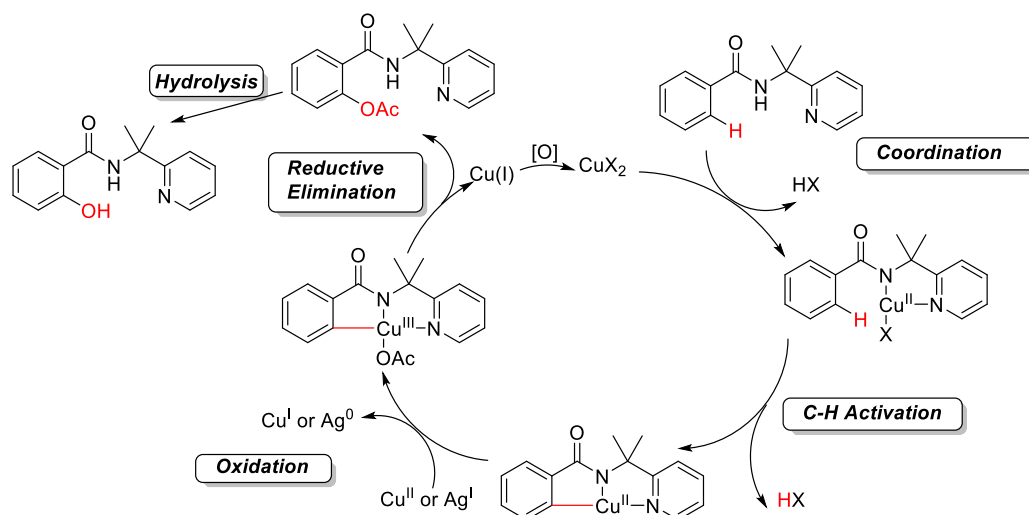


Figure 4.1.1. Directing groups for Cu mediated hydroxylation.^[1-7]

Shi and co-workers utilized 2-(pyridine-2-yl)isopropylamine (PIP) as a directing group for Cu catalyzed hydroxylation and acetoxylation.^[7] In this reaction, Ag(I) or Cu(II) oxidants were used with a phase transfer catalyst, tetrabutylammonium iodide (TBAI), to promote the generation of a Cu(III) intermediate. The proposed mechanism is shown in Scheme 4.1.2. Coordination of the Cu(II) salt to the substrate is followed by C–H activation

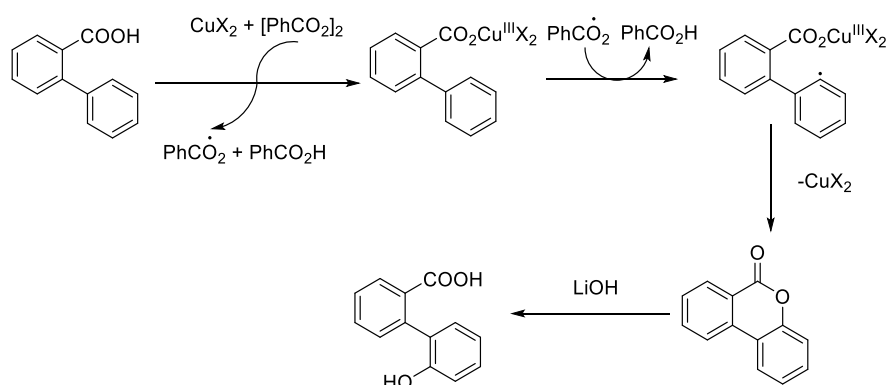
of the substrate, generating a tri-coordinate Cu(II) intermediate. Then, the Cu(II) intermediate is oxidized by Ag(I) or Cu(II) oxidant to give Cu(III). The Cu(III) intermediate reductively eliminates the product and regenerates the catalyst precursor, thus completing the catalytic cycle. The reaction with Ag(I) or Cu(II) oxidants achieved higher yield and a faster reaction rate than Yu's system which used O₂ as the oxidant.^[3-5] In support of the proposed mechanism, a high KIE of 5.3 was observed in acetoxylation with PIP directed benzene, and the presence of radical traps did not have an effect on either the yield or the reaction rate.



Scheme 4.1.2. Proposed mechanism for PIP group directed Cu catalyzed hydroxylation/acetoxylation.^[5]

In addition to the common practice of using an amide group to direct the hydroxylation reaction, benzoic acid has also proven to be a suitable candidate.^[8] In contrast to utilizing an amide directing group, a stoichiometric amount of benzoyl peroxide is required to achieve high conversion. The proposed mechanism is quite different from the PIP group directed Cu catalyzed hydroxylation/acetoxylation based on a much smaller KIE (1.22 versus 5.3) and the inhibition by radical traps. The proposed mechanism is shown in Scheme 4.1.3. The addition of Cu(II) and [PhCO₂]₂ generates a square-planar or square-

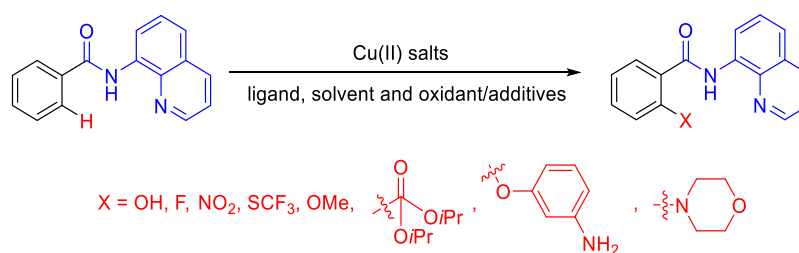
pyramidal Cu(III) intermediate. An aryl radical is then formed and undergoes CO₂ extraction from the phenyl radical. The formed free radical in the reaction mixture then triggers an H-atom abstraction from the *ortho* position of the benzene ring. Finally, the radical intermediate with the Cu(III) metal center engages in intramolecular C–O bond formation and regenerates the Cu(II) catalyst.



Scheme 4.1.3. Proposed mechanism for benzoic acid group directed Cu catalyzed hydroxylation.

Another well-known directing group for Cu catalyzed C–H bond functionalization is Daugulis's 8-aminoquinoline benzamide motif, which was originally used for Pd-catalyzed sp² and sp³ C–H bond arylation.^[9] Jana and co-workers reported Cu catalyzed hydroxylation based on this directing group. An excess amount (10 equiv. relative to Cu) of pyridine additive is required to facilitate this transformation. Without the pyridine additive, the only observed product is the result of substrate dimerization. In addition to the hydroxylation, Cu catalyzed fluorination, nitration, phosphorylation, etherification, sulfenylation, and amination were reported with Daugulis's directing group.^[10-16] The functional group structures are shown in Scheme 4.1.4. Shannon Stahl and co-workers have published a detailed study of Cu mediated etherification and chlorination using Daugulis's directing group as well.^[16] Under acidic conditions, the β position of the quinoline ring is

chlorinated, while the *ortho* position of the benzene ring is etherified under basic conditions. KIE values of 1 and 5.7 were observed for chlorination and etherification, respectively. Chlorination is proposed to occur through SET, while an organometallic mechanism was proposed for etherification.



Scheme 4.1.4. Cu catalyzed C–H bond functionalization with Daugulis’s directing group.

Although Cu catalyzed C–H bond functionalization using directing groups has been studied thoroughly, to our knowledge there are no reported examples of non-directed hydroxylation or acetoxylation catalyzed by Cu. In this Chapter, the acetoxylation of benzene mediated by Cu(II) salts is discussed.

4.2 Results and Discussions

4.2.1 *Cu(OAc)₂ Mediated Benzene Acetoxylation and Optimization of Reaction*

Conditions

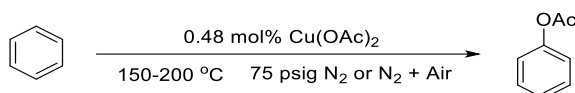
Phenyl acetates have been observed as a side product in our Rh catalyzed olefin hydrophenylation as the result of a reaction of the CuX_2 ($X = \text{OAc, OPiv, etc.}$) with benzene. Because this conversion occurs in the absence of a directing group, this oxidation phenomenon is interesting. The reaction conditions were optimized using Cu(OAc)_2 and benzene. Heating a 10 mL benzene solution of 0.48 mol% Cu(OAc)_2 with 75 psig nitrogen at 180 °C, phenyl acetate was obtained in 51% yield after 24 h based on the Cu(II) oxidant as the limiting reagent. For all reactions, the average yields and standard deviations are

calculated from the results of at least three separate experiments. Two equivalents of Cu(II) oxidant are required for the production of one equivalent of phenyl acetate. Some results are summarized in Table 4.2.1.

Acetic acid has been shown to stabilize Cu(OAc)₂ and prevent thermal decomposition.^[17] The addition of one equivalent of acetic acid increased the yield of phenyl acetate from 51% to 65%, but the addition of larger amounts of acetic acid did not lead to a further increase in yield (Table 4.2.1, entries 2, 4 and 5). The influence of temperature on the reaction (Table 4.2.1, entries 1-3) was also investigated. No significant production of phenyl acetate was detected when lowering the reaction temperature to 150 °C. When raising the temperature to 200 °C, the nitrogen pressure was reduced to 50 psig due to the pressure limit of the Fisher-Porter reactor. No significant effect on the yield or reaction rate was observed at 200 °C. Because the benzene was refluxing during the reaction, the actual temperature of the solution likely was lower than 200 °C. As a result, the optimal temperature was chosen to be 180 °C. The effect of varying Cu(OAc)₂ concentration was examined using a range of loadings 0.24 to 4.8 mol% (Table 4.2.1, entries 6-7). The amount time required for the reaction to reach completion was proportional to the Cu(II) oxidant loading, indicating that the reaction rate is likely zero order in the Cu(II) oxidant. The phenyl acetate yield increased from 65% to 84% when using a larger amount of Cu(OAc)₂. The prolonged reaction time at high temperatures could increase the possibility of the reduced copper(I) salt to undergo disproportionation to generate one half of an equivalent of a copper(II) species. In order to perform *catalytic* acetoxylation, regeneration of Cu(OAc)₂ during the reaction is necessary. As Cu(I) and Brønsted acid can be re-oxidized with O₂, one atmosphere of air was purged

into the reactor in an effort to regenerate $\text{Cu}(\text{OAc})_2$ *in situ*. However, the reaction rate is significantly inhibited by the air, and the yield after 24 h of reaction dropped from 65% to 9% (Table 4.2.1, entry 8).

Table 4.2.1. $\text{Cu}(\text{OAc})_2$ mediated benzene acetoxylation.



| Entry | Temp. (°C) | HOAc (equiv.) ^a | Cu loading (mol%) | Atmosphere | Yield (%) | Time (h) |
|-------|------------|----------------------------|-------------------|---|-----------|----------|
| 1 | 150 | 1 | 0.48 | 75 psig N ₂ | < 1 | 24 |
| 2 | 180 | 1 | 0.48 | 75 psig N ₂ | 60 (5) | 24 |
| 3 | 200 | 1 | 0.48 | 50 psig N ₂ | 65 (5) | 24 |
| 4 | 180 | 0 | 0.48 | 75 psig N ₂ | 51(4) | 24 |
| 5 | 180 | 2 | 0.48 | 75 psig N ₂ | 65 (2) | 24 |
| 6 | 180 | 2 | 0.24 | 75 psig N ₂ | 60 (2) | 12 |
| 7 | 180 | 1 | 4.8 | 75 psig N ₂ | 84 (2) | 132 |
| 8 | 180 | 1 | 0.48 | 1 atm Air + N ₂ ^b | 9 (2) | 24 |

^a The acid loading is relative to $\text{Cu}(\text{OAc})_2$. ^b The total pressure is 75 psig for gas mixture.

4.2.2 Cu(II) Oxidant Screening for Benzene C–H Functionalization

In our hypothesis, the Cu(II) salts likely plays two possible roles in the reaction: 1) Cu(II) could serve as a catalyst that activates a C–H bond of benzene to generate a Cu(II)–Ph intermediate; and 2) Cu(II) could serve as an oxidant to oxidize the Cu(II) metal center to Cu(III) which could promote the reductive elimination of phenyl acetate. By using more soluble Cu(II) salts, benzene C–H functionalization might be facilitated.

Two Cu(II) salts that are soluble in benzene, copper(II) pivalate ($\text{Cu}(\text{OPiv})_2$) and copper(II) 2-ethylhexanoate ($\text{Cu}(\text{OHex})_2$), were tested for the benzene acetoxylation reaction. The results are summarized in Table 4.2.2. Compared with $\text{Cu}(\text{OAc})_2$, the conversion to phenyl acetate was achieved at lower temperatures with both of the soluble Cu(II) salts than with $\text{Cu}(\text{OAc})_2$. With $\text{Cu}(\text{OPiv})_2$, benzene C–H functionalization was

observed between 150 and 180 °C. Raising the reaction temperature from 150 °C to 160 °C significantly improves the reaction rate without affecting the yield of phenyl pivalate. However, raising the temperature further to 180 °C results in a lower yield of the product (Table 4.2.2, entries 1, 3 and 4). Compared to Cu(OAc)₂, Cu(OPiv)₂ produces lower yields of functionalized products. For example, the reaction with Cu(OPiv)₂ give 40% yield after 28 h at 160 °C while with Cu(OAc)₂ gives 51% yield after 24h at 180 °C. Since a 3° carbon is adjacent to the carboxylate group in the pivalate, it may undergo C–C homolysis more rapidly, which would lead to the undesired decomposition of the Cu(OPiv)₂. In contrast to Cu(OPiv)₂, Cu(OHex)₂ only has a 2° carbon adjacent to the carboxylate group, and as such should exhibit improved thermal stability. In agreement with this hypothesis, Cu(OHex)₂ mediated C–H functionalization gave a 78% yield at 170 °C after 16 h, outperforming the yields obtained using Cu(OAc)₂ (50%) and Cu(OPiv)₂ (40%). Moreover, the use of acid additive inhibits the reaction rate with both Cu(OPiv)₂ and Cu(OHex)₂ (Table 4.2.2, entries 1, 2, 6 and 8), which is in contrast to observations with Cu(OAc)₂. The lower acidity of the acid additive may result in competition between benzene and acid coordination to Cu, which could reduce the rate of the reaction. In addition, the presence of air inhibits the Cu(OHex)₂ mediated reaction with or without acid additives (Table 4.2.2, entries 7 and 9).

Table 4.2.2. Cu(II) oxidant screening for benzene C–H functionalization.

0.48 mol% Cu(OPiv)₂ or Cu(OHex)₂
 acid additives or not
 150-180 °C 75 psig N₂ or N₂ + Air

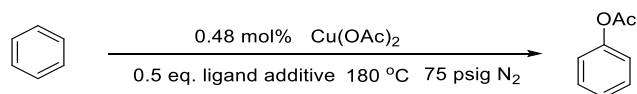
| Entry | Temp. (°C) | Acid (equiv.) ^a | Cu Source | Atmosphere | Yield (%) | Time (h) |
|-------|------------|----------------------------|-----------------------|------------------------|-----------|----------|
| 1 | 150 | 0 | Cu(OPiv) ₂ | 75 psig N ₂ | 44(2) | 110 |
| 2 | 150 | 2 | Cu(OPiv) ₂ | 75 psig N ₂ | 6 | 78 |
| 3 | 160 | 0 | Cu(OPiv) ₂ | 75 psig N ₂ | 40(1) | 28 |

| | | | | | | |
|---|-----|---|-----------------------|----------------------------|-------|----|
| 4 | 180 | 1 | Cu(OPiv) ₂ | 75 psig N ₂ | 28(1) | 6 |
| 5 | 160 | 0 | Cu(OHex) ₂ | 75 psig N ₂ | 86(2) | 44 |
| 6 | 170 | 0 | Cu(OHex) ₂ | 75 psig N ₂ | 78(2) | 16 |
| 7 | 170 | 0 | Cu(OHex) ₂ | 1 atm Air + N ₂ | 49(8) | 16 |
| 8 | 170 | 6 | Cu(OHex) ₂ | 75 psig N ₂ | 10 | 16 |
| 9 | 170 | 6 | Cu(OHex) ₂ | 1 atm Air + N ₂ | 8 | 16 |

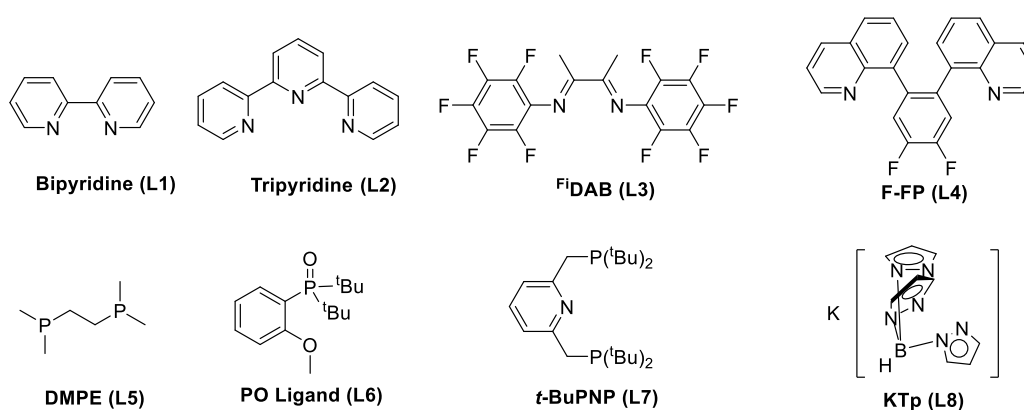
^aThe acid loading is relative to Cu(II) salts. HOPiv for Cu(OPiv)₂ and HOHex for Cu(OHex)₂.

4.2.3 Ligand Additives Screening

Ligand additives can be essential to achieve Cu mediated hydroxylation.^[3,5-7] In this work, Cu(OAc)₂ mediated acetoxylation was studied with a variety of ligands as additives. The results are summarized in Table 4.2.3 and the structures of the ligands are shown in Figure 4.2.1. The majority of the added ligands have a negative effect on the reaction. Ligand decomposition was observed immediately with DMPE, ^tBuPNP and ^FlDAB. The decomposed products such as oxidized DMPE was observed with GC-MS analysis. A moderate amount of biphenyl was produced in the reaction with added F-FP, indicating that the C–H cleavage occurred during the reaction. The PO ligand (**L6**, Figure 4.2.1) was the only one that accelerated the reaction without decreasing the yield of functionalized product. The **L6** loading was then optimized (Table 4.2.4). **L6** (0.1-0.5 equivalents) was added to the reaction and an acceleration of the reaction was observed under all studied conditions relative to the reaction without added ligand. The higher loading of the ligand resulted in a slightly higher reaction rate, but a decrease in the product yield also observed. The reactions with 0.4 and 0.5 equivalents of **L6** (relative to Cu(OAc)₂) were complete within 16 h, and the reaction with 0.1 to 0.3 equivalents **L6** were complete within 19 hours. Under optimized conditions with 0.1 equivalents **L6**, 83% yield of phenyl acetate was achieved. In addition, the yield can be increased further on the addition of acetic acid (Table 4.2.4, entry 6).

Table 4.2.3. Ligand additive screening for Cu(OAc)₂ mediated benzene acetoxylation.

| Entry | Ligand | 8 h Yield (%) | 16 h Yield (%) | 24 h Yield (%) |
|-------|--------------------|---------------|----------------|----------------|
| 1 | Bipyridine | 3.2 | 3.5 | 3.9 |
| 2 | Tripyridine | 0.8 | 2.0 | 2.2 |
| 3 | ^{Fi} DAB | 0.9 | 0.8 | 0.5 |
| 4 | F-FP | 1.5 | 1.4 | 1.5 |
| 5 | DMPE | N/A | N/A | N/A |
| 6 | PO ligand | 38 | 58 | 59 |
| 7 | ^t BuPNP | N/A | N/A | N/A |
| 8 | KTp | 0.5 | 0.6 | 0.6 |
| 9 | No ligand | 17(3) | 26(5) | 51(4) |

**Figure 4.2.1** Ligands structures.**Table 4.2.4.** Optimization of the L6 loading on Cu(OAc)₂ mediated benzene acetoxylation.

| Entry | Ligand (equiv.) ^a | Acid Additive | 16 h Yield (%) | 19 h Yield (%) |
|-------|------------------------------|---------------|----------------|----------------|
| 1 | 0.1 | N/A | 71 | 83 |
| 2 | 0.2 | N/A | 51 | 53 |
| 3 | 0.3 | N/A | 53 | 67 |
| 4 | 0.4 | N/A | 47 | 47 |
| 5 | 0.5 | N/A | 58 | 58 |
| 6 | 0.5 | 1 equiv. | 73 | 76 |

^aThe ligand loading is relative to Cu(II) salts.

In order to understand the nature of the acceleration of the reaction by the L6, di-tert-butylphenylphosphine (L9) was used for comparison. Ligands L6 and L9 share a similar

motif, however **L6** has a P=O linkage. Different amounts of **L9** were added to the reaction and an increase in the rate of the reaction was similar to **L6** observed (Table 4.2.5). The reaction with **L9** was complete after 14 h; however, the yield under each condition was lower when compared to reactions with ligand **L6**. Because phosphines are often readily oxidized, the structure of oxidized **L9** would be very similar to **L6**. Based on the charge transfer, the oxidation of one equivalent of **L9** would require two equivalents of Cu(II) oxidant, which may account for the decrease in the yield of phenyl acetate. Since the P=O linkage could be very beneficial for the acetoxylation reaction, a series of phosphines and phosphine oxides were studied (Figure 4.2.2). A 10 mL benzene solution of 0.48 mol% Cu(OAc)₂ with 0.1 equivalent of ligand was heated at 180 °C for 12 hours under 75 psig nitrogen. The yield of phenyl acetate after 12 h was used to compare each of the ligands. The results of a control reaction with Cu(OAc)₂ in the absence or presence of 1 equivalent of acetic acid as additive are presented in Figure 4.2.2. Most of the phosphines and phosphine oxides have a positive impact on the reaction rate. However, triphenylphosphine (PPh₃) does not, which could be the result of its ability to act as a strong reducing reagent. The phosphine oxide ligands, generally result in higher yields of functionalized product than the phosphine additives, with the exception of triphenyl phosphite (P(OPh)₃), which achieves over 70% yield in 4 h. When heating the Cu(OAc)₂ with P(OPh)₃ in benzene at 150 °C, 40% yield of phenyl acetate could be observed after 12 h. However, when heating the mixture through 72 h, only 4% additional phenyl acetate was produced compared to 12 hours, which indicated that most of the phenyl acetate was produced from ligand decomposition. After accounting for the production of phenyl acetate from ligand

decomposition, the actual yield using $P(\text{OPh})_3$ is 34%, which is slightly lower than the reaction in the absence of additives. In general, the less electron donating phosphine ligands lead to an improvement in the yield of phenyl acetate. Of all of the ligands that have been studied, the highest yields and reaction rates are obtained when using **L6**. The improved reaction rates observed when using phosphine oxide additives supports our hypothesis that the $P=O$ linkage of the phosphine oxide ligand assists in the electron transfer in the oxidation process from Cu(II) to Cu(III) . During the reaction, the $P=O$ linkage may be converted to $P-O$ radical which may have a suitable redox potential to mediated transformation from Cu(II) to Cu(III) .

Table 4.2.5. Comparison of the effects of various ligands with **L6** and **L9**.

| L6 | | | L9 | | |
|------------------|----------|------------------|-----------|------------------|-----------|
| Loading (equiv.) | Time (h) | Loading (equiv.) | Time (h) | Loading (equiv.) | Yield (%) |
| 0.1 | 19 | 0.1 | 19 | 0.1 | 35 |
| 0.2 | 19 | 0.2 | 19 | 0.2 | 46 |
| 0.3 | 19 | 0.3 | 19 | 0.3 | 37 |

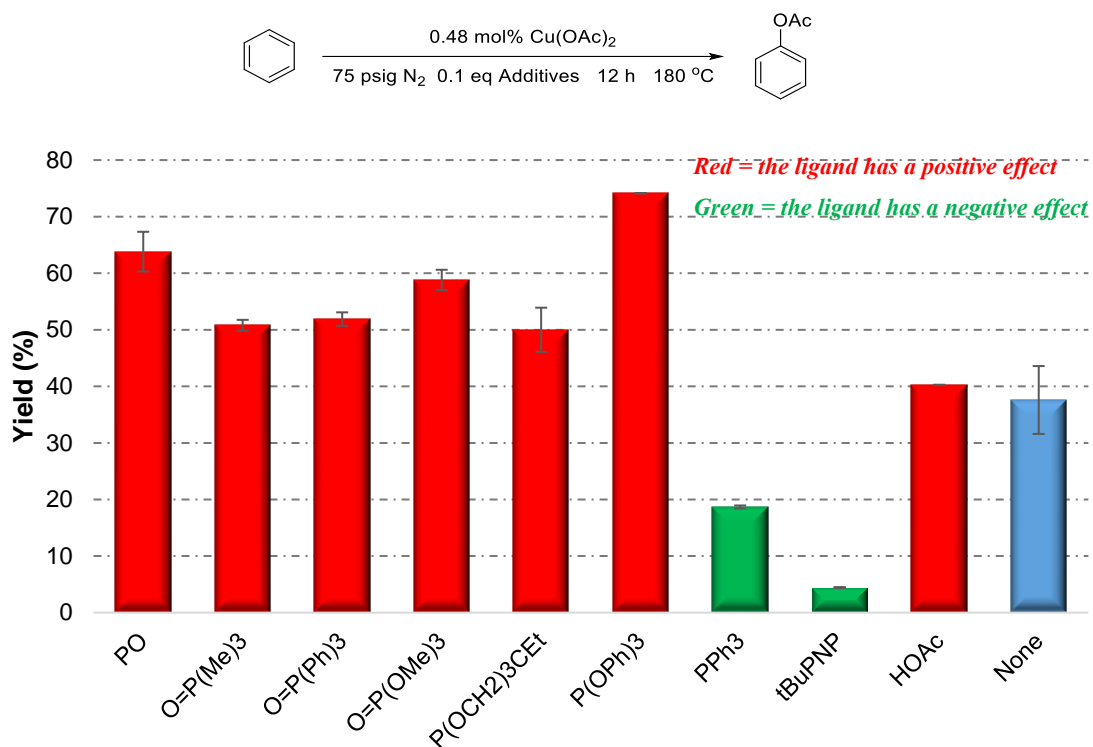


Figure 4.2.2. The results of the acetoxylation reaction with different phosphines and phosphine oxide ligands.

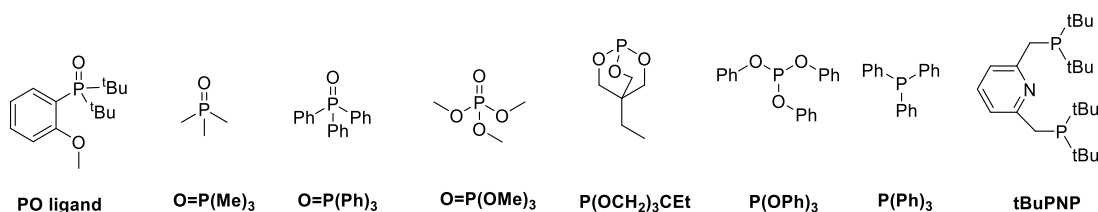


Figure 4.2.3. The structures of phosphine and phosphine oxide ligands.

4.2.4 Elucidation of the Reaction Mechanism

Previous reports of Cu mediated arene hydroxylation with directing groups have proposed reaction mechanisms involving free radical, SET or organometallic pathways.^{[1-}

^{9]} In order to elucidate the mechanism of Cu(II) salt mediated acetoxylation of benzene, one equivalent of various radical traps (e.g., benzoquinone (benzo), TEMPO and I₂) were added to the reaction mixture (Figure 4.2.4). In order to better represent the effect of radical trap, soluble Cu(OHex)₂ was used as the oxidant. The result with 1 atm of air is also included to serve as a comparison since oxygen could also serve as a possible radical trap

in the reaction. The reaction was carried out at 170 °C with 0.48 mol% Cu(OHex)₂ loading and was sampled every 4 h until completion. As presented in Figure 4.2.4, benzoquinone had no effect after the first 8 h, but decreased the yield from 66% to 50% after 12 h. The presence of air resulted in significant inhibition of the reaction, and the reaction rate is approximately two-fold slower than under anaerobic conditions. The addition of I₂ resulted in minimal phenyl hexanoate production; however, a large amount of iodobenzene was produced as the major product. This observation is similar to Jinqian Yu's study of 2-phenylpyridines, in which C–X formation occurs rather than C–O formation in the presence of nucleophilic anions. Notably, the addition of TEMPO accelerated the rate of the reaction and resulted in an approximate two-fold increase in the product yield. This observation suggests that TEMPO itself can serve as an oxidant for this reaction with higher oxidative efficiency than that of the disproportionation of the Cu(II) salt. TEMPO assisted Cu mediated oxidation was previously developed by Shannon Stahl's group for the aerobic oxidation of alcohols.^[18-22] The addition of TEMPO under their conditions reduced the reaction barrier and enabled the use of aerobic reaction conditions. Although the system achieved success for alcohol oxidation, this method was not applied to the oxidation of C–H bonds. Since the Cu(II) salt mediated functionalization of benzene's C–H bonds was inhibited by air, we considered that the addition of TEMPO might reduce this inhibition. When reducing the TEMPO loading to 0.2 equivalents, the reaction rate was identical to that of 1 equivalent addition until all of the Cu(OHex)₂ was consumed. The result indicated that the acceleration effect is not dependent on the TEMPO loading. In order to test the oxygen tolerance, the same reaction was carried out with 1 atm of air purged into the reactor.

The 8 h yield decreased from 88% to 65%, and the result remained 20% higher than those of anaerobic reactions without added TEMPO. When the reaction time of the aerobic reaction was extended to 24 h, no significant decrease in the rate of the reaction was observed. With added TEMPO, $\text{Cu}(\text{OHex})_2$ is an effective *catalyst* for the aerobic oxidation of benzene C–H bonds.

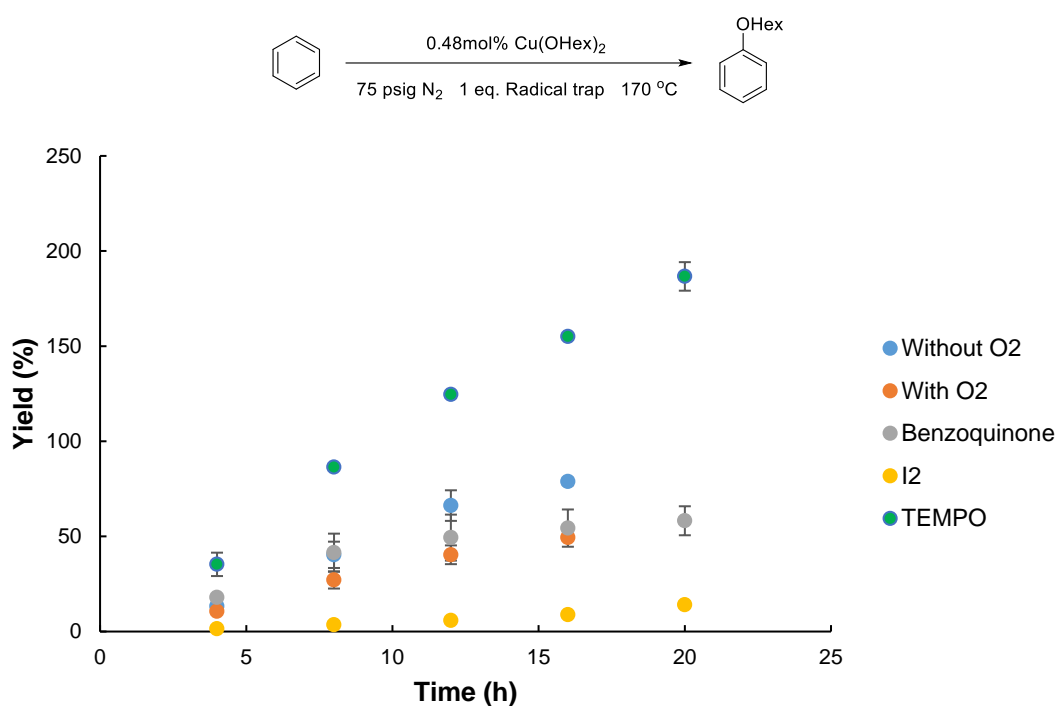


Figure 4.2.4. $\text{Cu}(\text{OHex})_2$ mediated benzene C–H functionalization with different radical traps.

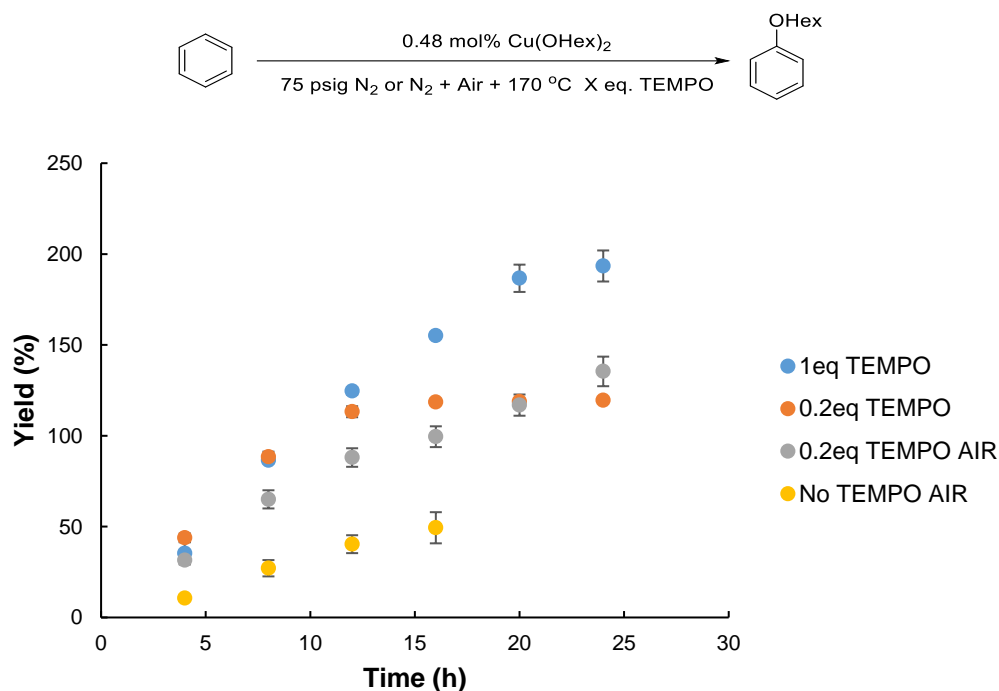


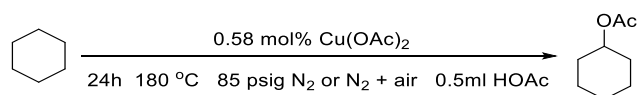
Figure 4.2.5. Cu(OHex)₂ mediated benzene C–H functionalization with different TEMPO loadings.

Two potential explanations of air inhibition on the reaction are: 1) oxygen in air serves as a radical trap to slow down the reaction, 2) the Cu mediated acetoxylation undergoes different pathways under aerobic and anaerobic conditions. The reaction could operate via an organometallic pathway under anaerobic conditions and a radical pathway in the presence of air. The first pathway is predicted to be faster than the second one, and the presence of oxygen facilitates the radical pathway. The first hypothesis regarding oxygen as a radical trap is in disagreement with the radical trap experiment (Figure 4.2.5). In order to evaluate the second assumption, two substrates, cyclohexane and toluene, were used for C–H functionalization.

The rationale for using cyclohexane as the substrate is due to the significant difference in its C–H bond dissociation energy (BDE) compared to those of arenes. The BDE of cyclohexane is ~96 kcal/mol, while the BDE of benzene is ~113 kcal/mol.^[23-24] If the

reaction were to operate through a radical pathway, the reaction rate likely would be highly dependent on the C–H BDE. The acetoxylation with cyclohexane should be much quicker than that of benzene. If the reaction were to undergo an organometallic pathway, the coordination of a sp^2 C–H bond of benzene to the Cu center would be much easier than that of a sp^3 C–H bond in cyclohexane. In addition, the Cu–C bond for a phenyl group will be stronger than that for a cyclohexyl group, which facilitates C–H activation. In this case, the acetoxylation of benzene is more accessible than that of cyclohexane. The reaction results with $\text{Cu}(\text{OAc})_2$ and cyclohexane are summarized in Table 4.2.6. In the absence of air, no acetoxyated product was detected in the reaction mixture, regardless of acid addition after 24 hours, while 52% cyclohexyl acetate was obtained with 1 atm air *in situ*. Acetoxylation of benzene was more accessible under anaerobic conditions (51% phenyl acetate vs < 1% cyclohexyl acetate), but cyclohexane functionalization was more favorable under aerobic conditions (9% phenyl acetate vs 52% cyclohexyl acetate). This result supports our hypothesis that the reaction occurs through an organometallic pathway under anaerobic conditions and a radical pathway in the presence of air.

Table 4.2.6. $\text{Cu}(\text{OAc})_2$ catalyzed acetoxylation of cyclohexane.



| Entry | Atmosphere | Acid (mL) | CyOAc Yield (%) | CyOH Yield (%) |
|-------|----------------------------|-----------|-----------------|----------------|
| 1 | 1 atm Air + N ₂ | 0.5 | 52 | <1% |
| 2 | 85 psig N ₂ | 0.5 | <1 | ND |
| 3 | 85 psig N ₂ | 0 | ND | ND |

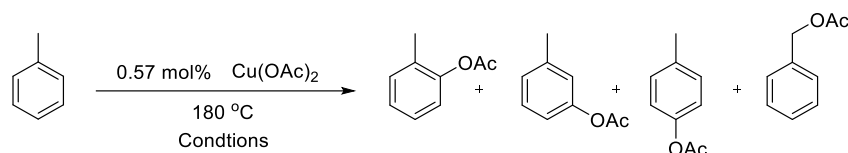
Toluene was also used as a substrate to further investigate the mechanism. The ratio of benzyl-acetate vs tolyl acetate was used to study the selectivity between the two reaction

pathways. A radical-based pathway should favor C–H activation at the benzyl position, while the organometallic pathway should be more likely to functionalize sp^2 C–H bonds. In addition, the *ortho:meta:para* (*o:m:p*) selectivity could be informative. If C–H activation occurred through bond coordination to the metal center, the steric bulk of the methyl group might inhibit coordination at the *ortho* position, which would favor the formation of *meta* and *para* products over *ortho* products.^[25] If C–H activation occurs through bond homolysis, to generate free radicals the *o:m:p* selectivity will be approximately 2:2:1 following the statistical distribution. Therefore, the Cu(OAc)₂ catalyzed acetoxylation of toluene under different conditions was tested in order to help elucidating the reaction mechanism (Table 4.2.7). As a result, when using Cu(OAc)₂ without additives under 70 psig. N₂ at 180 °C, a *meta*-selective acetoxylation was observed with a 1:1.9(0):1.1(0):0.9(1) *o:m:p:benzyl* ratio at 16 h, and after heating for 24 hours more sp^2 -selective product was formed with an *o:m:p:benzyl* ratio of 1:1.8(0):1.1(0):0.5(0) (Table 4.2.7, Entry 1). In the presence of 1 atm of air, there was a dramatic increase in the yield of the *benzyl* product with an *o:m:p:benzyl* ratio of 1:2.1(0):1.0(2):14.4(9) after 16 h (Table 4.2.7, Entry 2). Hence, it could be hypothesized that the non-radical and radical pathways are in competition during the acetoxylation reaction. Under anaerobic conditions the non-radical pathway is favored, while the reaction is dominated by the radical pathway under aerobic conditions.

The effect of TEMPO as an additive was also investigated with the Cu(OAc)₂ catalyzed acetoxylation with toluene under anaerobic and aerobic conditions (Table 4.2.7, Entries 3-4), and the major product was found to be the *meta*-tolyl acetate. This observation also supports our hypothesis of competing non-radical and radical mechanisms, and the *meta*-

selective reaction with TEMPO under aerobic conditions may lead to an air-recyclable Cu catalyzed acetoxylation reaction.

Table 4.2.7. Cu(OAc)₂ catalyzed acetoxylation of toluene.



| Entry | Atmosphere | Additive | <i>o:m:p:benzyl</i> (16 h) | <i>o:m:p:benzyl</i> (24 h) |
|------------------|------------------------------------|----------|----------------------------|----------------------------|
| 1 | 70 psig N ₂ | No | 1:1.9(0):1.1(0):0.9(1) | 1:1.8(0):1.1(0):0.5(0) |
| 2 | 1 atm Air + 70 psig N ₂ | No | 1:2.1(0):1.0(2):14(1) | 1:1.7(0):0.8(1):14(1) |
| 3 ^{a,b} | 70 psig N ₂ | TEMPO | 1:1.6:0.9:0.6 | 1:1.5:0.9:1.1 |
| 4 ^{a,c} | 1 atm Air + 70 psig N ₂ | TEMPO | 1:1.4:1.0:0.2 | 1:1.3:0.9:0.6 |

^a Using 1 equiv. of TEMPO relative to Cu(OAc)₂. ^b The *meta*-selective reaction seems to be completed at 8 h with a *o:m:p:benzyl* ratio of 1:1.6:1.0:0.1. ^c The *o:m:p:benzyl* ratio at 8 h is 1:1.5:1.0:0.0.

4.2.5 Attempt Towards Obtaining Catalytic Turnovers

In order to achieve catalytic turnovers for the Cu mediated acetoxylation reaction, 10 mL of benzene containing 0.01 mol% Cu(OAc)₂ and 200 equivalents of acetic acid were heated at 190 °C under 50 psig N₂ and 1 atm air as top pressure. The reaction was sampled at 12, 36, 60, 84, 108 and 142 h (Figure 4.2.6). Two separate trials are included in the turnover versus time plot. The increase in turnovers is linear with respect to time, indicating that no product inhibition or catalyst deactivation was observed during catalysis. However, the significant deviation between the two trials demonstrates inconsistent results.

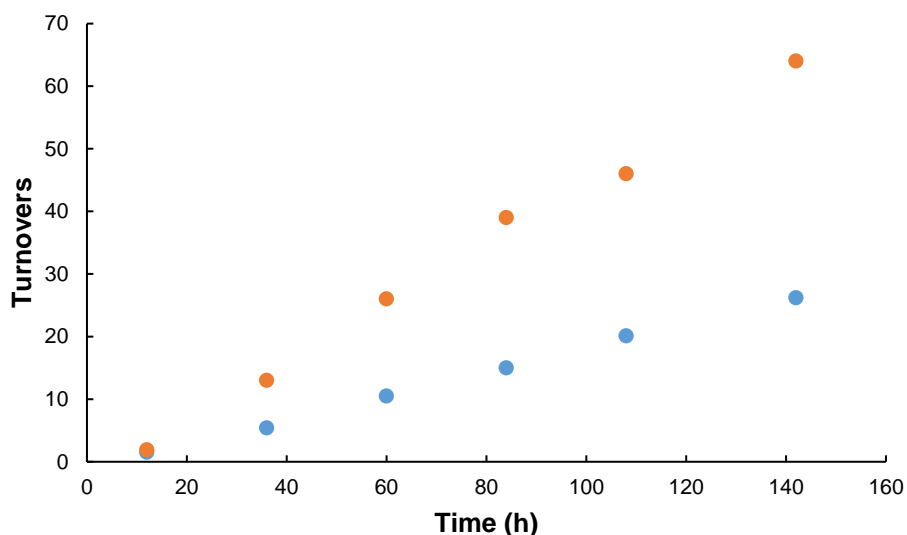


Figure 4.2.6. Catalytic acetoxylation of benzene with $\text{Cu}(\text{OAc})_2$. Reaction condition: 0.01 mol% $\text{Cu}(\text{OAc})_2$ and 200 equivalents of acetic acid were heated at 190 °C under 50 psig N_2 and 1 atm air as top pressure.

4.3 Conclusions

To our knowledge, there are no examples of $\text{Cu}(\text{II})$ salt mediated acetoxylation with un-directed arenes. We have demonstrated the acetoxylation of benzene using $\text{Cu}(\text{II})$ oxidants. Phenyl acetate was generated in 83% yield (based on $\text{Cu}(\text{II})$ salts) under optimized conditions with 0.1 equivalents of phosphine oxide ligand after 19 h. The $\text{P}=\text{O}$ linkage in the phosphine oxide is proposed to accelerate the reaction. The reaction rate was significantly higher under aerobic conditions than under anaerobic conditions, which indicates that the reaction operates by different pathways under each condition. Using cyclohexane and toluene as substrates, the reaction has been demonstrated to likely operate via a free radical pathway in the presence of oxygen and an organometallic pathway in its absence. In addition, the radical trap, TEMPO, was found to facilitate electron transfer during the reaction even under aerobic conditions. Over 60 TOs of phenyl acetate have been achieved with lower $\text{Cu}(\text{OAc})_2$ loading and no catalyst deactivation was observed after 142 h of reaction.

4.4 Experimental Section

Ligands L3, L4, L6 and L7 were prepared according to literature procedures.^[26-29] All other reagents were purchased from commercial sources and used as received.

Phenylacetate, phenyl pivalate, cyclohexyl acetate, cyclohexanol, benzo acetate, *o*-tolyl acetate, *m*-tolyl acetate, *p*-tolyl acetate production was quantified using linear regression analysis of gas chromatograms of standard samples of authentic product. A plot of peak area ratios versus molar ratios gave a regression line using hexamethylbenzene (HMB) as the internal standard.

Cu(II) salt mediated benzene C–H functionalization under anaerobic conditions.

A representative reaction is described (Table 4.2.1, entry 8). A stock solution containing hexamethylbenzene (0.1818 g, 1.12 mmol), and benzene (200 mL) was prepared in a volumetric flask. Thick-walled glass Fisher-Porter reactors were charged with stock solution (10 mL), acetic acid (31 μ L, 0.539 mmol) and Cu(OAc)₂ (0.0979 g, 0.539 mmol). The vessels were sealed, pressurized with nitrogen (75 psig) and subsequently stirred and heated to 180 °C. The color of the reaction mixture was deep blue at the beginning of the reaction and turned to yellow when all of the Cu oxidant was consumed. The reaction was sampled when the solution turned colorless. The reactors were cooled to room temperature and aliquots of the reaction mixture (< 200 μ L) were analyzed by GC/FID using relative peak areas versus the internal standard (hexamethylbenzene).

Cu(II) salt mediated benzene C–H functionalization under aerobic conditions.

A representative reaction is described (Table 4.2.1, entry 2). A stock solution containing hexamethylbenzene (0.1818 g, 1.12 mmol), and benzene (200 mL) was prepared in a

volumetric flask. Thick-walled glass Fisher-Porter reactors were charged with stock solution (10 mL), acetic acid (31 μ L, 0.539 mmol) and $\text{Cu}(\text{OAc})_2$ (0.0979 g, 0.539 mmol). The vessels were sealed and purged with 1 atm air, pressurized with nitrogen (75 psig) and subsequently stirred and heated to 180 $^{\circ}\text{C}$. The color of the reaction mixture was deep blue throughout the entire reaction. The reaction was sampled at 24 hours. The reactors were cooled to room temperature and aliquots of the reaction mixture (< 200 μ L) were analyzed by GC/FID using relative peak areas versus the internal standard (hexamethylbenzene).

Catalytic reaction with Cu(II) salt mediated benzene C–H functionalization. A stock solution containing hexamethylbenzene (0.1818 g, 1.12 mmol), and benzene (200 mL) was prepared in a volumetric flask. Thick-walled glass Fisher-Porter reactors were charged with stock solution (10 mL), acetic acid (128 μ L, 0.539 mmol) and $\text{Cu}(\text{OAc})_2$ (0.0020 g, 0.0112 mmol). The vessels were sealed and purged with 1 atm air, pressurized with nitrogen (50 psig) and subsequently stirred and heated to 190 $^{\circ}\text{C}$. The color of the reaction mixture was deep blue at the beginning of the reaction and turned to yellow when all of the Cu oxidant and oxygen were consumed. The reaction was sampled at 12, 36, 60, 84, 108 and 142 h. At each time point, the reactors were cooled to room temperature, sampled, purged with air (1 atm) and pressurized with nitrogen (50 psig) and reheated. The reactors were cooled to room temperature and aliquots of the reaction mixture (< 200 μ L) were analyzed by GC/FID using relative peak areas versus the internal standard (hexamethylbenzene).

Cu(II) salt mediated cyclohexane C–H functionalization. A representative reaction is described (Table 4.2.6, entry 2) for anaerobic conditions. A stock solution containing

hexamethylbenzene (0.1818 g, 1.12 mmol), and cyclohexane (200 mL) was prepared in a volumetric flask. Thick-walled glass Fisher-Porter reactors were charged with stock solution (10 mL), acetic acid (0.5 mL, 8.73 mmol) and Cu(OAc)₂ (0.0979 g, 0.539 mmol). The vessels were sealed, pressurized with nitrogen (85 psig) and subsequently stirred and heated to 180 °C. The color of the reaction mixture was deep blue at the beginning of the reaction and turned to light yellow when all of the Cu oxidant was consumed. The reaction was sampled at 24 h. The reactors were cooled to room temperature and aliquots of the reaction mixture (< 200 µL) were analyzed by GC/FID using relative peak areas versus the internal standard (hexamethylbenzene). The process of the reaction under aerobic conditions is similar except the reactor was purged with 1 atm air before pressurizing with nitrogen.

4.5 References:

- [1] Weber, M.; Weber, M.; Kleine-Boymann, M.. Phenol In *Ullmann's Encyclopedia of Industrial Chemistry*; Wiley-VCH Verlag GmbH & Co. KGaA: 2004.
- [2] Jeffrey S. Plotkin, "What's New in Phenol Production?", www.acs.org.
- [3] Chen, X.; Hao, X.-S.; Goodhue, C. E.; Yu, J.-Q., *J. Am. Chem. Soc.* **2006**, *128*, 6790-6791.
- [4] Wang, W.; Luo, F.; Zhang, S.; Cheng, J., *J. Org. Chem.* **2010**, *75*, 2415-2418.
- [5] Shang, M.; Shao, Q.; Sun, S.-Z.; Chen, Y.-Q.; Xu, H.; Dai, H.-X.; Yu, J.-Q., *Chemical science* **2017**, *8*, 1469-1473.

-
- [6] Sun, S.-Z.; Shang, M.; Wang, H.-L.; Lin, H.-X.; Dai, H.-X.; Yu, J.-Q., *J. Org. Chem.* **2015**, *80*, 8843-8848.
- [7] Li, X.; Liu, Y.-H.; Gu, W.-J.; Li, B.; Chen, F.-J.; Shi, B.-F., *Org. Lett.* **2014**, *16*, 3904-3907.
- [8] Gallardo-Donaire, J.; Martin, R., *J. Am. Chem. Soc.* **2013**, *135*, 9350-9353.
- [9] Zaitsev, V. G.; Shabashov, D.; Daugulis, O., *J. Am. Chem. Soc.* **2005**, *127*, 13154-13155.
- [10] Truong, T.; Klimovica, K.; Daugulis, O., *J. Am. Chem. Soc.* **2013**, *135*, 9342-9345.
- [11] Katayev, D.; Pfister, K. F.; Wendling, T.; Goossen, L. J., *Chem. Eur. J.* **2014**, *20*, 9902-9905.
- [12] Wang, S.; Guo, R.; Wang, G.; Chen, S.-Y.; Yu, X.-Q., *Chem. Commun.* **2014**, *50*, 12718-12721.
- [13] Roane, J.; Daugulis, O., *Org. Lett.* **2013**, *15*, 5842-5845.
- [14] Tran, L. D.; Popov, I.; Daugulis, O., *J. Am. Chem. Soc.* **2012**, *134*, 18237-18240.
- [15] Tran, L. D.; Roane, J.; Daugulis, O., *Angew. Chem. Int. Ed.* **2013**, *52*, 6043-6046.
- [16] Suess, A. M.; Ertem, M. Z.; Cramer, C. J.; Stahl, S. S., *J. Am. Chem. Soc.* **2013**, *135*, 9797-9804.
- [17] Meier, M.; Ruder, S.; Malona, J.; Frontier, A., e-EROS Encyclopedia of Reagents for Organic Synthesis. John Wiley & Sons: 2001; Vol.
- [18] Hoover, J. M.; Stahl, S. S., *J. Am. Chem. Soc.* **2011**, *133*, 16901-16910.
- [19] Ryland, B. L.; Stahl, S. S., *Angew. Chem. Int. Ed.* **2014**, *53*, 8824-8838.

-
- [20] Walroth, R. C.; Miles, K. C.; Lukens, J. T.; MacMillan, S. N.; Stahl, S. S.; Lancaster, K. M., *J. Am. Chem. Soc.* **2017**, *139*, 13507-13517.
- [21] Das, A.; Stahl, S. S., *Angew. Chem. Int. Ed.* **2017**, *56*, 8892-8897.
- [22] Rafiee, M.; Miles, K. C.; Stahl, S. S., *J. Am. Chem. Soc.* **2015**, *137*, 14751-14757.
- [23] Tian, Z.; Fattahi, A.; Lis, L.; Kass, S. R., *J. Am. Chem. Soc.* **2006**, *128*, 17087-17092.
- [24] Blanksby, S. J.; Ellison, G. B., *Acc. Chem. Res.* **2003**, *36*, 255-263.
- [25] McKeown, B. A.; Gonzalez, H. E.; Friedfeld, M. R.; Brosnahan, A. M.; Gunnoe, T. B.; Cundari, T. R.; Sabat, M., *Organometallics* **2013**, *32*, 2857-2865.
- [26] Vaughan, B. A.; Webster-Gardiner, M. S.; Cundari, T. R.; Gunnoe, T. B., *Science* **2015**, *348*, 421-424.
- [27] O'Reilly, M. E.; Johnson, S. I.; Nielsen, R. J.; Goddard, W. A.; Gunnoe, T. B., *Organometallics* **2016**, *35*, 2053-2056.
- [28] Feller, M.; Diskin-Posner, Y.; Leitun, G.; Shimon, L. J. W.; Milstein, D., *J. Am. Chem. Soc.* **2013**, *135*, 11040-11047.
- [29] Lee, S. Y.; Hartwig, J. F., *J. Am. Chem. Soc.* **2016**, *138*, 15278-15284.

5 Brønsted acid-catalysed intramolecular hydroamination of unactivated alkenes

This chapter is adapted from “Chen J., Goforth S. K., McKeown B. A., et al. Brønsted acid-catalysed intramolecular hydroamination of unactivated alkenes: metal triflates as an in situ source of triflic acid. Dalton Transactions, 2017, 46: 2884-2891.” Copyright 2017 Royal Society of Chemistry

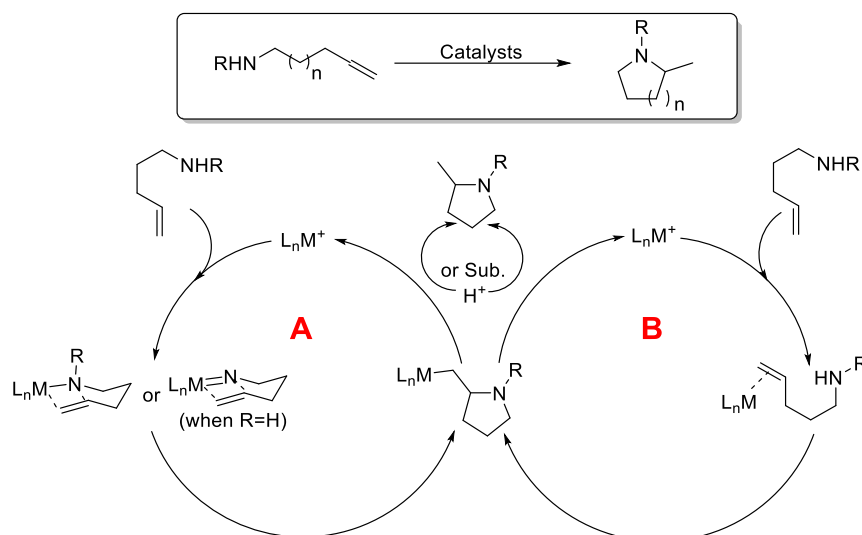
5.1 Introduction

Heterocyclic fragments are common moieties in a wide range of bioactive compounds. According to an analysis of drug candidates prepared by three leading pharmaceutical companies, the synthesis of 84 of 128 (65%) drug candidates involves C–N bond formation.^[1] “Amide formation avoiding poor atom economy reagents” has been listed as a key green chemistry research area.^[1] In order to construct nitrogen-containing heterocyclic frameworks, substantial effort has been devoted towards effective formation of C–N bonds. Currently, most synthetic methods are based on acid chloride intermediates or coupling reagents such as *N*-ethyl-*N*'-(3-dimethylaminopropyl)carbodiimide hydrochloride.^[2] However, those methods are not “atom economical” due to the production of stoichiometric by-products such as SO₂ and HCl. As a result, atom economical methods of C–N bonds formation are highly desired.

Hydroamination of alkenes or alkynes is one of the most straightforward methods to form C–N bonds and *N*-containing heterocycles. This method involves direct addition of amines to carbon-carbon multiple bonds. In the absence of catalysts, hydroamination of unactivated olefins is generally unfavorable due to a high activation energy barrier caused by repulsion between the lone pair of the amine nitrogen and the electron-rich carbon-

carbon multiple bond.

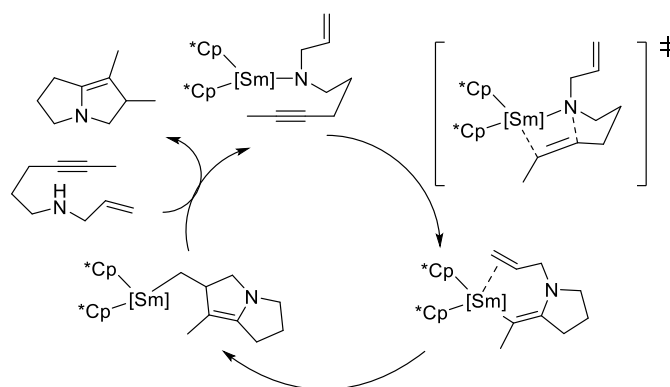
A variety of efficient catalysts have been developed for hydroamination of C-C multiple bonds. Two mechanisms are often suggested for these catalysts, where C-N bond formation is initiated by the activation of either N-H or C=C moiety (Scheme 5.1.1).^[3]



Scheme 5.1.1. Proposed mechanisms for intramolecular hydroamination of alkene with different types of catalysts

Traditionally, the most widely used catalysts are rare-earth and alkaline earth complexes.^[4-12] The general mechanism is initiated by activation of the N-H bond to form a M-N bond followed by rate-determining C=C multiple bond insertion into the M-N bond, after which the catalyst is regenerated by rapid protonolysis with other amine substrate (Scheme 5.1.1, route A). The reaction intermediates are consistent with Baldwin's guidelines for ring formation, the ease of the catalytic reactions increases with decreasing ring size ($5 > 6 > 7$).^[9] For alkaline earth complexes, strong electron-donating ligands are needed for stabilizing the structure and ligands such as $N(\text{SiMe}_3)_2$ or $\text{CH}(\text{SiMe}_3)_2$ are needed to initialize the reaction. In addition, Ca complexes are generally more reactive than those of Mg. Rare-earth complexes are the earliest reported and most reactive catalysts for hydroamination.^[10-15] Marks and co-workers developed a series of organolanthanide

complexes to accomplish this conversion.^[10] Both inter- and intra- molecular hydroamination can be catalyzed by organolanthanide complexes.^[12,15] In addition, bicyclization through hydroamination of C-C multiple bonds can be achieved, and a simplified mechanism is shown in Scheme 5.1.2. With the help of asymmetric aminodiolate ligands, the rare-earth-metal complexes can catalyze intermolecular asymmetric hydroamination of alkenes with over 90% ee value.^[11] However, short catalyst lifetimes due to catalyst poisoning by amine substrates, limited scope and modest selectivity are known as disadvantages of organolanthanide catalysts.



Scheme 5.1.2. Simplified mechanism for organolanthanide catalyzed bicyclization.

Group 4 metal complexes follow a similar pathway and substrate scope. The difference is that the catalytically active species are often proposed to be metal imido complexes generated by α -elimination of metal amides.^[16-22] Although those metal catalysts have many attractive features including high turnover frequencies and excellent stereoselectivities, their sensitivity to oxygen and moisture has limited their use.

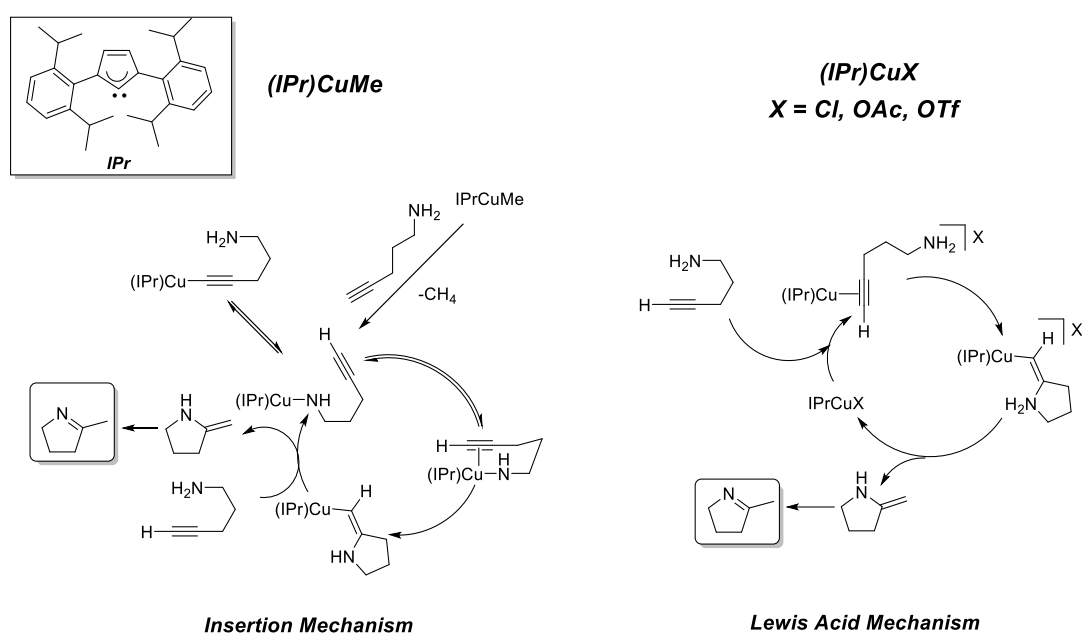
There is a push towards less oxophilic late transition metals (*e.g.*, Rh, Pd, Au) catalysts^[23-32] developed as a mean of decreasing sensitivity to oxygen and moisture as well as expanding substrate functional group tolerance. Conversely, those catalysts often are proposed to initiate the catalytic cycle by π -coordination of the carbon-carbon multiple

bond to reduce its electron density, which is followed by exo-metallic attack of the nucleophilic amine (Scheme 5.1.1, route B). Among those catalysts, Lewis acidic metal complexes with d^8 and d^{10} electron configurations exhibit high activities. Protonolysis of Pd–C bond is proposed to be the turnover-limiting step due to inhibition by amine substrates.^[31] Late transition metal catalysts are often more effective with secondary amine than primary amines. Tobisch and co-workers reported a special designed pyrazolato ligand supported Ir complex, which can catalyze intramolecular hydroamination through a cooperative activation of amino alkenes. In the catalytic cycle the pyrazolato ligand can benefit the proton transfer and lead to lower reaction barrier.^[27] Although late transition metal catalysts have better longevity and oxygen and moisture tolerance, the high price of the catalysts limits their use.

Copper complexes are considered as prospective low-cost catalysts. Hii and co-workers reported the use of copper triflates for hydroamination of arylsulfonamides to vinylarenes, norbornene, and cyclohexadiene.^[33] Sawamura and co-workers reported an effective copper alkoxide catalyst in different intramolecular hydroamination reactions. With the help of alcohol solvent, the reaction can bear primary and secondary amino group.^[34]

Our group have reported NHC–Cu–amido complexes (monomeric Cu complexes supported by *N*-heterocyclic carbene (NHC) ligand) for the intermolecular addition of amines to electron-deficient olefins.^[35,36] Recently our group expanded the use of the (NHC)–Cu–Me complex as a catalyst precursor for intramolecular hydroalkoxylation and hydroamination of alkynes.^[37] It was proposed that the Cu complex first reacts with an -OH group to release methane and form a Cu–O bond. The Cu coordinates to the carbon-

carbon triple bond to initiate an alkyne insertion into the Cu–O bond. In the last step, protonolysis of Cu–C bond produces the product and regenerate the catalyst. However, the same mechanism cannot be applied to hydroamination, since kinetic studies suggested a different mechanism. In addition, when catalytic amounts metal triflates are added, a significant increase in the reaction rate could be observed. Two different proposed pathways are shown in Scheme 5.1.3.

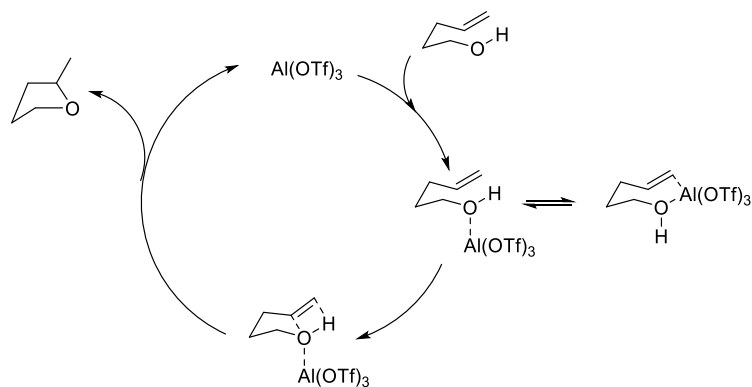


Scheme 5.1.3. Proposed two different mechanisms for NHC ligand supported Cu complexes catalyzed hydroamination.

Metal triflates or a combination of metal halides and silver triflate have been reported to catalyze intramolecular addition of N–H bonds across alkenes. However, the mechanisms for the reactions are undetermined. For example, Bi(OTf)₃ has been shown to generate HOTf *in situ*, which is the catalyst,^[39] however, with a PF₆[−] counter ion, the mechanism is proposed to be Lewis acid catalyzed hydroamination.^[42,43] In addition, Hartwig and co-workers found that triflic acid is an effective catalyst for hydroamination of protected alkenylamines and compared catalysis result with metal triflate based

reactions.^[44,45] Other Brønsted acids are catalysts for the hydroamination of unsaturated C–C bonds. Salicylic acid, triflic acid, phosphoric acid, trifluoroacetic acid and other protic catalysts, or even ionic liquids, can be used to catalyze inter- or intramolecular hydroamination with secondary or activated amines.^[46-57] Ackermann and co-workers reported that ammonium salts such as $[\text{PhMe}_2\text{NH}][\text{B}(\text{C}_6\text{F}_5)_4]$ catalyze intramolecular olefin hydroamination. The majority of their amine substrates were secondary, although primary amines could be converted to cyclic fluorinated amides with the aid of two equivalents of trifluoroacetic anhydride.

Al(III) complexes with supporting ligands have been demonstrated to be competent catalysts for the hydroamination of alkenylamines.^[58-60] Al–C bond is not cleaved during the reaction and the reaction is not inhibited by base additives, which indicates that the Al complex is possibly the true catalyst during the reaction. The inexpensive and commercially available Al(III) reagent $\text{Al}(\text{OTf})_3$ (OTf = trifluoromethanesulfonate) is known to catalyze related hydroalkoxylations of alkenylalcohols.^[61] The proposed mechanism is shown in Scheme 5.1.4. HOTf can reach the similar catalytic results to $\text{Al}(\text{OTf})_3$. However, with base additive, $\text{Al}(\text{OTf})_3$ catalyzed hydroalkoxylation was not affected but the reaction with HOTf was quenched. We investigated $\text{Al}(\text{OTf})_3$ as a catalyst for hydroamination of alkenylamines and we found evidence that the mechanism is different from that of hydroalkoxylation.



Scheme 5.1.4. Proposed mechanisms for $\text{Al}(\text{OTf})_3$ catalyzed hydroalkoxylations.

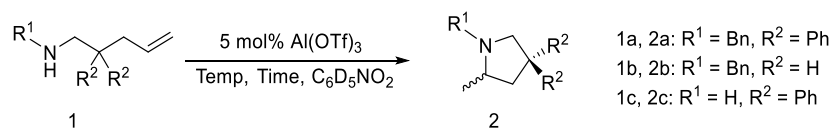
5.2 Results and Discussion

5.2.1 $\text{Al}(\text{OTf})_3$ Catalyzed Hydroamination: Alkenylamine Substrate Scope

A series of primary and secondary alkenylamine substrates were tested for hydroamination. Detailed substrate structure and catalysis result are summarized in Table 5.2.1. All reactions were performed in sealed NMR tubes with 5 mol% $\text{Al}(\text{OTf})_3$ as catalyst and d_5 -nitrobenzene as solvent with 0.8 M amine substrate. Preliminary investigations demonstrated successful cyclization of both secondary amines, **1a** and **1b**, and primary amine, **1c**. The reaction of secondary amine substrate **1a** shows the highest reaction rate, likely aided by the Thorpe-Ingold effect, and was converted in 24 h at 110 °C (entry 1). **1b** requires a higher temperature of 150 °C as well as a longer reaction time (46 h) to reach similar conversion (entry 2). The reaction of **1c**, a primary alkenylamine, also required a high temperature (150 °C, entry 4) to promote the reaction. After only 16 h at 150 °C, the cyclic amine **2c** was produced in 76% yield, which is nearly identical to that reported for the same reaction catalyzed by a phenylene-diamine ligated Al complex after 38 h at the same temperature.^[58] In addition, product **2c** is not stable at extended times under reaction

conditions and begins to decompose into multiple products which could not be clearly identified through analysis of the NMR spectra.

Table 5.2.1. Al(OTf)₃-catalysed hydroamination of alkenylamines.^a



| Entry | Substrate | Product | Temp. (°C) | Time (h) ^b | NMR Yield ^{b,c} |
|-------|-----------|-----------|------------|-----------------------|--------------------------|
| 1 | 1a | 2a | 110 | 24 | 89 |
| 2 | 1b | 2b | 150 | 46 | 74 |
| 3 | 1c | 2c | 110 | 24 | 0 |
| 4 | 1c | 2c | 150 | 16 | 76 |

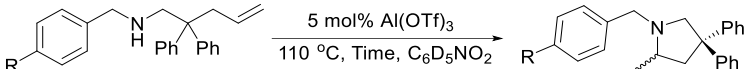
^aAll reactions were performed in sealed NMR tubes containing C₆D₅NO₂ with 0.8 M substrate and 5 mol% Al(OTf)₃.

^bFinal times and yields/conversions were recorded when either the conversion reached 95% or the percent yield began decreasing due to product decomposition. ^cDetermined by ¹H NMR spectroscopy using hexamethyldisiloxane as internal standard (the standard deviations for % yields are < 5%).

With promising results from our initial investigations, a series of secondary amine substrates with different functional groups at the *para* position of the benzylamine group of **1a** were used to study the tolerance towards electron-withdrawing and electron-donating groups (Table 5.2.2). In all cases, the intramolecular olefin hydroamination proceeded with good to excellent yield, indicating good scope and functional group tolerance in the phenyl ring. Electron-withdrawing groups such as -Br⁻, -NO₂ and -COOMe appear to reduce the rate of the reaction or the reaction times are significantly longer to reach the completion (Table 5.2.2 entries 1-3). Electron-donating group such as -OMe can facilitate the reaction; however, the effect is not significant compared to the phenyl derivative giving 93% conversion and 89% yield after 24 h respectively (Table 5.2.2 entry 4 and Table 5.2.1 entry 1). The correlation between decreasing amine basicity and decreasing reaction rate suggests that the basicity of the amine moiety may be an important attribute to facilitate intramolecular nucleophilic attack of nitrogen on the olefin (*vide infra*). This result is

different from that of Pd catalyzed olefin hydroamination, in which protonolysis of Pd–C bond is the turnover-limiting step. Decreased basicity of the amine moiety will increase the reaction rate and yield.^[31]

Table 5.2.2. Effect of electron-withdrawing and electron-donating groups in the *para* position of the phenyl ring for hydroamination of alkenylamines using Al(OTf)₃.^a



| Entry | -R | 24 h NMR Yield (Conv.) | Time (h) ^b | Final NMR Yield (Conv.) ^{b,c} |
|-------|--------------------|------------------------|-----------------------|--|
| 1 | -NO ₂ | 73 (74) | 52 | 92 (>95) |
| 2 | -Br | 78 (83) | 38 | 93 (>95) |
| 3 | - | 70 (70) | 52 | >95 (>95) |
| 4 | CO ₂ Me | 93 (95) | 28 | >95 (>95) |

^aAll reactions were performed in sealed NMR tubes containing C₆D₅NO₂ with 0.8 M substrate and 5 mol% Al(OTf)₃.

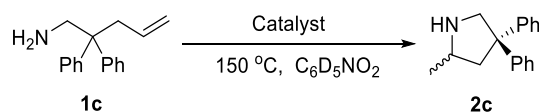
^bFinal times and yields/conversions were recorded when either the conversion reached 95% or the percent yield began decreasing due to product decomposition. ^cDetermined by ¹H NMR spectroscopy using hexamethyldisiloxane as internal standard (the standard deviations for % yields are < 5%).

5.2.2 Lewis and Brønsted Acid Catalyzed Hydroamination: Catalyst Screening

In order to determine the role of the Al species in the reaction, a variety of other simple Lewis acids were tested as catalysts for the hydroamination of **1c** (Table 5.2.3). When comparing the 16 h yield, Al(OTf)₃ gives 76% yield (Table 5.2.3, entry 1). However, only moderate yields were observed for most of other metal salts with the exception of Bi(OTf)₃, which provided a comparable yield (78%) of **2c** after 16 h (Table 5.2.3, entry 3). Product decomposition is observed with Bi(OTf)₃ after 16h, which leads to a lower final yield compared to Al(OTf)₃. AgOTf and Mg(OTf)₂ show comparable final yield, but the reaction rates are much slower (Table 5.2.3, entry 8 and 11). Interestingly, even very weak Lewis acid such as KOTf and NaOTf show some reactivity. The wide range of activity by the various catalysts suggests two possible catalysis pathways: (1) the metal is directly involved in the olefin hydroamination mechanism, and Al(OTf)₃ and Bi(OTf)₃ are the most

active catalysts; or (2) the metal triflates generate another species that is the actual catalyst, and the Al and Bi triflates are more efficient than the other metal triflates in catalyst generation. In a related study involving stoichiometric Zn salts for the amination of alkenyl benzylamines, balanced Lewis acidity was a crucial factor for higher yield and conversion. The reaction with Zn(OTf)₂ being outperformed by the weaker Lewis acids ZnCl₂ and ZnI₂.^[47] The non-metal Lewis acid BBr₃ can also catalyze the reaction, which suggests that a strong Lewis acid is capable of mediating the intramolecular olefin hydroamination or that BBr₃ reacts with amine to generate HBr or other Brønsted acid intermediate *in situ*, which catalyzes the reaction.

Table 5.2.3. Screening Lewis acids as catalyst precursors for intramolecular olefin hydroamination using 2,2-diphenyl-4-pentenylamine (**1c**).^a



| Entry | Catalyst (mol%) | 16 h NMR Yield (Conv.) | Time (h) ^b | Final NMR Yield (Conv.) ^{b,c} |
|-------|---|------------------------|-----------------------|--|
| 1 | Al(OTf) ₃ (5) | 76 (82) | 24 | 83 (>95) |
| 2 | Al(OTf) ₃ (1) | 32 (36) | — | — |
| 3 | Bi(OTf) ₃ (5) | 78 (82) | 24 | 71 (> 95) |
| 4 | AlCl ₃ (5) | 14 (19) | 170 | 46 (56) |
| 5 | Cu(OTf)(C ₆ H ₆) (5) | 24 (36) | 45 | 55 (67) |
| 6 | Cu(MeCN) ₄ PF ₆ (5) | 45 (55) | 52 | 37 (95) |
| 7 | Zn(OTf) ₂ (5) | 49 (60) | 36 | 50 (> 95) |
| 8 | Mg(OTf) ₂ (5) | 47 (57) | 52 | 81 (95) |
| 9 | NaOTf (5) | 21 (24) | 82 | 22 (44) |
| 10 | KOTf (5) | 12 (15) | 70 | 24 (40) |
| 11 | AgOTf (5) | 44 (48) | 82 | 79 (95) |
| 12 | BBr ₃ (5) | 42 (47) | — | — |

^aAll reactions were performed in sealed NMR tubes containing C₆D₅NO₂ with 0.8 M substrate and different loading of catalyst. ^bFinal times and yields/conversions were recorded when either the conversion reached 95% or the percent yield began decreasing due to product decomposition. ^cDetermined by ¹H NMR spectroscopy using hexamethyldisiloxane as internal standard (the standard deviations for % yields are < 5%).

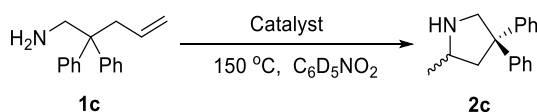
We need to be cautious when making a conclusion on the mechanism with metal triflate catalyzed olefin or alkyne hydroamination and hydroalkoxylation. Metal

triflates have been shown to generate HOTf *in situ* under reaction conditions. In addition, HOTf is an effective catalyst for hydroamination and hydroalkoxylation with specific classes of substrates.^[44,61-63] This has been observed for the hydroamination of more reactive amide substrates, particularly sulphonamides,^[46] as well as the hydroalkoxylation of unactivated alcohol substrates.^[64] These papers particularly noted that more than 1 mol% of HOTf is essential to the reaction and more than 5 mol% HOTf is harmful to the reaction. For the primary alkenylamine in this study, we have found that the intramolecular hydroamination is more effective with a higher concentration of HOTf. Using 1 mol% HOTf, the yield of **2c** is 25% after 16 h at 150 °C but increased to 64% when the amount of HOTf was increased to 5 mol% (Table 5.2.4, entries 7 and 8). The acceleration continues with high loading of HOTf and reaction is complete with over 15 mol% HOTf at 16h. In a related study by Michon and coworkers, HBF₄, can be generated *in situ* from AgBF₄ and was able to catalyze the hydroamination of more reactive secondary alkenylamines but failed in the case of the primary alkenylamines.^[65] In addition, Li and coworkers identified trifluoroacetic acid (HTFA) as a hydroamination catalyst for secondary alkenylamines.^[47] When using 10 mol% HTFA in C₆D₅NO₂, we observed a comparable but slightly decreased yield of 84% versus the previously reported 89% for hydroamination of secondary amine **1a** in 1,4-dioxane. In order to compare the catalytic ability between two Brønsted acids, a range of HTFA concentrations was tested using **1c** as substrate (Table 5.2.4, entries 1-4). However, the reactions resulted in < 16% yield of **2c** under all conditions. This reduced activity, compared to our observations with HOTf, was initially surprising

noting that Li and coworkers observed HTFA to be the superior catalyst for the hydroamination of **1a**. However, the solvents are different in the two studies. Their catalyst optimization was performed in xylene, and we have observed that non-polar solvents diminish the performance of HOTf (*vide infra*). Other common acids, such as acetic acid and HCl are reported as catalysts for hydroxylation or hydroamination of C-C multi bonds using activated amines; however, some of them are not a catalyst for hydroamination reaction with **1c** (Table 5.2.4, entries 5 and 6). These observations may be explained by a difference in mechanism. In the hydroxylations of alkenyl alcohols or hydroaminations of sulphonamides, the triflic acid or other strong Brønsted acid may be regenerated in the catalytic cycle due to the weak basicity of the substrate. However, for hydroaminations of amines, the substrates' stronger basicity precludes the presence of a strong acid like HOTf in the solution. The real catalyst may be an ammonium triflate salt formed from the combination of triflic acid and amine substrate.

The data from base additive experiment supports this hypothesis.

Table 5.2.4. Screening Brønsted acid as catalyst precursors for intramolecular olefin hydroamination using 2,2-diphenyl-4-pentenylamine (**1c**).^a



| Entry | Catalyst (mol%) | 16 h NMR Yield (Conv.) | Time (h) ^b | Final NMR Yield (Conv.) ^{b,c} |
|-------|-----------------|---------------------------|-----------------------|---|
| 1 | HTFA (5) | 4(14) | 90 | 11(46) |
| 2 | HTFA (10) | 5(22) | 90 | 12(47) |
| 3 | HTFA (20) | 8(31) | 90 | 16(49) |
| 4 | HTFA (30) | 14(45) | 90 | 15(57) |
| 5 | HOAc (5) | — | 67 | < 10(25) |
| 6 | HCl (5) | — | 50 | 20(30) |
| 7 | HOTf (5) | 60 (64) | 24 | 74 (85) |
| 8 | HOTf (1) | 25 (32) | — | — |
| 9 | HOTf(10) | 76 (81) | — | — |

| | | | | |
|----|----------|---------|---|---|
| 10 | HOTf(15) | 84 (95) | — | — |
| 11 | HOTf(20) | 87 (95) | — | — |

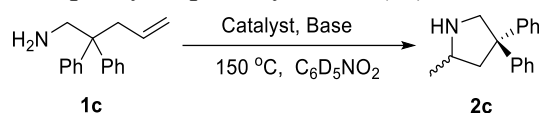
^aAll reactions were performed in sealed NMR tubes containing C₆D₅NO₂ with 0.8 M substrate and different loading of catalyst. ^bFinal times and yields/conversions were recorded when either the conversion reached 95% or the percent yield began decreasing due to product decomposition. ^cDetermined by ¹H NMR spectroscopy using hexamethyldisiloxane as internal standard (the standard deviations for % yields are < 5%).

5.2.3 Base Additives Study

In studies by Pons and Dunach, hydroalkoxylations using unactivated alkenylalcohols were found to be catalyzed by either 5 mol% Al(OTf)₃ or HOTf.^[61] This could be consistent with Al(OTf)₃ acting as a precatalyst for formation of HOTf as the active catalyst. However, it was found that the HOTf catalyzed reaction was inhibited with addition of 5 mol% 2,6-lutidine, while no inhibition of the Al-catalysed reaction was observed. The HBF₄ catalyzed hydroamination of secondary alkenylamines was also inhibited by the addition of base.^[65] In this study, the addition of weak bases such as 5 mol% 2,6-lutidine and pyridine did not affect the yields of both the Al(OTf)₃ and the HOTf catalyzed reactions using **1c** (Table 5.2.5). Even increasing the loading of 2,6-lutidine to 30 mol%, no specific yield decrease was observed. Due to these surprising results, we tested other bases for their effect on both the Al(OTf)₃ and HOTf catalysed reactions (Table 5.2.5). The additions of 5 mol% Et₃N and 2,6-di-*tert*-butylpyridine did not significantly affect the yield of **2c** after 16 h for either the Al(OTf)₃ or HOTf catalyzed reactions. In fact, several of these added bases led to small increases in yield and selectivity. However, large quantities (30 mol%) of Et₃N or Na₂CO₃ greatly hindered both Al(OTf)₃ and HOTf-mediated reactions (Table 5.2.5, entries 7, 8, 15 and 16). Since different bases have different effects on the catalytic results, pyridinium and 2,6-lutidinium triflate salts were prepared and tested as catalysts directly (Table 5, entries 17 and 18). These salts gave comparable yields and selectivities to the HOTf catalyzed reaction indicating that the high acidity of HOTf is not required for catalysis. In the

presence of a large excess of amine and smaller quantities of a strong Brønsted acid, the strongest acid in solution will be the protonated amine due to the leveling effect. If the basicity of base additive is less than the amine substrate, the additive will not inhibit the reaction. Comparing with the catalysis results of other strong acids in Table 5.2.4, the high activity of the pyridinium triflate salts suggests that the triflate ion itself might also play an important role in these catalytic olefin hydroamination reactions. For example, the triflate ion may act as an efficient proton shuttle. Another possibility is that the increased basicity of other ions (e.g., TFA) may result in a stable ammonium intermediate and prevent proton transfer to the olefinic fragment. In this case, we could conclude that HOTf acts as a catalyst precursor to generate the ammonium triflate, which is likely the actual catalyst for this reaction.

Table 5.2.5. Base additive effects on Al(OTf)₃ and HOTf catalyzed intramolecular olefin hydroamination using 2,2-diphenyl-4-pentenylamine (**1c**).^a



| Entry | Catalyst | Base (mol %) | 16 h NMR Yield (Conv.) ^b | Time (h) ^b | Final NMR Yield (Conv.) ^{b,c} |
|-------|----------------------|---------------------------------------|-------------------------------------|-----------------------|--|
| 1 | Al(OTf) ₃ | — | 76 (82) | 24 | 83 (>95) |
| 2 | Al(OTf) ₃ | 2,6-lutidine (5) | 78 (81) | 24 | 87 (92) |
| 3 | Al(OTf) ₃ | 2,6-lutidine (30) | 83 (84) | 24 | 87 (>95) |
| 4 | Al(OTf) ₃ | pyridine (5) | 77 (86) | 24 | 87 (>95) |
| 5 | Al(OTf) ₃ | 2,6-Di- <i>tert</i> -butylpyridine(5) | 71 (72) | 24 | 87 (89) |
| 6 | Al(OTf) ₃ | Et ₃ N (5) | 75 (77) | 24 | 89 (92) |
| 7 | Al(OTf) ₃ | Et ₃ N (30) | 36 (42) | 38 | 68 (80) |
| 8 | Al(OTf) ₃ | Na ₂ CO ₃ (30) | 43 (53) | 38 | 60 (75) |
| 9 | HOTf | — | 60 (64) | 24 | 74 (85) |
| 10 | HOTf | 2,6-lutidine (5) | 56 (60) | 24 | 76 (82) |
| 11 | HOTf | 2,6-lutidine (30) | 61 (70) | 24 | 77 (86) |
| 12 | HOTf | pyridine (5) | 67 (72) | 32 | 86 (92) |
| 13 | HOTf | 2,6-di- <i>tert</i> - | 53 (57) | 32 | 77 (82) |

| | | butylpyridine(5) | | | |
|----|---------------------|--------------------------------------|---------|----|---------|
| 14 | HOTf | Et ₃ N (5) | 52 (55) | 32 | 77 (80) |
| 15 | HOTf | Et ₃ N (30) | 33 (31) | 38 | 62 (67) |
| 16 | HOTf | Na ₂ CO ₃ (30) | 33 (43) | 38 | 45 (62) |
| 17 | [2,6-lutidinium]OTf | — | 57 (64) | 44 | 83 (92) |
| 18 | [pyridinium]OTf | — | 52 (60) | 44 | 74 (92) |

^aAll reactions were performed in sealed NMR tubes containing C₆D₅NO₂ with 0.8 M substrate and different loading of catalyst. ^bFinal times and yields/conversions were recorded when either the conversion reached 95% or the percent yield began decreasing due to product decomposition. ^cDetermined by ¹H NMR spectroscopy using hexamethyldisiloxane as internal standard (the standard deviations for % yields are < 5%).

5.2.4 Kinetic Study of Hydroamination

In order to investigate the mechanism of Al(OTf)₃ catalyzed olefin hydroamination, a series of kinetic experiments were performed. Both the Al(OTf)₃- and the HOTf-mediated hydroaminations with **1c** were found to be first order with respect to amine substrate (Figure 5.2.1 plot a). The reaction rate (k_{obs}) is accelerated with increased initial catalyst loading signifying that the reaction is also first order with respect to catalyst precursor (Figures 5.2.1, plot b and c). If these two catalysts follow two different mechanisms, there will be a substrate competition between them, which may slow down the Al(OTf)₃ catalysed reaction. In this case, possible substrate competition was investigated by performing the same kinetic experiments with 5 mol% Al(OTf)₃ and varying amount of added HOTf. The linear plots of k_{obs} versus concentration of HOTf are consistent with a reaction that is first order in substrate and first order in HOTf (Figure 5.2.1, plot d). This result suggests that the Al(OTf)₃ catalyzed reaction is running as a background reaction and the rate is unaffected by the addition of HOTf. Since no reaction inhibition was observed, the same reaction mechanism may be operative for both the Al(OTf)₃ and HOTf

mediated reactions. This observation suggests that HOTf is *in situ* generated from the $\text{Al}(\text{OTf})_3$, which then serves as the catalyst precursor for amine hydroamination.

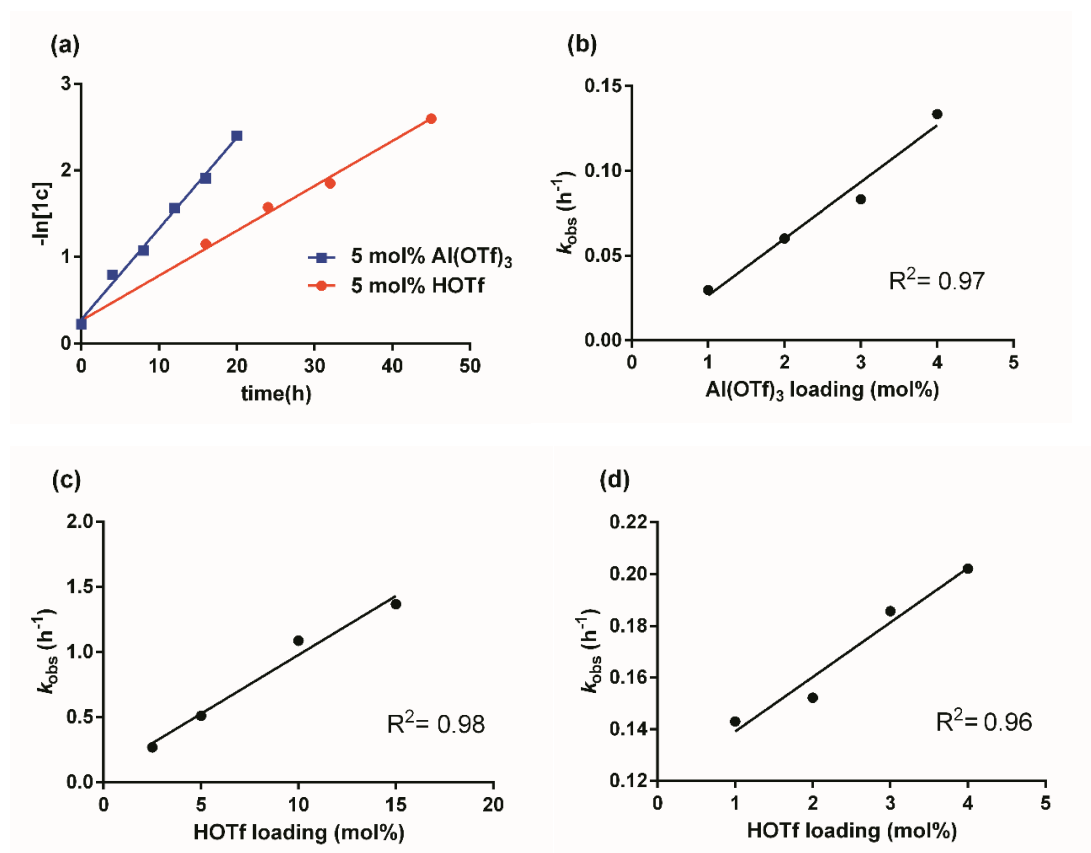


Figure 5.2.1. Kinetic data for determination of reaction order with respect to **1c** and catalysts. All reactions were performed in sealed NMR tubes containing $\text{C}_6\text{D}_5\text{NO}_2$ with 0.8 M substrate and different loading of catalyst. (a) Determination of the rate order of **1c**: linear fit of $-\ln[1c]$ versus time for reactions with 5 mol % of $\text{Al}(\text{OTf})_3$ or HOTf. (b) Determination of the reaction order of $\text{Al}(\text{OTf})_3$: k_{obs} as a function of $\text{Al}(\text{OTf})_3$ loading. (c) Determination of the reaction order of HOTf: k_{obs} as a function of HOTf loading. (d) Determination of the reaction order of HOTf with 5 mol% $\text{Al}(\text{OTf})_3$: k_{obs} as a function of HOTf loading.

Experiment for Kinetic isotope effects (KIEs) were performed for further investigation of the mechanism. The reactions used HOTf and $\text{Al}(\text{OTf})_3$ with one equivalent relative to amine substrate with added H_2O or D_2O to determine the KIEs. Statistically identical KIEs of $k_{\text{H}}/k_{\text{D}} = 1.53 \pm 0.17$ and 1.49 ± 0.18 , are observed for the reaction with $\text{Al}(\text{OTf})_3$ and HOTf, respectively. (Figure 5.2.2). In addition, KIE

experiments with protio- and deuterio-substrates under the same reaction condition were performed (Scheme 5.2.1, Figure 5.2.3). Likewise, an identical KIE ($k_{\text{H}}/k_{\text{D}} = 1.4 \pm 0.1$ and 1.5 ± 0.2) was also obtained for $\text{Al}(\text{OTf})_3$ and $\text{Bi}(\text{OTf})_3$ catalysts. These results are consistent with the *in situ* generation of HOTf, which suggests that all metal triflates might undergo a similar mechanism. In order to exclude the influence of water on the reaction, different amounts of H_2O were added to the reaction. The effects on reaction rate or products were negligible (Table 5.2.6).

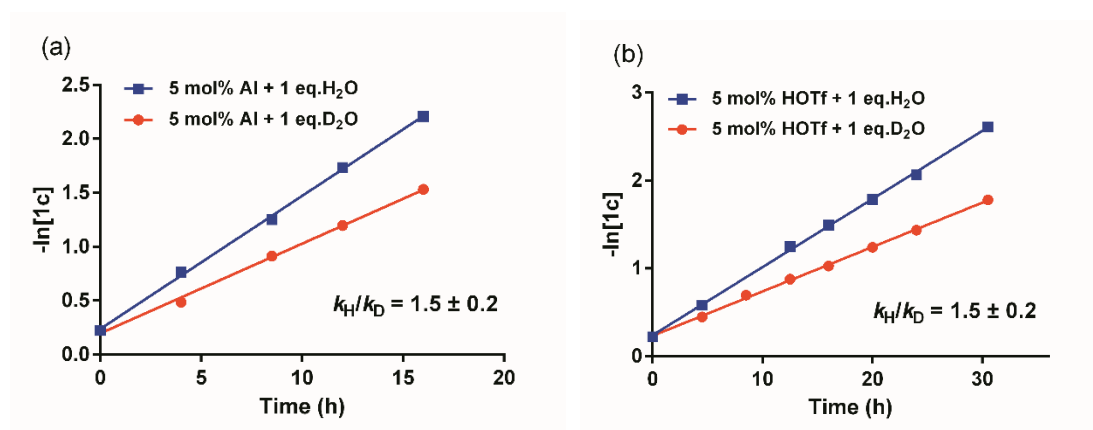
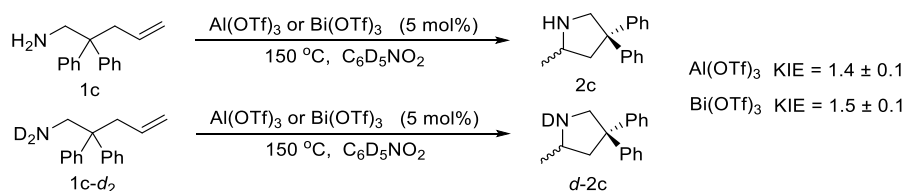


Figure 5.2.2. KIE determination for HOTf and $\text{Al}(\text{OTf})_3$ catalysed hydroamination of **1c**. All reactions were performed in sealed NMR tubes containing $\text{C}_6\text{D}_5\text{NO}_2$ with 0.8 M substrate, 5 mol% catalyst and one equivalent H_2O or D_2O (relative to amine substrate). (a) Determination of KIE for $\text{Al}(\text{OTf})_3$ catalysed reaction: linear fit of $-\ln[1c]$ versus time for reactions with 1 equivalent of H_2O or D_2O (relative to amine substrate). (b) Determination of KIE for HOTf catalysed reaction: linear fit of $-\ln[1c]$ versus time.



Scheme 5.2.1. Kinetic isotope effect experiments with $\text{Al}(\text{OTf})_3$ and $\text{Bi}(\text{OTf})_3$.

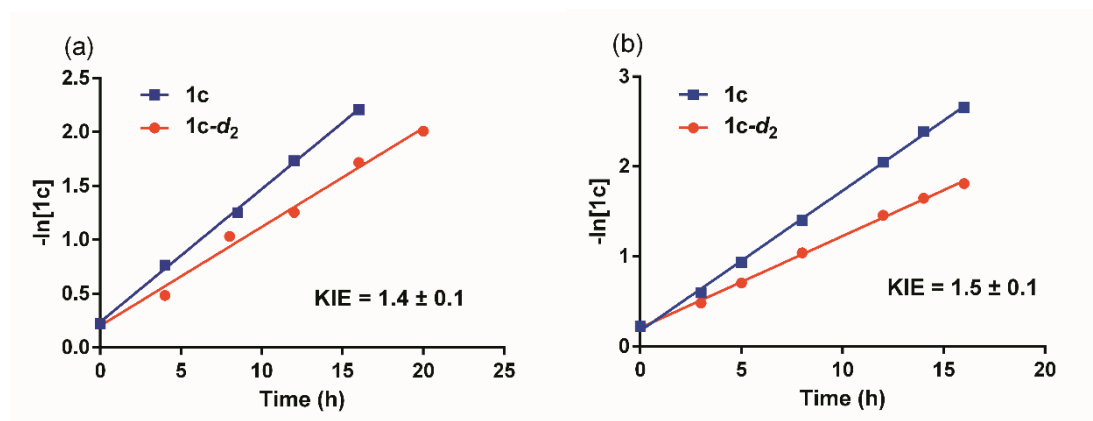
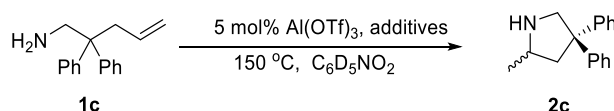


Figure 5.2.3. KIE determination for $\text{Al}(\text{OTf})_3$ and $\text{Bi}(\text{OTf})_3$ catalysed hydroamination of **1c** or **1c-d₂**. All reactions were performed in sealed NMR tubes containing $\text{C}_6\text{D}_5\text{NO}_2$ with 0.8 M substrate, 5 mol% catalyst at 150 °C. (a) Determination of KIE for $\text{Al}(\text{OTf})_3$ catalysed reaction: linear fit of $-\ln[1c]$ and $-\ln[1c-d_2]$ versus time (b) Determination of KIE for $\text{Bi}(\text{OTf})_3$ catalysed reaction: linear fit of $-\ln[1c]$ and $-\ln[1c-d_2]$ versus time.

Table 5.2.6. Influence of water on $\text{Al}(\text{OTf})_3$ catalyzed hydroamination.^{a,b,c}



| Entry | Catalysts | Additives | NMR Yield (%) | NMR Conv. (%) |
|-------|----------------------------------|-------------------------------|---------------|---------------|
| 1 | 5 mol% $\text{Al}(\text{OTf})_3$ | / | 76 | 82 |
| 2 | 5 mol% $\text{Al}(\text{OTf})_3$ | 0.25 eq. H_2O | 80 | 81 |
| 3 | 5 mol% $\text{Al}(\text{OTf})_3$ | 0.5 eq. H_2O | 85 | 86 |
| 4 | 5 mol% $\text{Al}(\text{OTf})_3$ | 1 eq. H_2O | 76 | 81 |
| 5 | 5 mol% $\text{Al}(\text{OTf})_3$ | 2 eq. H_2O | 83 | 86 |

a) All reactions were performed in sealed NMR tubes containing $\text{C}_6\text{D}_5\text{NO}_2$ with 0.8 M substrate, 5 mol% $\text{Al}(\text{OTf})_3$ and different amount water. b) yields/conversions were recorded at 16h and determined by ^1H NMR using hexamethyldisiloxane as internal standard (the standard deviations for % yields are < 5%). c) H_2O 's loading are relative to $\text{Al}(\text{OTf})_3$

5.2.5 Solvent Effect Study

The solvent effect on catalyst performance using $\text{Al}(\text{OTf})_3$ and HOTf was investigated by using deuterated solvents of varying polarity including dimethyl sulfoxide (DMSO), 1,2-dichlorobenzene (1,2-DCB), toluene and 1,4-dioxane (Table 5.2.7). The reaction rates were much slower compared to nitrobenzene. Of these four solvents, only the reaction

performed in 1,2-DCB give comparable yields to those in $C_6D_5NO_2$ after 5 days instead of only approximately 30 h for the reaction in $C_6D_5NO_2$. Catalysis in the slightly polar solvent 1,4-dioxane required approximately 5 days to reach maximum yield, but with much lower yield compared to nitrobenzene. The decrease in efficiency was even more pronounced in DMSO and toluene (entries 1, 2, 5 and 6), which may due to the poorer solvation of possible ionic intermediates. Although yields in each solvent were different, $Al(OTf)_3$ and HOTf showed comparable results to each other in all of the solvents.

Table 5.2.7. Solvent effect on the hydroamination of benzyl(2,2-diphenyl-4-pentenyl)amine (**1a**).

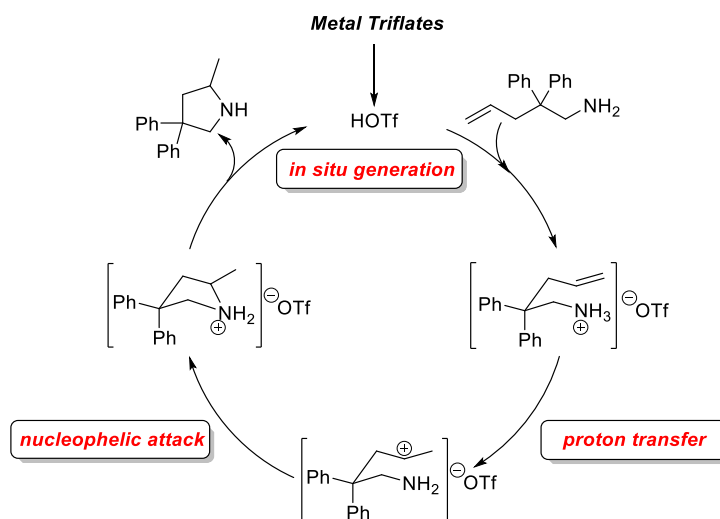
| Entry | Solvent | Catalyst | 24 h NMR Yield ^b | Time (h) ^b | Final NMR Yield ^{b,c} |
|-------|----------------------|-------------|-----------------------------|-----------------------|--------------------------------|
| 1 | DMSO | $Al(OTf)_3$ | 11 | 137 | 46 |
| 2 | DMSO | HOTf | 5 | 128 | 40 |
| 3 | 1,2-DCB ^d | $Al(OTf)_3$ | 38 | 137 | 89 |
| 4 | 1,2-DCB | HOTf | 19 | 137 | 74 |
| 5 | toluene | $Al(OTf)_3$ | 3 | 137 | 44 |
| 6 | toluene | HOTf | 7 | 137 | 38 |
| 7 | 1,4-dioxane | $Al(OTf)_3$ | 15 | 133 | 57 |
| 8 | 1,4-dioxane | HOTf | 15 ^c | 133 | 38 |

^aAll reactions were performed in sealed NMR tubes with 0.8 M substrate in different solvents with 5 mol% catalyst. ^bFinal times and yields/conversions were recorded when either the conversion reached 95% or the percent yield began decreasing due to product decomposition. ^cDetermined by 1H NMR spectroscopy using hexamethyldisiloxane as internal standard (the standard deviations for % yields are < 5%). ^d1,2-DCB = 1,2-dichlorobenzene.

5.3 Proposed Mechanism and Conclusion.

We report intramolecular hydroamination of unactivated secondary and primary alkenylamines catalyzed by $Al(OTf)_3$. Comparable or increased efficiency to other reported Al catalysts was observed using catalytic amounts of simple aluminium salt, $Al(OTf)_3$. However, HOTf or even pyridinium triflate salts are found to produce comparable catalytic results. Compared to other Brønsted acids (e.g., HTFA and HCl), HOTf shows higher catalytic activity. Due to the levelling effect of amine substrate, the acidic species are

probably the same protonated amine substrates. The reactivity difference indicates that the triflate anion is likely of significance in mediating the reactions. The solvent was also found to have a significant effect. Polar solvents are more effective for the HOTf initiated reaction and stabilize the ion pair intermediate. Identical kinetic results are observed for the $\text{Al}(\text{OTf})_3$ and the HOTf-mediated reactions. In addition, base additives have very similar effects on both Lewis acid and Brønsted acids catalyzed reaction. These observations suggest that $\text{Al}(\text{OTf})_3$ may only serve as a source to generate triflic acid *in situ*. The triflic acid may then act as a catalyst precursor which would react with the basic amine substrates to produce ammonium salts as the active catalyst for the hydroaminations. The proposed mechanism is shown in Scheme 5.3.1. These results serve as a caution for studies that propose metal salts as the operative active catalyst in hydroaminations of unactivated alkenylamines; rigorous controls should be used to verify the nature of the active catalyst. The remarkable activity of Brønsted acids, even relatively weak pyridinium salts, to serve as hydroamination catalysts is illustrated particularly through their success toward hydroamination of a less reactive primary alkenylamine which, to our knowledge, has not been previously reported in the absence of additional co-catalysts or additives.



Scheme 5.3.1. Proposed mechanism for metal triflate catalyzed hydroamination**5.4 Experimental Section**

The substrates benzyl(2,2-diphenyl-4-pentenyl)amine (**1a**),^[29] N-benzyl-4-pentenyl-1-amine (**1b**),^[39] 2,2-diphenyl-4-pentenylamine (**1c**),^[66] 4-bromobenzyl(2,2-diphenyl-4-pentenyl)amine,^[29] methyl 4-[(2,2-diphenyl-4-pentenylamino)-methyl]benzoate,^[29] and 4-nitrobenzyl(2,2-diphenyl-4-pentenyl) amine^[29] were synthesized according to literature procedures.

Synthesis of 4-methoxybenzyl(2,2-diphenyl-4-pentenyl)amine. A 25 mL methanol solution containing **1c** (1.51 g, 6.37 mmol) and 4-methoxybenzaldehyde (0.91 g, 6.68 mmol) was stirred at room temperature for 3.5 h. A small excess of NaBH₄ (0.268 g, 7.1 mmol) was added at room temperature and stirred for 12 h. The reaction was quenched by the addition of water at 0 °C. The solution was made alkaline by the addition of 1 M NaOH (50 mL), resulting in a suspension. The suspension was extracted with CH₂Cl₂ (3 × 50 mL). The combined organic extracts were washed with brine (3 × 50 mL) and dried with MgSO₄. The solvent was then removed under vacuum to provide a colorless oil, which was then purified by column chromatography on silica gel (eluent: hexanes:EtOAc = 8:1 with 2% Et₃N) to give the title compound (1.47 g, 65 %) as a viscous colorless oil that formed a white solid upon standing. ¹H NMR (600 MHz, CD₂Cl₂): δ 7.30 (4H, t, ³J_{HH} = 8 Hz, H^o-Ph), 7.18-7.25 (6H, m, H^m-Ph and H^p-Ph), 7.16 (2H, d, ³J_{HH} = 8 Hz, H^o-4-C₆H₄OMe), 6.84 (2H, d, ³J_{HH} = 8 Hz, H^m-4-C₆H₄OMe), 5.40 (1H, ddt, ³J_{HH} = 17, 11, 7, vinyl CH), 5.02 (1H, d, ³J_{HH} = 17 Hz, vinyl CH₂), 4.93 (1H, d, ³J_{HH} = 10 Hz, vinyl CH₂), 3.79 (3H, s, C₆H₄OCH₃), 3.67 (2H, s, CH₂), 3.25 (2H, s, CH₂), 3.08 (2H, d, ³J_{HH} = 7 Hz, CH₂), 0.85 (1H, br s, NH)

^{13}C NMR (150 MHz, CD_2Cl_2): δ 159.0 ($\text{C}_6\text{H}_4\text{OMe}$), 147.4 (Ph), 135.4 (vinyl CH), 133.4 ($\text{C}_6\text{H}_4\text{OMe}$), 129.4 ($\text{C}_6\text{H}_4\text{OMe}$), 128.4 (Ph), 128.3 (Ph), 126.3 (Ph), 117.7 (vinyl CH_2), 113.9 ($-\text{C}_6\text{H}_4\text{OMe}$), 55.6 (CH_2), 55.5 (OMe), 54.0 (benzyl- CH_2), 50.4 (quaternary C), 41.9 (CH_2)

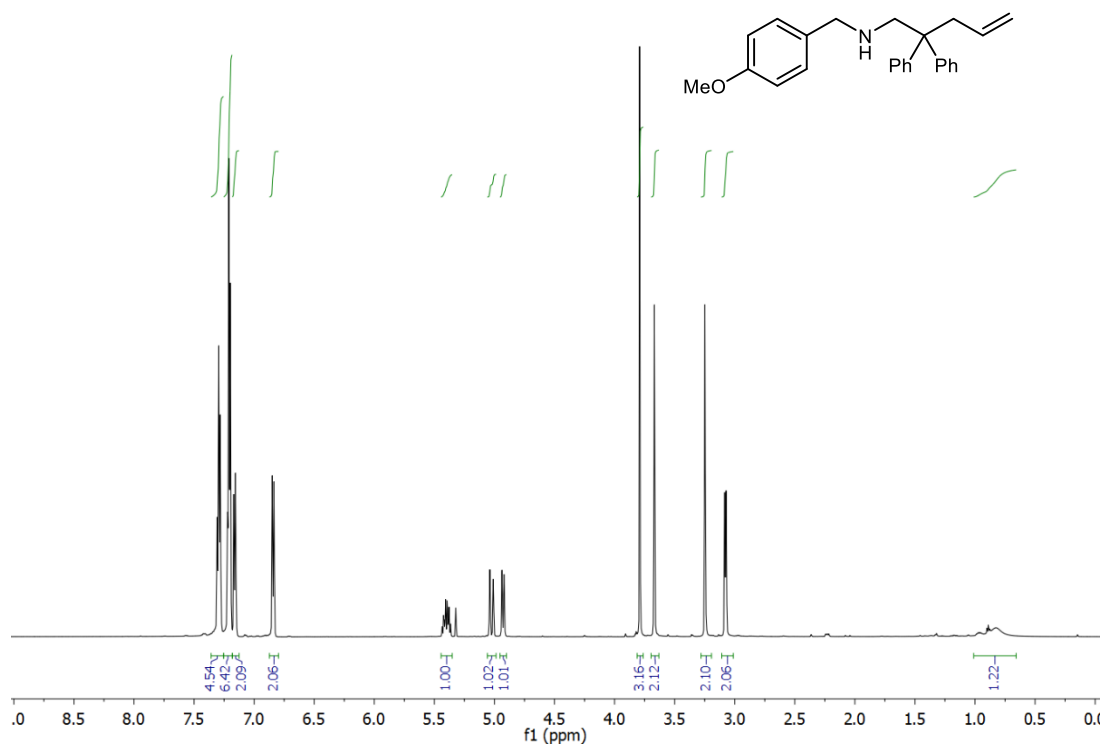


Figure 5.4.1. ^1H NMR spectrum (600 MHz, CD_2Cl_2) of 4-methoxybenzyl(2,2-diphenyl-4-pentenyl)amine.

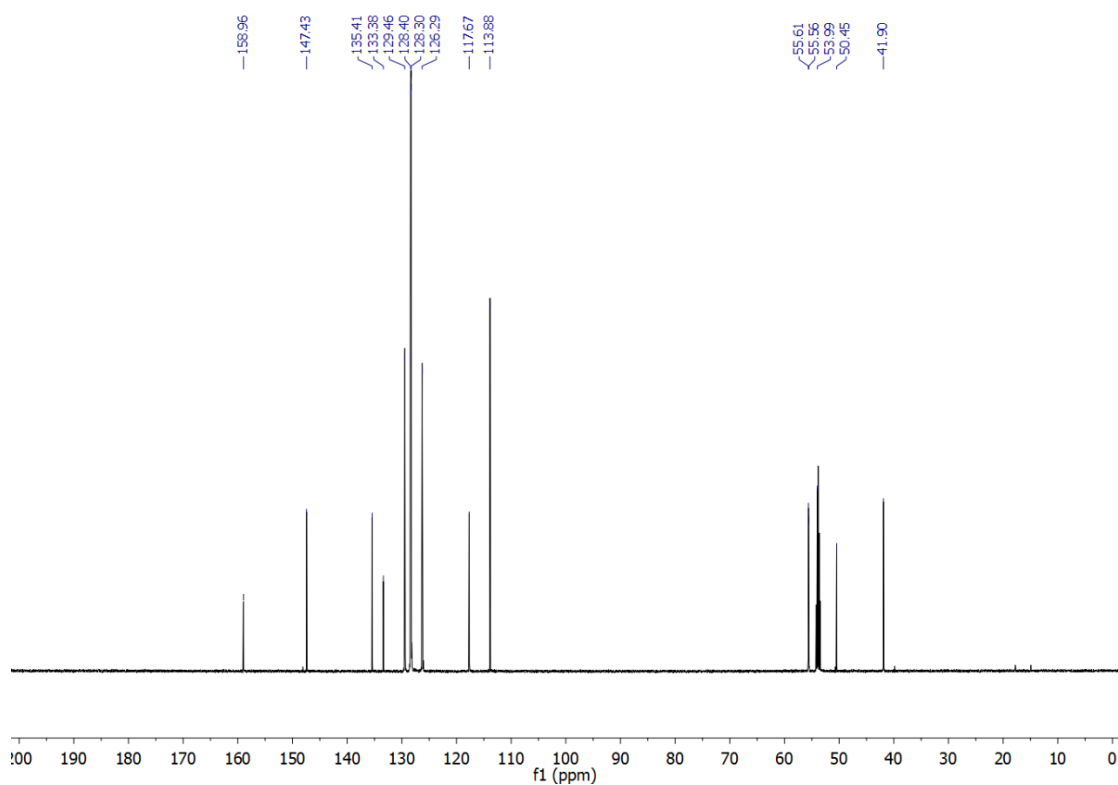


Figure 5.4.2. $^{13}\text{C}\{^1\text{H}\}$ NMR spectrum (150 MHz, CD_2Cl_2) of 4-methoxybenzyl(2,2-diphenyl-4-pentenyl)amine.

Synthesis of benzyl(2,2-diphenyl-4-pentenyl)amine- d_1 ($\mathbf{1c-d}_2$). Anaerobic conditions are not required. The compound **1c** (1.01 g, 4.29 mmol) was stirred in D_2O (10 mL) at reflux for 24 h. The solvent was removed under vacuum to afford **1c- d_2** (0.95 g, 95 %) as a pale yellow oil. ^1H NMR spectroscopy was used to verify > 95 % deuterium incorporation.

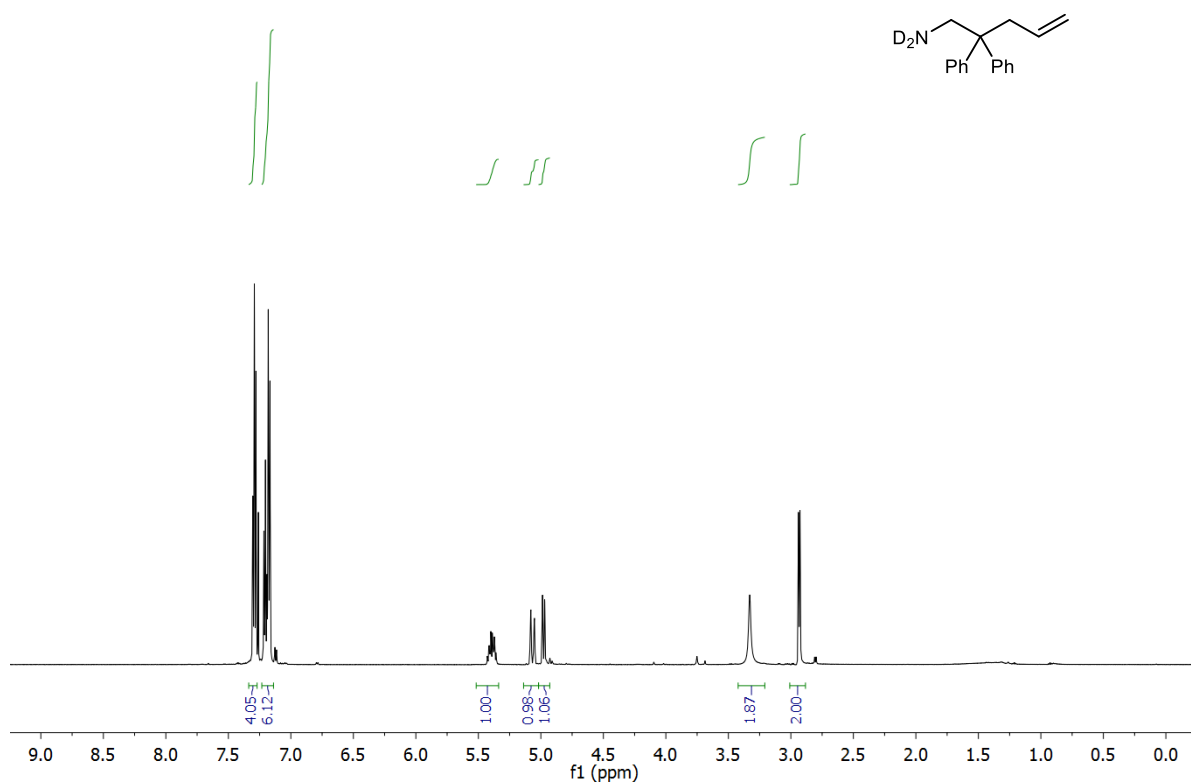
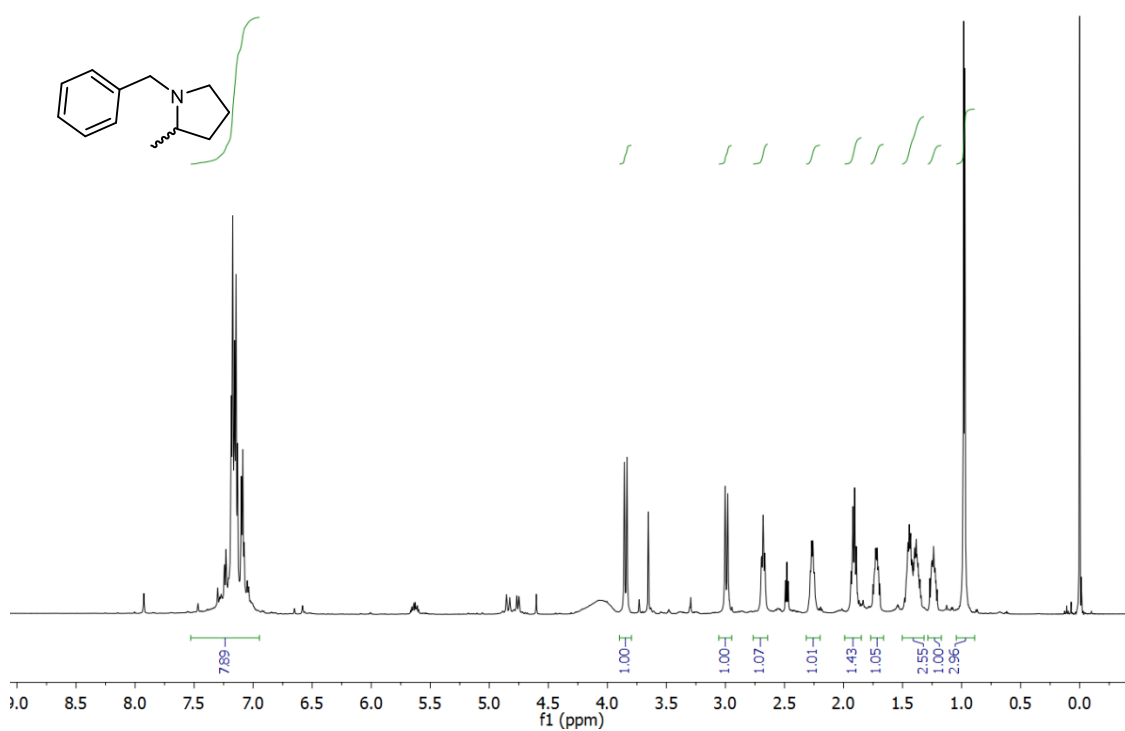
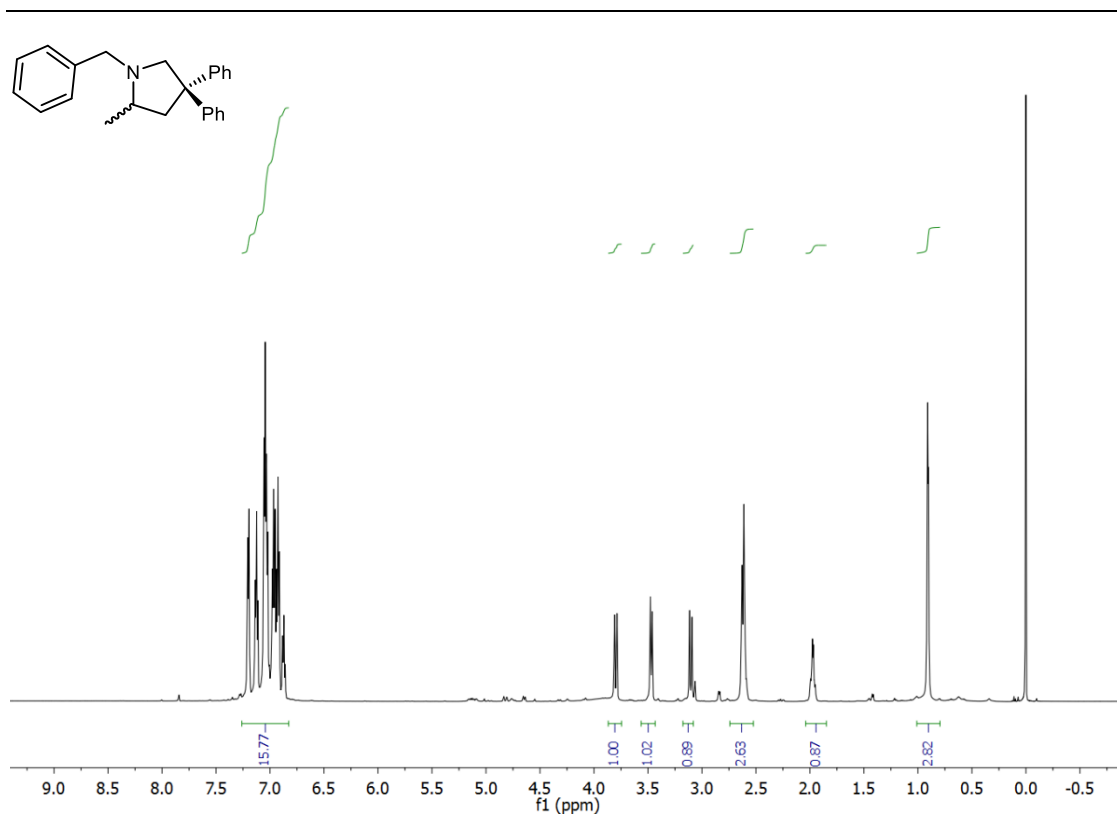


Figure 5.4.3. ¹H NMR spectrum (600 MHz, CDCl₃) of **1c-d₂**.

General Procedure for Catalytic Intramolecular Hydroamination. A representative catalytic reaction is described. A 0.8 M stock solution was prepared by dissolving compound **1c** (0.2846 g, 1.2 mmol) in nitrobenzene-*d*₅ (1.5 mL). The stock solution was then distributed among 3 NMR tubes (3 x 0.5 mL) containing Al(OTf)₃ (9.5 mg, 0.02 mmol) and a sealed capillary of hexamethyldisiloxane, as the internal standard. The NMR tubes were sealed and initial ¹H NMR spectra obtained. The NMR tubes were then heated in an oil bath at 150 °C. Every 4 hours, the reaction was paused by rapid cooling to 0 °C using an ice bath and analyzed by ¹H NMR spectroscopy. ¹H NMR spectra were collected using 8 transients with a 10 second pulse delay. Yields and conversion were calculated from the integration of resonances for **1c**, **2c**, and the internal standard. The resulting cyclized products were not isolated.



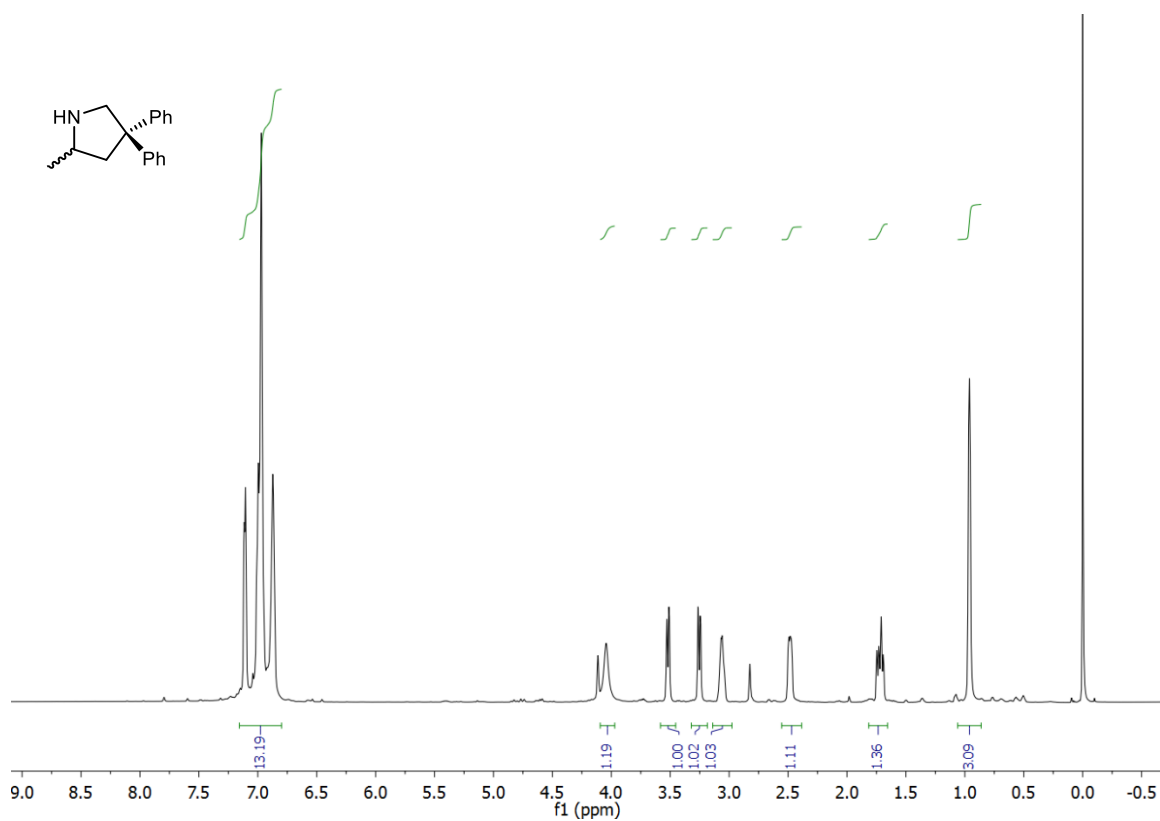


Figure 5.4.6. ^1H NMR spectrum (600 MHz, $\text{C}_6\text{D}_5\text{NO}_2$) of hydroamination product of **1c**.^{a,b}

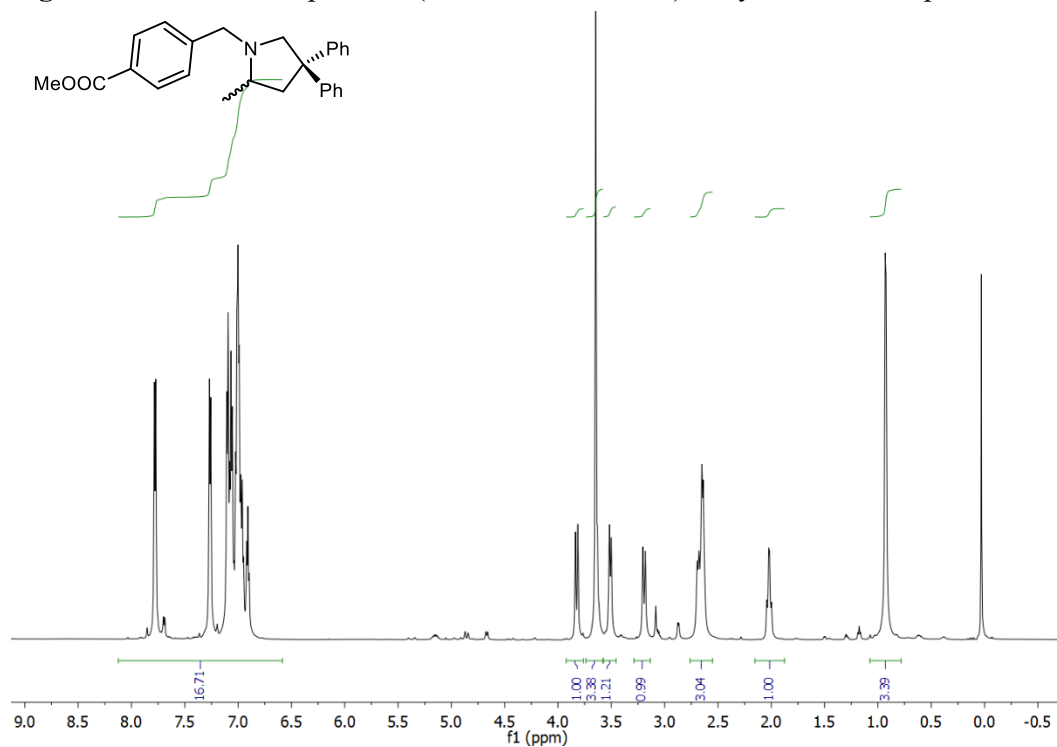


Figure 5.4.7. ^1H NMR spectrum (600 MHz, $\text{C}_6\text{D}_5\text{NO}_2$) of hydroamination product of methyl 4-[(2,2-diphenyl-4-pentylamino)-methyl]benzoate.^{a,b}

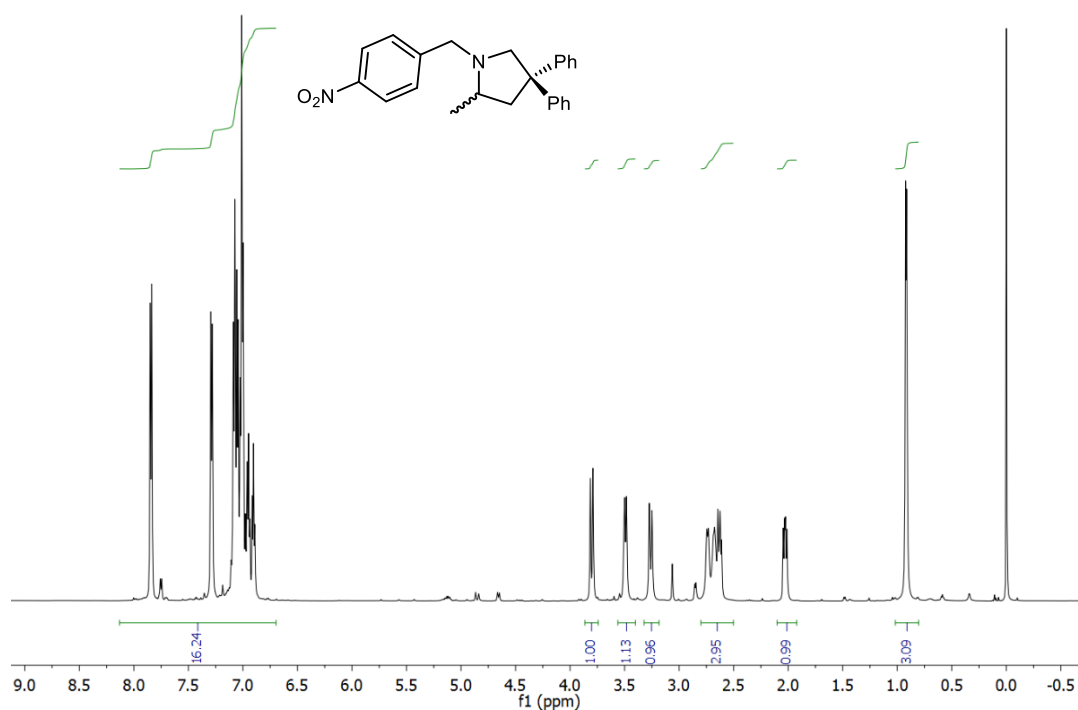


Figure 5.4.8. ¹H NMR spectrum (600 MHz, C₆D₅NO₂) of hydroamination product of 4-nitrobenzyl(2,2-diphenyl-4-pentenyl)amine.^{a,b}

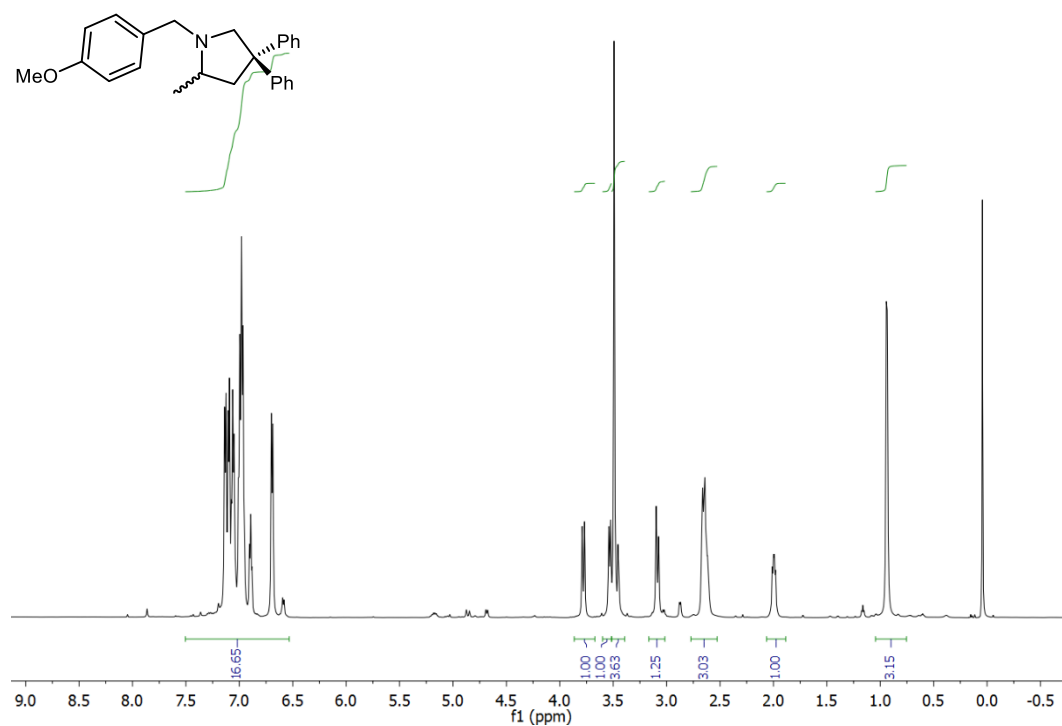


Figure 5.4.9 ¹H NMR spectrum (600 MHz, C₆D₅NO₂) of hydroamination product of 4-methoxybenzyl(2,2-diphenyl-4-pentenyl)amine.^{a,b}

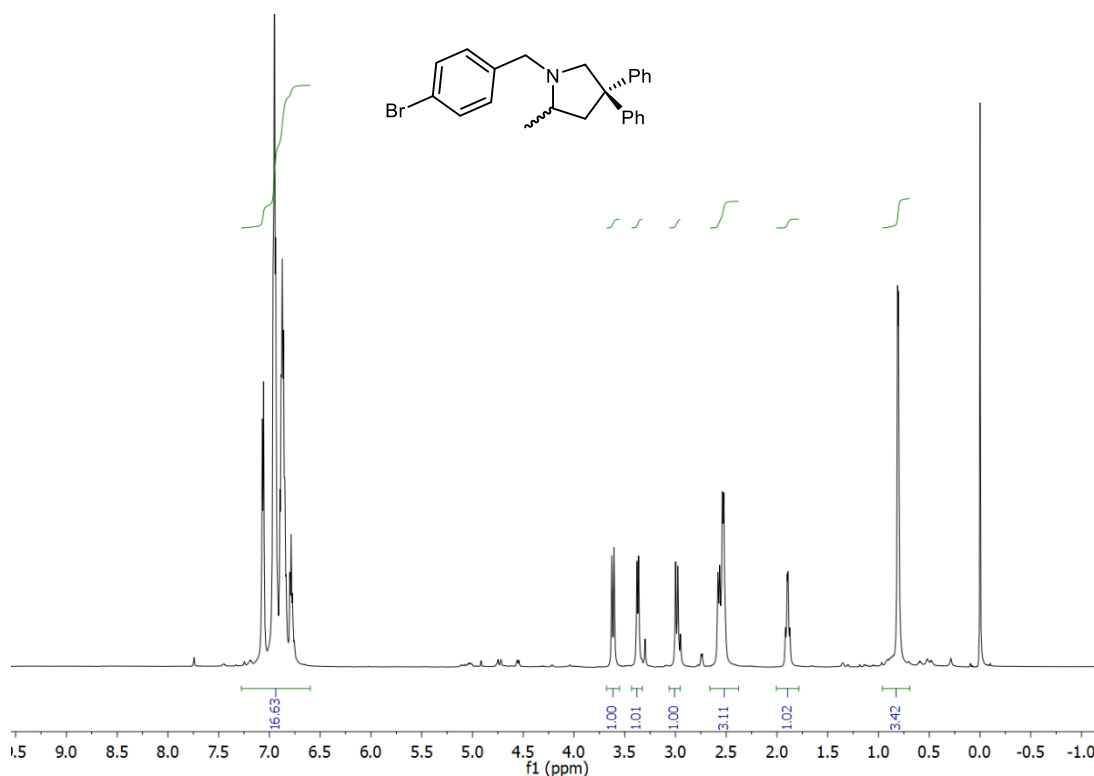


Figure 5.4.10 ¹H NMR spectrum (600 MHz, C₆D₅NO₂) of hydroamination product of 4-bromobenzyl(2,2-diphenyl-4-pentenyl)amine.^{a,b}

a: The proton peak shows up at 0.0 ppm is inner standard HMDSO.

b: The integration of aromatic region do not fit the structure due to the overlap with solvent peaks.

Sample Preparation for Kinetic Isotope Effects Experiments. (1) Using water

additives: The reaction NMR tubes were prepared using the typical catalytic intramolecular hydroamination procedure with 5 mol% of either Al(OTf)₃ or HOTf. Before sealing the NMR tubes, H₂O (7.2 μL) or D₂O (7.2 μL) was added separately to each tube. (2) *Using protic or deuterated substrates:* A 0.8 M stock solution was prepared by dissolving either compound **1c** (0.2846 g, 1.2 mmol) or **1c-d₂** (0.2870 g, 1.2 mmol) in nitrobenzene-*d*₅ (1.5 mL). The stock solution was then distributed among 3 NMR tubes (3 x 0.5 mL) containing either Al(OTf)₃ (9.5 mg, 0.02 mmol) or Bi(OTf)₃ (13,1mg, 0.02mmol) and a sealed capillary of hexamethyldisiloxane, as the internal standard. The remainder of the experiments were performed in the same manner as for the representative catalytic intramolecular hydroamination procedure above.

5.5 References

- [1] Carey, J. S.; Laffan, D.; Thomson, C.; Williams, M. T., *Org. Biomol. Chem.* **2006**, *4*, 2337-2347.
- [2] Constable, D. J. C.; Dunn, P. J.; Hayler, J. D.; Humphrey, G. R.; Leazer, J. J. L.; Linderman, R. J.; Lorenz, K.; Manley, J.; Pearlman, B. A.; Wells, A.; Zaks, A.; Zhang, T. Y., *Green Chemistry* **2007**, *9*, 411-420.
- [3] Müller, T. E.; Hultsch, K. C.; Yus, M.; Foubelo, F.; Tada, M., *Chem. Rev.* **2008**, *108*, 3795-3892.
- [4] Crimmin, M. R.; Casely, I. J.; Hill, M. S., *J. Am. Chem. Soc.* **2005**, *127*, 2042-2043.
- [5] Crimmin, M. R.; Arrowsmith, M.; Barrett, A. G. M.; Casely, I. J.; Hill, M. S.; Procopiou, P. A., *J. Am. Chem. Soc.* **2009**, *131*, 9670-9685.
- [6] Arrowsmith, M.; Hill, M. S.; Kociok-Köhn, G., *Organometallics* **2014**, *33*, 206-216.
- [7] Zhang, X.; Emge, T. J.; Hultsch, K. C., *Organometallics* **2010**, *29*, 5871-5877.
- [8] Neal, S. R.; Ellern, A.; Sadow, A. D., *J. Organomet. Chem.* **2011**, *696*, 228-234.
- [9] Hultsch, K. C.; Hampel, F.; Wagner, T., *Organometallics* **2004**, *23*, 2601-2612.
- [10] Hong, S.; Marks, T. J., *Acc. Chem. Res.* **2004**, *37*, 673-686.
- [11] Reznichenko, A. L.; Hultsch, K. C., *Organometallics* **2013**, *32*, 1394-1408.
- [12] Zhang, Y.; Yao, W.; Li, H.; Mu, Y., *Organometallics* **2012**, *31*, 4670-4679.
- [13] Baldwin, J. E., *J. Chem. Soc., Chem. Commun.* **1976**, 734-736.
- [14] Manna, K.; Ellern, A.; Sadow, A. D., *Chem. Commun.* **2010**, *46*, 339-341.
- [15] Ryu, J.-S.; Li, G. Y.; Marks, T. J., *J. Am. Chem. Soc.* **2003**, *125*, 12584-12605.

-
- [16] Brahms, C.; Tholen, P.; Saak, W.; Doye, S., *Eur. J. Org. Chem.* **2013**, *2013*, 7583-7592.
- [17] Manna, K.; Everett, W. C.; Schoendorff, G.; Ellern, A.; Windus, T. L.; Sadow, A. D., *J. Am. Chem. Soc.* **2013**, *135*, 7235-7250.
- [18] Wang, X.; Chen, Z.; Sun, X.-L.; Tang, Y.; Xie, Z., *Org. Lett.* **2011**, *13*, 4758-4761.
- [19] Helgert, T. R.; Hollis, T. K.; Valente, E. J., *Organometallics* **2012**, *31*, 3002-3009.
- [20] Chong, E.; Qayyum, S.; Schafer, L. L.; Kempe, R., *Organometallics* **2013**, *32*, 1858-1865.
- [21] Gribkov, D. V.; Hultsch, K. C., *Angew. Chem. Int. Ed.* **2004**, *43*, 5542-5546.
- [22] Clark, W. D.; Cho, J.; Valle, H. U.; Hollis, T. K.; Valente, E. J., *J. Organomet. Chem.* **2014**, *751*, 534-540.
- [23] Liu, Z.; Yamamichi, H.; Madrahimov, S. T.; Hartwig, J. F., *J. Am. Chem. Soc.* **2011**, *133*, 2772-2782.
- [24] Kashiwame, Y.; Kuwata, S.; Ikariya, T., *Organometallics* **2012**, *31*, 8444-8455.
- [25] Shen, X.; Buchwald, S. L., *Angew. Chem. Int. Ed.* **2010**, *49*, 564-567.
- [26] Nguyen, T. O.; Man, B. Y.-W.; Hodgson, R.; Messerle, B. A., *Aust. J. Chem.* **2011**, *64*, 741-746.
- [27] Tobisch, S., *Chem. Eur. J.* **2012**, *18*, 7248-7262.
- [28] Hesp, K. D.; Tobisch, S.; Stradiotto, M., *J. Am. Chem. Soc.* **2010**, *132*, 413-426.
- [29] Bender, C. F.; Widenhoefer, R. A., *J. Am. Chem. Soc.* **2005**, *127*, 1070-1071.
- [30] Bender, C. F.; Hudson, W. B.; Widenhoefer, R. A., *Organometallics* **2008**, *27*, 2356-2358.

-
- [31] Cochran, B. M.; Michael, F. E., *J. Am. Chem. Soc.* **2008**, *130*, 2786-2792.
- [32] Lavery, C. B.; Ferguson, M. J.; Stradiotto, M., *Organometallics* **2010**, *29*, 6125-6128.
- [33] Taylor, J. G.; Whittall, N.; Hii, K. K., *Org. Lett.* **2006**, *8*, 3561-3564.
- [34] Ohmiya, H.; Moriya, T.; Sawamura, M., *Org. Lett.* **2009**, *11*, 2145-2147.
- [35] Munro-Leighton, C.; Blue, E. D.; Gunnoe, T. B., *J. Am. Chem. Soc.* **2006**, *128*, 1446-1447.
- [36] Munro-Leighton, C.; Delp, S. A.; Blue, E. D.; Gunnoe, T. B., *Organometallics* **2007**, *26*, 1483-1493.
- [37] Pouy, M. J.; Delp, S. A.; Uddin, J.; Ramdeen, V. M.; Cochrane, N. A.; Fortman, G. C.; Gunnoe, T. B.; Cundari, T. R.; Sabat, M.; Myers, W. H., *ACS Catal.* **2012**, *2*, 2182-2193.
- [38] Komeyama, K.; Morimoto, T.; Takaki, K., *Angew. Chem. Int. Ed.* **2006**, *45*, 2938-2941.
- [39] Mathia, F.; Szolcsányi, P., *Org. Biomol. Chem.* **2012**, *10*, 2830-2839.
- [40] Cheng, X.; Xia, Y.; Wei, H.; Xu, B.; Zhang, C.; Li, Y.; Qian, G.; Zhang, X.; Li, K.; Li, W., *Eur. J. Org. Chem.* **2008**, *2008*, 1929-1936.
- [41] Taylor, J. G.; Whittall, N.; Hii, K. K., *Org. Lett.* **2006**, *8*, 3561-3564.
- [42] Qin, H.; Yamagiwa, N.; Matsunaga, S.; Shibasaki, M., *Chemistry – An Asian Journal* **2007**, *2*, 150-154.
- [43] Qin, H.; Yamagiwa, N.; Matsunaga, S.; Shibasaki, M., *J. Am. Chem. Soc.* **2006**, *128*, 1611-1614.

-
- [44] Rosenfeld, D. C.; Shekhar, S.; Takemiya, A.; Utsunomiya, M.; Hartwig, J. F., *Org. Lett.* **2006**, *8*, 4179-4182.
- [45] Schlummer, B.; Hartwig, J. F., *Org. Lett.* **2002**, *4*, 1471-1474.
- [46] McKinney Brooner, R. E.; Widenhoefer, R. A., *Chem. Eur. J.* **2011**, *17*, 6170-6178.
- [47] Liu, G.-Q.; Cui, B.; Sun, H.; Li, Y.-M., *Tetrahedron* **2014**, *70*, 5696-5703.
- [48] Yang, L.; Xu, L.-W.; Xia, C.-G., *Synthesis* **2009**, *2009*, 1969-1974.
- [49] Wang, Y.-M.; Li, T.-T.; Liu, G.-Q.; Zhang, L.; Duan, L.; Li, L.; Li, Y.-M., *RSC Advances* **2014**, *4*, 9517-9521.
- [50] Ackermann, L.; Althammer, A., *Synlett* **2008**, *2008*, 995-998.
- [51] Ackermann, L.; Kaspar, L. T.; Althammer, A., *Org. Biomol. Chem.* **2007**, *5*, 1975-1978.
- [52] Marcseková, K.; Doye, S., *Synthesis* **2007**, *2007*, 145-154.
- [53] Li, Z.; Zhang, J.; Brouwer, C.; Yang, C.-G.; Reich, N. W.; He, C., *Org. Lett.* **2006**, *8*, 4175-4178.
- [54] Anderson, L. L.; Arnold, J.; Bergman, R. G., *J. Am. Chem. Soc.* **2005**, *127*, 14542-14543.
- [55] McBee, J. L.; Bell, A. T.; Tilley, T. D., *J. Am. Chem. Soc.* **2008**, *130*, 16562-16571.
- [56] Griffiths-Jones, C. M.; Knight, D. W., *Tetrahedron* **2010**, *66*, 4150-4166.
- [57] Mirabdolbaghi, R.; Dudding, T., *Org. Lett.* **2015**, *17*, 1930-1933.
- [58] Koller, J.; Bergman, R. G., *Chem. Commun.* **2010**, *46*, 4577-4579.
- [59] Koller, J.; Bergman, R. G., *Organometallics* **2010**, *29*, 3350-3356.
- [60] Khandelwal, M.; Wehmschulte, R. J., *J. Organomet. Chem.* **2012**, *696*, 4179-4183.

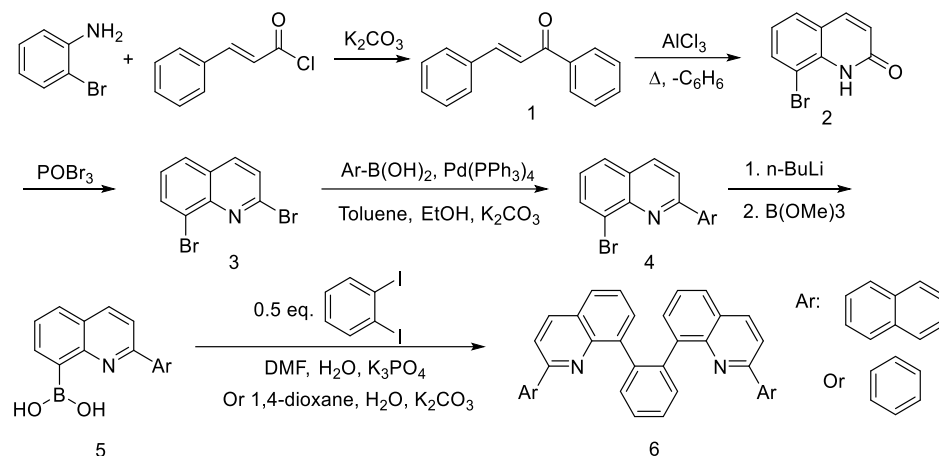
-
- [61] Taylor, J. G.; Adrio, L. A.; Hii, K. K., *Dalton Transactions* **2010**, 39, 1171-1175.
- [62] Muratore, M. E.; Holloway, C. A.; Pilling, A. W.; Storer, R. I.; Trevitt, G.; Dixon, D. J., *J. Am. Chem. Soc.* **2009**, 131, 10796-10797.
- [63] Dang, T. T.; Boeck, F.; Hintermann, L., *J. Org. Chem.* **2011**, 76, 9353-9361.
- [64] Coulombel, L.; Rajzmann, M.; Pons, J.-M.; Olivero, S.; Duñach, E., *Chem. Eur. J.* **2006**, 12, 6356-6365.
- [65] Michon, C.; Medina, F.; Capet, F.; Roussel, P.; Agbossou-Niedercorn, F., *Adv. Synth. Catal.* **2010**, 352, 3293-3305.
- [66] Hirner, J. J.; Roth, K. E.; Shi, Y.; Blum, S. A., *Organometallics* **2012**, 31, 6843-6850.

6 Future Outlook

6.1 Future Direction of Reductive Elimination of Rh–Me

The “capping arene” ligand supported Rh(III) complexes have successfully achieved reductive elimination of MeX. The ligand was designed to block an axial coordination site by using steric bulk in order to favor reductive elimination by destabilizing the higher oxidation state Rh(III) relative to Rh(I). The Rh(I) catalyst with “capping arene” ligand can resist oxidation with O₂ at 150 °C and the “capping arene” supported Rh(III)-Me complex can reductively eliminate MeX in high yield.

Designing a related series of ligands that could block more than one coordination site could result in enhanced reaction rate of reductive elimination for similar complexes. A proposed synthetic route for a di-“capping arene” ligand is shown in Scheme 6.1.1. This new “capping arene” ligand is based on the motif of 6-FP [6-FP = 8,8'-(1,2-phenylene)diquinoline]. Two additional phenyl or naphthyl groups are located on the α position of quinoline ring. After coordination to the metal center, the two phenyl or naphthyl groups would add steric bulk to the upper position in axial coordination site, which may further destabilize the Rh(III) state. In another approach, the substituents on the benzene ring could be varied to reduce its propensity to bind to the metal center (Figure 6.1.1). By adding electron withdrawing groups such as -NO₂, -F or -CF₃, the coordination ability of the benzene ring will be reduced. In addition, adding groups with large steric bulk like -^tBu or -ⁱPr, the coordination could also be inhibited.



Scheme 6.1.1. Proposed synthetic routes for di-“capping arene” ligands.

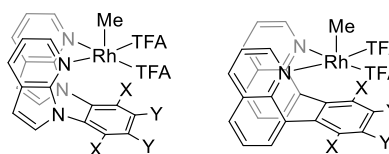


Figure 6.1.1. Structure for proposed “capping arene” ligands.

The ultimate goal for this study is to identify a potential catalyst for the selective partial oxidation of hydrocarbons. The $(5\text{-FP})\text{Rh}(\text{TFA})(\eta^2\text{-C}_2\text{H}_4)$ [5-FP = 1,2-bis(*N*-7-azaindoly)benzene] has proven to be an effective catalyst for oxidative olefin hydroarylation with benzene and olefins.^[1] Based on DFT calculations, the benzene C–H activation is proposed as the rate determining step. In this case, the “capping arene” supported Rh complex should be capable for arene C–H activation, and it may be possible to achieve alkane C–H activation as well. In addition, $(5\text{-FP})\text{Rh}(\text{TFA})_2\text{Me}$ has been demonstrated to reductively eliminate MeTFA in the presence of a Ag oxidant. By coupling these two reactions, we may be able to catalytically functionalize the C–H bonds of hydrocarbons. In same initial experiments, benzene will be used as substrate and $\text{PhI}(\text{OAc})_2$ as oxidant. Under similar conditions, $\text{Pd}(\text{OAc})_2$ is an effective catalyst for benzene acetoxylation.^[2-7] Since the capping arene Rh complex has shown great potential in both C–H activation and reductive elimination, we believe this is a promising route for alkane

or arene functionalization.

6.2 Future Direction of Hydroarylation with Rh Catalysts

Although (5-FP)Rh(TFA)(η^2 -C₂H₄) demonstrates high longevity and reactivity towards oxidative olefin hydroarylation, additional advances would be required for commercialization. Tethering the catalyst to heterogenous supports may improve catalyst longevity and open the possibility of flow reactors. Recently, polymer-supported palladium carbene complexes have been shown to be effective for arene acetoxylation.^[8] The NHC ligand supported Pd catalysts have C=C in the supporting ligand and could co-polymerize with monomers of the heterogenous support. Additionally, the pore sizes of the heterogenous catalysts can be tuned by controlling the polymerization conditions and ligand structure. Since the steric bulk around the metal center is essential for the high linear:branched selectivity for alkenyl arenes by our Rh catalyst, heterogenous supports with different pore sizes could result in improved L:B selectivity.

Although high turnover numbers are achieved with the “capping arene” supported Rh catalyst, the overall conversion of benzene remains low (<10%) due to challenges with product inhibition. Developing a more suitable solvent system may be a potential approach. As acetic acid results in stabilization of the Cu(II) oxidant stabilization and acidic media is essential for the olefin hydroarylation reactions using oxygen as the sole oxidant, acidic acid is a candidate for these future solvent screening studies. Further, as water is a side product of the reaction and the accumulated moisture might become an issue with high benzene conversion reaction, the addition of acetic anhydride could be beneficial.

In the Pt- and Ru-catalyzed olefin hydroarylation reaction with benzene and ethylene,

varying the electron donating ability of ligand affects the selectivity of the reaction, resulting in the formation of ethylbenzene or styrene.^[9-15] However, no such phenomenon was observed with our Rh catalysts. Although styrene is a more valuable product than ethylbenzene, the production of phenyl alkanes, which can be directly used with sulfonating reagents to make alkylbenzene sulfonates, may be more valuable overall. In order to favor the production of phenyl alkanes, a strongly electron donating ligand must be required. *N*-heterocyclic carbene (NHC) ligands are well-known for their strong donating ability. A series of ligands shown in Figure 6.2.1 are proposed to be suitable candidates. Mono-, di- and tri-NHC ligands can be tested with Rh. The R groups of the ligand can be easily modified to tune the steric bulk around the metal center. In this case, phenyl alkane products could be produced with high L:B ratios.

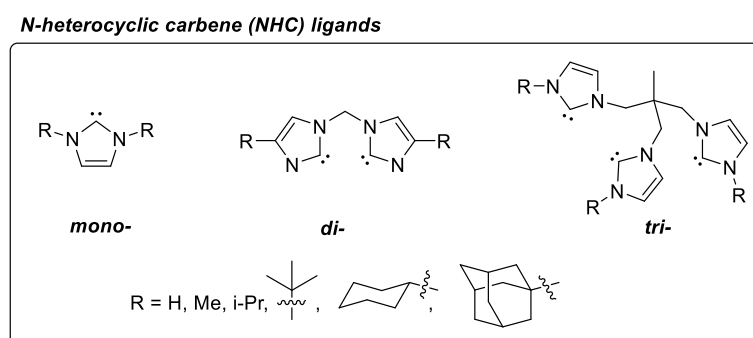


Figure 6.2.1. Structures of proposed NHC ligands.

6.3 Future Direction of Copper Catalyzed Arene C–H Functionalization

TEMPO has proven to be effective in accelerating the acetoxylation reactions with benzene and $\text{Cu}(\text{OAc})_2$. A series of radicals with N–O linkage will be tested for comparison (Figure 6.3.1). 4-Acetamido-TEMPO shows higher reactivity toward alcohol oxidation, and we may also observe an improvement in the benzene acetoxylation reactions by using modified TEMPO reagents.^[18] A series of additional radical precursors with N–O linkages

will also be tested in efforts to improve the reaction rate. The NHPI/PINO redox couple in particular has a higher redox potential (~ 0.9 V).^[19] In addition, since the reaction has been demonstrated to likely occur via an organometallic pathway, the addition of ligands for copper may benefit the reaction. Again, ligands shown in Figure 6.3.3 are effective additives for alcohol oxidation under different conditions and they may benefit our Cu/TEMPO system as well.^[20-22]

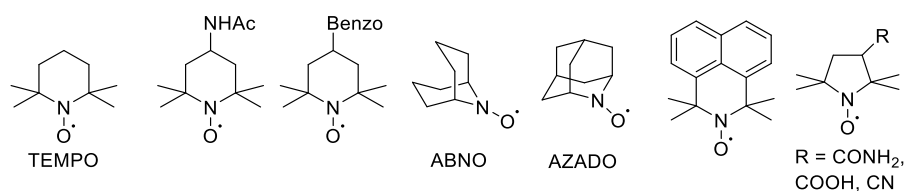


Figure 6.3.1. Structures of TEMPO and additional radicals with N-O linkages.

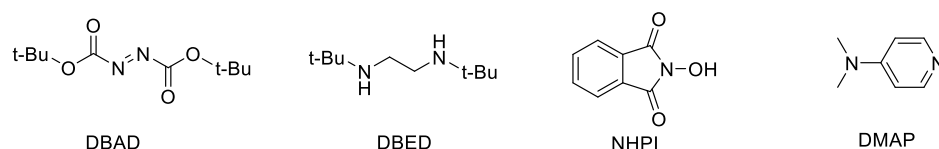


Figure 6.3.2. Structures of radical precursors with N-O linkages.

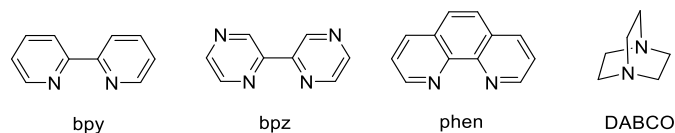


Figure 6.3.3. Structures of potential ligands to support Cu(OAc)₂.

With the addition of various nucleophilic anions, Cu(II) can catalyze the functionalization of aryl C–H bonds with directed arenes.^[23] Since we have successfully achieved iodination with the addition of iodine, other additives including TMSCN, PhSH, H₂O, AgNO₂ and AgF will be tested for possible corresponding functionalization. In addition, other arenes will also be tested for Cu-mediated C–H functionalization. Different site selectivity will be expected when comparing with traditional acid-catalyst mediated benzene functionalization.

6.4 References:

- [1] Chen, J.; Nielsen, R. J.; Goddard, W. A.; McKeown, B. A.; Dickie, D. A.; Gunnoe, T. B., *J. Am. Chem. Soc.* **2018**, *140*, 17007-17018.
- [2] Emmert, M. H.; Gary, J. B.; Villalobos, J. M.; Sanford, M. S., *Angew. Chem. Int. Ed.* **2010**, *49*, 5884-5886.
- [3] Emmert, M. H.; Cook, A. K.; Xie, Y. J.; Sanford, M. S., *Angew. Chem. Int. Ed.* **2011**, *50*, 9409-9412.
- [4] Cook, A. K.; Sanford, M. S., *J. Am. Chem. Soc.* **2015**, *137*, 3109-3118.
- [5] Cook, A. K.; Emmert, M. H.; Sanford, M. S., *Org. Lett.* **2013**, *15*, 5428-5431.
- [6] Gary, J. B.; Cook, A. K.; Sanford, M. S., *ACS Catal.* **2013**, *3*, 700-703.
- [7] Shrestha, A.; Lee, M.; Dunn, A. L.; Sanford, M. S., *Org. Lett.* **2018**, *20*, 204-207.
- [8] Majeed, M. H.; Shayesteh, P.; Wallenberg, L. R.; Persson, A. R.; Johansson, N.; Ye, L.; Schnadt, J.; Wendt, O. F., *Chem. Eur. J.* **2017**, *23*, 8457-8465.
- [9] Burgess, S. A.; Joslin, E. E.; Gunnoe, T. B.; Cundari, T. R.; Sabat, M.; Myers, W. H., *Chemical Science* **2014**, *5*, 4355-4366.
- [10] Joslin, E. E.; Quillian, B.; Gunnoe, T. B.; Cundari, T. R.; Sabat, M.; Myers, W. H., *Inorg. Chem.* **2014**, *53*, 6270-6279.

-
- [11] Morello, G. R.; Cundari, T. R.; Gunnoe, T. B., *J. Organomet. Chem.* **2012**, *697*, 15-22.
- [12] Jia, X.; Gary, J. B.; Gu, S.; Cundari, T. R.; Gunnoe, T. B., *Isr. J. Chem.* **2017**, *57*, 1037-1046.
- [13] McKeown, B. A.; Gonzalez, H. E.; Friedfeld, M. R.; Brosnahan, A. M.; Gunnoe, T. B.; Cundari, T. R.; Sabat, M., *Organometallics* **2013**, *32*, 2857-2865.
- [14] McKeown, B. A.; Prince, B. M.; Ramiro, Z.; Gunnoe, T. B.; Cundari, T. R., *ACS Catal.* **2014**, *4*, 1607-1615.
- [15] McKeown, B. A.; Gonzalez, H. E.; Friedfeld, M. R.; Gunnoe, T. B.; Cundari, T. R.; Sabat, M., *J. Am. Chem. Soc.* **2011**, *133*, 19131-19152.
- [16] Díez-González, S.; Nolan, S. P., *Coord. Chem. Rev.* **2007**, *251*, 874-883.
- [17] Ahrens, S.; Zeller, A.; Taige, M.; Strassner, T., *Organometallics* **2006**, *25*, 5409-5415.
- [18] Rafiee, M.; Miles, K. C.; Stahl, S. S., *J. Am. Chem. Soc.* **2015**, *137*, 14751-14757.
- [19] Nutting, J. E.; Rafiee, M.; Stahl, S. S., *Chem. Rev.* **2018**, *118*, 4834-4885.
- [20] Mannam, S.; Alamsetti, S. K.; Sekar, G., *Adv. Synth. Catal.* **2007**, *349*, 2253-2258.
- [21] Markó, I. E.; Giles, P. R.; Tsukazaki, M.; Brown, S. M.; Urch, C. J., *Science* **1996**, *274*, 2044-2046.

[22] Ragagnin, G.; Betzemeier, B.; Quici, S.; Knochel, P., *Tetrahedron* **2002**, *58*, 3985-3991.

[23] Chen, X.; Hao, X.-S.; Goodhue, C. E.; Yu, J.-Q., *J. Am. Chem. Soc.* **2006**, *128*, 6790-6791.